U.PORTO

FEUP FACULDADE DE ENGENHARIA
UNIVERSIDADE DO PORTO

Decentralized Cloud-Based Approaches for Cross-Sector Demand Side Management

Mohamed Lotfi

Supervisor: Prof. João P.S. Catalão (FEUP and INESC TEC)

Co-Supervisor: Prof. Cláudio D. Monteiro (FEUP)

Co-Supervisor: Prof. Gerardo J. Osório (UPT)

Programa Doutoral em Sistemas Sustentáveis de Energia

November 2021

Faculdade de Engenharia da Universidade do Porto

Decentralized Cloud-Based Approaches for Cross-Sector Demand Side Management

Mohamed Lotfi

Dissertation submitted to Faculdade de Engenharia da Universidade do Porto
to obtain the degree of

Doctor Philosophiae in Sustainable Energy Systems

Jury President:
Dr. **João Abel Peças Lopes**, Universidade do Porto, Portugal

Jury Members:
Dr. **Gianfranco Chicco**, Politecnico de Torino, Italy
Dr. **Javier Contreras Sanz**, Universidad de Castilla-La Mancha, Spain
Dr. **Carlos Henggeler Antunes**, Universidade de Coimbra, Portugal
Dr. **Luís António Fialho Marcelino Ferreira**, Universidade de Lisboa, Portugal
Dr. **Manuel António Cerqueira da Costa Matos**, Universidade do Porto, Portugal
Supervisor: Dr. **João Paulo da Silva Catalão**, Universidade do Porto, Portugal

---

November 2021

VIRTVTIBVS MAIORVM VT SIT OMNIBVS DOCVMENTO

"Às Virtudes dos Maiores, para que sirva a todos de ensinamento."

"To the virtues of the greatest, so that it may serve everyone as a teaching."

The author of this thesis, Mohamed Lotfi, gratefuly acknowledges the co-financing of this work by Portuguese and European Union funds through the *Fundação para a Ciência e a Tecnologia (FCT)*, under grant number *PD/BD/142810/2018*.

The grant was awarded to pursue the Doctoral Program in Sustainable Energy Systems at FEUP as part of the MIT Portugal Program. The author was hosted by INESC TEC as a research assistant at the centre for power and energy systems (CPES). In addition, the work involved a 6-month research visit to the Faculty of Energy Systems and Nuclear Science at Ontario Tech University (Canada). This visit was authorized by FCT and funded by the same aforementioned grant.

The work in this thesis has contributed to the ESGRIDS Project: *Enhancing Smart GRIDS for Sustainability — ESGRIDS. Ref. POCI-01-0145-FEDER-016434*, COMPETE 2020, Portugal. This contribution was authorized by FCT (25% time allocation).

The work in this thesis has contributed to the UNiTED Project: *Unlocking demand response potential with Next generation innovative optimization Tools Empowering prosumers and Distribution grid benefits — UNiTED*, Ref. POCI-01-0145-FEDER-029803, FCT, Portugal. This contribution was authorized by FCT (25% time allocation).

Abstract

Technological advances are enabling decentralized energy systems to be more economically competitive on larger scales with their centralized counterparts. Suitable information exchange, data analysis, and communication solutions are needed to operate and manage these physically decentralized systems. The transition thereto is accelerated by increased unsustainability of traditional models to cope with emerging technical, socio-economic, and environmental problems.

In the electrical energy sector, rapid Internet-of-Things (IoT)-enabling of smart grids (SGs), the proliferation of distributed generation (DG), and the emergence of peer-to-peer (P2P) trading and decentralized economies are collectively paving the way for the emergence of the Internet-of-Energy (IoE). In this IoE paradigm being a fully decentralized network of energy prosumers, traditional top-down centralized models are being rendered obsolete, with the "demand" side participation in the operation and control of the IoE being centerpiece. Active participation by energy end-users began decades ago with the first waves of electricity market liberalization that incentivized the participation of consumers as active players in the market through the introduction of Demand Response (DR) belonging to the wider category of Demand-Side Management (DSM) programs. SGs have been a key enabler to modern data-driven DR and DSM schemes, with smart metering data providing input to underlying optimization and forecasting tools. Between P2P energy trading and the development of the IoE (seen as an evolution of SGs), there is a clear emergence of what is referred to as democratic energy systems in which fundamental aspects are (1) significant citizen participation, (2) decentralized decision making in operation, management, planning, and trading, and (3) renewable energy source (RES) dominated generation. Concurrently, the fourth industrial revolution (I4.0) currently underway is resulting in increased intertwining between sectors that are the major consumers of energy (residential, transport, and industry). In addition, with the electrification of transport being a top priority and smart industries emerging as vital pillars of modern economies, the adaptation of DSM and DR schemes for cross-sector applications becomes of paramount importance. More physically decentralized and interconnected energy systems motivate the investigation of decentralized data models to manage them as opposed to centralized operators.

In this context, the work in this thesis builds on architectures, approaches, and emerging technologies in the IoE paradigm to develop disruptive energy management tools that cover the full spectrum and dimensions of this transition: 1) grid operation (cloud-based coordination, forecasting, and power flow management tools), and 2) cross-sector end-user energy management adaptation to future scenarios (namely: the residential, transport, and industry sectors).

Keywords: Energy Management, Smart Grids, Demand Response, Decentralized Systems, Machine Learning, Optimal Scheduling.

Resumo

Graças ao avanços tecnológicos dos últimos anos, os sistemas de energia descentralizados têm-se tornados mais competitivos economicamente, e em maior escala, do que seus equivalentes centralizados. A troca de informação adequada, a análise de dados, e as tecnologias de comunicação, são domínios necessários para a operação e adequada gestão dos sistemas fisicamente descentralizados, os quais têm tido um crescimento acelerado, por causa do aumento de insustentabilidade dos modelos tradicionais em tratar os problemas técnicos, socioeconómicos e ambientais da atualidade.

No setor de energia elétrica, devido à rápida adaptação do conceito "*Internet-of-Things*" (IoT) nas redes inteligentes (SGs), a proliferação da geração distribuída (GD), o surgimento do conceito de comércio "*peer-to-peer*", e as economias descentralizadas, coletivamente pavimentam o caminho para o surgimento do novo paradigma denominado por *"Internet-of-Energy"* (IoE). o IoE é uma rede totalmente descentralizada de prosumers energéticos, onde os modelos tradicionais de produção de eletricidade se tornam obsoletos. Na operação e controlo da IoE, a participação do lado da "procura" fica no centro da ação.

A participação ativa dos utilizadores finais de eletricidade começou há décadas atrás com a liberalização do mercado de eletricidade, os quais incentivaram a participação dos consumidores como agentes ativos no mercado, através da introdução do conceito de "*Demand Response*" (DR), e da categoria mais generalizada de programas de "*Demand-Side Management*" (DSM). Nesta senda, as definições sobre as SGs foram as principais facilitadoras dos esquemas modernos de DR e DSM baseados em dados, com dados monitorizados por medidores inteligentes, os quais fornecem os dados para as ferramentas de otimização e previsão.

Na atualidade, entre a negociação P2P e o desenvolvimento da IoE, existe uma evidente manifestação de que é identificado como "sistemas democráticos de energia", cujos aspetos fundamentais se resumem: (1) a significativa participação dos cidadãos, (2) tomada de decisão descentralizada para operação, gestão, planeamento e negociação, e, (3) geração dominada pelas fontes renováveis. Ao mesmo tempo, com a quarta revolução industrial (I4.0) a decorrer, permite também o aumento da interligação entre os setores que são os grandes consumidores de eletricidade, (residencial, transportes e indústria). Também, com a prioridade global na eletrificação dos transportes, as indústrias inteligentes são vistas como pilares vitais das economias modernas, onde a adaptação dos esquemas DSM e DR para aplicações intersectoriais se mostram de grande importância.

O trabalho desta tese baseia-se nas arquiteturas, métodos e tecnologias emergentes no paradigma IoE, para desenvolver ferramentas de gestão de energia disruptivas que cobrem todo o espectro e as dimensões da transição energética: 1) o funcionamento da rede (coordenação baseada em nuvem, com ferramentas de previsão e gestão de fluxo de potência), e 2) adaptação da gestão da energia dos utilizadores finais, dos vários setores, e dos cenários futuros (nos setores residencial, transporte, e a indústria).

Acknowledgments

There are so many people that I am immensely grateful to for helping me throughout this long and tough journey. I've been truly blessed with wonderful companionship during my PhD years.

First and foremost, there are three people without whom this work would not have been possible. First, the true "Legend", the "Godfather", the "Greatest" Prof. Catalão! I will never, ever, be able to thank you enough for everything you have done for me, dearest Professor! Words simply won't suffice. You truly are a "Legend", and I am truly lucky to have had the honor of having you as my supervisor and mentor. Second, the "Innovator", the "Genius", Prof. Cláudio! You inspired me to be innovative and pursue originality! I will always be grateful that you put me on this path! Third, the "Angel", "Golden Heart", Prof. Gerardo! You have not only helped a lot scientifically, but you have treated me with patience and kindness as an older brother and a true friend! Thank you, Professors, for showing me how true mentors and supervisors should be like.

I would like to thank the great Professors of the PDSSE program at FEUP: Professor Vitor Leal, for encouraging and inspiring me to join the program; Prof. Peças Lopes and Prof. Manuel Matos for demonstrating how it is to be great teachers and inspiring leaders to younger researchers like myself. It was a true honor to be taught by legends such as yourselves. Of course, the PDSSE program cannot be mentioned without thanking Ms. Célia Couto, who has been extremely professional and helpful even during the very tough times.

I would like to thank Prof. Hossam Gaber for inviting me as a visiting scholar to Ontario Tech University. It was a life-changing experience and working with him taught me a lot of scientific knowledge and life wisdom. I also sincerely thank Ms. Cristina Preece for all her relentless support and help. I truly felt home during my visit and I will always be grateful for your hospitality.

Special thanks go to my dear colleagues at INESC TEC. I thank Mohammad Javadi, Sérgio Santos, and Matthew Gough for being great colleagues and collaborators.

My friends Marco and Konstantinos, you two were wonderful companions in this journey. I will never forget our "Mediterranean Alliance", our scientific and philosophical debates. It was an honor knowing you gentlemen, I wish you all the best!

Last but not least, I thank my family: my dear parents and siblings, for their endless and unconditional love support.

To all my dear friends and family: I can only hope this thesis makes all of you proud.

Mohamed Lotfi, Porto, 2021

"Tudo vale a pena se a alma não é pequena"

Fernando Pessoa

Prologue and Thesis Synopsis

1 Research Questions

Primary Research Question:

Can fully decentralized distributed data models (based on IoT[1] and P2P[2] networks) ensure techno-economic sustainability for electric power systems and cross-sector end-users?

Secondary Research Questions:

Can individual and proprietary data models from the IoE[3] paradigm be used to leverage DSM[4] and DR[5] services from individual prosumers and microgrids (cluster of prosumers) thereby improving global operation of dispersed energy systems?

Can local (fully decentralized) optimization and data analytics functions enable global integration of demand-side flexibility in the energy market, system operation, and planning?

Can optimal prosumption scheduling of individual agents in a decentralized energy system (using information signals from other individual agents contrary to top-down centralized control) result in global optimal operation?

Do decentralized data models provide an effective and sustainable solution for the operation of physically decentralized energy systems?

Could new models be created and developed to enable a fully decentralized P2P energy and information trading platform?

In the future cloud-based IoE paradigm, how can energy management models be adapted for end-users in different sectors (namely: residential, transport, and industry).

[1] Internet-of-Things (IoT)
[2] Peer-to-Peer (P2P)
[3] Internet-of-Energy (IoE)
[4] Demand Side Management (DSM)
[5] Demand Response (DR)

2 Novel Contributions and Thesis Structure

This **work builds** on architectures, approaches, and emerging technologies in the **IoE paradigm** to **develop disruptive energy management tools that cover the full spectrum and dimensions** of this transition: **1) grid operation** (cloud-based coordination, forecasting, and power flow management tools), and **2) cross-sector end-user energy management adaptation** to future scenarios (namely: the residential, transport, and industry sectors).

Embracing the adopted scientific hypothesis pertaining to the IoE paradigm, this thesis is also structured in a "decentralized" manner. While the order of the chapters provides the ideal flow of information to describe the work performed in this thesis; an effort was made to ensure that each chapter can also be read separately with minimal need to refer to other chapters.

Each chapter has its separate nomenclature, which is especially important due to the fact that research was conducted on different sectors, with different variable and mathematical notation conventions used in their corresponding fields of research. A unified list of references is used to duly link the bibliography across the entire document.

This thesis is structured into **four parts and ten chapters**:

PART I (Chapters 1 and 2) serves to introduce the setting within which this work is conducted (the emergence of the IoE paradigm and energy prosumers) by conducting a thorough analysis of scientific literature, legislations, and expert reviews. The necessary criteria for tools developed to be compatible with the IoE paradigm are defined. Then, PART II (Chapters 3, 4, and 5) and PART III (Chapters 6, 7, and 8) form the core of the thesis, presenting the developed methods and analyses performed.

PART II (Chapters 3, 4, and 5) focuses on the work done with regards to grid operation. Chapter 3 demonstrates how modern-day energy management systems can be coordinated through a cloud based approach to achieve synergistic benefits both for the global system and the end-users (local prosumers). Chapters 4 and 5 proceed to develop new algorithms for fully decentralized forecasting and power flow management of next-generation power systems. In Chapter 4, a novel KDE method is developed and enables fully decentralized local forecasting for prosumers without depending on private/proprietary data or divulging their own, being compatible with the cloud based IoE paradigm. In Chapter 5, a novel machine learning algorithm is proposed and formulated to enable the transition into a cloud-based fully decentralized power system operation.

PART III (Chapters 6, 7, and 8) focuses on the work done with regards to adapting energy management models of end-users from different sectors to future scenarios. In Chapter 6, a combined prosumption scheduling and trading tool based on energy value is presented. In Chapter 7, a comprehensive optimization model for charging infrastructure deployment, charge scheduling, battery sizing, and route design for fully electric public transport networks is developed and used to analyze future scenarios. In Chapter 8, a novel graph-based model for fully autonomous task scheduling in smart industries is presented to minimize energy consumption.

PART IV (Chapters 9 and 10) is the final part of this thesis. In Chapter 9 the research questions of the this thesis are revisited and answered in detail based on, and referencing, the research work presented in all previous chapters. Chapter 10 summarizes the final conclusions and discusses future prospects building on the work developed in this thesis.

3 Publications

The research work performed throughout the course of this thesis has contributed to a large number of scientific publications. As a direct extraction of the thesis body, 5 journal papers and 7 conference papers, 1 book chapter, and 1 newsletter article have been produced. In addition, research performed throughout the course of the work on overlapping research topics has resulted in an additional 5 journal papers and 6 conference papers.

Thus, the work performed throughout the course of this thesis contributed to the preparation of a total of **10 journal papers, 13 conference papers, 1 book chapter, and 1 newsletter article**.

Direct Extractions - International Journals

M. Lotfi, C. Monteiro, G.J. Osorio, M. Javadi, M.S. El-Moursi J.P.S. Catalão, "A Fully Decentralized Machine Learning Algorithm for Optimal Power Flow with Cooperative Information Exchange," in *International Journal of Electrical Power & Energy Systems*.
Minor Revisions, Resubmitted.

M. Lotfi, T. Almeida, M. Javadi, G.J. Osorio, C. Monteiro, J.P.S. Catalão, "Coordinating Energy Management Systems in Smart Cities with Electric Vehicles," in *Applied Energy*, 2022.
Accepted for Publication.

M. Lotfi, G.J. Osório, M. Javadi, A. Ashraf, M. Zahran, G. Samih, J.P.S. Catalão, "A Dijkstra-Inspired Graph Algorithm for Fully Autonomous Tasking in Industrial Applications," in *IEEE Transactions on Industry Applications*, vol. 57, no. 5, pp. 5448-5460, Sept.-Oct. 2021.
Published: https://doi.org/10.1109/TIA.2021.3091418

M. Lotfi, P. Pereira, N. G. Paterakis, H. A. Gabbar and J. P. S. Catalão, "Optimal Design of Electric Bus Transport Systems With Minimal Total Ownership Cost," in *IEEE Access*, vol. 8, pp. 119184-119199, 2020.
Published: https://doi.org/10.1109/ACCESS.2020.3004910

M. Lotfi, M. Javadi, G. J. Osório, C. Monteiro, and J. P. S. Catalão, "A Novel Ensemble Algorithm for Solar Power Forecasting Based on Kernel Density Estimation," *Energies*, vol. 13, no. 1, p. 216, Jan. 2020.
Published: http://dx.doi.org/10.3390/en13010216

Direct Extractions - International Conferences

M. Lotfi, S. Fikry, G. J. Osório, M. Javadi, S. F. Santos and J. P. S. Catalão, "A Hybrid Probabilistic Algorithm for Computationally Efficient Estimation of Power Generation in AC Optimal Power Flow," *2020 IEEE 14th International Conference on Compatibility, Power Electronics and Power Engineering (CPE-POWERENG)*, 2020, pp. 169-174.
Published: https://doi.org/10.1109/CPE-POWERENG48600.2020.9161685

M. Lotfi, A. Ashraf, M. Zahran, G. Samih, M. Javadi, G.J. Osório, J.P.S. Catalão, "A Dijkstra-Inspired Algorithm for Optimized Real-Time Tasking with Minimal Energy Consumption," *2020 IEEE International Conference on Environment and Electrical Engineering and 2020 IEEE Industrial and Commercial Power Systems Europe (EEEIC / I&CPS Europe)*, 2020, pp. 1-6.
Best PhD Paper Award (1st Place)
Published: https://doi.org/10.1109/EEEIC/ICPSEurope49358.2020.9160688

M. Lotfi, P. Pereira, N. Paterakis, H.A. Gabbar, J.P.S. Catalão, "Optimizing Charging Infrastructures of Electric Bus Routes to Minimize Total Ownership Cost," *2020 IEEE International Conference on Environment and Electrical Engineering and 2020 IEEE Industrial and Commercial Power Systems Europe (EEEIC / I&CPS Europe)*, 2020, pp. 1-6.
Published: https://doi.org/10.1109/EEEIC/ICPSEurope49358.2020.9160687

M. Lotfi, T. Almeida, M. Javadi, G.J. Osório, J.P.S. Catalão, "Coordinated Operation of Electric Vehicle Parking Lots and Smart Homes as a Virtual Power Plant," *2020 IEEE International Conference on Environment and Electrical Engineering and 2020 IEEE Industrial and Commercial Power Systems Europe (EEEIC / I&CPS Europe)*, 2020, pp. 1-6.
Published: https://doi.org/10.1109/EEEIC/ICPSEurope49358.2020.9160684

M. Lotfi, C. Monteiro, M.S. Javadi, M. Shafie-khah and J.P.S. Catalão, "Optimal Prosumer Scheduling in Transactive Energy Networks Based on Energy Value Signals," *2019 International Conference on Smart Energy Systems and Technologies (SEST)*, 2019, pp. 1-6.
Published: https://doi.org/10.1109/SEST.2019.8849017

M. Lotfi, J.P.S. Catalão, M.S. Javadi, A.E. Nezhad and M. Shafie-khah, "Demand Response Program Implementation for Day-Ahead Power System Operation," *2019 IEEE Milan PowerTech*, 2019, pp. 1-6.
Published: https://doi.org/10.1109/PTC.2019.8810850

M. Lotfi, C. Monteiro, M. Shafie-khah, J.P.S. Catalão, "Evolution of Demand Response: A Historical Analysis of Legislation and Research Trends," *2018 Twentieth International Middle East Power Systems Conference (MEPCON)*, 2018, pp. 968-973.
Published: https://doi.org/10.1109/MEPCON.2018.8635264

Direct Extractions - Miscellaneous

_Book Chapter (Elsevier):

M. Lotfi, C. Monteiro, M. Shafie-khah, J.P.S. Catalão, Chapter 3 - "Transition toward blockchain- based electricity trading markets", in: *Blockchain-based Smart Grids*, Academic Press, 2020, Pages 43-59, ISBN 9780128178621.
Published: https://doi.org/10.1016/B978-0-12-817862-1.00003-8

_Newsletter Article (Peer-Reviewed):

M. Lotfi, J.P.S. Catalão, H.A. Gabbar, "The Rise of Energy Prosumers and Energy Democracy: History and Future Prospects", *IEEE Smart Grid Newsletter*, July, 2020.
Published: https://smartgrid.ieee.org/newsletters/july-2020/the-rise-of-energy-prosumers-and-energy-democracy-history-and-future-prospects

Overlapping Research - Journal Papers

G.J. Osório, **M. Lotfi**, M. Gough, M. Javadi, H.M.D. Espassandim, M. Shafie-khah, J.P.S. Catalão, "Modeling an Electric Vehicle Parking Lot with Solar Rooftop Participating in the Reserve Market and in Ancillary Services Provision," in *Journal of Cleaner Production*, vol. 318, 128503, 2021.
Published: https://doi.org/10.1016/j.jclepro.2021.128503

O. Abedinia, **M. Lotfi**, M. Bagheri, B. Sobhani, M. Shafie-khah and J.P.S. Catalão, "Improved EMD-Based Complex Prediction Model for Wind Power Forecasting," in *IEEE Transactions on Sustainable Energy*, vol. 11, no. 4, pp. 2790-2802, Oct. 2020.
Published: https://doi.org/10.1109/TSTE.2020.2976038

M. S. Javadi, **M. Lotfi**, A. E. Nezhad, A. Anvari-Moghaddam, J. M. Guerrero and J. P. S. Catalão, "Optimal Operation of Energy Hubs Considering Uncertainties and Different Time Resolutions," in *IEEE Transactions on Industry Applications*, vol. 56, no. 5, pp. 5543-5552, Sept.-Oct. 2020.
Published: https://doi.org/10.1109/TIA.2020.3000707

M. Gough, **M. Lotfi**, R. Castro, A. Madhlopa, A. Khan, and J.P.S. Catalão, "Urban Wind Resource Assessment: A Case Study on Cape Town," *Energies*, vol. 12, no. 8, p. 1479, Apr. 2019.
Published: https://doi.org/10.3390/en12081479

G. Osório, **M. Lotfi**, M. Shafie-khah, V. Campos, and J. Catalão, "Hybrid Forecasting Model for Short-Term Electricity Market Prices with Renewable Integration," *Sustainability*, vol. 11, no. 1, p. 57, Dec. 2018.
Published: https://doi.org/10.3390/su11010057

Overlapping Research - Conference Papers

M. Javadi, **M. Lotfi**, G.J. Osório, A. Ashraf, A.E. Nezhad, M. Gough, J.P.S. Catalão, "A Multi-Objective Model for Home Energy Management System Self-Scheduling using the Epsilon- Constraint Method," *2020 IEEE 14th International Conference on Compatibility, Power Electronics and Power Engineering (CPE-POWERENG)*, 2020, pp. 175-180.
Published: https://doi.org/10.1109/CPE-POWERENG48600.2020.9161526

G. J. Osório, **M. Lotfi**, V. M. A. Campos and J. P. S. Catalão, "Extended Hybrid Wind Power Forecasting Approach to Short-Term Decisions," *2020 IEEE International Conference on Environment and Electrical Engineering and 2020 IEEE Industrial and Commercial Power Systems Europe (EEEIC / I&CPS Europe)*, 2020, pp. 1-6.
Published: https://doi.org/10.1109/EEEIC/ICPSEurope49358.2020.9160581

T. Almeida, **M. Lotfi**, M. Javadi, G. J. Osório and J. P. S. Catalão, "Economic Analysis of Coordinating Electric Vehicle Parking Lots and Home Energy Management Systems," *2020 IEEE International Conference on Environment and Electrical Engineering and 2020 IEEE Industrial and Commercial Power Systems Europe (EEEIC / I&CPS Europe)*, 2020, pp. 1-6.
Published: https://doi.org/10.1109/EEEIC/ICPSEurope49358.2020.9160594

A. B. Bahgat, **M. Lotfi**, O. M. Shehata, E. I. Morgan and J. P. S. Catalao, "Multi - Agent Task Allocation to Minimize Costs of Energy Consumption in the Presence of a Price-Based Demand Response Program," *IECON 2019 - 45th Annual Conference of the IEEE Industrial Electronics Society*, 2019, pp. 4151-4156.
Published: https://doi.org/10.1109/IECON.2019.8926713

H. M. D. Espassandim, **M. Lotfi**, G. J. Osório, M. Shafie-khah, O. M. Shehata and J. P. S. Catalão, "Optimal Operation of Electric Vehicle Parking Lots with Rooftop Photovoltaics," *2019 IEEE International Conference on Vehicular Electronics and Safety (ICVES)*, 2019, pp. 1-5.
Published: https://doi.org/10.1109/ICVES.2019.8906320

M. S. Javadi, **M. Lotfi**, M. Gough, A. E. Nezhad, S. F. Santos and J. P. S. Catalão, "Optimal Spinning Reserve Allocation in Presence of Electrical Storage and Renewable Energy Sources," *2019 IEEE International Conference on Environment and Electrical Engineering and 2019 IEEE Industrial and Commercial Power Systems Europe (EEEIC / I&CPS Europe)*, 2019, pp. 1-6.
Published: https://doi.org/10.1109/EEEIC.2019.8783696

Contents

List of Figures

List of Tables

Part I

The Rise of the "Demand" Side: History, Present, and Future

Chapter 1

Evolution of Demand Side Management and Demand Response

In the past two decades, interest in Demand Response (DR) schemes has grown exponentially. The need for DR has been driven both by sustainability (environmental and socioeconomic) and cost efficiency. The main premise of DR is to influence the timing and magnitude of consumption to match energy supply by sharing the benefits with consumers, ultimately aiming to optimize generation cost. As such, the first and primary enabler to DR was the establishment of contemporary electricity markets. Increased proliferation of Distributed Energy Resources (DER) and micro generation further motivated the participation of consumers as active players in the market. This immensely popularized DR and the wider category of Demand-Side Management (DSM) programs. Smart Grids (SG) have been an enabler to modern DR schemes, with smart metering data providing input to the underlying optimization and forecasting tools. The more recent emergence of the Internet of Energy (IoE), seen as the evolution of SG, is driven by increased Internet of Things (IoT)-enabling and high penetration of scalable and distributed energy resources. In this IoE paradigm being a fully decentralized network of energy prosumers, DR will continue to be a vital aspect of the grid in future Transactive Energy (TE) schemes, aiming for a more user-centered, energy-efficient, cost-saving, energy management approach. This chapter investigates original motives and identifies the first mentions of DR in the legislative and scientific literature. Afterwards, the evolution of DR is tracked over the past four decades, attempting to study the co-influence of legislation and research by performing a thorough statistical analysis of research trends on the IEEE Xplore digital library. Finally, the current state of DR programs is presented and future prospects are discussed.

Chapter Highlights and Novel Contributions:

- Origins of DR and DSM and initial motives for their inception are identified and regional differences investigated (namely: USA, UK, and EU, as pioneers of DR and DSM development).
- The historical evolution of DR and DSM is analyzed using a novel scientometric approach of both legislative and scientific research literature from the past four decades.
- A co-influence between legislation and academic research trends on DR is identified and a timeline of its evolution identifying important milestones is presented.
- With the history and status-quo of DR investigated, the emergence of the IoE as a future paradigm is identified, being a fully decentralized network of energy prosumers.

Relevant Publication(s):

M. Lotfi, C. Monteiro, M. Shafie-khah, J.P.S. Catalão, "Evolution of Demand Response: A Historical Analysis of Legislation and Research Trends," *2018 Twentieth International Middle East Power Systems Conference (MEPCON)*, 2018, pp. 968-973.
Published: https://doi.org/10.1109/MEPCON.2018.8635264

M. Lotfi, J.P.S. Catalão, M.S. Javadi, A.E. Nezhad and M. Shafie-khah, "Demand Response Program Implementation for Day-Ahead Power System Operation," *2019 IEEE Milan PowerTech*, 2019, pp. 1-6.
Published: https://doi.org/10.1109/PTC.2019.8810850

Chapter Nomenclature

Abbreviation	Definition
CPP	Critical Peak Pricing
DER	Distributed Energy Resources
DG	Distributed Generation
DR	Demand Response
DSM	Demand Side Management
EDP	Extreme Day Pricing
EEA	European Economic Area
EU	European Union
FiT	Feed in Tariff
I4.0	Fourth Industrial Revolution
IBP	Incentive Based Programs
IoE	Internet of Energy
IoT	Internet of Things
LF	Load Factor
PBP	Price Based Programs
RES	Renewable Energy Resources
RTP	Real Time Pricing
SG	Smart Grid
SM	Smart Meter
TE	Transactive Energy
ToU	Time of Use
UK	United Kingdom
USA	United States of America

1.1 Introduction

1.1.1 The Problem with Conventional Power Systems

Conventional electric power systems were designed with over-dimensioned generation capacity to provide for peak load. Presently, around 20% of generation capacity is used exclusively for peak demand periods, accounting for 5% of the year [5]. By analyzing wholesale price duration curves such as in [6], one can calculate that those 5% of annual demand (18 days) exhibit hourly electricity prices reaching more than six times the average price. Another calculation indicates that one in every ten Euros of the average annual electricity wholesale price is due to costs associated with peak demand periods.

Peak demand price spikes are due to the economics of energy generation and supply. Baseload power plants are generally ones with high capital investment and low running costs (e.g. steam, nuclear, and hydroelectric). Peaking power plants generally have lower capital investment and high running costs, with fast start-up being a necessity to respond to sudden demand peaks (e.g. gas and diesel generators) [7]. On a year-average, baseload power plants operate at an 85% load factor (LF), with the overall LF of generation capacity being 55% [8]. Power plants at lower LF operate less efficiently which results in higher cost per unit of generated electricity. Consequently, in peak demand periods caused by sudden imbalance of supply and demand (e.g. unforeseen rise in demand, unforeseen fall in supply, or transmission failure), price spikes in a spot market occur as generators have an opportunity to compensate losses in off-peak periods [9, 10]. Furthermore, thermal peaking plants operating at low annual LFs increases their CO_2 and greenhouse gas emissions [11, 12] and thus current power systems also have an environmental problem aside from being economically inefficient with most generation capacity being redundant.

While large-scale renewable energy sources (RES) are increasingly used as an economic low-emission alternative for both baseload and peak generation (mainly solar and wind) [7], their intermittent, non-dispatchable, stochastic, and geographically-constrained nature does not make them a reliable solution [13]. Meanwhile, although they result in a direct reduction of emissions, RES do not contribute to power system inertia (although synthetic inertia may be used with wind farms, it does not equal that of traditional generation [14, 15]), and thus create a need to maintain spinning and non-spinning reserves which indirectly, once again, increase the cost and emissions of the power system [16]. Therefore, the problem can be summarized in the following points:

- Generation capacity is planned according to peak demand which constitutes only 5% of the year.
- 20% of total installed generation capacity is only used during peak demand periods.
- The average annual LF of total installed generation capacity is 55%.
- A lower LF results in lower efficiency, which results in higher cost and emissions per unit of generated electricity.
- RESs decrease emissions but are volatile, geographically constrained, and unreliable.
- RESs decrease inertia, and it is necessary to still maintain reserves.

1.1.2 Demand Response as a Solution

During the 1990s, proliferation of distributed energy resources (DER) and distributed generation (DG) has made electricity consumers increasingly active participants in power generation. This, occurring simultaneously with the electricity market liberalization movement globally, has ignited a shift from the supply to the demand side, viewing electricity consumers as active participants in the industry. As such, interest in demand-side management (DSM) has grown exponentially. With the subsequent rise of Smart Grids (SG) and advanced communication infrastructures, DSM approaches have become more sophisticated and capable of dramatically enhancing power system efficiency. There are three main categories of DSM: 1) On-Site Backup and Storage, 2) Energy Efficiency and Conservation, and 3) Demand Response (DR) as can be seen in Fig. 1.1 and Fig. 1.2. Some studies seem to use both terms interchangeably and the source of this confusion is caused by the early development stages of DSM and DR. This historical confusion leads to some authors interchangeably using DSM and DR and is elaborated further in Section 1.3. However, the current official definitions both in academic literature and in legislation are that DR is a subset of DSM [17, 18, 19].

DSM approaches deal with the broader perspective of managing and decreasing energy consumption from the consumer-side. On-site backup provides capacity for demand-side generation and storage to participate in load-balancing or ancillary services. When DSM and DR are confused as previously highlighted, it is rather energy efficiency and conservation that is confused with DR. Fig. 1.1 highlights the difference between both approaches. While efficiency and conservation measures aim at reduction of overall electricity demand (baseline and peak alike), DR is concerned with specifically reducing peak demand, shifting load to off-peak periods and smoothing out the demand curve. This, as explained earlier, contributes to economic and environmental benefits and more reliable grid operation.

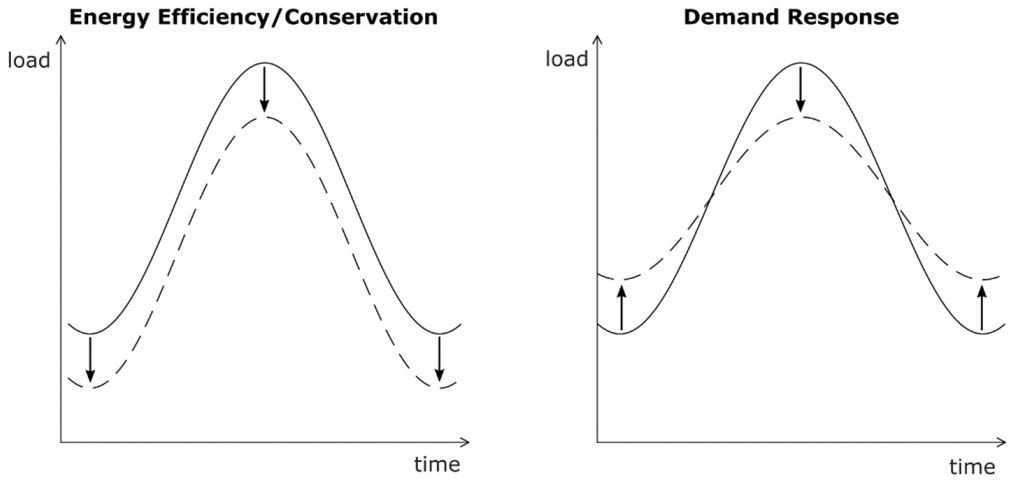

Figure 1.1: Comparing two of the DSM Approaches: Energy Efficiency and Conservation (left) vs. Demand Response (right).

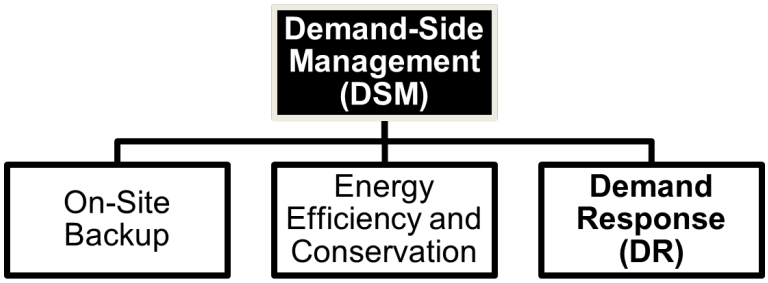

Figure 1.2: Relationship between DSM and its subsets: On-Site Backup (and Storage), Energy Efficiency and Conservation, and DR.

1.2 Origins of Demand Response

For most of its history, the electric power industry was a monopoly, with electricity companies being largely state owned and vertically integrated (performing generation, transmission, and distribution). This is because economies of scale have historically been the main driver of the industry, and it was widely perceived that one large utility would be more efficient in delivering electricity demands rather than several competing smaller ones [20, 21].

During the 1970's technological advance caused generation economies of scale at the unit level to be exhausted at 500 MW [22], thereby dismantling the long-held natural monopolistic perception of energy generation [23]. Moreover, the 1960's and 1970's witnessed the beginning of global environmental awareness.

This subsequently manifested in enaction of government environmental policies, best characterized by the US Clean Air Act of 1970 [24] and the first European Action Program in 1973 [25], which both sought to restrict pollutants and greenhouse gas emissions. Meanwhile, the 1973 oil crisis raised concerns on security of electricity supply and the need to diversify the power generation mix, which was largely dependent on fossil fuels, to incorporate renewable and clean energy sources [26, 27].

This triad of events in the 1970's (economic viability of small generation units, environmental awareness of greenhouse gas emissions, and concerns on security of supply largely dependent on fossil fuels) sparked a global wave of electricity market reform bent on socio-economic and environmental sustainability of electrical power systems through two simultaneous motions: 1) deregulation, unbundling, and liberalization of the electricity industry, and 2) incorporation of clean and renewable energy sources into the energy mix. The atmosphere created by the combined effect of competing electric utilities and proliferation of small renewable generation made it necessary to start considering the demand side as active participants in the electricity industry rather than passive users. It was during this period that the evolution of DSM (and subsequently DR) as an effective policy began.

Two main historic drivers of DSM and DR were identified: 1) Markets and Legislation and 2) Scientific Research; and the progress of DR was tracked in both through the past four decades to highlight its evolution from its origins to the current state.

1.3 Historical Evolution of Demand Response

1.3.1 Markets and Legislation

After the investigation of DR origins in the previous Section, it was possible to name three major players: USA, UK, and the EU to focus on; as they were the first to incentivize and implement DSM programs in general and DR programs in particular; and continue to be top influencers of global energy markets and policies. By surveying the full body of legislative and statutory publications of the USA, UK, and EU pertaining to energy and electricity, it was possible to propose a general classification of five stages in the development of DR programs in legislation:

- **Step 1:** Market deregulation/liberalization;
- **Step 2:** Incentivization of RES and DG/DER (While not yet fully established at this stage, fully developed DER services incorporate DG, Distributed Storage (DS), and DR services.);
- **Step 3:** Implementation of DSM programs for energy efficiency and decreased emissions;
- **Step 4:** Use of Smart Meters (SM) and emergence of DR capability as an additional DSM tool;
- **Step 5:** DR programs in Smart Grids (SG).

The following Sections present all energy and electricity-related legislation for the USA, UK, and EU, identifying the legislations corresponding to the above five stages.

United States of America (USA)

The USA has been the pioneer in electricity market deregulation and liberalization. It is often mentioned in literature that the first case of market liberalization happened in Chile by the Chile Electricity Act of 1982 [6, 28]. However, that was found to be preceded by the Public Utility Regulatory Policies Act [29] in the USA in 1978; which is the first case of legislation found allowing non-utility generators to participate in an electric power market. While this opened the door to a quasi-deregulated/liberalized US electricity market, it wasn't until 1992 [30] that it was fully so on the federal level.

It is important to mention that in the USA there is a distinction between federal law and state law, so while this directs federal activities and strategies individual states have a good degree of independence as to the degree of regulation they have on local electricity markets. This was particularly evident after the California crisis in 2001, when many states chose to reverse or slow down their motion towards deregulation at the time [21].

The first mention of DR in legislation was also found in USA Energy Policy Act of 2005 [31]:

"install time-based meters and communications devices for each of their customers which enable such customers to participate in time-based pricing rate schedules and other demand response programs.",

which coincides with the first mention of DSM (i.e., DR was the first DSM measure mentioned by USA legislation). All legislations including subsequent ones which direct the development of USA's DR national action plan, in addition to rollout of SM and SG are detailed in Table 1.1 [24, 29, 30, 31, 32, 33].

Table 1.1: List of USA legislations pertaining to development of DSM and DR.

Year	Legislation Title	Description
1978	**Public Utility Regulatory Policies Act [29]**	- Allowed "non-utility generators" to participate in energy supply - Created an electric power market with "non-utility generators"
1992	**Energy Policy Act of 1992 [30]**	- Energy deregulation / allowing private competition in the wholesale market - Incentivize renewable energy production
2005	**Energy Policy Act of 2005 [31]**	- Incentivize installation of Smart Meters (first mention of SM) - Incentivize participation in demand response programs, and request a study of the potential benefits of DR (first mention of DR) - Incentivize renewable energy production via tax incentives
2007	**Energy Independence and Security Act of 2007 [32]**	- Directs developing DR programs to reduce peak loads and increase energy efficiency; requests a study on the use of DR to provide ancillary services - Directs the establishment of a SG infrastructure (first mention of SG), and provide funding for Smart Grid applications - Increase taxes on oil industries and promote renewable energy sources.
2009	**American Recovery and Reinvestment Act of 2009 [33]**	- Significantly increase funding and incentives for Smart Grid applications.

United Kingdom (UK)

The UK swiftly followed the US in implementing market liberalization policies in 1989 [34]. In 2006, "dynamic demand technologies" were first mentioned [35]:

"contribution ... being made by dynamic demand technologies to reducing emissions of greenhouse gases in Great Britain."

While this corresponds to DR by current definitions, the objective was in fact to implement DSM with an environmental focus rather than an economic one (as was the case with USA). All relevant legislation for the UK was listed and cited in detail in Table 1.2 [34, 35, 36, 37]. The first literal mention of DR only came much later, in 2011 [37].

Table 1.2: List of UK legislations pertaining to development of DSM and DR.

Year	Legislation Title	Description
1989	**Electricity Act 1989 [34]**	- Liberalization of electric power generation in the UK - Promotion of microgeneration / renewable sources
2006	**Climate Change and Sustainable Energy Act 2006 [35]**	- The capacity of "dynamic demand technologies" to reduce greenhouse gas emissions is requested to be reported, and is defined (first mention of DR)
2008	**Energy Act 2008 [36]**	- Licensing Smart Meters (first mention of SM) - Licensing Feed-in-Tariffs (FiT) for small-scale generation
2011	**Energy Act 2011 [37]**	- Requested an assessment of, and defining, "demand side response" (first literal mention of DR)

European Union (EU)

The EU was the last of the three to liberalize electricity markets, doing so in 1996 [38]. At the same time, it was the first to mention DSM programs in 2003 [39]:

"'energy efficiency/demand-side management' means a global or integrated approach aimed at influencing the amount and timing of electricity consumption in order to reduce primary energy consumption and peak loads by giving precedence to investments in energy efficiency measures, or other measures"

When first introduced by legislation, DSM in the EU was confined to (the term even used interchangeably with) energy efficiency and conservation (Fig. 1.2). Same as the UK (part of EU at the time despite not being in Eurozone or EEA), the focus of EU was directed towards environmental sustainability and security of supply, opposed to more economic and profit-driven motives of the USA. An important observation to note is that all three (USA, UK, and the EU) shared security of supply as a common motive when first enacting DSM / DR measures in legislation.

This is more evident by realizing that despite being the first to mention DSM in legislation, EU was the last to mention DR in 2012, as shown in Table 1.3 [38, 40, 39, 41, 42] and visualized later in Fig. 1.5.

Table 1.3: List of EU legislations pertaining to development of DSM and DR.

Year	Legislation Title	Description
1996	**Directive 96/92/EC [38]**	- Liberalization and unbundling of electric utilities - Establishing the European internal electricity market
2001	**Directive 2001/77/EC [40]**	- Targets for renewable energy generation
2003	**Directive 2003/54/EC [39]**	- Expanded liberalization and unbundling of the electricity market - Directs the use of Demand-Side Management (first mention of DSM)
2009	**Directive 2009/28/EC [41]**	- Set EU 2020 strategy with 20% target for renewable energy generation, emissions reduction, and consumption reduction - Set 80% target for consumers with SM by 2020 (first mention of SM) - Suggests the use of FiT to promote small-scale renewable generation
2012	**Directive 2012/27/EU [42]**	- Directs use of DR (first mention of DR) - Deployment of SG (first mention of SG)

1.3.2 Scientific Research

To study the scientific research trends during the same time period, a Python web-crawler was developed and was used to track the exact volume of literature pertaining to keywords/technologies identified as directly influential to development of DR on the IEEE Xplore digital library.

Fig. 1.3 shows that scientific research on DG was first published in 1990, during the wave of electricity market liberalization and after DSM has been studied in literature since 1985. DER first appeared in literature in 2000, after market liberalization. This is probably due to motivations to micro-generate and store energy amidst liberal markets.

Sparked first by the EU Directive 2001/77/EC [40] and then by the UK Climate Change & Sustainability Act [35], research on MG began in 2001 and started increasing in 2005, respectively. The enactment of EU Directive 2009/28/EU [41] (promoting small-scale generation), as expected, tended to mark an exponential growth in research on both MG and DER.

Fig. 1.4 shows that although DR scientific research began in 1989, while that on SG was first published more than a decade later, the two only started to attain a significant volume and increase together. This is expected, since DR programs are an essential component of modern SGs [43]. Being low voltage distribution grids capable of operating isolated from the main grid and acting as a controllable load, SG were an essential part of DSM development [44].

The series of legislations by the USA, UK, and EU as shown in the figure clearly ignited the growth of scientific research on both SG and DR. The figure also shows the volume of correlated research (DR & SG), with 40% of all DR research currently being directly related to SG applications. This suggests that currently, DR is heavily influenced by SG technologies and grid architectures.

Finally, the legislation and scientific research trends were combined in a complete timeline for the historical emergence and evolution of DR, incorporating all milestones from previous analyses (Fig. 1.5). The timeline provides a clearer visualization of the reasoning given in the previous section about USA being more economically-driven while the EU being more environmentally driven, shown by the emergence of DR much later in the EU, in-line with the expectation of [45].

Here, it is necessary to specify some limitations posed by the automated method that was utilized to track the historical research trends, and clarify resulting ambiguities:

- The first captured publication with the IEEE keyword of "Smart grids" was from 1997 [46]. Here, the label of "Smart grids" is misleading, as the first paper on SG as intended was actually published in 2004, titled "Transforming the U.S. electricity system" [47]. This is captured in Fig. 1.4 and Fig. 1.5 with the discontinuity of research between 1997 and 2004 clearly visible.

- Conversely, while the first captured publication with the IEEE keyword of "Distributed generation" was from 1990, scientific research on DG technologies was available before 1990 (and even before 1985), albeit under the name “dispersed generation” [48, 49, 50].

While it is important to duly clarify these two anomalies, they do not affect the performed analysis and the relevant observations made.

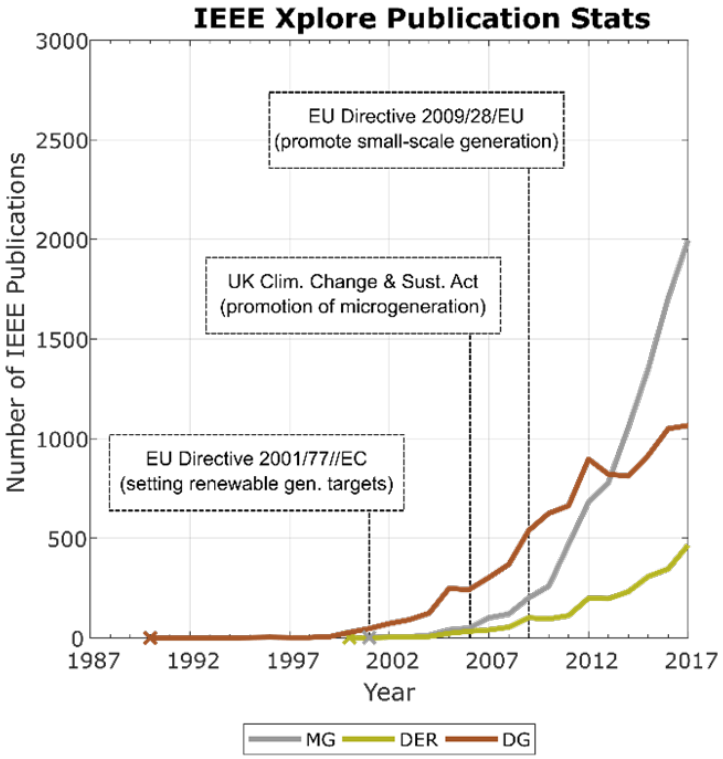

Figure 1.3: Research trends on IEEE Xplore for MG, DER, and DG.

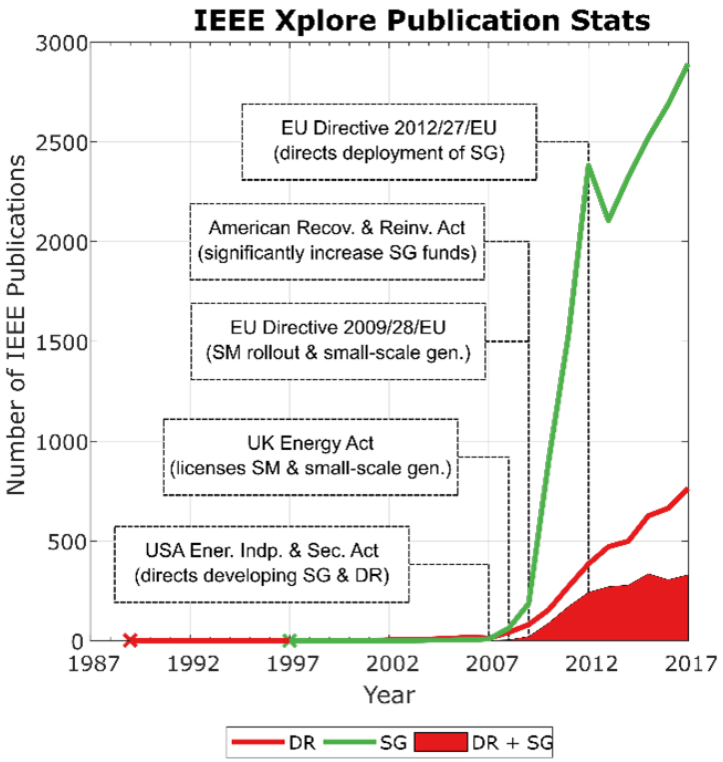

Figure 1.4: Research trends on IEEE Xplore for DR, SG, and DR correlated with SG (DR + SG).

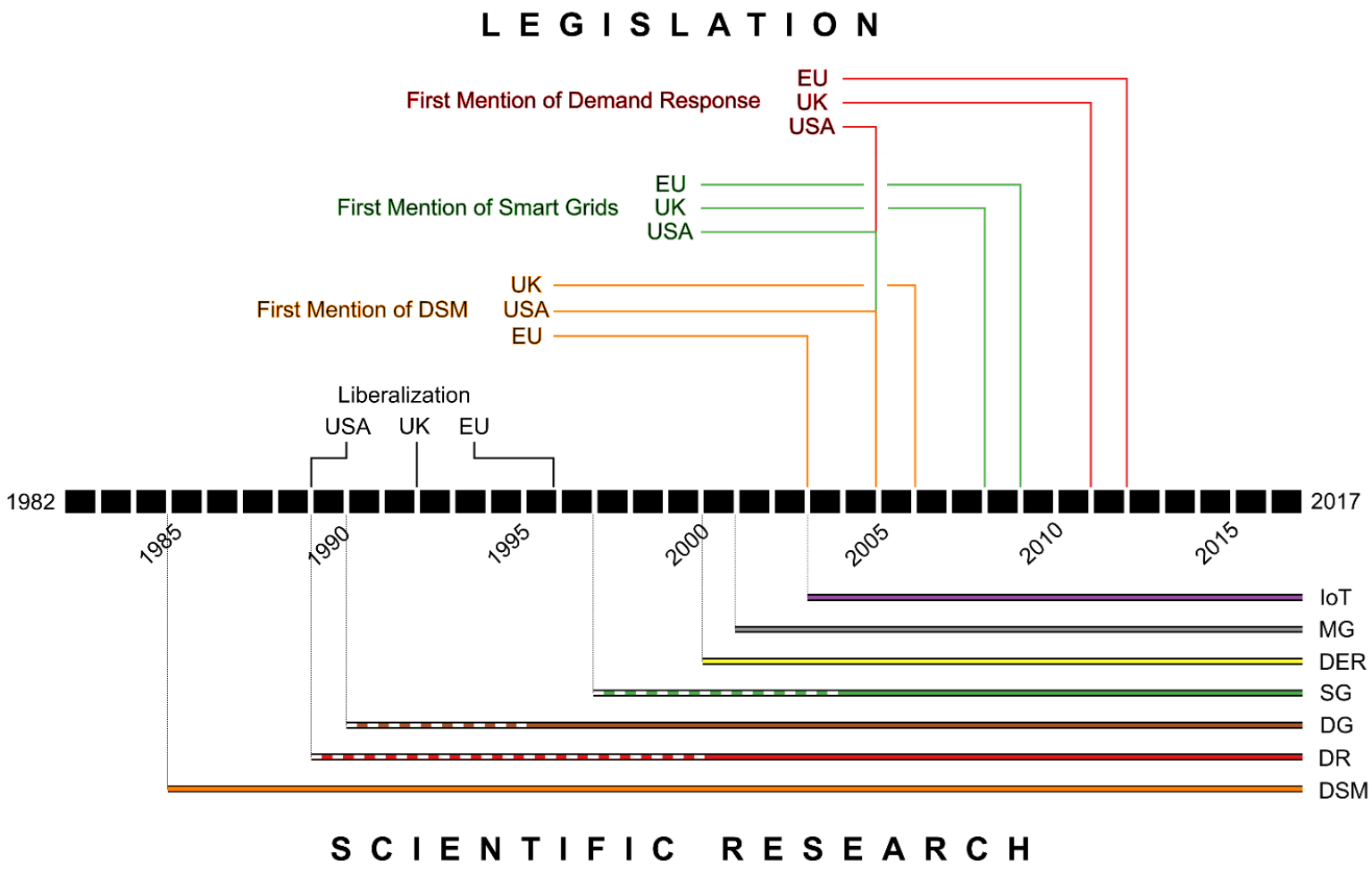

Figure 1.5: Timeline showing all important legislative milestones (top) and tracking scientific research on IEEE Xplore (bottom) for each topic/technology of relevance to DR and DSM development (dashed lines mean discontinuous research i.e., <1/year)

1.4 Status-Quo of Demand Response and Future Prospects

As demonstrated, DR programs became an indispensable component of modern SGs. DR adoption provides effective means of minimizing operating costs, enhancing reliability, and mitigating risk in SGs. Today, numerous DR schemes exist, however the core concept remains unchanged: contradict traditional strategies of increasing supply to match required demand by making users adapt or change their electricity usage, shifting loads from peak to off-peak periods. Contemporary DR programs all fall into two main categories [51, 13, 52]:

1. **Mandatory DR** - Incentive-Based Programs (IBP) (also known as system-led, emergency-based, or direct DR).
2. **Voluntary DR** - Price-Based Programs (PBP) (also known as market-led, economic- based, or indirect DR).

Mandatory DR (IBPs) involves contracting users to give a central operator the authority to "schedule, reduce, or disconnect" their loads. Voluntary DR (PBPs) on the other hand lets users reschedule their own usage motivated by fluctuating market prices, which would ideally be cheaper during off-peak hours. In this way, consumers are stimulated to modify their consumption behavior in a way that is more favorable for system operation as they "share" the economic benefits by following the price signals [13]. Many PBPs exist, including but not limited to Time of Use (ToU) tariffs, Peak Shaving, Critical Peak Pricing (CPP), Extreme Day Pricing (EDP), and Real-Time Pricing (RTP), each designed for a specific purpose. The ToU scheme is the most straightforward while RTP is the most sophisticated. In ToU, tariffs are defined for preset peak and off-peak periods. In RTP schemes, customers pay hourly varying tariffs reflecting the real conditions of the power market. In this respect, the day-ahead or hourly-ahead prices are given to those customers participating in the RTP. Such a mechanism can be effectively implemented in liberalized electricity markets [43].

With residential users constituting up to 40% of global energy demand and being the significant contributors to peak demand periods and irregularities, DR scheme designers have the traditionally specifically targeted residential usage across different economies [53]. For this, Voluntary DR (PBPs) is more common since they are more compatible with and accepted by residential users [45]. Despite being more sophisticated to implement, PBPs can substantially impact the load profile favorably, especially with respect to hours of peak demand and price fluctuations over different hours of the day. PBPs are capable of effectively influencing consumers to adapt their consumption behavior to better match electricity supply conditions, and thereby mitigate such effects [51].

Historically, Mandatory DR (IBPs) has been more popular in the other dominant energy demand sectors (i.e., transport and industry). However, only recently have researchers paid more attention to developing PBPs for these sectors, due to the current paradigm shift in the context of the fourth industrial revolution (I4.0) and resulting intertwining of the different sectors [54, 55, 56].

Increased IoT-enabling of SG and high penetration of scalable and distributed energy resources in recent years is resulting in the emergence of the Internet of Energy (IoE) [57]. In this IoE paradigm being a fully decentralized network of energy prosumers, DR will continue to be a vital aspect of the grid in future Transactive Energy (TE) schemes [58], which aim for more user-centered, energy-efficient, cost-saving, energy management approaches [59, 54].

Concurrently, the I4.0 paradigm shift is resulting in increased intertwining between sectors that are the major consumers of energy (residential, transport, and industry). In addition, with the electrification of transport being a top priority and smart industries emerging as vital pillars of modern economies, the adaptation of DSM and DR schemes for cross-sector applications becomes of paramount importance. More physically decentralized and interconnected energy systems motivate the investigation of decentralized data models to manage them as opposed to centralized operators. Motivated by the financial sector decentralization caused by the rise of digital currencies and Blockchain as an enabling technology, there is an interest now in adapting this new management model which is compatible with the emerging IoE paradigm. This is investigated further in the next chapter.

1.5 Chapter Conclusions

In this chapter, a thorough historical analysis of DR as a vital DSM approach was presented, investigating the historical origins of DR along with the original motives for its inception. USA, UK, and EU were identified as the pioneers of DSM and DR. Afterwards, an extensive historical review of their legislations was performed, identifying all relevant legislation and milestones in the evolution of DR. Research trends on IEEE Xplore were analyzed to track relevant technologies, and a comparative analysis was performed between legislation and research trends. A clear co-influence between both was demonstrated, and regional differences were highlighted. The status of contemporary DR programs is discussed in detail. Finally, the emergence of the IoE being a fully decentralized network of energy prosumers was identified, aiming for more user-centered, energy-efficient, and cost-saving, energy management approaches. The IoE paradigm along with the increased intertwining between sectors that are now the major consumers of electrical energy (residential, transport, and industry) necessitates the adaptation of DSM and DR schemes for cross-sector applications in this emerging paradigm.

Chapter 2

Decentralization of Power Systems: The Internet-of-Energy Paradigm

It may be surprising to recall that Blockchain was largely unheard of merely a decade ago. Being first launched in 2008 in the advent of Bitcoin (the world's first digital crypto-currency), it is indeed astounding how the technology rapidly became a major enabler of all sorts of decentralized platforms, which are now ever so important in this digital era of extensive Internet-of-Things (IoT) enabling. In order to understand how Blockchain-based systems took center stage in modern electricity trading frameworks, it is necessary to look back at the sequence of events which resulted in the need for Blockchain, its creation, success as the first fully decentralized commercial platform, and subsequent expansion to the energy sector. In fact, Blockchain seems to have emerged at the most convenient timing for the energy sector, which in itself was transforming in favor of more decentralized structures and decision making. Therefore, Blockchain appeared as a reliable solution to several challenges facing the energy sector, and with perfect timing. That being said, this convenience is absolutely no coincidence. These simultaneous events happened, and continue to happen, in the context of a much larger revolution, the fourth industrial revolution.

Chapter Highlights and Novel Contributions:

- The fourth industrial revolution (I4.0) is introduced, and its design principles are listed.
- The Internet-of-Things (IoT) effect on the energy sector is studied in detail, and the emergence of the Internet-of-Energy (IoE) with IoT-enabling of Smart Grids (SGs) is established.
- The design requirements for all technical models and processes developed for the IoE paradigm are defined.
- Fully decentralized economies based on Blockchain technology are investigated, and the adoption of Blockchain by the energy sector is discussed in detail.
- The decentralization of the energy sector in different dimensions (decentralization of generation, information, and markets) is elaborated.
- The paradigm shift towards peer-to-peer energy trading, along with next-generation IoE systems is discussed.

Relevant Publication(s):

M. Lotfi, C. Monteiro, M. Shafie-khah, J.P.S. Catalão, Chapter 3 - "Transition toward blockchain-based electricity trading markets", in: *Blockchain-based Smart Grids*, Academic Press, 2020, Pages 43-59, ISBN 9780128178621.
Published: https://doi.org/10.1016/B978-0-12-817862-1.00003-8

M. Lotfi, J.P.S. Catalão, H.A. Gabbar, "The Rise of Energy Prosumers and Energy Democracy: History and Future Prospects", *IEEE Smart Grid Newsletter*, July, 2020.
Published: https://smartgrid.ieee.org/newsletters/july-2020/the-rise-of-energy-prosumers-and-energy-democracy-history-and-future-prospects

Chapter Nomenclature

Abbreviation	Definition
ADMM	Alternating Direction Method of Multipliers
CPS	Cyber Physical Systems
DSM	Demand Side Management
DER	Distributed Energy Resources
I4.0	Fourth Industrial Revolution
GDPR	General Data Protection Regulation
dena	German Energy Agency
IoE	Internet of Energy
IoT	Internet of Things
E-LAN	Local Area Energy Networks
OPF	Optimal Power Flow
P2P	Peer to Peer
PV	Photovoltaic
PwC	PricewaterhouseCoopers

2.1 Introduction

2.1.1 The Fourth Industrial Revolution

Previous industrial revolutions all had one thing in common: each of them was triggered by a uniquely identifiable technological breakthrough. Steam engines fueled mechanization in the first, electricity sparked mass production in the second, and electronics and computers made automation possible in the third. The fourth industrial revolution currently underway is prominently different from its predecessors for two main reasons.

First, it was not triggered by a single breakthrough; rather it is the result of a combination of simultaneous technological and scientific advances. By increasingly overlapping digital, physical, and biological systems (Fig. 2.1), it is giving rise to cyber-physical systems (CPS) [60]. These fourth generation industry systems (I4.0) are designed based on the following principles [61]:

- decentralized decisions;
- information transparency (data analytics and information provision);
- interoperability and interconnection; and
- technical assistance (e.g., virtual assistance)

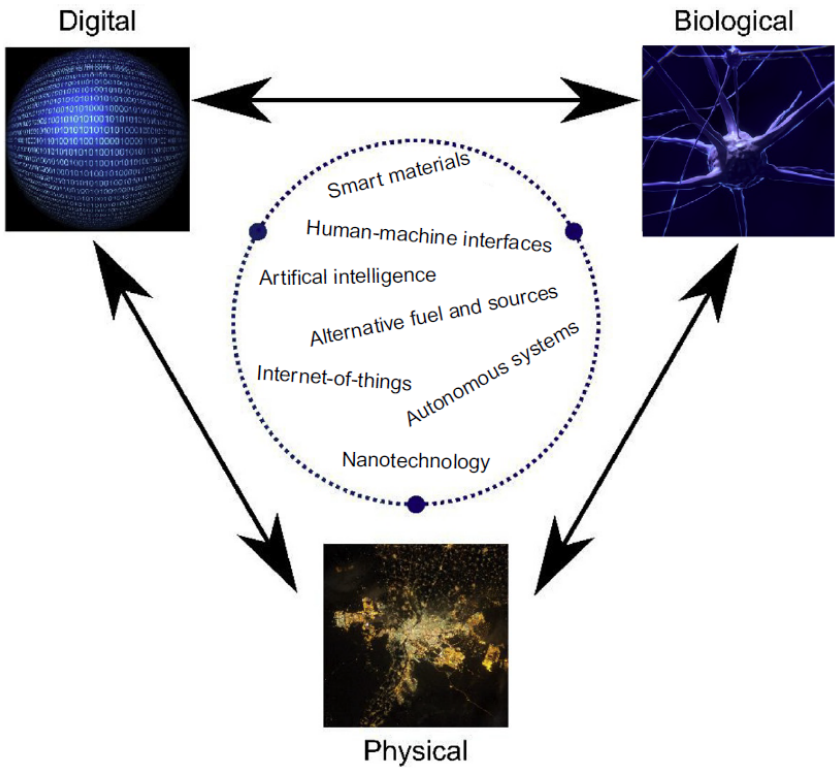

Figure 2.1: The fourth industrial revolution: a synergy of simultaneous technological breakthroughs contributing to the rise of CPS by overlapping digital, physical, and biological systems.

The second difference between the fourth industrial revolution and its predecessors is the rate at which technological advance has been occurring. With an exponential rate rather than a linear one, it continues to be disruptive to almost all industries globally. This often left decision and policy makers significantly lagging behind, often being caught in "traditional, linear (and non-disruptive) thinking" [62, 63]. As such, the transfer of novel innovative solutions between different sectors which are facing similar emerging challenges is often delayed. The adoption of Blockchain by the energy sector is a perfect example of this. Having first appearing as an enabling technology for decentralized commercial systems, it took time to attract the attention of the energy sector which at the time was struggling to find a solution to manage increasing decentralization caused by proliferation of micro-generation and the rise of small-scale prosumers. This section presents the concurrent events which lead to Blockchain now being a key enabler of peer-to-peer energy trading and show the exact series of milestones leading to the current status.

2.1.2 An Interconnected World: The Rise of the Internet-of-Things

In its earliest days, the Internet was originally developed to connect and transfer data between computers. With the advent of smartphones (technically small computers), the Internet became a network which also provided nonstop connectivity between people. As electronics and IT evolved, "things" which are not by nature computing or communication devices started being connected to the Internet. The term "Internet of Things" started circulating around 2003 but was first officially used in 2005, when the International Telecommunication Union published a report titled "Internet of Things," describing the rise of IoT as follows [64]:

"developments are rapidly under way to take this phenomenon an important step further... enabling new forms of ***communication between people and things, and between things themselves****. A new dimension has been added...:* ***from anytime, any place connectivity for anyone, we will now have connectivity for anything****"*

This changed everything. The emergence of IoT propelled global interconnectedness to an unprecedented level, opening the door for previously inconceivable possibilities for technological, social, and economic advancement. The IoT has been one of the main technologies driving the fourth industrial revolution.

Table 2.1: Number of IoT-connected devices (conventional and "things") and a summary of predicted changes from 2016 to 2021.

Type of device	IoT connected in 2016 (billion)	IoT connected in 2021 (billion)	Percentage change
All	17.6	28 (Ericsson) [67] 30.7 (IHS) [68]	+60% <-> +75%
Conventional (computers, smartphones, etc.)	11.2	7.2 (Ericsson/ Gartner) 2.6 (IHS/IDC)	-35% <-> -75%
"Things" (appliances, sensors, etc.)	6.4	20.8 (Gartner) [66] 28.1 (IDC) [69]	+225% <-> +340%

More than a decade later, IoT continues to grow at an exponentially increasing rate. In 2016, there was a total of around 17.6 billion devices connected to the Internet of which 11.2 (64%) are conventional devices such as smartphones and laptops while 6.4 (36%) are other devices, "things," such as appliances, meters, etc. [65]. In a press statement, Gartner stated its prediction of the latter figure (nonconventional devices/things) growing to 20.8 billion by 2020 [66]. IDC published a market forecast which put this number at 28.1 billion. Ericsson and IHS have both published reports forecasting the total number of Internet connected devices (conventional and things) at 28 and 30.7, respectively [67, 68]. By analyzing those numbers (Table 2.1), one can see that the number of new "things" to be IoT connected was set increase dramatically by 225% (by most conservative forecasts), compared to a mere 60% growth in the overall number of IoT-connected devices.

This rapid uncontrollable growth of IoT is unleashing unprecedented data traffic on the Internet, creating two main problems: data redundancy and data security/privacy. In an IoT stakeholders survey [70], 41% of respondents said "timely collection and analysis of data" was a major challenge since there was "too much data to analyze effectively," "difficult to capture useful data," and "data is analyzed too slowly to be actionable." Those responses precisely describe the data redundancy problem in modern IoT-enabled systems.

A major solution effort to data redundancy was the development cloud computing. IoT refers to the connection of devices to the Internet and cloud computing refers to how those devices work together to deliver data, applications, or services [71]. IBM defines cloud computing as the "delivery of on-demand computing resources ... over the Internet on a pay-for-use basis" [72]. Another effort to tackle the data redundancy problem has been the development of more advanced and efficient distributed data analysis algorithms.

In fact, it is interesting to see that according to all forecasts the number of conventional devices is expected to decrease, despite the enormous overall IoT growth. This can be attributed to the fact that with the increased use of things like smart sensors or smart actuators, the need for many computers currently used solely to provide the Internet link for such devices will cease to exist. In addition, the emergence of cloud computing and more advanced data analytics will facilitate shared processing and storage resources, reducing the required number of dispensable computing and storage devices.

As for the second (security/privacy) problem, it is hardly possible to come across any IoT-related discussion without the mention of the topic. With everything from personal appliances to industrial machinery being connected to an extended global network, the potential damage of cyberattacks and unsolicited disclosure could be devastating. It is therefore not surprising that another report by Gartner [73] predicted that IoT security spending growth is set to overtake overall IoT spending growth by 2017, which was an impressively accurate prediction. In the survey of IoT stakeholders mentioned earlier, the top challenge in IoT projects reported by 58% of respondents was "Business processes or policies" in which they complained that privacy concerns over confidential data posed a major issue preventing data collection [70]. The approval of the European Union's General Data Protection Regulation (GDPR) in 2016 [74] and other similar legislation worldwide made data security and privacy not only a concern, but also a legally binding obligation for all sectors affected by IoT enabling.

Those sectors were therefore expected to explore and implement novel solutions to address data redundancy and security issues. While the issue of data redundancy was quickly handled early on, privacy and security issues remained a major concern. This was due to two reasons. One of the main reasons for this is the fact that the latter is not only dependent on the availability of feasible technical solutions, but also involves social, political, and economical debate.

The energy industry is and will continue to be one of the most affected by the growth of IoT. Of the 20.8 billion nonconventional devices expected to be online by 2020/2021, around 1.4 billion will be from the energy industry, and 1.5 billion from home energy management devices. This meant that 10% of all IoT endpoints will be energy or energy management devices. Therefore, the energy sector began to realize in that period that incorporating compatible and feasible solutions for both data redundancy and privacy problems will be a necessity for the design future energy system structures in an IoT-dominated world. This unstoppable IoT enabling of energy systems on all levels reinforced an increasingly popular vision in scientific literature: the Internet of Energy (IoE). This vision of IoE being the product of IoT enabling of smart grids (SGs) was first mentioned in a news article in 2010 [75]. The article envisioned scalable and self-sufficient energy networks through Internet enabling. Computational power required for coordination and management of energy supply and demand is provided by cloud resources. The other stated requirement was sufficient energy storage resources, which is becoming increasing efficient and affordable.

As such, scientific literature started showing great attention to this IoE paradigm [76, 77, 78, 79, 80, 81, 82] with multiple other associated variants such as Local Area Energy Networks (E-LAN) [83] and Smart Grids 2.0 [84].

The consensus in the all the aforementioned scientific literature was that **technical models and processes developed in an IoE paradigm should be:**

1. **distributed (fully decentralized),**
2. **efficient at data analysis (with efficient forecasting and optimization capabilities),**
3. **scalable**, and
4. **user-friendly (plug and play)**.

Those correspond exactly with I4.0 design requirements listed earlier, making this IoE framework a perfectly suitable as an I4.0 solution model.

2.1.3 Decentralized Economies: The Success of Blockchain

Following the 2008 global financial crisis, the world's first digital cryptocurrency (Bitcoin) was proposed [85]. The introduced platform allowed peer-to-peer (P2P) transactions to take place, eliminating the need for intermediary financial authorities, being the world's first fully decentralized commercial system of its kind. It was a tremendous success. In 2010, 1 Bitcoin was valued at 0.08 USD, and rose exponentially to reach a peak value of 17,000 USD in 2017, maintaining a market capital well above 100 Billion USD since then. This astonishingly rapid success is primarily attributed to the underlying technology: Blockchain, a cryptographically secured distributed database containing blocks of transactions.

The platform possesses two distinguishing characteristics allowing it to provide a decentralized system: security and global consensus. The latter is provided by the fact that everyone in the network is constantly validating and updating the state of the system collectively. Since each block in the chain is linked to the previous one, all users can verify if contents have not been modified. Keys are function of both the encrypted contents of the block and the previous block's key, thus involve a puzzle to be solved requiring computational effort. Keys are generated by miners: users providing the distributed computational effort and rewarded accordingly. The platform's decentralized nature makes it immune to many cyber attacks, even if a large number of users are targeted.

With the conception of Ethereum in 2012 and its launch in 2015, Blockchain 2.0 introduced smart contracts: digitally written and signed awaiting satisfaction of certain conditions to come into effect [86]. Ethereum's Blockchain 2.0 with its smart contracts was an equally massive success, amassing a market capital of over 1 Billion USD within less than a year of its launch, which exponentially grow to steadily remain above 10 Billion USD since 2017 (Fig. 2.2).

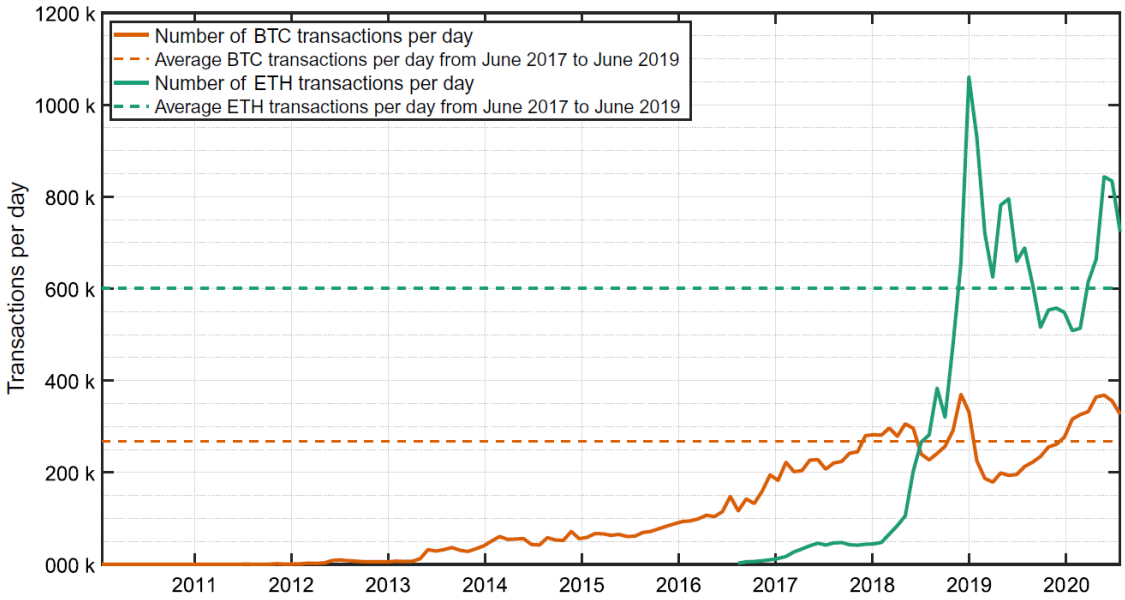

Figure 2.2: The phenomenal success of blockchain technology is shown by the number of daily transactions taking place on Bitcoin and Ethereum, currently the world's two largest cryptocurrencies.

With hundreds of billions of market capital, Blockchain-based trading platforms have clearly gained society's trust, which became impossible to miss. Official recognition of cryptocurrencies and their underlying technology was inevitable. In 2012, the European Central Bank first recognized digital currencies [87] and later in 2015 just before Ethereum was about to be launched, a follow-up report was released with an extensive analysis of the success of their decentralized platforms [88]. This consolidated the acknowledgement of Blockchain-based systems. During the past 2 years (between June 2017 and June 2019), there has been an average of more than 250,000 daily Bitcoin transactions, and more than 600,000 Ethereum daily transactions. Bitcoin and Ethereum continue to dominate as the two leading digital currencies with market capitals well above 10 and 100 Billion USD since 2017, respectively. However, there are numerous other Blockchain-based cryptocurrencies which have emerged, with hundreds of thousands of daily transactions.

The massive success and recognition of Blockchain with its smart contracts as a decentralized commercial system has led many people to investigate the application in different sectors, particularly those that are shifting most toward a decentralized structures. The secure cryptographic algorithm of Blockchain and its immunity to many cyberattacks is even more reason why it is currently seen as an enabling technology as it may potentially offer a solution to many data security/privacy problems caused by IoT enabling.

2.2 Enabling the Decentralization of the Energy Sector

Around the same time when Blockchain-based commercial platforms were rising and gaining global recognition, the energy sector was going through a massive transformation of its own. Motivated by a triad of causes (security of supply, environmental protection, and economic efficiency), legislation was being passed worldwide eagerly promoting demand-side management (DSM) strategies, specifically demand response (DR) programs. DR inherently relies on the availability of two main things: distributed energy resources (DERs) and SG infrastructure (with smart metering and communication devices). In 2012, the EU passed a directive to direct the rollout of SGs to implement DR programs (and multiple similar legislation was passed worldwide contemporarily) [89]. This ultimately meant that power and energy systems were about to rapidly witness two major transformations: physical decentralization due to DER installations and information decentralization due to smart metering and SG rollout. It is important to elaborate that **decentralization occurs at three different and distinguishable layers**:

- **Decentralization of power systems**: This is related to the physical disaggregation of power generation, for example, DERs.
- **Decentralization of information systems**: Due to interconnection of even the smallest devices as in the IoT paradigm.
- **Decentralization of energy markets**: Is the case with P2P trading of generated energy by prosumers.

An advantage of decentralized systems is their capacity to make better use of the local endogenous resources and reduce costs and losses of transporting these resources, consequently leading to more environmental sustainability. Economic sustainability depends on the scale factor; big centralized systems are more efficient with low unitary costs. Small decentralized systems are less efficient with high unitary costs. However, recent technological developments of decentralized systems are enabling them to be economically competitive with their centralized counterparts. The three levels of decentralization are interinfluential and complementary.

Between P2P energy trading and IoE there is a clear emergence of what is referred to as ***democratic energy systems*** *in which fundamental aspects are (1) significant citizen participation and (2) decentralized decision making in operation, management, planning, and trading, and (3) RES dominated generation.*

2.2.1 P2P Energy Markets: The Emerging Paradigm Shift

Conventional electrical power systems had unidirectional energy flow from generation to consumption. A centralized structure was best suited for this model with different utilities managing operation, planning, and energy market operations. Increased penetration of prosumers with DERs made electric power systems more decentralized and rendering the conventional model obsolete. First, energy was now being generated at both ends of the conventional chain and therefore roles of operators and utilities need to be redefined or the structure shuffled altogether. Second, DERs are increasingly incorporated into energy networks without being given any operational role or access to the wholesale market which is not sustainable [90].

In the beginning, feed-in-tariffs were offered with the intention of incentivizing small consumers to install small renewable energy generation (e.g., rooftop solar PV). Consumers generating electricity with renewable sources would be able to feed any surplus energy into the grid and are paid for it, albeit at a rate which is significantly lower than the electricity market price. This among other reasons started creating distrust between large utilities and system operators on one hand and DER owners on the other. With the decreasing price of renewable installations and the ease of acquiring them, small prosumers start looking for alternatives of trading electricity which can eliminate need for a middle man such as P2P trading.

After witnessing its capability to provide fully decentralized commercial trading platforms, it was clear that Blockchain offered the ideal solution for newly emerged prosumers and their desire for citizen-run democratic energy systems. Multiple successful tests of Blockchain-based P2P platforms started being carried out, albeit on small scales. Prior to the launch of Ethereum's Blockchain 2.0 and smart contracts in 2015, the role of Blockchain was limited to enabling a secure and reliable distributed ledger of transactions, and thereby the early experiment with Blockchain in P2P energy trading were strictly limited to its use to record financial transactions.

2012 was an important year in the transition to Blockchain-based applications in the energy sector. The EU directive for SG rollout was approved, incentivizing researchers and stakeholders to seek new innovative data models and manage these new smart interconnected microgrids with DERs [89]. The first academic article putting forth the concept of "transactive energy" was published in 2013, proposing a vision of decentralized and self-sustaining microgrids capable of autonomous transactive operation [91].

This sparked a new trend in academic research, attempting and designing solutions based on this transactive energy vision. It is important to recall that at the time of the first transactive energy publication (early 2013), only first generation Blockchain platforms have been in operation. Without smart contracts, and being limited only to financial transactions, the potential of Blockchain being a suitable enabler for such a system was extremely limited. Thus, in the early years of research on transactive energy, Blockchain was seldom mentioned.

With the proposal of Blockchain 2.0 in late 2012 and the launch of Ethereum in late 2015, successfully incorporating smart contracts, this second generation of Blockchain technology was suitable to provide for the needs of the energy sector. Smart contracts made energy trading possible in the way that was being envisioned by researchers on transactive energy networks. Therefore, a few months after the successful launch of Ethereum and the witness of its success, the first academic research papers proposing a validated methodology for Blockchain applications to energy systems and peer-to-peer electricity trading were made toward the end of 2015 and the beginning of 2016 (Fig. 2.3) [92, 93, 94].

2.2.2 Expansion of Blockchain Applications

Once the first proposals were presented for the application of Blockchain in the energy sector, its expansion became exponential. In 2016, recognition of Blockchain as an inevitable enabler of future energy grids and markets became obvious around the world. The major reports were published in 2016 by global consultancy firms and governmental agencies which investigated the status-quo of Blockchain applications at the time and predicated its great potential in the years to come.

PricewaterhouseCoopers (PwC) released a report [54] in highlighting the opportunities Blockchain offers for energy producers and consumers. The report started by stating that Blockchain's transaction model which shifts from centralized structures to P2P can reduce costs and speed up processes resulting in more flexible systems. The report highlights that while some level of maturity is being reached in the financial sector, the technology is still being developed for other applications with some barriers in the way, primarily conflict resolution and legal and regulatory requirements for fully decentralized systems. The Brooklyn Microgrid project was a successful experiment in which a microgrid consisting of a group of 10 households directly traded surplus solar energy generated using a Blockchain system. Smart meters were used in conjunction with Blockchain's smart contracts to keep track of energy produced and to automatically effect transactions, respectively. An energy token system was used for energy payments. Most start-ups working on Blockchain applications at the time were developing cryptocurrencies specific for energy trading.

The report emphasized the opportunity Blockchain offers for prosumers of electricity in a P2P system, by providing more flexible and autonomous systems. In addition, the report highlights that Blockchain could potentially be employed to a wide range of uses other than energy transactions, which include documentation of ownership (of energy generated), guarantees of origin, renewable energy certificates, and others. While Blockchain could radically transform the energy sector, the report stated that current legal and regulatory frameworks need to be adjusted to cope with large-scale decentralized transactions models to be made possible.

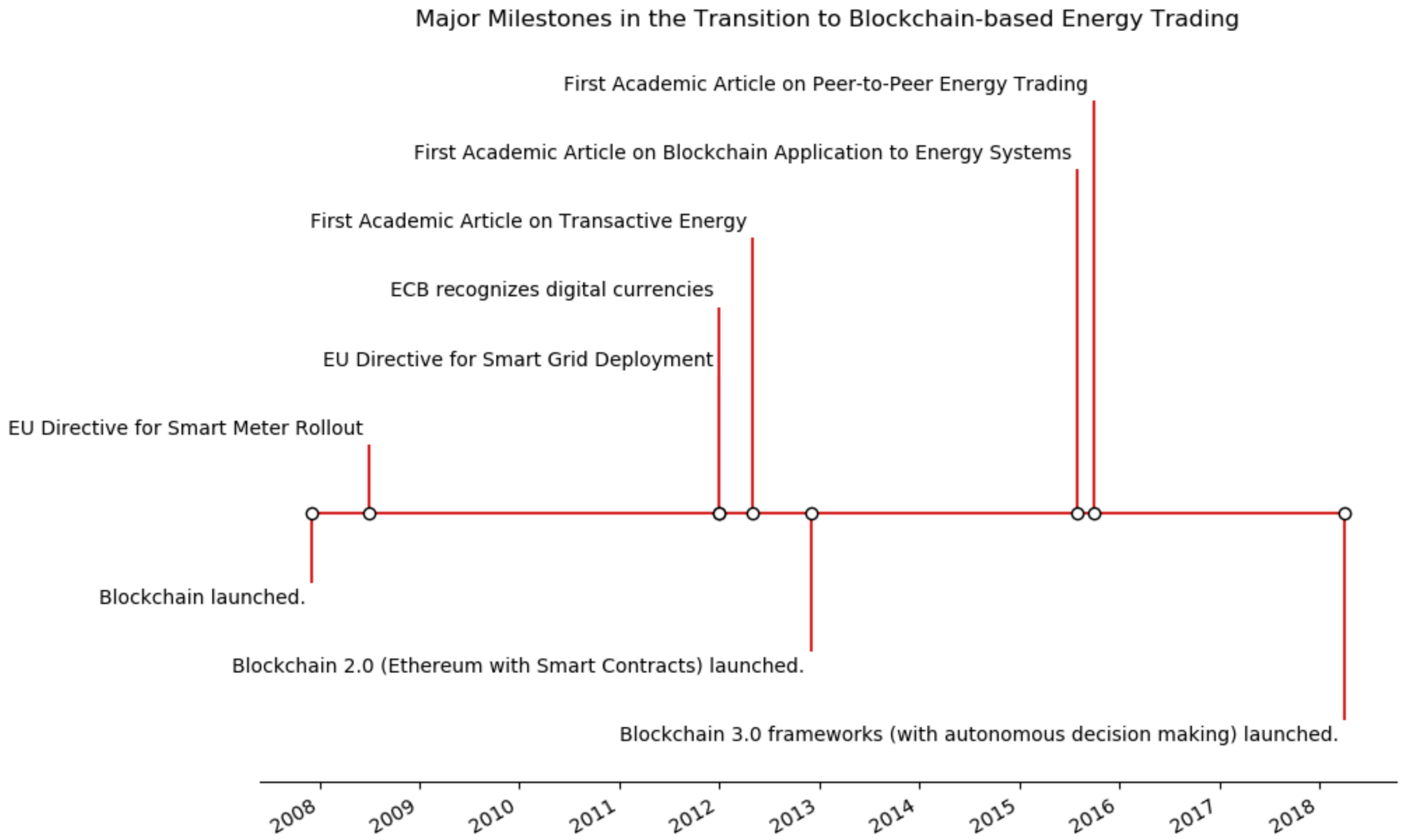

Figure 2.3: Timeline of major milestones and milestones taking place in the transition toward blockchain-based energy trading.

The German Energy Agency (dena) conducted a survey [95] among 70 decision makers in the German energy industry regarding Blockchain applications; 69% said they had already heard of existing Blockchain applications in the energy sector and 52% either have Blockchain implementations or ongoing plans thereof; 81% of the respondents are confident that Blockchain will likely have a significant influence on the industry. Potential use cases that they envision were (in decreasing order of potential): security, decentralized generation, P2P trading, mobility, metering and data transfer, trading platforms, automation, billing, grid management, and communication. Blockchain's potential in cost reduction and as an enabler for new business models was reported. Since it was expected to be more disruptive compare to current technological alternatives, it had a higher chance of being the dominant design in applications where P2P trading has not yet been established on a large scale. Despite changing the structure of energy trading, if Blockchain applications prove to have monetary or timely advantages over existing solutions, the critical number of market participants would be convinced to abandon current platforms in favor of Blockchain. Rapid successful launching of prototypes around the world might make Germany and the EU lagging behind globally with current regulator frameworks being completely unsuitable and uncompliant with Blockchain applications. Thus, they urged policymakers to consider it as a top priority.

Another report [96] studied the development of Blockchain use cases by assuming the role of RD developers. First, global consensus was identified as the primary disruptive element of Blockchain technology in the energy sector.

This makes it an enabler technology for platforms with fully decentralized control which is particularly useful in situations where transacting parties lack trust. In addition, Blockchain offers more efficient structures by removing the need for data to be synchronized with and by an intermediary, which is particularly useful in industry-level applications. For global and cross-country applications, the main potential of Blockchain technology lied in its ability to offer interoperability between devices and systems. As such, the report identified that interoperability and flexibility is the target state which Blockchain development in the energy sector must aim for. A conceptual use case which involved using Blockchain in conjunction with smart meters was made and evaluated with industry specialists. The report recommended that being a disruptive technology to the energy sector, companies planning on developing Blockchain energy applications should build strategic understanding of use cases in collaboration with Blockchain technology developers by insourcing the knowledge.

An article [94] published in 2016 modeled and simulated a case of P2P energy trading in an SG. The proposed model was a fully decentralized private trading platform based on Blockchain with multisignatures and anonymous encrypted message propagation streams. The system was resistant against significant common cyberattacks. In addition, the privacy of trading parties was found to be well protected by the system. By comparison with the results with a simulated centralized system, it concluded that the proposed system is a feasible application of Blockchain technology to develop secure and efficient fully decentralized energy trading platforms.

Another study [97] investigated new models for managing distribution grids. They proposed creating virtual distribution grids as a layer above the physical one. A Blockchain-based platform would be used for transactions of surplus energy from homes in a distributed architecture. The proposed model was neither implemented nor tested. However, the paper attempted to provide Blockchain usage model in the energy industry which is compatible with the current market structures. A journal article published in 2017 [98] studied the energy market in Perth, Australia, where a recent successful experiment with a Blockchain-trading platform was performed (similar Brooklyn). It showed that proliferation of cheap renewable generation and battery storage technologies are going to soon result in a paradigm shift in the energy industry to what they referred to as "citizen utilities." The paper states that an inevitable shift to distribute and bidirectional energy systems and more decentralized energy markets will take place, where Blockchain will be the basis of transactions such systems. The response of traditional market players would be what the paper called a "fight, flight, or innovate" one: fight will be the case if markets are resistant and in denial of the new paradigm shift; flight is if energy utilities take no action and possibly divesting investment in traditional markets; and innovate is if current utilities embrace the new technologies driving the paradigm shift.

This analysis concludes that there is a rapid change to a new energy market model which is operated not by utilities, but by consumers and that this should be facilitated in what the author called "democratization of power."

2.3 Blockchain 3.0: The Enabler of Next-generation Energy Systems

Up to this stage, all published works and conducted experiments considered the capabilities of Blockchain 2.0. The cryptographically secured, consensus-based, approach enabled the elimination of financial mediators. Similarly, smart contracts enabled a fully decentralized market where energy can be traded. However, there was still a major pillar missing from the IoE vision for a fully autonomous transactive energy network. As mentioned earlier, there are three distinguishable layers of energy systems: the grid, the markets, and the information infrastructure. While Blockchain 2.0 solutions provided a way of managing the latter two in a fully decentralized fashion, it was not sufficient to be applied on the first. Operation and control of power systems require the solution of complex optimization and forecasting models, and it was still extremely challenging at that stage to develop a fully decentralized operation or control framework for electrical grids which would justify the dispensability of a (central) grid operator.

Only one academic paper at the time (when this work began) had proposed a Blockchain-based solution for distributed optimization and control of electric grids in a P2P market architecture [99]. A decentralized optimal power flow (OPF) model for scheduling DERs on a microgrid was built and tested. Distributed optimization (namely ADMM) was used to decompose the OPF problem making it compatible with Blockchain architecture. The cost function was decomposed into a set of local functions, and a global function which is a function of the local ones. In this manner, the scheduling and dispatch routine could be performed in a fully decentralized fashion using Blockchain and smart contracts. The model was tested on a 55-bus microgrid with a dispatchable central generator, uncontrolled plug loads, nondispatchable renewable energy sources, shapeable loads, deferrable loads, and batteries. A day-ahead scheduling problem was considered with 1-h intervals. Blockchain and smart contracts used to perform optimization and control actions, and clearing prices, recording energy consumption (smart meters), and billing contracts (payment, charges, and penalties). The optimal cost based on ADMM was 0.4% larger than the centralized one. Shorter time horizons, ancillary services, or stochastic behavior were not considered. The aim was providing proof of the feasibility of using Blockchain for distributed optimization and control grid applications. The success was due to the combination of Blockchain 2.0 and ADMM and set the standard for future studies which attempted to develop the next generation of Blockchain which allowed not only for decentralized financial and information transactions, but also for autonomous operation of power systems.

This set the stage for the development of what came to be known as Blockchain 3.0 platforms. The evolution of Blockchain (Fig. 2.4) can thus be summarized as follows:

- **Blockchain 1.0**: A fully distributed ledger of transactions which are cryptographically secured and rely on global consensus.
- **Blockchain 2.0**: Includes smart contracts, which are digitally written and signed awaiting satisfaction of certain conditions to come into effect, executing peer-to-peer transactions.
- **Blockchain 3.0**: A fully decentralized platform capable of autonomous operation relying on distributed mathematical models. This self-managing system can determine optimal strategies to ensure global benefit, and thereby constructing smart contracts accordingly.

The ultimate objective of employing Blockchain 3.0 is to achieve the ideal structure of an IoE transactive energy network, possessing fully autonomous and fully decentralized operation, aiming at the benefit of end-users first and foremost.

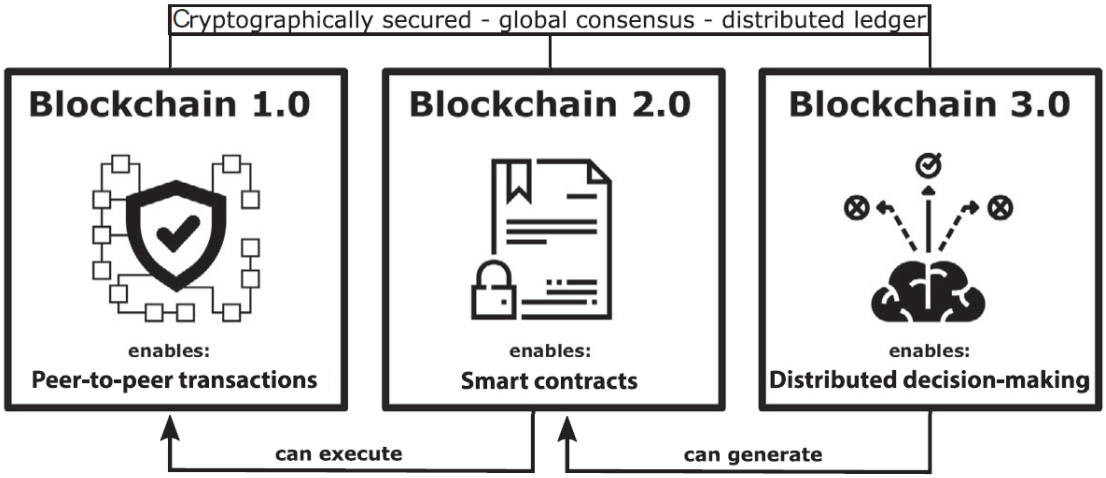

Figure 2.4: Timeline of major milestones and milestones taking place in the transition toward blockchain-based energy trading.

2.4 The Cloud-Based Internet of Energy

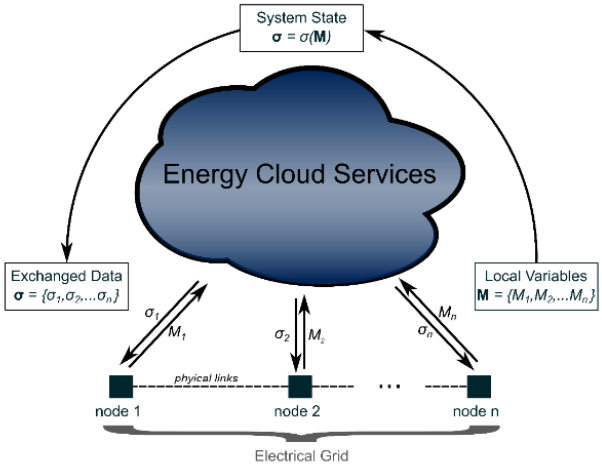

Figure 2.5: Energy cloud services concept. Local optimization and forecasting is performed and each agent, broadcasting signals into the cloud. The system state is updated iteratively through this cooperative information exchange.

As mentioned earlier "If IoT refers to the connection of devices to the internet; cloud computing refers to how those devices work together to deliver data, applications, or services" [72]. Extending this to the grid operation of the IoE paradigm, cloud services allow connected nodes, or agents, to work cooperatively to deliver required data, applications, or services to the larger energy system they are part of. Each agent broadcasts some local variables, contributing to a collective state for participants of this energy cloud service, as illustrated in 2.5. This model will be constructed in the next part of the thesis.

2.5 Chapter Conclusions

Blockchain seems to have emerged at the most convenient timing for the energy sector, which in itself was transforming in favor of more decentralized structures and decision making. Therefore, Blockchain appeared as a reliable solution to several challenges facing the energy sector, and with perfect timing. That being said, this convenience is absolutely no coincidence. These simultaneous events happened, and continue to happen, in the context of a much larger revolution, the fourth industrial revolution (I4.0). In this chapter, the latter is introduced, and its design principles are listed. The Internet-of-Things (IoT) effect on the energy sector was investigated in detail, and the emergence of the Internet-of-Energy (IoE) with IoT-enabling of Smart Grids (SGs) is established. The design requirements for all technical models and processes developed for the IoE paradigm were defined. Fully decentralized economies based on Blockchain technology were investigated, and the adoption of Blockchain by the energy sector was discussed in detail. The decentralization of the energy sector in different dimensions (decentralization of generation, information, and markets) was elaborated. The paradigm shift towards peer-to-peer energy trading, along with next-generation IoE systems was established.

Part II

Transition to Cloud-Based Operation of Smart Grids

Chapter 3

Synergistic Coordination of Smart City Energy Management Systems

The smart cities paradigm is focused on optimizing resource management using modern software tools and communication infrastructures. In this paradigm, Electric Vehicles (EVs) create an everlasting link between the transport and power sectors. Optimal management of energy resources is of key importance, and with mobile EVs playing a pivotal role in smart city power flows, coordination of energy management systems (EMSs) at their parking locations can bear global benefits. In this chapter, novel models for local EMSs are considered. Namely, a home energy management system (HEMS) and an EV parking lot energy management system (PLEMS) were implemented using mixed-integer linear programming (MILP). Cloud-based coordination of the local EMSs is then conceptualized, being centered around the EVs arrival and departure schedules, without sharing private information. The proposed coordination framework is computationally implemented and simulated based on a real-life case study. The results show that the proposed cloud coordination of local EMSs is both technically beneficial for power grids and economically beneficial for EV owners.

Chapter Highlights and Novel Contributions:

- A novel EV PLEMS model is presented as an EV aggregating agent participating in both energy and ancillary markets.
- A novel HEMS model is presented to minimize both the homeowners' electricity bill and their discomfort levels, considering dynamic electricity tariffs.
- A cloud-based EMS coordination framework is proposed and different scenarios are defined.
- A real-world case study is simulated, accounting for traffic uncertainties affecting transit times, real PV generation ,load profiles, and electricity market data. Power flow simulations are performed to obtain a complete techno-economic evaluation.
- Synergistic coordination of the EMSs is evaluated. Technical and economic benefits for all participants (grid operator, EV owners, and PLEMS aggregator) are demonstrated.

Relevant Publication(s):

M. Lotfi, T. Almeida, M. Javadi, G.J. Osorio, C. Monteiro, J.P.S. Catalão, "Coordinating Energy Management Systems in Smart Cities with Electric Vehicles," in *Applied Energy*
Submitted, Under Review.

M. Lotfi, T. Almeida, M. Javadi, G.J. Osório, J.P.S. Catalão, "Coordinated Operation of Electric Vehicle Parking Lots and Smart Homes as a Virtual Power Plant," *2020 IEEE International Conference on Environment and Electrical Engineering and 2020 IEEE Industrial and Commercial Power Systems Europe (EEEIC / I&CPS Europe)*, 2020, pp. 1-6.
Published: https://doi.org/10.1109/EEEIC/ICPSEurope49358.2020.9160684

Chapter Nomenclature

Abbreviation	Definition
ANN	Artificial Neural Network
DER	Distributed Energy Resources
DG	Distributed Generation
DI	Discomfort Index
DR	Demand Response
DSM	Demand Side Management
DSO	Distribution System Operator
EMS	Energy Management System
ERSE	Portuguese Energy Regulation Services Entity
ESS	Energy Storage System
EV	Electric Vehicle
EVPL	Electric Vehicle Parking Lot
GEMS	Grid Energy Management System
HEMS	Home Energy Management System
IoT	Internet of Things
ISO	Independent System Operator
MILP	Mixed Integer Linear Programming
MIP	Mixed Integer Programming
MPC	Model Predictive Control
MPPT	Maximum Power Point Tracking
MV	Medium Voltage
PL	Parking Lot
PLEMS	Parking Lot Energy Management System
PV	Photovoltaic
RES	Renewable Energy Resources
SG	Smart Grid
TSO	Transmission System Operator

3.1 Introduction

3.1.1 Background and Motivation: The Smart Cities Paradigm

Accelerated transition towards smart cities can clearly be observed globally. Severe environmental alerts combined with exponential growth of human populations (and urban population densities) makes it imperative to develop sustainable cities to manage resources as efficiently as possible [100].

With modern day crises being mainly due to inefficient management of resources, smart cities are no longer seen as a luxury, but a necessity for the sustained wellbeing of humanity.

The cornerstones of any smart city are 1) the employment of Internet-of-Things (IoT)-enabling to collect data, 2) to use the collected data to optimize the resource management efficiency, and 3) iterate this process to improve the design of the processes by which resources are allocated and used [101].

Indeed, the development of an IoT infrastructure has been a key enabler of the transition towards smart cities. The other key enabler is cloud computing, allowing data to be stored, accessed, and processed by different users simultaneously [102]. While the development of smart cities impacts all sectors, some are more affected than others. The electrical power and transport sectors are being heavily impacted by this transition.

In fact, both sectors are becoming increasingly intertwined in this new paradigm [103].

3.1.2 The Intertwining of Electric Power and Transport Sectors

The electric power sector has seen many profound changes in the past few decades. Concerns over security of supply have led a wave of electricity market liberalization and the activation of demand-side management (DSM) policies. In this competitive electricity market, DERs became valuable assets in the demand-side. Typically, local DERs are small-scale distributed generation (DG) and energy storage systems (ESSs) [89].

More recently, with the urgency of minimizing greenhouse gas emissions, renewable energy sources (RESs) have become the preferred means of generating electricity, both on the demand-side (e.g., DERs) and on the generation utilities side (e.g., wind and solar farms). Meanwhile, the same government climate actions which mandated shifting to cleaner energy production have also affected another emission-heavy sector: the transport sector. Electrification of transport, particularly the proliferation of Electric Vehicles (EVs), has been at the forefront of this change [104].

At the same time, transport electrification inherently creates an everlasting link between the electric power and transport sectors, with the latter now becoming a major component of the demand-side and DSM. In fact, EVs intersect multiple elements of smart cities: connection to the power grid as a DER, asset of final energy users as citizen-owned vehicles for personal transport, using road and transit infrastructure, and dependence on cloud services such as navigation services, traffic and weather data, electricity prices, etc. This is illustrated in Fig. 3.1.

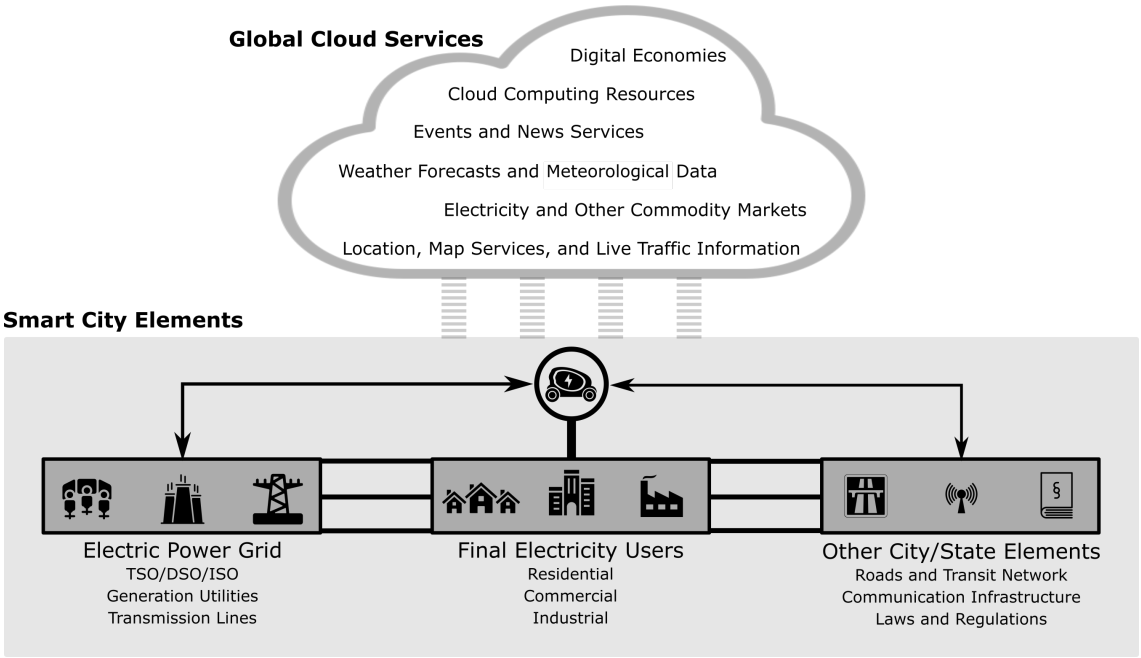

Figure 3.1: Elements of a smart city interdependent through the presence of EVs.

The simultaneous proliferation of RESs and EVs has been proven (both in literature and in real-life) to successfully reduce emissions significantly [105]. On the one hand: EVs eliminate local emissions of their combustion engine counterparts, while on the other hand charging their batteries from electricity generated by low-emission sources due to high levels of RESs.

However, having a high penetration of DERs and EVs causes multiple technical challenges in the operation of the electrical power grid. While modern smart grids (SG) are designed taking into account this fact, critical reliability issues are still encountered if the integration of both is performed in an uncontrolled manner.

Energy Management Systems (EMS) have already been used ever since DSM measures, especially Demand Response (DR) and dynamic pricing policies, were introduced. Their main objective has been to schedule energy consumption in order to make the best of the off-peak low electricity prices. In modern SGs, EMSs are developed accounting for technical constraints of the power grid and therefore they are a great tool to mitigate the technical challenges of high RES and EV penetration, while maintaining the economic incentives to the demand-side.

3.1.3 State-of-the-Art: Energy Management Systems EVs

Home Energy Management Systems (HEMS) which include EVs have been extensively studied in scientific literature. With accurate modeling, the HEMS scheduling results in decreased electricity bills through optimized utilization of local DERs (PV panels and EVs) and maximizing self-consumption during peak hours, while increasing the grid-independence [106].

A Mixed-Integer Linear Programming (MILP) model for a HEMS was introduced in [107]. The proposed model incorporated an ESS EV, PV, dynamic DR tariffs, and shiftable loads. By considering the homeowners' preferences for the usage time of each shiftable load, a discomfort index (DI) was calculated as a proportional value to the amount of load shifted. Multi-objective MILP optimization was then used to obtain the day-ahead schedule that provides the optimal tradeoff between minimizing the electricity bill and user discomfort. The results showed that the HEMS scheduling of the DERs and EV provided higher economic benefits for the homeowners through increased self-consumption while contributing to grid stability. Another recent study [108] investigated different operating strategies for another HEMS model, which also considered PV installations, an EV, shiftable loads, an ESS, and dynamic DR tariffs, and reiterated the same findings and conclusions.

A recent study [109] proposed a more complex HEMS model which addressed real-life uncertainties in user behavior and solar generation using a combination of algorithms: Model Predictive Control (MPC), Artificial Neural Networks (ANN), Markov chain, and conditional probability techniques. The analysis performed clearly showed the capability of the HEMS to significantly decrease the electricity bills compared to non-optimized rule-based methods (e.g., homeowners manual scheduling by simply following the dynamic DR tariffs). The paper also presented an important finding by simulating different time resolutions for the HEMS implementation. It was found that decreasing the time resolution from 1 hour to 15 minutes had little impact on the cost savings (<1%), while significantly increasing the computational effort (40x). This sets an important guideline on the choice of the time resolution.

In [103], a novel analysis was presented in which the coordination between the HEMS and the Grid Energy Management System (GEMS) was studied. The two EMSs shared information such as day-ahead driving schedules of the EVs and forecasted power profiles. The paper demonstrated that by coordinating the operation between the HEMS and GEMS, the electricity bills of the homeowners can be further decreased in addition to reduced PV curtailment.

All previous works [103, 106, 107, 108, 109] demonstrated techno-economic benefits of employing HEMSs incorporating EVs and DERs. However, in smart cities with high EV presence, traditional parking lots (PLs) can be converted to grid-connected EVPLs. EVPLs provide parking and charging services to EV owners at an agreed-upon tariff. By aggregating a large number of EVs, they are also capable of making a significant profit by being an ancillary services provider to the grid at a medium-voltage (MV) level. Being commercial establishments, their EMSs have one objective: maximize profits. In addition, the EVPLs make use of installed local generation (rooftop PVs) to further increase their net profits. Accordingly, recent works have proposed models for EVPL EMSs (PLEMSs). Recent studies on PLEMSs are surveyed subsequently.

A dynamic programming algorithm for a PLEMS was proposed in [110]. The intended application was the commercial areas where EVs are parked during power grid's peak hours. By using the aggregated potential of stationed EVs, the PLEMS was capable of determining the optimal charging schedule for each EV, which maximized the owner's profits by providing ancillary services to the grid while committing to the agreed upon charging rate for the total parked duration of each EV.

A PLEMS was implemented in [111] using fuzzy logic inference. In this study, the main focus was not to assess the PL's profitability, but rather its capability to mitigate grid overloading (which would be the case in uncontrolled EV charging at the EVPL) without sacrificing the charging commitments made to the EV owners. The PLEMS was shown to be successful at achieving this goal.

A combined EMS which aimed at maximizing the parking lot owner's profit while minimizing the distribution system operator's (DSO's) costs was proposed in [112]. In this sense, the PL would be incorporated as a subproblem in the GEMS. A stochastic MILP optimization model was used to account for the uncertainty of grid-connected RESs using a weighted-scenario based approach. The results showed that the implemented EMS effectively reduced the DSO's costs while maximizing the EVPL profits. In [113], an EVPL with rooftop PV installations was modeled and a real-time PLEMS was proposed, taking into account power grid constraints and dynamic electricity pricing. The PLEMS determined near-optimal charging/discharging of the parked EVs to increase the EVPL's profit.

Building on [112] and [113], a PV-equipped EV parking lot was modeled in [114]. The proposed MILP model for day-ahead operational planning showed that the designed PLEMS significantly increasing the EVPL's profits, without sacrificing neither the EVs' charging requirements, nor the grid constraints. On the contrary, a significant portion of the additional profit came from providing ancillary services to the grid, which enhanced grid reliability and reduced power losses.

From the conducted literature survey, the following is noted:

- HEMSs have been extensively studied in literature, demonstrating their capability to minimize electricity bills (with minimal sacrifice of comfort) by shifting loads and optimizing EV charging/discharging according to dynamic DR tariffs.
- PLEMSs have been proposed in recent studies, mainly aiming at either maximizing the EVPL's profit or that of the grid operator. The aggregated capacity of parked EVs allow the EVPL to do so by participating in the ancillary services market.
- Only one study [103] considered the coordination between two EMSs (HEMS and the GEMS) in the presence of consumer EVs. No studies were found that studied the simultaneous operation of PLEMSs and HEMSs.

3.2 Methodology

3.2.1 Conceptual Model

The conceptual model devised for this study is shown in Fig. 3.2. In this model, residents of different neighborhoods commute daily to an EVPL. The latter has rooftop PV installations and a PLEMS. Individual houses have their own DERs (specifically, PV panels and ESSs) and a HEMS. The EVPL and all houses are connected to the same SG, with dynamic DR electricity prices, bidirectional power flows, and open access to participate in providing ancillary services.

The following scenarios will be studied and compared:

- **Scenario 1 – No EMSs**: In this (base) scenario, the houses have neither DERs nor an EMS installed. In this case, the houses are "traditional" homes with unscheduled operation of the appliances and uncontrolled charging of the EVs (i.e., once they arrive, they are plugged in until fully charged). In this scenario, the parking lot is nothing more than a parking space for the EVs.
- **Scenario 2 – HEMS only**: In this scenario, the houses are smart homes, with DERs (PV panels and batteries) installed and a HEMS operating to schedule all electricity usage (including EV charging). Each home has its own HEMS. The parking lot still exists only as a parking space for the EVs.
- **Scenario 3 – PLEMS only**: In this scenario, the houses are traditional houses, as they were in Scenario 1. The EVPL is converted to a commercialized smart EVPL, which has its own DERs (rooftop PV panels) and an EMS.
- **Scenario 4 – All EMSs**: In this scenario, both the houses and the parking lot are converted to their smart versions, equipped with DERs and EMSs. In this scenario, the EMSs coordination is studied. The EV owners include their arrival and departure times in the HEMS preferences, which shares this information with the PLEMS. The latter in turn shares back the expected SoC of the EV upon departure from the PL.

The techno-economic benefits of DERs, HEMSs, and PLEMSs, separately, have all been already established in previous studies and in the real world. Since the objective of this study is to investigate the synergies that can be obtained through the coordinated operation of these systems in the presence of EVs, the main comparison to be performed is between scenarios 1 and 4. With this being said, scenarios 2 and 3 are important to include as control scenarios, to identify if any observation is due to the synergy of the EMSs or if it already results from one of the individual EMSs on its own. The mathematical formulation used to model these scenarios is presented subsequently.

It duly noted that the PLEMS and HEMS models, detailed subsequently, have been developed as original work also throughout the course of this thesis.

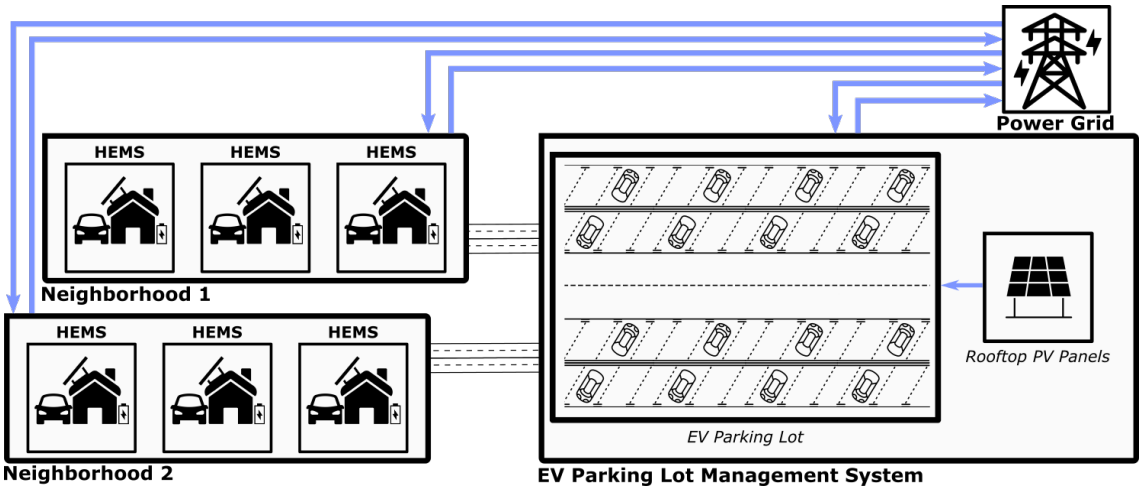

Figure 3.2: Conceptual model for the interaction between various EMSs with EVs.

3.2.2 Parking Lot Energy Management System

The EVPL and its grid interaction are modeled using a MILP formulation. The optimal day-ahead charging and discharging schedule of parked EVs is determined to maximize the EVPL's profit. The model considers the presence of rooftop PV panels and DR participation to sell energy to the grid or participate in the reserve and regulation markets in response to offers by the independent system operator (ISO). The day-ahead schedule is obtained by discretizing the 24 hours into NT^{PLEMS} time slots of size ΔT^{PL} hours, as shown in (3.1).

$$\Delta T^{PL} = \frac{24}{NT^{PLEMS}} \tag{3.1}$$

During each timeslot $t = 1 \ldots NT^{PLEMS}$, there are N_t^{PL} EVs parked in the PL, which changes every timeslot as shown in (3.2).

$$N_t^{PL} = N_{t-1}^{PL} + N_t^{arr} - N_t^{dep} \quad \forall t = 1 \ldots NT^{PLEMS} \tag{3.2}$$

In every timeslot there is a number of N_t^{arr} and N_t^{dep} newly arriving and departing EVs, respectively. The total number of EVs which use the PL is expressed as N^{EVPL}, and each individual EV is assigned an index $EVID = 1 \ldots N^{EVPL}$. A binary variable Φ_t^{EVID} indicates whether or not an EV $EVID$ is inside the PL during timeslot t or not, as shown in (3.3).

$$\Phi_t^{EVID} = \begin{cases} 1, & TARRPL_{EVID} \leq t \leq TDEPPL_{EVID}, \\ 0, & \text{otherwise} \end{cases}, \quad \forall EVID = 1 \ldots N^{EVPL}, t = 1 \ldots NT^{PLEMS} \tag{3.3}$$

Each EV's arrival and departure time to/from the EVPL is expressed as $TARRPL_{EVID}$ and $TDEPPL_{EVID}$, respectively. In (3.4) the total aggregated stored energy by the EVPL in timeslot t E_t^{PL} is calculated as the sum of energy stored of individual batteries of parked EVs (E_t^{EVID}). Similarly, in (3.5) the maximum storage capacity of the EVPL ($E_t^{PL,cap}$) is the sum of that of all parked EVs ($E_t^{EVID,cap}$). The corresponding SoC of individual EVs and the PL is defined in (3.6) and (3.7), respectively.

$$E_t^{PL} = \sum_{EVID=1}^{N^{EVPL}} \left(\Phi_t^{EVID} \cdot E_t^{EVID}\right) \tag{3.4}$$

$$E_t^{PL,cap} = \sum_{EVID=1}^{N^{EVPL}} \left(\Phi_t^{EVID} \cdot E_t^{EVID,cap}\right) \tag{3.5}$$

$$SOC_t^{EVID} = \frac{E_t^{EVID}}{E_t^{EVID,cap}}, \forall EVID = 1 \ldots N^{EVPL}, \quad \forall t = 1 \ldots NT^{PLEMS} \tag{3.6}$$

$$SOC_t^{PL} = \frac{E_t^{PL}}{E_t^{PL,cap}}, \forall t = 1 \ldots NT^{PLEMS} \tag{3.7}$$

For each timeslot, the total power injected from the grid to the PL and the total power injected from the PL to the grid are expressed in (3.8) and (3.9), respectively.

$$P_t^{G2PL} = P_t^{G2PL,en} + P_t^{G2PL,reg,down} \tag{3.8}$$

$$P_t^{PL2G} = P_t^{PL2G,en} + P_t^{PL2G,reg,up} + P_t^{PL2G,res} \tag{3.9}$$

In (3.8), the total power injected to the PL (P_t^{G2PL}) is equal to that corresponding to the energy purchased from the grid ($P_t^{G2PL,en}$) and that injected by the grid for the regulation-down offer ($P_t^{G2PL,reg,down}$). In (3.9), the total power injected from the PL to the grid (P_t^{PL2G}) is equal to the sum of that: 1) sold to the energy market ($P_t^{PL2G,en}$), 2) injected for the regulation-up offer ($P_t^{PL2G,reg,up}$), and 3) providing the reserve market offer ($P_t^{PL2G,res}$).

In (3.10)-(3.12), a condition is set such that the PL can either be injecting energy to or absorbing energy from the grid during each timeslot.

$$\text{FPL2G}_{\text{t}} = \begin{cases} 1, & P_t^{PL2G} > 0 \\ 0, & \text{otherwise} \end{cases}, \quad \forall t = 1 \ldots NT^{PLEMS} \tag{3.10}$$

$$\text{FG2PL}_{\text{t}} = \begin{cases} 1, & P_t^{G2PL} > 0 \\ 0, & \text{otherwise} \end{cases}, \quad \forall t = 1 \ldots NT^{PLEMS} \tag{3.11}$$

$$FPL2G_t \cdot FG2PL_t = 0, \quad \forall t = 1 \ldots NT^{PLEMS} \tag{3.12}$$

The binary variables $FPL2G_t$ and $FG2PL_t$ correspond to whether power is being injected from or to the PL in timeslot t, respectively. Constraint (3.12) allows only one of the two to be true at the same time. With all previous definitions, the power balance constraints can be defined as shown in (3.13)-(3.15).

$$P_t^{G2PL} + P_t^{PV2PL} \leq \gamma^{PL,ch} \cdot N_t^{PL} \quad \forall t = 1 \dots NT^{PLEMS} \tag{3.13}$$

$$P_t^{PL2G} \leq \gamma^{PL,dis} \cdot N_t^{PL} \quad \forall t = 1 \dots NT^{PLEMS} \tag{3.14}$$

$$\Delta T^{PL} \cdot P_t^{PV2PL} \leq \left(SOC^{PL,max} \cdot E_{t-1}^{PL,cap} - SOC_{t-1}^{PL} \cdot E_{t-1}^{PL} \right) - E_t^{arr} + E_t^{dep}, \quad \forall t = 1 \dots NT^{PLEMS} \tag{3.15}$$

For each timeslot, the sum of the power injected from both the grid and the local PV installations to the PL (P_t^{G2PL} and P_t^{PV2PL}, respectively) must be less than or equal to the number of EVs currently stationed multiplied by the charging rate ($\gamma^{PL,ch}$).This constraints the power injected to the PL to the maximum charging capability of EVs currently stationed.

Similarly, P_t^{PL2G} must not exceed the maximum discharge capability ($\gamma^{PL,dis} \cdot N_t^{PL}$). The presence of local PV generation makes it necessary to add the third power balance constraint shown in (3.15).

The energy charged by the PV panels is equal to the power injected (P_t^{PV2PL}) multiplied by the size of the time slot (ΔT^{PL}). The energy charged by the PV panels during any time slot must not exceed the difference between the maximum allowable energy capacity and actual energy level of the previous timeslot ($SOC^{PL,max} \cdot E_{t-1}^{PL,cap} - SOC_{t-1}^{PL} \cdot E_{t-1}^{PL}$), minus the energy to be added by newly arriving EVs (E_t^{arr}), plus that removed by departing ones (E_t^{dep}).

The aggregated energy stored by the PL at each timeslot can be related to the previous timeslot using (3.16), where $\eta_t^{PL,ch}$ and $\eta_t^{PL,dis}$ correspond to the overall charging and discharging efficiencies of the parked EVs, respectively.

$$E_t^{PL} = E_{t-1}^{PL} + \Delta T \cdot \eta_t^{PL,ch} \left(P_t^{G2PL} + P_t^{PV2PL} \right) - \Delta T \cdot \frac{1}{\eta_t^{PL,dis}} \cdot \left(P_t^{PL2G} \right), \quad \forall t = 1 \dots NT^{PLEMS} \tag{3.16}$$

Finding the optimal charging and discharging schedule for parked EVs involved the amount to be charged or discharged from each EV, as shown in (3.17) and (3.18), respectively. For each stationed EV at timeslot t, the SoC increment or decrement ($SOC_t^{EVID,up}$) and $SOC_t^{EVID,down}$, respectively) is defined such that the EV can only be either charging or discharging.

$$SOC_t^{EVID,up} = \begin{cases} 0, & \Phi_t^{EVID} = 0 \\ 0, & \mathrm{SOC}_t^{EVID,dep} \leq SOC_t^{EVID} - SOC_{t-1}^{EVID} \\ SOC_t^{EVID,dep} & -SOC_t^{EVID} - SOC_{t-1}^{EVID}, \text{ otherwise} \end{cases}, \quad \forall EVID = 1 \ldots N^{EVPL}, \forall t = 1 \ldots NT^{PLEMS} \tag{3.17}$$

$$SOC_t^{EVID,down} = \begin{cases} 0, & \Phi_t^{EVID} = 0 \\ 0, SOC_t^{EVID} - SOC_{t-1}^{EVID} \leq SOC_t^{EVID,dep} \\ SOC_t^{EVID,dep} - SOC_t^{EVID} - \mathrm{SOC}_{t-1}^{EVID}, & \text{otherwise} \end{cases}, \quad \forall EVID = 1 \ldots N^{EVPL}, \forall t = 1 \ldots NT^{PLEMS} \tag{3.18}$$

In (3.19) and (3.20), the set of all EVs' charging and discharging schedules are compiled, respectively.

$$SOC_t^{up} = \left\{ SOC_t^{1,up}, SOC_t^{2,up}, \ldots, SOC_t^{N^{EVPL},up} \right\} \tag{3.19}$$

$$SOC_t^{down} = \left\{ SOC_t^{1,down}, SOC_t^{2,\text{ down}}, \ldots, SOC_t^{N^{EVPL},down} \right\} \tag{3.20}$$

The MILP model for the PLEMS is now fully constrained. Additional constraints such as the active and reactive power flows (power factor limits) and voltage limits are added according to the grid requirements [114, 115].

To maximize the EVPL's profit, incomes and costs must first be defined. Those are listed and described in detail in Table 3.1. Unit prices are based on the electricity market being considered [114, 115]. Accordingly, the objective function ($\text{Profit}^{\text{EVPL}}$) is presented in (3.21), and the decision vector (**XPL**) is defined in (3.22)-(3.23).

$$\begin{gathered} \max_{\mathbf{XPL}} \left(\text{ Profit }^{\text{EVPL}} \right) = \\ \max_{\mathbf{XPL}} \sum_{t=1}^{NT^{PLEMS}} (\mathrm{IN1_t} + \mathrm{IN2_t} + \mathrm{IN3_t} + \mathrm{IN4_t} + \mathrm{IN5_t} + \mathrm{IN6_t} \\ -\mathrm{C1_t} - \mathrm{C2_t} - \mathrm{C3_t} - \mathrm{C4_t} - \mathrm{C5_t} - \mathrm{C6_t} - \mathrm{C7_t} - \mathrm{C8_t}) \end{gathered} \tag{3.21}$$

$$\mathbf{XPL} = \{\mathbf{XPL}_1, \mathbf{XPL}_2, \ldots, \mathbf{XPL}_{NT^{PLEMS}}\} \tag{3.22}$$

$$\begin{gathered} \mathbf{XPL}_t = \left\{ SOC_t^{up}, SOC_t^{down}, \right. \\ P_t^{PV2PL}, P_t^{G2PL,en}, P_t^{PL2G,en}, \\ \left. P_t^{G2PL,\text{ reg,down}}, P_t^{PL2G,\text{ reg,up}}, P_t^{PL2G,\text{ res}} \right\} \end{gathered} \tag{3.23}$$

Table 3.1: Profit and cost terms for the PLEMS.

Term	Description	Unit Price
Income: IN1_t	Energy sold to grid as active power injection from the PL, $\propto \left(P_t^{PL2G,en}\right)$	λ_t^{en} €/kWh
Income: IN2_t	Energy sold for the ISO-requested reserve, $\propto \left(P_t^{PL2G,res}\right)$	λ_t^{res} €/kWh
Income: IN3_t	Tariff paid by EV owners for energy charged to their EVs, $\propto \left(P_t^{G2PL} + P_t^{PV2PL}\right)$	$\lambda_t^{\text{EV,ch}}$ €/kWh
Income: IN4_t	Hourly tariff paid by EV owners for to park in the PL, $\propto \left(P_t^{G2PL} + P_t^{PV2PL}\right)$	$\lambda_t^{\text{EV,park}}$ €/h
Income: IN5_t	Energy exchanged for the ISO-requested regulation-up, $\propto \left(P_t^{PL2G,reg,up}\right)$	$\lambda_t^{\text{reg,up}}$ €/kWh
Income: IN6_t	Energy exchanged for the ISO-requested regulation-down, $\propto \left(P_t^{PL2G,\text{ reg, down}}\right)$	$\lambda_t^{\text{reg,down}}$ €/kWh
Cost: C1_t	Energy purchased from the grid as active power injection to the PL, $\propto \left(P_t^{G2PL,en}\right)$	λ_t^{en} €/kWh
Cost: C2_t	Tariff paid to EV owners for energy discharged from their EVs.	$\lambda_t^{EV,\text{ dis}}$ €/kWh
Cost: C3_t	Compensation paid to EV owners for battery degradation by V2G in energy market.	Cd^{en} €/kWh
Cost: C4_t	Compensation paid to EV owners for battery degradation by V2G in reserve market.	$\text{Cd}^{\text{ en}}$ €/kWh
Cost: C5_t	Compensation paid to EV owners for battery degradation by V2G in regulation market.	$\text{Cd}^{\text{ reg}}$ €/kWh
Cost: C6_t	Penalty paid for failing to provide the ISO-requested reserve	$0.02 \cdot \lambda_t^{\text{res}}$ €/kWh
Cost: C7_t	Penalty paid for failing to deliver the ISO-requested regulation-up	$0.02 \cdot \lambda_t^{\text{reg, up}}$ €/kWh
Cost: C8_t	Penalty paid for failing to deliver the ISO-requested regulation-down	$0.02 \cdot \lambda_t^{\text{reg,down}}$ €/kWh

3.2.3 Home Energy Management System

The implemented HEMS models a smart home incorporating an EV, local PV generation, dynamic DR tariffs, and shiftable loads. By considering the homeowner's preferences for the usage time of each shiftable load, MILP optimization is used to obtain the day-ahead schedule that minimizes the electricity bill. The mathematical formulation of the model is presented in this section.

With residential DR participation, the final electricity bill is the difference between energy bought from the grid and energy sold back. The objective function (Z), to be minimized, is defined in (3.24): The total power injected from the grid to the home (bought) for each timeslot t is represented as P_t^{G2H} at a unit price of λ_t^{buy}. In this model, the energy stored by the ESS is used directly for self-consumption never injected into the grid. Therefore, P_t^{H2G} (total power sold to the grid at a unit price λ_t^{sell}) is equal to excess PV generation. Similar to the PLEMS, the HEMS day-ahead time discretization is shown in (3.25), Such that scheduling is performed for each timeslot $t = 1 \ldots NT^{HEMS}$, and the duration of each timeslot is ΔT^{HEMS}.

$$\min Z = \min \sum_{t=1}^{NTHEMS} \Delta T^{HEMS} \left(P_t^{G2H} \lambda_t^{buy} - P_t^{H2G} \lambda_t^{\text{sell}} \right) \tag{3.24}$$

$$\Delta T^{HEMS} = \frac{24}{NT^{HEMS}} \tag{3.25}$$

Two stages are defined: 1) before HEMS implementation, which are the baseline operation intervals based on the end-user preferences; and 2) after HEMS implementation, where the flexible loads are optimally scheduled based on the DR tariffs.

The initial stage (before HEMS implementation) is first modeled by defining the operating intervals of each load i from a total number of N^{shift} shiftable loads. This is defined as the baseline interval for each load i as shown in (3.26), with $LB_{i,b}$ and $UB_{i,b}$ being the baseline lower and upper bounds, respectively. The binary variable $B_{i,t}$ is set to 1 during the timeslots t when the load i is operating and 0 for all timeslots outside its operating interval.

$$B_{i,t} = \begin{cases} 0 & t < LB_{i,b} \\ 1 \quad LB_{i,b} \leq t \leq UB_{i,b}, & \forall t = 1 \ldots NT^{HEMS} \\ 0 & t > UB_{i,b} \end{cases} \tag{3.26}$$

In the second stage (HEMS implementation), flexible loads are shifted from the baseline intervals to reduce costs according to dynamic DR tariffs (i.e., shifting from peak to off-peak periods). However, not all loads are indefinitely shiftable and so users set allowable lower and upper intervals for each load to operate, represented as $LB_{i,u}$ and $UB_{i,u}$, respectively. The output of the HEMS would include the new scheduled slots for each load as shown in (3.27). The binary variable $S_{i,t}$ corresponds to the timeslots that the load i is scheduled to operate by the HEMS, in the interval between $LB_{i,s}$ and $UB_{i,s}$. The scheduled operating interval must lie within the limits set by the user, as set by constraints (3.28) and (3.29).

$$S_{i,t} = \begin{cases} 0 & t < LB_{i,s} \\ 1 \quad LB_{i,s} \leq t \leq UB_{i,s}, & \forall t = 1 \ldots NT^{HEMS} \\ 0 & t > UB_{i,s} \end{cases} \tag{3.27}$$

$$LB_{i,S} \geq LB_{i,u}, \quad \forall i = 1, \ldots, N^{\text{shift}} \tag{3.28}$$

$$UB_{i,s} \leq UB_{i,u}, \quad \forall i = 1, \ldots, N^{\text{shift}} \tag{3.29}$$

Moreover, (3.30) indicates that while the scheduled of each shiftable load is shifted, the operating duration is unchanged.

$$\sum_{t=1}^{NT^{HEMS}} S_{i,t} = \sum_{t=1}^{NT^{HEMS}} B_{i,t}, \quad \forall i = 1, \ldots, N^{\text{shift}} \tag{3.30}$$

The total day-ahead energy demand of the house (E^{HD}) is shown in (3.31) and is the sum of two terms: the energy demand of scheduled loads and the base load (P_t^{HBase}). Due to the constraint by (3.30), the total energy demand before and after scheduling is unchanged. The power demand for each timeslot (P_t^{HD}) is expressed in (3.32).

$$E^{HD} = \sum_{i=1}^{N^{\text{shift}}} \sum_{t=1}^{NT^{HEMS}} \left(\frac{S_{i,t} \cdot P_i}{\Delta T^{HEMS}} \right) + \sum_{t}^{NT} \frac{P_t^{HBase}}{\Delta T^{HEMS}} \tag{3.31}$$

$$P_t^{HD} = \sum_{i=1}^{N^{shift}} (S_{i,t} \cdot P_i) + P_t^{HBase} \tag{3.32}$$

The model considers the presence of an ESS and local PV generation. For the ESS, constraints (3.33)-(3.38) are applied. Binary variables ESSCH $_t$ and (ESSDIS $_t$) indicate whether the ESS is charging or discharging during timeslot t, respectively. The ESS can only be either charging or discharging in a given timeslot as indicated by (3.33).

In (3.34) and (3.35), the charging and discharging power ($P_t^{HESS,ch}$ and $P_t^{HESS,dis}$, respectively) of the ESS are limited by the maximum charging and discharging rates ($\gamma^{HESS,ch}$ and $\gamma^{HESS,dis}$, respectively). In (3.36), the energy stored by the ESS is updated for timeslot t, considering that of the previous timeslot and charged/discharged energy. The SoC in (3.37) is the ratio of current energy stored to the rated capacity (^{HESS,Cap}) and is constrained by the minimum and maximum allowable limits in (3.38). While EV charging is considered a shiftable load to be scheduled by the HEMS, the technical constraints (3.33)-(3.38) apply to the EV battery while it is parked at home.

$$\text{ESSCH}_t \cdot \text{ESSDIS}_t = 0, \quad \forall t = 1 \ldots NT^{HEMS} \tag{3.33}$$

$$P_t^{HESS,ch} \leq \text{ESSCH}_t \cdot \gamma^{HESS,ch}, \quad \forall t = 1 \ldots NT^{HEMS} \tag{3.34}$$

$$P_t^{HESS,dis} \leq \text{ESSDIS}_t \cdot \gamma^{HESS,dis}, \quad \forall t = 1 \ldots NT^{HEMS} \tag{3.35}$$

$$E_t^{HESS} = E_{t-1}^{HESS} + \left(\eta^{HESS,ch} \cdot P_t^{HESS,ch} - \frac{1}{\eta^{HESS,dis}} \cdot P_t^{HESS,dis} \right) \cdot \Delta T^{HEMS}, \quad \forall t = 1 \ldots NT^{HEMS} \tag{3.36}$$

$$SOC_t^{HESS} = \frac{E_t^{HESS}}{E^{HESS,Cap}}, \quad \forall t = 1 \ldots NT^{HEMS} \tag{3.37}$$

$$SOC^{HESS,min} \leq SOC_t^{HESS} \leq SOC^{HESS,\max}, \quad \forall t = 1 \ldots NT^{HEMS} \tag{3.38}$$

The net power generated by the home PV panels (P_t^{HPV}) in a given timeslot must either be self-consumed (P_t^{HPV2H}) or sold to the grid (P_t^{HPV2G}) as indicated by (3.39).

$$P_t^{HPV} = P_t^{HPV2H} + P_t^{HPV2G}, \quad \forall t = 1 \ldots NT^{HEMS} \tag{3.39}$$

The final constraint for the HEMS is the power balance constraint, which is shown in (3.40) for each timeslot t.

$$P_t^{HPV2H} + P_t^{G2H} = P_t^{HD} + P_t^{HESS,ch} - P_t^{HESS,dis} + P_t^{HPV2G}, \quad \forall t = 1 \ldots NT^{HEMS} \tag{3.40}$$

3.2.4 Coordinating the Energy Management Systems

The primary link between the individual EMSs are the EVs. In (3.41) and (3.42), the arrival/departure times to/from the home and PL are related using TCOM (commuting time) for each EV. Given the arrival and departure time from only one of the two locations, accurate commuting times can be obtained by means of online cloud applications such as map and navigation services, which account for real traffic data. Thus, the EV owner can only provide the departure time from home and departure time from the PL, and the other times can be automatically computed. Similarly, the SoC of the EV battery at the destination is equal to that upon departure from the source minus the SoC lost during the commute, as in (3.43) and (3.44).

$$t^{EVID,arr,PL} = t^{EVID,dep,H} + TCOM^{EVID,2PL}, \quad \forall EVID \tag{3.41}$$

$$t^{EVID,arr,H} = t^{EVID,dep,PL} + TCOM^{EVID,2H}, \quad \forall EVID \tag{3.42}$$

$$SOC^{EVID,arr,PL} = SOC^{EVID,dep,H} - \Delta\mathrm{SOC}^{EVID,2PL}, \quad \forall EVID \tag{3.43}$$

$$SOC^{EVID,arr,H} = SOC^{EVID,dep,PL} - \Delta\mathrm{SOC}^{EVID,2H}, \quad \forall EVID \tag{3.44}$$

The SoC lost during the commute (ΔSOC) can be calculated based on the commute distance ($DCOM$) and average driving efficiency of the EV model ($\eta^{\mathrm{drive,EVID}}$, %/km), as shown in (3.45) and (3.46).

$$\Delta\mathrm{SOC}^{EVID,2PL} = DCOM^{EVID,2PL} \cdot \eta^{drive,EVID}, \quad \forall EVID \tag{3.45}$$

$$\Delta\mathrm{SOC}^{EVID,2H} = DCOM^{EVID,2H} \cdot \eta^{\mathrm{drive,EVID}}, \quad \forall EVID \tag{3.46}$$

Using (3.41)-(3.46), it is possible to coordinate the operation of the PLEMS and individual HEMSs without needing to share private information by either side. The HEMS only needs to share the EV arrival time at PL, EV departure time from PL, and arrival SoC. Meanwhile, the PLEMS shares each EV's departure SoC with its HEMS. Any extra information needed by the EMSs (e.g., PV forecasts, electricity market data, traffic data, etc.) is obtained through public cloud/web applications and repositories. The interaction and information flow between the EMSs and different elements is illustrated in Fig. 3.3.

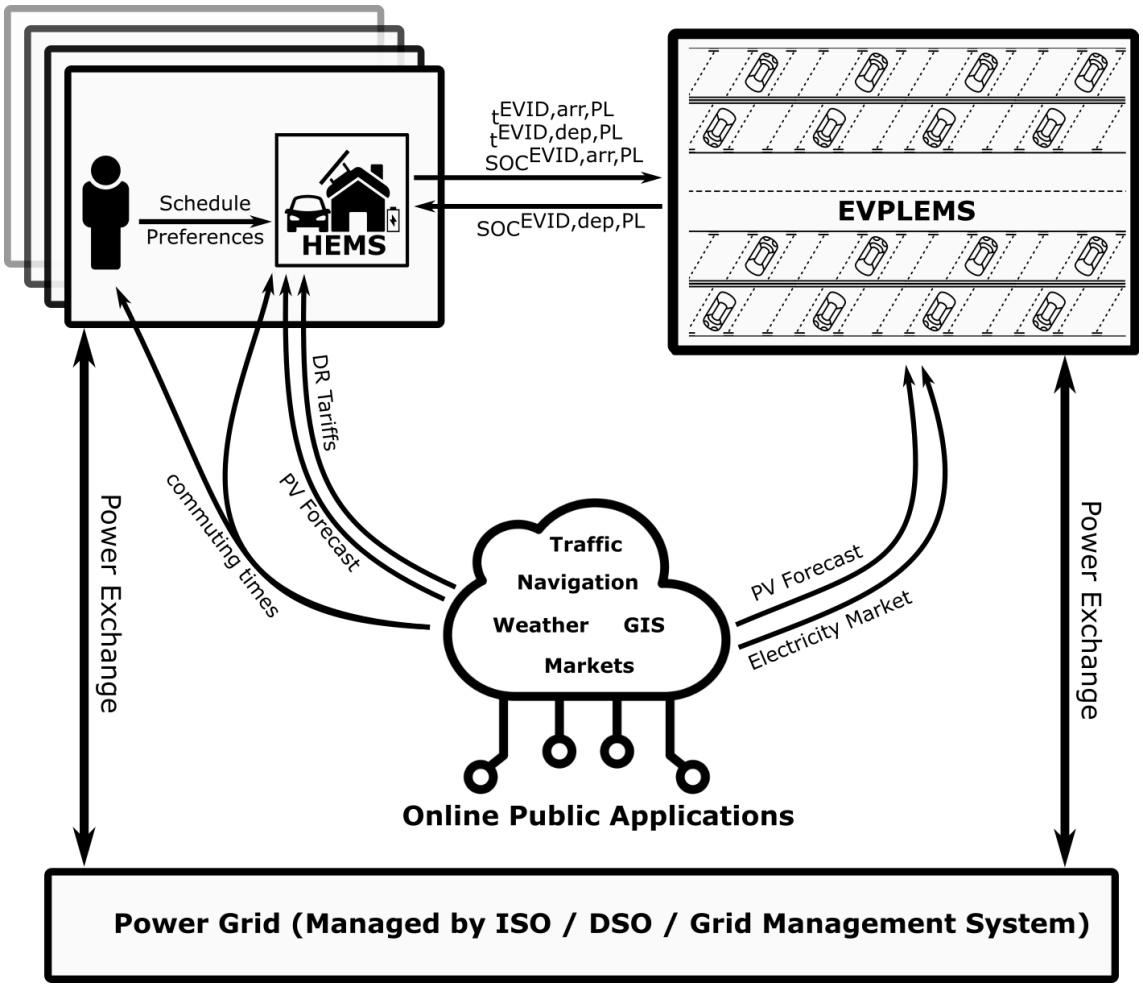

Figure 3.3: An illustration of the interactions and information flow between the PLEMS, HEMSs, cloud/web public services and repositories, and the power grid in the considered scheme.

3.3 Case Study

To simulate the proposed scheme, a case study based on real-world conditions was designed. By computationally simulating the four scenarios described in Section 3.2.1, possible synergies (or drawbacks) resulting from the interaction between the EMSs can be observed and evaluated.

The modeled EVPL was based on one of the parking spaces of the Faculty of Engineering of University of Porto (FEUP). This EVPL, along with variations of it, has been used in [114] to test the PLEMS system. It is assumed that a total of 108 EVs are enlisted in this EVPL (students and staff members). The EVPL has PV panels installed with a rated output power of 100 kW [116]. As a common EV model in Portugal, the Nissan Leaf, with a 30 kWh battery was used to model all EVs. The full specifications of the Nissan Leaf can be found in [105].

Table 3.2: Average SoC lost in commute and expected variations.

Location	**Mean SoC Lost in Commute to/from EVPL**	**Variation with Traffic (as std. deviation)**
Neighborhood 1	0.2	0.02
Neighborhood 2	0.3	0.03

The smart homes corresponding to each of the 108 EVs have local PV installations with a 3 kW rated output power and the LG RESU 6.5 kWh lithium-ion ESS. The complete specifications of the home PV panels and ESS can be found in [117] and [107], respectively. The homes are in one of two neighborhoods located in different places of the metropolitan area of Porto. In this way, the effect of different commuting times can be compared. Neighborhoods 1 and 2 have 72 and 36 homes, respectively (total of all 108 homes).

The average SoC lost when commuting between the EVPL and each of the neighborhoods is shown in Table 3.2. In this table, the variation of the SoC lost (accounting for traffic conditions) is represented as a standard deviation from the mean value. Given the nature of study and work times at the faculty, some EV owners have a morning schedule, while others have an afternoon schedule.

On average, the ones with morning schedules arrive at the EVPL at 9:00 and leave by 18:00, while the ones with an afternoon schedule arrive at 14:00 and leave by 21:00. Variations in the individual arrival and departure times of individual EV owners were considered, with the arrival and departure times varying from the average ones as show in Table 3.3. The "Max" value represents the latest possible arrival time (11:30 for the morning and 16:30 for the afternoon).

By accounting for the uncertainties in both the commuting times and commuting time and the arrival/departure times, real-life conditions are captured. A code script was made to generate individual arrival/departure times and transit times for each EV, for each day simulated.

Finally, power grid is simulated using the IEEE 33-bus test system. The locations of the EVPL and the neighborhoods both on the map and on the power grid are illustrated in Fig. 3.4.

Table 3.3: Morning and afternoon schedules and variations.

Work Schedule		**Mean**	**Std. Deviation**	**Max**
Morning	Arrival Time	9:00	50 min	11:30
	Departure Time	18:00		-
Afternoon	Arrival Time	14:00	50 min	16:30
	Departure Time	21:00		-

Neighborhoods 1 and 2 are connected to buses 22 and 25, respectively, and the EVPL to bus 33. Typical commercial and residential load profiles provided by the Portuguese Energy Regulation Services Entity (ERSE) [118] were used for the other buses as shown in Table 3.4. The power exchange at buses 22, 25, and 33 is according to the EMSs output. All parameters assumed for the PLEMS and HEMS are according to those in [116, 117]. Accordingly, one day of operation is simulated using the following steps:

- **Step 1**: Generate individual schedules for each EV: arrival, departure, and transit times.
- **Step 2**: Run PLEMS code to determine departure SoC of each EV, and power exchange with the grid at bus 33.
- **Step 3**: Run HEMS code for each individual home to determine power exchange with the grid at buses 22 and 25.
- **Step 4**: At each timestep, run AC optimal power simulation for the power grid.

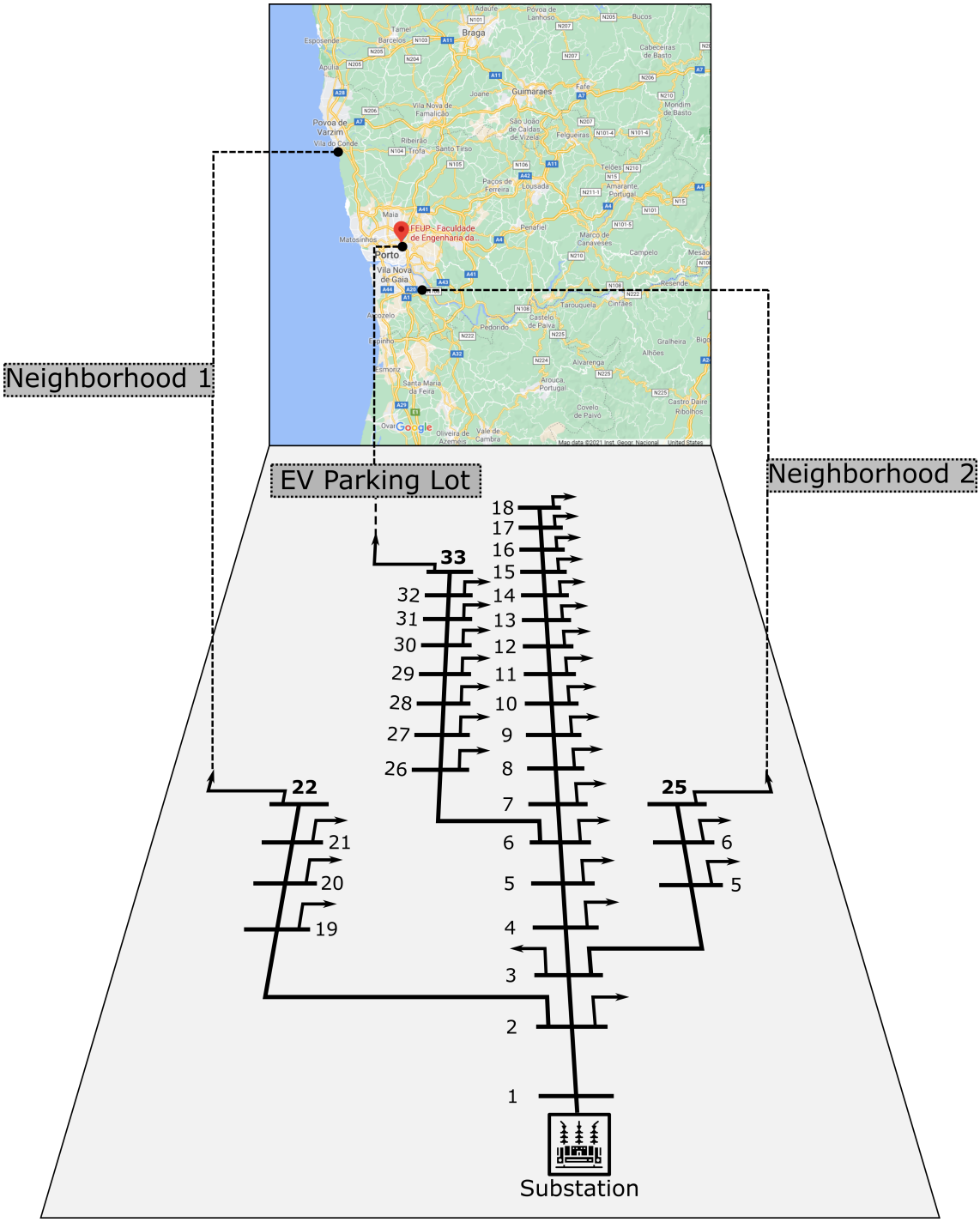

Figure 3.4: The map location of the EVPL and two neighborhoods used in the case study, and the corresponding buses on the IEEE 33-bus test system.

3.4 Simulation and Results

In this section, the results of the simulations are shown and discussed. Two separate studies were performed. The first is done from the technical perspective, where the objective is to analyze the effect of the EMSs coordination on the power flow in the grid. The second analysis is performed from an economic perspective, illustrating the point of view of the EV owners to analyze the cost-efficiency of the proposed EMS coordination scheme. All simulations were run on a standard laptop computer with an Intel Corei7-8550U CPU @ 1.80 GHz, 16.0 GB RAM, and a Windows 10 64 bit operating system. The General Algebraic Modelling System (GAMS) environment was used to implement the PLEMS and HEMS, applying the Mixed Integer Programming (MIP) solver. MATPOWER 7.1 on MATLAB 2019b was used for the power flow simulations.

3.4.1 Technical Viability: Power Flow Analysis

To incorporate effects of seasonal variations, two working days were analyzed: a winter day (21-Jan-2019) and a summer day (01-Jul-2019), both a Monday for consistency.

For the homeowners, the summer and winter residential tariffs are shown in Fig. 3.5, according to commercial tri-hourly electricity tariffs in Portugal, which can be seen found in [119]. For the EVPL, the energy, reserve, and regulation prices are according to the Iberian market, which are available online by the Portuguese TSO (REN) [120]. The energy price in the Iberian market is also plotted in Fig. 3.5. It is assumed that both the PL and homes use maximum power point tracking (MPPT) PV installations, and it is also assumed the normalized (unit) MPPT generation is the same for both.

Accordingly, real PV generation data was obtained from a smart home [116] in Porto for the given days and the normalized MPPT generation is shown in Fig. 3.6. After generating the daily arrival/departure and commuting schedules for all 108 EVs, the aggregated load profiles of Neighborhood 1 and 2 are shown in Fig. 3.6. It is noteworthy that the two neighborhoods do not have the same profile, due to the variations of the individual schedules. The energy exchanged between the grid and each of the EMSs installed is shown for the neighborhoods and the PL in Fig. 3.8 and 3.9, respectively.

In Fig. 3.10, active power losses are plotted for all four scenarios. As mentioned in II.A, evaluating these intermediate scenarios can provide some insight of the contribution of each EMS to the final result. In Figs. 3.11 and 3.12, scenarios 1 (base) and 4 (final) are compared for all variables of interest (voltages at buses 22, 25, and 33, total power supplied by grid, and total power losses) between the summer and winter cases.

In Fig. 3.10 it is observed that applying only the HEMSs has a slight but consistently favorable effect on grid losses. This is expected, since the HEMS favors self-consumption and only injects to the grid in times of excess PV generation, which is also a time of high load demand.

Table 3.4: Loads connected to the simulated power grid.

Bus	Load	Bus	Load	Bus	Load
1	Slack Bus	12	Commercial - BTN	23	Residential – BTE1
2	Commercial - BTN	13	Commercial - BTN	24	Residential – BTE1
3	Commercial - BTN	14	Commercial - BTN	25	***Neighborhood 2***
4	Commercial - BTN	15	Commercial - BTN	26	Residential – BTE1
5	Commercial - BTN	16	Commercial - BTN	27	Residential – BTE1
6	Commercial - BTN	17	Commercial - BTN	28	Residential – BTE1
7	Commercial - BTN	18	Commercial - BTN	29	Residential – BTE1
8	Commercial - BTN	19	Residential – BTE1	30	Residential – BTE1
9	Commercial - BTN	20	Residential – BTE1	31	Residential – BTE1
10	Commercial - BTN	21	Residential – BTE1	32	Residential – BTE1
11	Commercial - BTN	**22**	***Neighborhood 1***	**33**	***EVPL***

By looking at Fig. 3.11(c)-(d) and 3.12(c)-(d), it can be seen that very minimal (barely observable) change occurs in the voltage profiles at the neighborhoods buses. With or without EMSs, the p.u. voltage at the neighborhood buses is very close to 1 for both the winter and summer days. Meanwhile, the PLEMS can be seen to have a more significant impact on the power flow results.

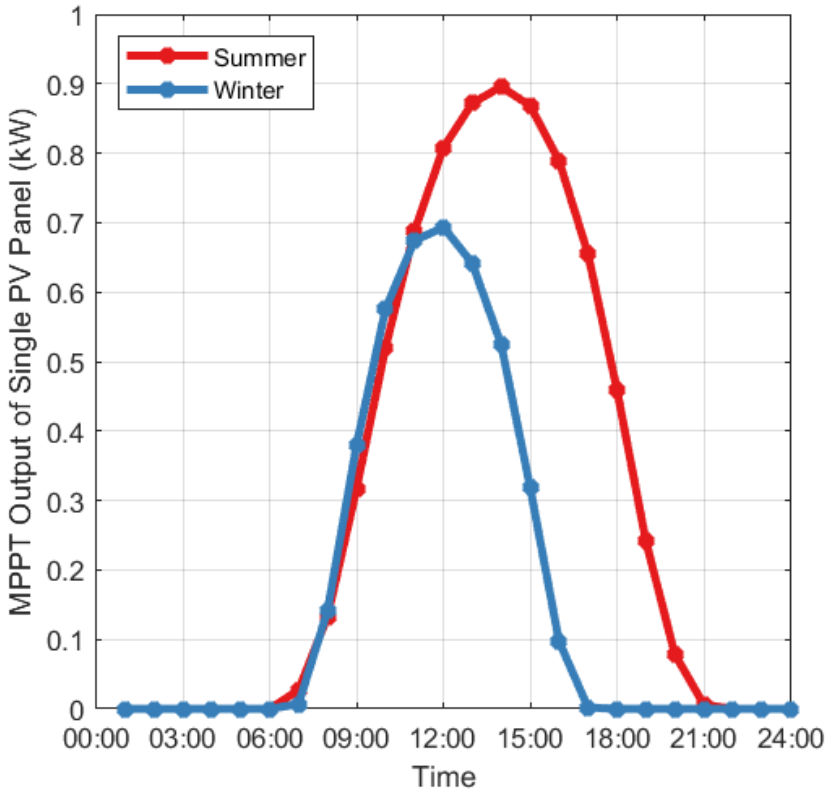

Figure 3.6: Normalized MPPT PV output for the summer and winter days.

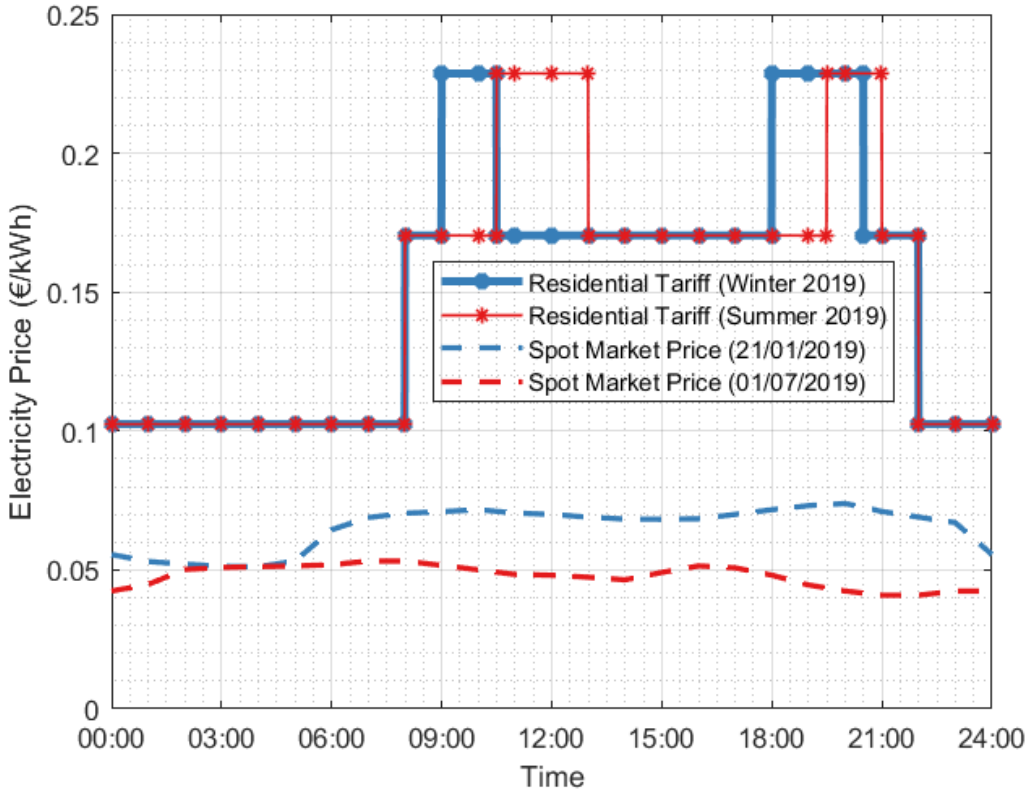

Figure 3.5: Residential tariffs and Iberian market prices for summer and winter days.

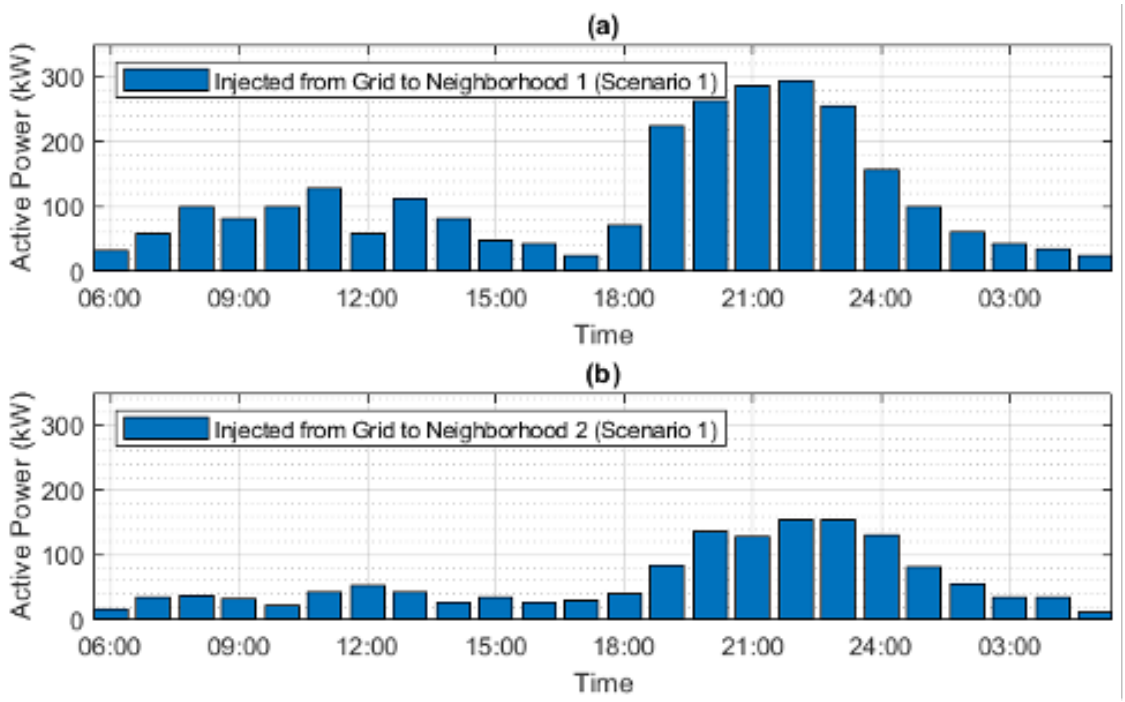

Figure 3.7: Active power load profile with no EMSs (scenario 1) in the summer day for a) Neighborhood 1 and b) Neighborhood 2.

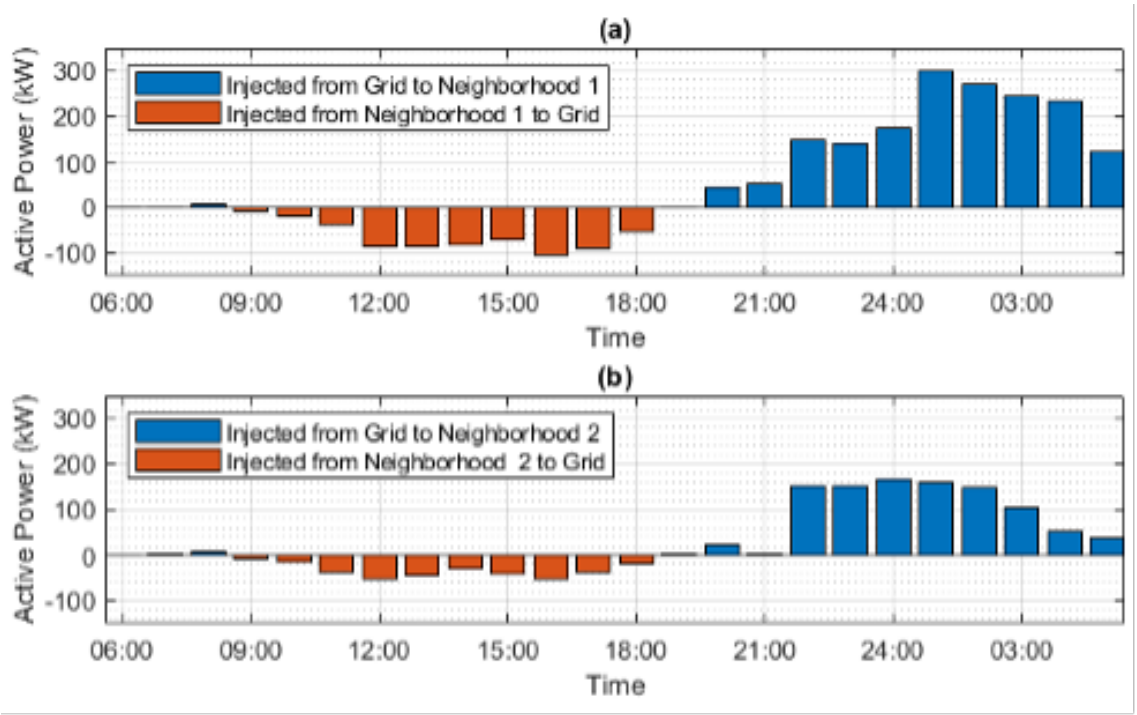

Figure 3.8: Active power exchanged with grid with coordinated EMSs (scenario 4) in the summer day for (a) Neighborhood 1 and (b) Neighborhood 2.

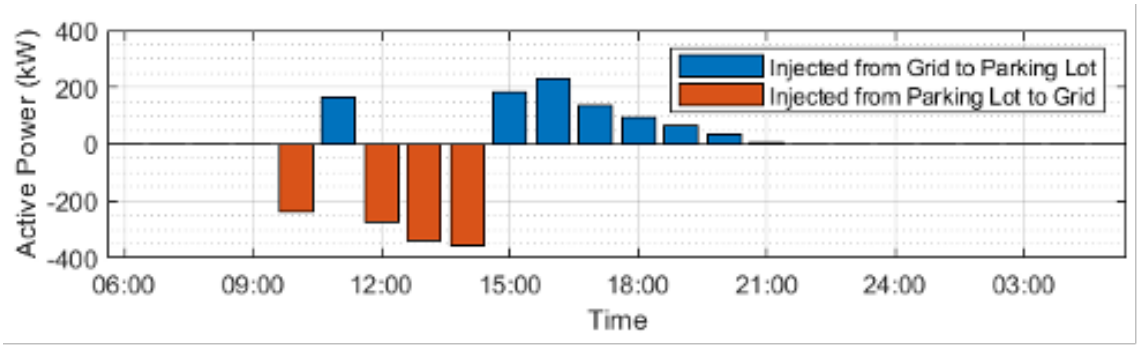

Figure 3.9: Active power exchanged with grid with coordinated EMSs (scenario 4) in the summer day for the EVPL.

From Fig. 3.10 it can be seen that the intermediate scenario 3 (with the PLEMS and without the HEMSs) is very similar to the final scenario 4 (with all EMSs). In scenario 3, during the summer day the power losses are dramatically decreased in the morning (at 09:00). In this time the majority of EVs are arriving to the PL and are available to operate in V2G modes, and PV generation starts. With both factors combined, the EVPL starts to inject power to the grid and this is met with the observed drop both in power losses and power supplied by the grid.

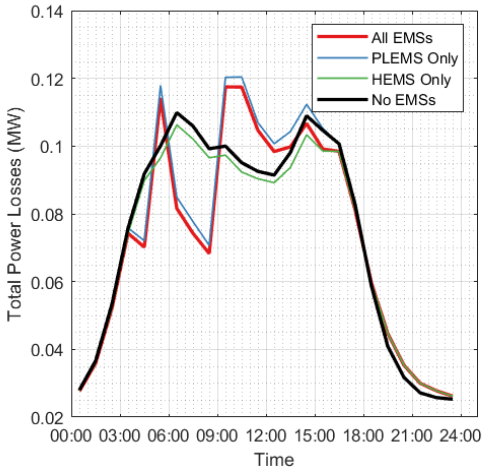

Figure 3.10: Comparison of active power losses for all scenarios (summer).

In Fig. 3.11(d) it can be seen that this corresponds to an observable over-voltage due to the injected power to the grid. In the winter, the exact opposite occurs at this time, since the morning surge of EVs occurs when PV generation is not enough and an undervoltage occurs since power has to be consumed from the grid.

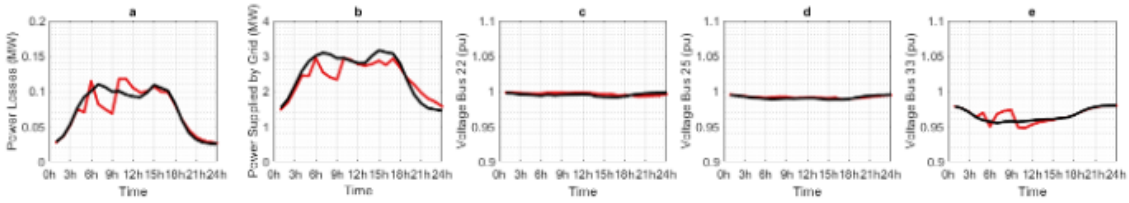

Figure 3.11: Power flow results for the summer day: (a) grid active power losses, (b) active power supplied by the grid, (c) voltage at Neighborhood 1, bus 22 (d) voltage at Neighborhood 2, bus 25, and (e) voltage at EVPL, bus 33. Black line represents base scenario (no EMSs) red line represents final scenario (all EMSs).

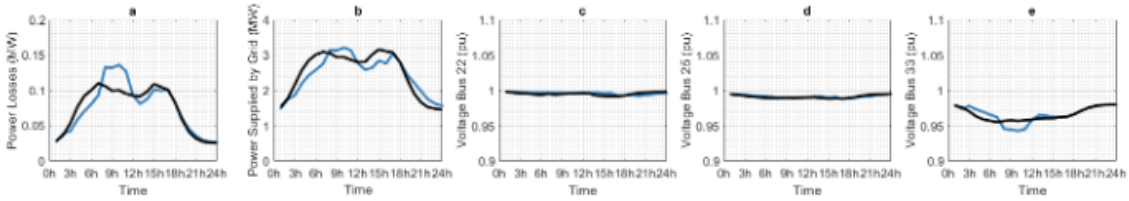

Figure 3.12: Power flow results for the winter day: (a) grid active power losses, (b) active power supplied by the grid, (c) voltage at Neighborhood 1, bus 22 (d) voltage at Neighborhood 2, bus 25, and (e) voltage at EVPL, bus 33. Black line represents base scenario (no EMSs) red line represents final scenario (all EMSs).

Table 3.5: Results from the power flow analysis.

Season	Winter		Summer	
Scenario	No EMSs	All EMSs	No EMSs	All EMSs
Total Energy Supplied (MWh)	59.8	58.6	59.8	57.2
Total Energy Losses (MWh)	1.8	1.8	1.8	1.7

Around 12:00, the opposite occurs. The PL is full at this time and requires energy from the grid to charge the parked EVs (as seen in Fig. 3.9). However, due to PV generation and self-consumption, this is still met with a decrease in system losses and power supplied by the grid; and an undervoltage can be observed. Since this is around the peak PV generation time, the same effect is observed in the winter albeit with less magnitude.

The total power loss and power supplied by the grid for both days are reported in Table 3.5. This effect results in the observed shift of the peak power losses time of the day. From this study, the following inferences can be drawn:

- A synergistic effect is observed in which an added benefit is obtained by applying all the EMSs compared to each one separately.
- Overall, all observed power flow variables show added benefits for the summer day compared to the winter one.
- The employed HEMSs have a slight but consistently favorable effect on the power grid.
- The employed PLEMS has a more significant effect on the power grid. During the summer the morning surge results in a drop in grid power losses and an overvoltage at the PL bus. During the winter, the morning surge causes a significant undervoltage due to insufficient PV generation.
- The employed PLEMS has a more significant effect on the power grid. During the summer the morning surge results in a drop in grid power losses and an overvoltage at the PL bus. During the winter, the morning surge causes a significant undervoltage due to insufficient PV generation.
- All voltages in the network, for all cases, are well within the allowed safety range (0.9-1.1).

3.4.2 Economic Viability: Cost Analysis for EV Owner

With the technical viability of the proposed scheme confirmed, a second study was performed to analyze the economic aspect from the EV owners' point of view. As it is advised to investigate the worst-case scenario for economic purposes, the winter case was used. The simulations were extended for the entire week, rather than one day, for the working week corresponding to 21/25-Jan-2019. A single EV was extracted and analyzed to obtain the total electricity costs for the full working week. The results of this study are shown in Fig. 3.13 (a)-(d), and Table 6. By tracking the full SoC variation during the working week, the total electricity bill for the EV owner can be calculated based on the: i) cost of purchasing electricity at home, ii) profit from selling energy to grid at home, iii) tariffs paid to the PL for parking and charging, iv) income from the parking lot for V2G compensation.

The breakdown of the week electricity bill for the EV under study is shown in Table 3.6.

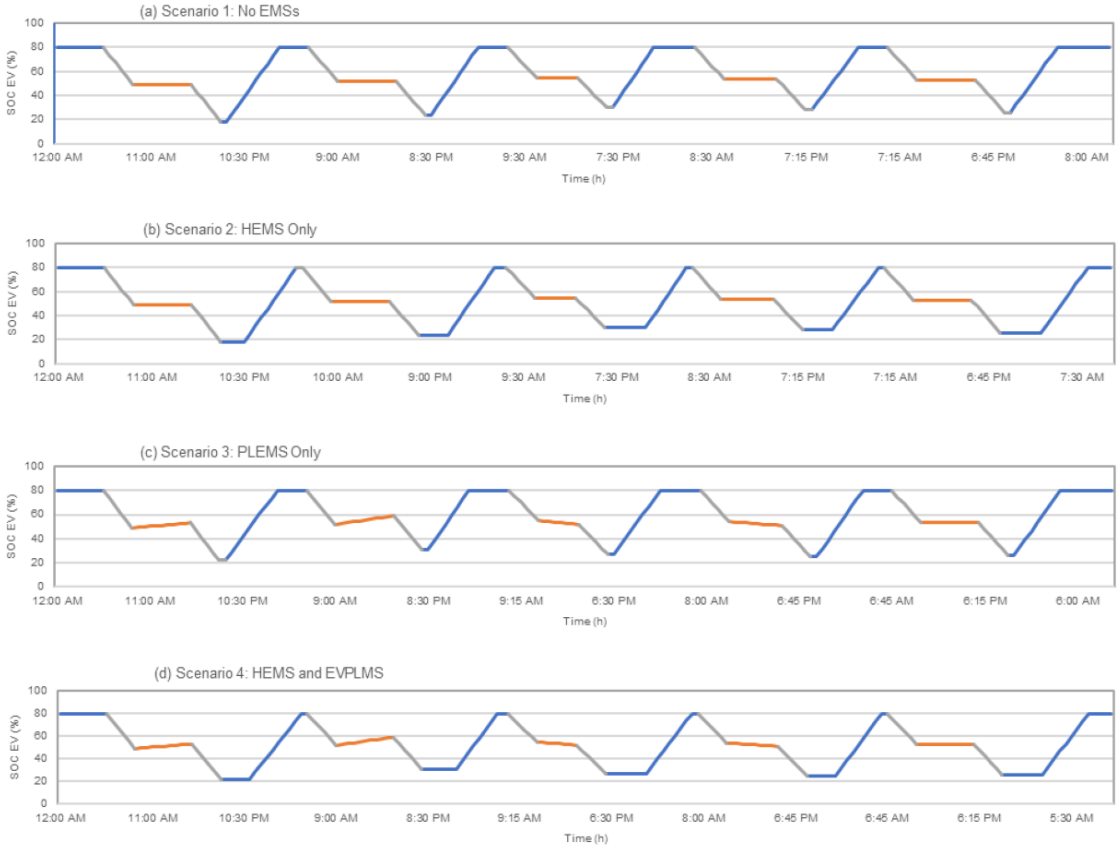

Figure 3.13: SoC variation during the full winter working week for the EV under study in the case of (a) no EMSs, (b) only HEMSs, (c) PLEMS only, (d) all EMSs.

- Employing the HEMS introduces a significant reduction in the weekly electricity bill compared to the base case (-14%).

Table 3.6: Total electricity bill for the owner of the EV.

Scenario	Day					Total
	1	2	3	4	5	
S1	€ 1.37	€ 1.08	€ 1.03	€ 1.11	€ 1.21	€ 5.79
S2	€ 1.25	€ 0.93	€ 0.81	€ 0.96	€ 1.05	€ 4.99
S3	€ 1.61	€ 1.48	€ 0.87	€ 0.94	€ 1.21	€ 6.11
S4	€ 1.46	€ 1.32	€ 0.64	€ 0.82	€ 1.05	€ 5.30

- Employing the PLEMS alone has a negative effect on the EV owner. This is expected since the PLEMS's objective function is to maximize the EVPL's profit.
- Employing the HEMS along with PLEMS overcomes the adverse effect of the previous scenario and results in a net reduction in the bill compared to the base scenario (-9%).

Overall, the employment of the coordinated EMSs has been shown to be both technically beneficial for the power grid and economically beneficial for the EV owners.

3.5 Chapter Conclusions

An innovative coordination framework was proposed and implemented for different EMSs in a smart city. The model was conceptualized based on the coordination between individual HEMSs belonging to the EV owners and a PLEMS at their workplace. The HEMS only needed to share the EV arrival time at the PL, EV departure time from the PL, and arrival SoC. Meanwhile, the PLEMS shared each EV's departure SoC with its HEMS. Any extra information needed by the EMSs (e.g., PV forecasts, electricity market data, traffic data) was obtained through public cloud/web applications and repositories. The individual EMSs and the proposed coordination framework were implemented and tested based on real-world data and by simulating a day-ahead operation. Two studies were performed. In the first, a power flow analysis was made to analyze the technical viability of the proposed approach. In the second, an economic analysis was made by calculating an EV owner's electricity bill for a full working week under different scenarios of EMS coordination. The results of both studies showed that the proposed EMS coordination framework was both technically beneficial for power grids and economically beneficial for the EV owners.

In this chapter, the cloud-based coordination of modern day SG EMSs was investigated and the techno-economic benefits analyzed. In the next two chapters, the transition to a fully cloud-based operation of future SGs is demonstrated through the development of novel fully decentralized algorithms for forecasting (chapter 4) and power flow management (chapter 5).

Chapter 4

Fully Decentralized Forecasting of Renewable Power Generation

A novel ensemble algorithm based on kernel density estimation (KDE) is proposed to forecast distributed generation (DG) from renewable energy sources (RES). The proposed method relies solely on publicly available historical input variables (e.g., meteorological forecasts) and the corresponding local output (e.g., recorded power generation). Given a new case (with forecasted meteorological variables), the resulting power generation is forecasted. This is performed by calculating a KDE-based similarity index to determine a set of most similar cases from the historical dataset. Then, the outputs of the most similar cases are used to calculate an ensemble prediction. The method is tested using historical weather forecasts and recorded generation of a real PV installation located in Portugal. Despite only being given averaged data as input, the algorithm is shown to be capable of predicting uncertainties associated with high frequency weather variations, outperforming a deterministic prediction based on solar irradiance data. Moreover, the algorithm is shown to outperform a neural network (NN) in most test cases while being exceptionally faster (32 times). Given that the proposed model only relies on public and locally-metered data, it is a convenient tool for use by owners or operators of DG installations, including small-scale prosumers, to effectively forecast their expected generation without depending on private/proprietary data or divulging their own. In this manner, the proposed algorithm can be deployed in a fully decentralized cloud-based system, providing highly accurate forecasting capability locally and without the need for a central coordinating entity.

Chapter Highlights and Novel Contributions:

- A novel KDE-based method for fully decentralized local forecasting is developed, relying only on publicly available historical variables and locally metered data.
- The algorithm can run despite inconsistency or loss of data points. Using KDE, the most suitable inputs are "activated" from the historical dataset based on a newly proposed similarity index.
- The proposed method was tested by considering meteorological and recorded power generation from a real PV installation around the city of Coimbra, in the center region of Portugal.
- The method was capable of predicting uncertainties associated with high frequency variations, outperforming both a deterministic prediction and a NN forecast.
- The developed method enables fully decentralized local forecasting for prosumers without depending on private/proprietary data or divulging their own, being compatible with the cloud based IoE paradigm.

Relevant Publication(s):

M. Lotfi, M. Javadi, G. J. Osório, C. Monteiro, and J. P. S. Catalão, "A Novel Ensemble Algorithm for Solar Power Forecasting Based on Kernel Density Estimation," *Energies*, vol. 13, no. 1, p. 216, Jan. 2020.
Published: http://dx.doi.org/10.3390/en13010216

Chapter Nomenclature

Abbreviation	Definition
ANN	Artifical Neural Network
DER	Distributed Energy Resources
DG	Distributed Generation
EMD	Empirical Mode Decomposition
GFS	Global Forecasting System
KDE	Kernel Density Estimation
MAE	Mean Absolute Error
ML	Machine Learning
MPPT	Maximum Power Point Tracking
NN	Neural Network
NRMSD	Normalized Mean Root Square Deviation
PV	Photovoltaic
RES	Renewable Energy Resources
RF	Random Forest
RMSD	Root Mean Square Deviation

4.1 Introduction

Accurate prediction of power generation from renewable energy sources (RES) is a challenging task, posing problems for short-term operation of modern power systems [105]. This difficulty is due to the high uncertainties and complexity of both the associated variables and the equipment used for generation and grid connection. On the one hand, generation from RES is a function of multiple meteorological factors (temperature, humidity, wind flow, etc.) which are in and of themselves highly chaotic in nature and difficult to quantify [121, 122]. On the other hand, the equipment used is also a source of significant uncertainty with reliability issues and failures commonly occurring in installed power electronics, inverter-side, grid-side, and even the metering apparatus [123].

The combined effect of chaotic input variables and complex energy conversion models render deterministic approaches infeasible for the prediction of distributed generation (DG) from RES. As such, statistical and/or probabilistic models are commonly employed not only to forecast DG but also to predict market behavior in the case of high RES deployment [124, 125] which allows for a computationally efficient way of accounting for uncertainties in inputs.

In recent years, there has been increased interest in the use of ensemble methods for power system applications. Ensemble techniques have a decades-long track record in meteorological prediction, proving their potential to effectively predict highly chaotic processes [126]. The main premise of ensemble methods is to overcome both input and model uncertainties by compiling a set (ensemble) of separate predictions into a forecast of most likely outcomes. Each separate prediction is a result of varying input variables within their uncertainty range in addition to the model uncertainty. Therefore, a combination of these separate predictions yields a range of possible outputs representing a confidence/uncertainty region surrounding a most likely scenario.

In Fig. 4.1, the concept of an ensemble forecast is visualized considering the case of DG production from RESs. Various meteorological factors are independent input variables and are associated with a significant level of uncertainty. In addition, the physical energy conversion models of DG units are also associated with a high uncertainty, leading to a significant change in energy generation as a result of small perturbances in the meteorological variables. Ensemble methods combine different scenarios based on both input and model uncertainties and establish a confidence interval around a most likely outcome. One can see that the employment of an ensemble technique involves the (continuously improving) prediction of some variable based on historical data, without knowledge of the physical model relating the inputs with the outputs. This is, in fact, the definition of machine learning (ML), and, as such, ensemble methods are often classified accordingly [127].

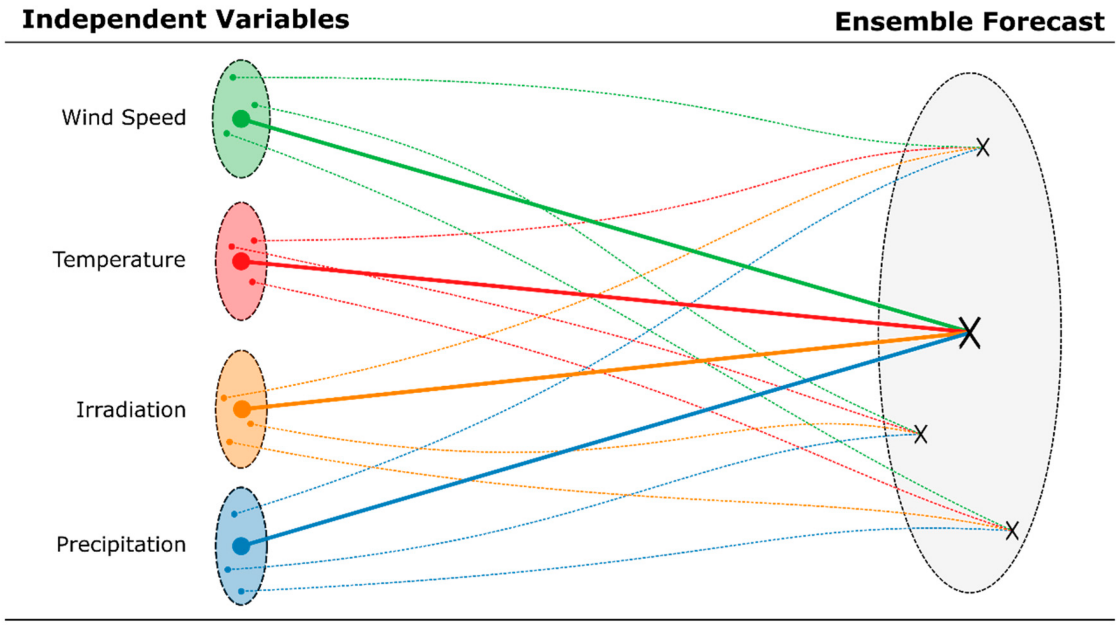

Figure 4.1: Visualization of an ensemble forecast. Rather than employing a deterministic/point method (thick lines) to obtain the output from input variables, an ensemble of predictions is made from varied input conditions (dashed lines), constructing an uncertainty region and most likely output value(s).

4.2 State-of-the-Art

As mentioned, the use of ensemble methods is gaining popularity with the increased complexity and uncertainty of distributed energy resources (DERs). Before presenting the proposed method, a review of recent works is presented to highlight the state-of-the-art scientific literature on ensemble methods applications to power systems in recent years.

In Reference [128], different strategies for combining forecasts of solar photovoltaic (PV) generation were presented. In this study, the ensemble prediction was obtained by combining different probabilistic models rather than an ensemble of results of the same model. It used three models (i.e., QKNN, QRF, and QR) and the inputs were historical PV power and weather data. By testing using the GEFCOM 2014 data, the results showed that the use of an ensemble of various probabilistic forecasts resulted in a significant increase in forecasting accuracy for solar photovoltaic (PV) systems as opposed to the use of individual ones, regardless of the ensemble strategy and/or scenarios considered.

In Reference [129], the advantages and disadvantages of applying an ensemble to improve empirical mode decomposition (EMD) techniques were reported, which are mentioned as being commonly applied to wind forecasting. While the ensemble improved EMD models are associated with additional computational burden, they are reported to outperform other techniques, specifically in tackling the challenge of mode mixing. In addition, the authors reported it was significantly more beneficial to apply ensemble decomposition to artificial neural network (ANN) models as compared to using optimization methods to tune the ANN parameters. The previous statements were shown to hold for all time resolutions in wind power forecasting. In Reference [127], a comparison of numerous commonly used ensemble, ANN, and other ML techniques was performed for solar power forecasting. Random Forest (RF), an ensemble method, was found to exhibit the best performance. Two main conclusions were made by the study: (1) a seasonal bias was shown with spring and winter being more challenging to forecast than summer and autumn (keeping in mind that the data were from Norwich, UK) and, more importantly, that (2) a combination of simple algorithms yielded better and more reliable results than any individual algorithm on its own, regardless of its complexity.

In Reference [130], a short-term probabilistic forecasting method was proposed based on a competitive ensemble of different base predictors of PV power. The method was implemented using different probabilistic approaches which were trained as base predictors in order to obtain an ensemble of the predictive distribution with optimal characteristics of accuracy and reliability. In Reference [131], the reliability, robustness, and computational burden of a proposed PV power forecasting model based on the RF method was combined with the extra trees technique on an hourly basis and compared against supervised support vector regression. For a fair and comparative analysis, the models used comparable forecasting data, applicable for forecasting hourly PV power.

A probabilistic PV power forecasting model was proposed in Reference [132] and applied to several French PV plants considering six days of lead time with a resolution of thirty minutes. The proposed model was derived from multiple forecasts considering the national numerical weather predictions and including ensemble forecasts. Then, a free online parameter learning technique generated a weighted combination of the individual PV outputs, and the resulting weights were later sequentially computed before each forecast, using only historical data, with the goal of minimizing the continuous ranked probability score criterion.

An analog ensemble forecasting method for day-ahead regional with hourly resolution was presented in Reference [133]. The proposed model considered publicly available weather forecasts and power measurement data, considering some historical sets of temperature, irradiance, and terrain slopes as well, among others. To process the input data, clustering and blending strategies were used to improve the PV forecasting results which were compared and validated against several numerical models based on weather forecasts.

Photovoltaic power variability was studied in Reference [134], proposing a data-driven ensemble modeling technique to improve the forecasting of PV output. Also, three different models were analyzed within a recursive arithmetic average technique, considering stand-alone forecasting results. To prove the superiority of the proposed model, the comparison was carried out considering a considerable number of different training and testing samples, showing that the ensemble model generally outperforms different stand-alone forecasting models.

A PV forecasting model in Reference [135] used an ANN ensemble scheme based on particle swarm optimization with trained feed-forward neural network. The proposed model was constructed considering five different structures with varying network complexities, in order to improve the forecasting results. Then, the model was combined using trim aggregation after removing the error boundaries. Exogenous data, such as physical specification and environmental, were used as model inputs. Moreover, a clearness index was used to classify days accordingly with their features, considering a yearly basis analysis with a real case study. It was shown that ensemble schemes improve the forecast results in comparison with benchmark models.

In Reference [136], an hourly PV power forecasting model was presented based on clustering and ensemble prediction using the RF method. First, clustering was used to improve the computational burden by selecting the necessary weather variables. Then, the RF method with different parameters was implemented as a component model to find weather regimes making up the ensemble prediction. Finally, weighted computation was carried to analyze the different forecasting weather regimes in order to obtain the final results. Ridge regression was used to determine the weight of each weather variable automatically.

In Reference [137], a hybrid PV forecasting model combined the ML method with the Theta statistical method. Multiple ML components were used: long short-term memory, gate recurrent unit, and unsupervised learning. Structural and data diversity were key to improving the accuracy of the model. Four different approaches were implemented for validation, considering two real case studies. The proposed hybrid model was shown to be superior to traditional ML without statistical components.

In Reference [124], a new ensemble technique was employed to improve probabilistic forecasting of day-ahead price forecasting of the Iberian market. An approach based on kernel density estimation (KDE) was used to "activate" the best set of input variables which minimize the forecasting error. This study is an example of numerous others applying probabilistic and ML techniques for electricity price forecasting which has been increasing exponentially in the past decade as shown by Reference [6]. The latter shows that, while non-existent before 2003, probabilistic methods (or hybrid ones) have quickly gained ground as one of the main approaches used contemporarily for price forecasting [138, 139, 140].

The analysis in Reference [141] has shown that, for the case of price forecasting, while combining different forecasts in an ensemble framework does not necessarily always bring about improved accuracy, it does contribute to more reliable forecasting by decreasing the risk associated with an individual method.

Based on the conducted literature review, the following points were noted and were carried forth in the formulation, analysis, and discussion made throughout this chapter:

- The use of combinatorial ensemble techniques is shown to significantly improve the accuracy of RES-based DG forecasting in addition to guaranteeing a more reliable and/or robust prediction;
- An ensemble of simple probabilistic/statistical techniques is shown to produce better and more robust DG forecasting than individual complex models;
- KDE has been recently employed to "activate" input sets for probabilistic price forecasting models, showing great success in improving the accuracy. This was only found to be tested on price forecasting, and no studies were found using this methodology for DG forecasting [124].

4.3 Proposed Methodology

Consider an output variable P that has a value which depends on a set of inputs $\mathrm{V} := \{v_1, v_2, \ldots N_V\}$ through some unknown model f:

$$P = f(\mathrm{V}) = f(v_1, v_2, \ldots N_V) \tag{4.1}$$

where N_V is the number of independent variables which affect output P. For the purpose of generalization, the inputs V are considered multidimensional, such that:

$$v_1 = \{v_{1,1}, v_{1,2}, \ldots v_{1,H_1}\} \tag{4.2}$$

In this case, H_1 is the number of dimensions of v_1. Now, consider scenario "new" for which we are trying to predict the output P_{new}, given a set of conditions V_{new}:

$$P^{\text{new}} = f(\mathrm{V}^{\text{new}}) = f(v_1^{\text{new}}, v_2^{\text{new}}, \ldots N_V^{\text{new}}) \tag{4.3}$$

The goal is to predict the value of P_{new} given only the new conditions V_{new} and a historical set of N_o cases (with no knowledge of f):

$$P^{old,o} = f\left(\mathrm{V}^{old,o}\right) = f\left(v_1^{old,o}, v_2^{old,o}, \ldots N_V^{old,o}\right), \quad \forall \quad o = 1,2,\ldots,N_o \tag{4.4}$$

While the model function f is assumed to be chaotic, in this model we assume that the number of independent input variables and their dimensions remain constant and, therefore, the following equations hold:

$$N_V^{\text{new}} = N_V^{\text{old},o} = N_V; H_i^{\text{new}} = H_i^{\text{old},o} = N_H; \quad \forall o = 1,2,\ldots,N_o; i = 1,2,\ldots,N_V \tag{4.5}$$

At this stage, the objective was to select a subset of N_s cases which were most suitable to form an ensemble prediction of P_{new}. To do this, the KDE function similar to Reference [124] was used to calculate a similarity index $_{sold,new}$ between the new case and each of the old cases in the historical dataset. In this case, the most similar N_s cases (with the highest similarity index) can be activated by means of the product of kernel functions of each variable. This is visualized in Fig. 4.2.

The Gaussian kernel functions were used to construct the similarity index KDE, as they are most suitable for cases when little or no knowledge of the model is known.

$$s_{old,new} = \left(\prod_i^{N_V}\prod_j^{N_H} e^{-\frac{1}{2}\left(\frac{v_{i,h}^{old} - v_{i,h}^{neu}}{b_i}\right)^2}\right)^{\frac{1}{N_V N_H}} \tag{4.6}$$

The bandwidth value b_i can be used to increase or decrease the sampling window (relative to the full range of the historical samples) for each variable in the same manner that KDE works, i.e., the narrower the bandwidth, the higher assumed correlation between variable v and the output P. Therefore, the value of b_i for each variable i can be expressed by means of a tuning coefficient α_i:

$$b_i = \alpha_i \left(\max_{\mathrm{o}}\left(v_i^{old,o}\right) - \min_{\mathrm{o}}\left(v_i^{old,o}\right)\right); \quad \forall \quad o = 1,2,\ldots,N_o; i = 1,2,\ldots,N_V \tag{4.7}$$

In this way, this normalized tuning coefficient is varied from 0 (exclusive) to 1 (inclusive), corresponding to a bandwidth value between zero (exclusive) and the maximum range of the historical value of the variable (inclusive):

$$0 < \alpha_i \leq 1 \quad \forall \quad i = 1,2,\ldots,N_V \tag{4.8}$$

The similarity index in (4.6) can be simplified in case all input independent variables are scalars. In this case, N_H is equal to one, and the equation is reduced accordingly:

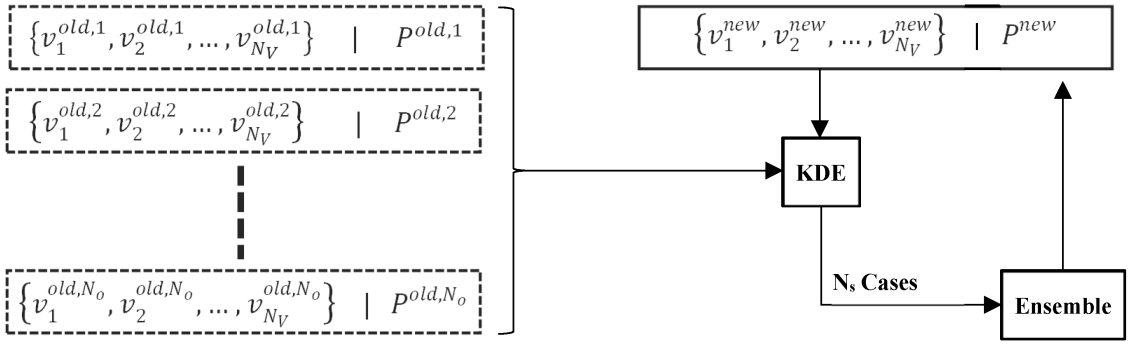

Figure 4.2: Demonstration of how the proposed Kernel Density Estimation (KDE)-based similarity index is used to extract N_s cases to form an ensemble prediction of the new output value.

$$s_{old,new} = \left(\prod_{i}^{N_V} e^{-\frac{1}{2}\left(\frac{v_i^{old} - v_i^{new}}{b_i}\right)^2} \right)^{\frac{1}{N_V}} \tag{4.9}$$

Given a new case, the similarity index is calculated for all old cases in the historical dataset. We can now construct a sorted array S which has elements that correspond to the index of the old case; this array thus contains the indices of the historical dataset, sorted from most to least similar to the current case based on their calculated similarity index in (4.9):

$$\mathrm{S} = [k_1, k_2 \ldots k_{N_o}] \tag{4.10}$$

In this case, k_1 is the index o of the historical case with the highest, k_2 to the second highest, etc. Now, the top N_s samples can be selected to perform the ensemble prediction. The simplest prediction is to calculate the mean value of the top N_s P_{old} values:

$$\hat{P}^{\text{new}} \approx \frac{\sum_{i=1}^{N_s} P_{k_i}^{\text{old}}}{Ns} \tag{4.11}$$

To obtain a confidence/uncertainty interval around this expected output, percentile ranks can be used by constructing a cumulative distribution function of the top N_s values. By doing so, a confidence interval can be determined as follows:

$$\hat{P}_{lb,x\%}^{\text{new}} \leq \hat{P}^{\text{new}} \leq \hat{P}_{ub,x\%}^{\text{new}} \tag{4.12}$$

$$\hat{P}_{lb,x\%}^{\text{new}} = \rho_{\frac{1}{2}(100-x)\%} \left(\left\{ P_{k_1}^{\text{old}}, P_{k_2}^{\text{old}}, \ldots, P_{k_{Ns}}^{\text{old}} \right\} \right) \tag{4.13}$$

$$\hat{P}_{ub,x\%}^{\text{new}} = \rho_{\frac{1}{2}(100+x)\%} \left(\left\{ P_{k_1}^{\text{old}}, P_{k_2}^{\text{old}}, \ldots, P_{k_{Ns}}^{\text{old}} \right\} \right) \tag{4.14}$$

What (4.12) means is that for a confidence of $x\%$, P^{new} lies between the lower and upper bounds equal to $\hat{P}^{\text{new}}_{lb,x\%}$ and $\hat{P}^{\text{new}}_{ub,x\%}$, respectively; which are calculated, as per (4.13) and (4.14), by means of the percentile $\rho_{\frac{1}{2}(100-x)\%}$ and $\rho_{\frac{1}{2}(100+x)\%}$ of the top N_s values $\left(\left\{P^{\text{old}}_{k_1}, P^{\text{old}}_{k_2}, \ldots, P^{\text{old}}_{k_{Ns}}\right\}\right)$, respectively. These constitute the confidence bounds of the forecast.

It must be noted that there are clearly more complex means of calculating $x\%$, P^{new}, and the confidence bounds. However, the main focus of this study was to highlight the use of the similarity index to extract the set S, and the choice of the simplest ensemble prediction afterwards was intentional to demonstrate the power of such a selection algorithm even with the most basic ensemble applied.

4.4 Case Study and Validation

4.4.1 PV Installation in Portugal

In order to test and validate the proposed algorithm, a real case study was used based on solar PV installations located in the vicinity of the city of Coimbra in the center region ("*Região do Centro*") of Portugal as shown in Fig. 4.3. The technical specifications of the plant are listed in Table 4.1. Historical forecasts and measurements are available for the same installation for a full year from 15 March 2015 to 15 March 2016 as detailed in Table 4.2. Annual plots of all variables are provided in Appendix A.

In this case, the historical weather forecasts were the input variables (V) and are publicly provided by the Global Forecasting System (GFS) model with a 22 km resolution. The GFS's data are available for any region of the world and is publicly available online [142]. The forecasts are made at 18:00 (UTC time) of each day for the day-ahead with a 3 h resolution (average of each 3 h interval of the day: 0:00, 3:00, 6:00, ..., 21:00). The provided forecasts are for wind speed, temperature, solar irradiance, precipitation, and humidity.

The output AC power of the inverter was recorded for the same year. A 20 kW SMA Sunny Tripower inverter was installed with 2 maximum power point trackers (MPPTs) installed (4 strings per inverter). The logging frequency of the AC power output was approximately 5 min. For this study, the recorded AC power was synchronized with the forecasts by applying a 3 h average (averaging can be seen in Figure A.6). It is important to stress that the proposed prediction method was only given the averaged output power as input. However, high-resolution data were used for validation to test if uncertainties associated with high frequencies were captured.

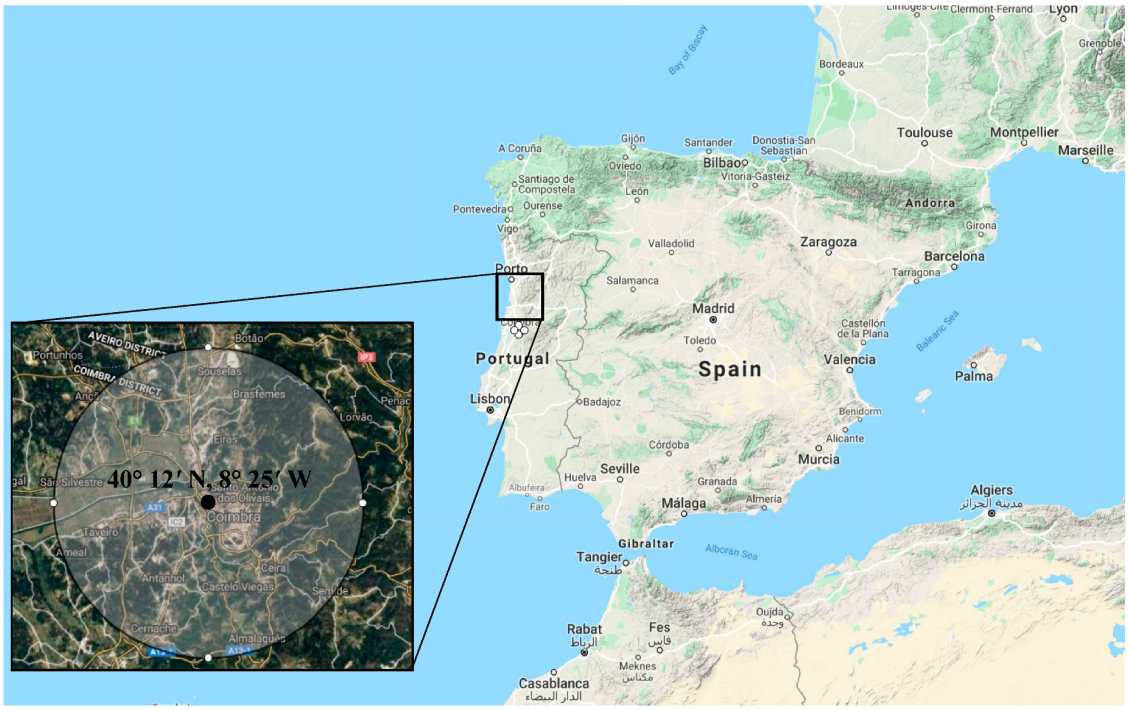

Figure 4.3: Region in the center of Portugal used as a case study. The PV installations used in the current analysis were located within a 10 km radius of the city of Coimbra (40°12' N, 8°25' W).

Table 4.2: Variables in the historical dataset provided (from 15 March 2015 to 15 March 2016).

Historical Variable	Data Source	Spatial Resolution	Temporal Resolution	Units
Wind Speed	Meteorological Forecast	22 km	3 h	m/s
Temperature	Meteorological Forecast	22 km	3 h	°C
Solar Irradiance	Meteorological Forecast	22 km	3 h	W/m^2
Precipitation	Meteorological Forecast	22 km	3 h	mm
Humidity	Meteorological Forecast	22 km	3 h	%
Inverter AC Power (Output)	Real Measurement	-	∼5 min	kW

Table 4.1: Technical specifications of the PV plant used as a case study.

Parameter	Value	Units
Number of Panels (300 kWp each)	53	-
Panel Area (each)	1.713	m^2.
Total Installed Capacity	18	kWp
Inverter Capacity	20	kW
Nominal DC Voltage	600	V
Overall Efficiency	20	%

4.4.2 Numerical Irradiance-Based Forecast

Given that the GFS data and the output power were synchronized, and since MPPTs were installed with the inverters, one can use the following equation to predict the maximum possible power output from the current installation for each data point.

$$P_t \approx P_t^{irr} = \eta_{avg} N_p A_p R_t^{wf} \tag{4.15}$$

where P_t^{irr} is the predicted power output at time t calculated numerically from the irradiance forecast, η_{avg} is the overall average energy conversion efficiency of the PV plant (accounting for the PV conversion and inverter efficiency), N_p and A_p are the number of panels and the area of each panel (in m^2), respectively, and R_t^{wf} is the direct incident solar irradiance (in W/m^2) obtained from the weather forecast for time t.

4.4.3 Seasonal Test Weeks

Also, in order to check for seasonal effects and/or bias, four test weeks were extracted from the annual data corresponding to all four seasons. The annual measured output power, annual predicted maximum output (based on irradiance estimation in (4.15), and detailed plots thereof for all four representative weeks are shown in Fig. 4.4.

By inspecting the plots shown in Fig. 4.4, particularly comparing the maximum theoretical output based on irradiance and recorded power, two important observations are worthy of noting:

- During the summer, the maximum power output prediction based on (4.15) was greater than the recorded value. This is what one would expect, and the operating efficiency and/or reliability of the installation would seldom reach the maximum theoretical power output;
- During the winter, the prediction based only on solar irradiation failed to predict any value of output power (one can see that the predicted values were zeros throughout the winter and also by looking at the plot of the winter week). This is due to the fact that the meteorological forecasts provided by GFS are averaged over large temporal and spatial resolutions. As a result of the averaging, the forecast irradiance dissipates to zero during the winter.

As such, it is clear that relying solely on the irradiance models, is insufficient to make any prediction of the expected power output of the solar PV installations.

Therefore, the objective of this case study was to check if the proposed method, taking into consideration GFS data as input variables and the recorded (and synchronized) AC power output of the plant, would be capable of accurately forecasting the power output under different meteorological conditions.

Table 4.3: Description of input variables for the historical dataset and value chosen for bandwidth coefficient for the KDE-based similarity index calculator.

Bandwidth Coefficient	Value
α_{v1} (hour of the day)	0.4
α_{v2} (day of the year)	1.0
α_{v3} (wind speed forecast)	0.8
α_{v4} (temperature forecast)	0.5
α_{v5} (solar irradiance forecast)	0.1
α_{v6} (precipitation forecast)	0.8
α_{v7} (humidity forecast)	0.5

The GFS meteorological data are plotted for the entire year in Fig. A.1, Fig. A.2, Fig. A.3, Fig. A.4, Fig. A.5 and Fig. A.6 in the Appendix A. Zoomed-in plots are also provided for each test week in order to show the seasonal differences and highlight some visible correlation between the weather conditions and the recorded AC power output. The plots of spring, summer, autumn, and winter are shown in Fig. 4.5, Fig. 4.5, Fig. 4.5 and Fig. 4.5, respectively.

4.4.4 Implementation and Validation

To test the proposed algorithm in Section 4.3, the power output for each of the four test weeks was forecasted, only taking as input variables the meteorological forecasts provided by GFS. The hour of the day and day of the year were appended to the array of input variables in order to give the potential of favoring closer times/dates. The input variable array for this case was as follows:

$$V = \{v_1, v_2, v_3, v_4, v_5, v_6, v_7\} \tag{4.16}$$

The description of each variable and the choice of the bandwidth tuning coefficients, as in (4.7) and (4.8), are provided in Table 4.3. As explained in Section 4.3, the smaller the value of α, the higher the assumed correlation between the output variable and its corresponding input variable. The values used in this study were assumed based on the well-established physical relationships between each meteorological variable and the target one (PV output power). For instance, solar irradiance was associated with the most dependence and thus a value of 0.1 was chosen, etc. This can heuristically be set based on visual inspection of Fig. 4.5, Fig. 4.6, Fig. 4.7, and Fig. 4.8.

In order to investigate the performance of the proposed algorithm, the results obtained for the four test weeks are against the numerical irradiance-based forecast based on (4.15), and an ANN (trained using the same data). A feed-forward ANN was used with 1 hidden layer and 10 neurons. The performance of all three methods was compared in terms of computational time and accuracy. Since the ANN was trained using the Levenberg–Marquardt algorithm [143], its results and computational time both varied in every run due to the random data division and training process employed. Therefore, to evaluate the results in a fair manner, the ANN was run a sufficiently large number of times (10,000 runs), and the average runtime and forecast results were used for comparison.

To quantify the forecast error, three criteria were used: the mean absolute error (MAE), root mean square deviation (RMSD), and the normalized root mean square deviation (NRMSD). The MAE provides a simple overall measurement of the mean error between forecasted $\hat{P}$ and real P values:

$$MAE = \frac{\sum_{t=1}^{N_t} \left| \hat{P}_t - P_t \right|}{N_T} \tag{4.17}$$

where the subscript t corresponds to the value at time step t and Nt is the total number of time steps. The RMSD is based on the on the quadratic mean:

$$RMSD = \sqrt{\frac{\sum_{t=1}^{N_t} \left(\hat{P}_t - P_t \right)^2}{N_T}} \tag{4.18}$$

Both the MAE and RMSD provide a scale-dependent measure of the deviation between the forecasted and real values. The NRMSD provides a normalized measure as a percentage which is sometimes more favorable when comparing different models.

$$NRMSD = \frac{RMSD}{(P_{\max} - P_{\min})} \cdot 100\% \tag{4.19}$$

P_{max} and P_{min} are the maximum and minimum values of the real data, respectively. As such, the NRMSD provides a scale-independent measure. The MAE, RMSD, NRMSD, and computational time are all used to assess the performance of the different approaches for all four test weeks.

The proposed algorithm was developed as original code by the authors using the MATLAB R2019b environment on a standard laptop computer with the following specifications: Intel Core i7-8550U CPU @ 1.80 GHz, 16.0 GB RAM, Windows 10 64 bit operating system. The neural network used for validation was based on the MATLAB 2019b Statistics and Machine Learning Toolbox [143].

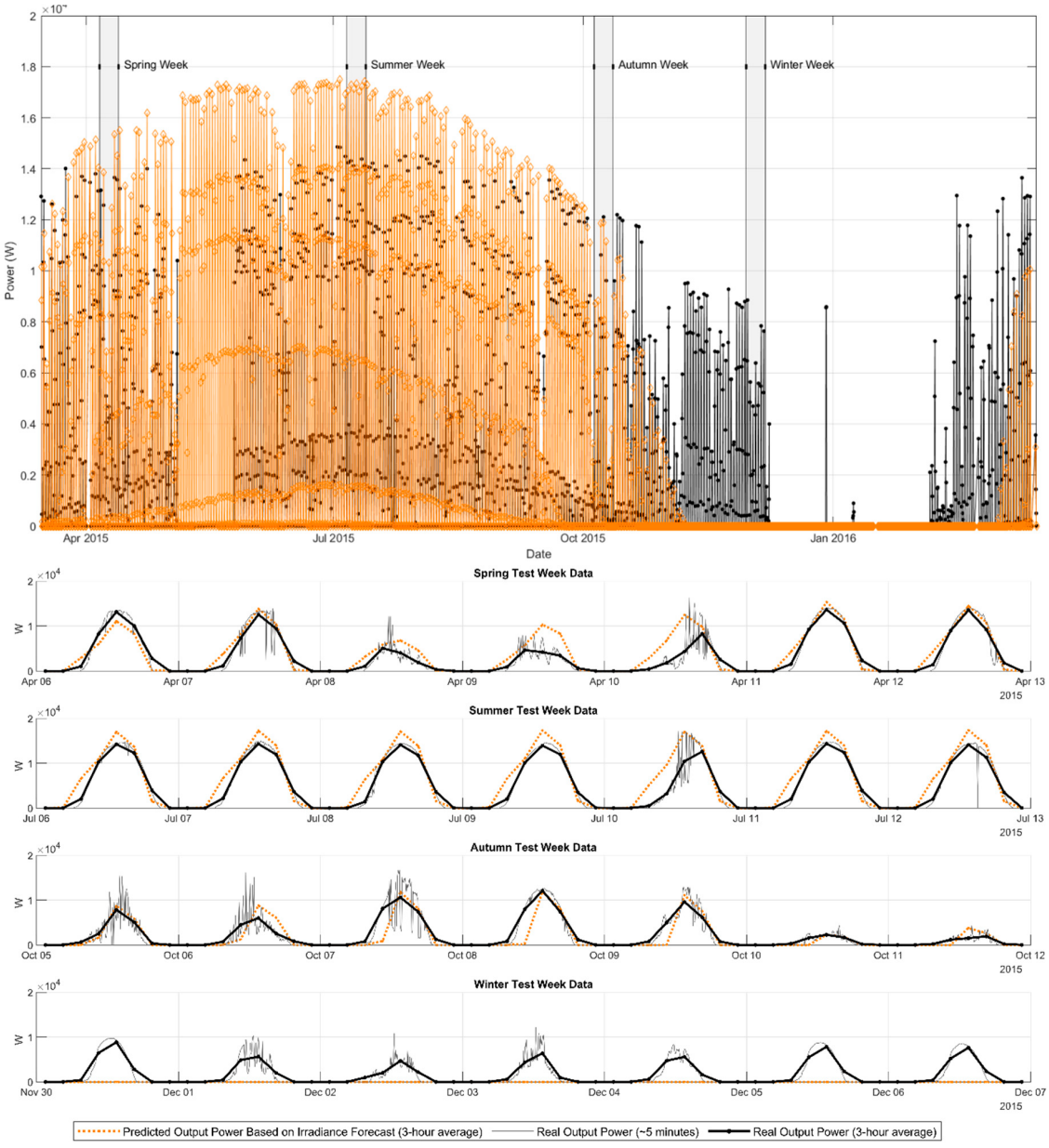

Figure 4.4: Annual plot of recorded AC power output, annual plot of maximum theoretical power output based on solar irradiance estimation and average efficiencies, and four test weeks representing all four seasons (top); and for each test week, zoomed-in plots of recorded AC power output (un-averaged), 3 h averaged recorded AC power output (synchronized with GFS data), and maximum theoretical power output based on solar irradiance estimation and average efficiencies (bottom).

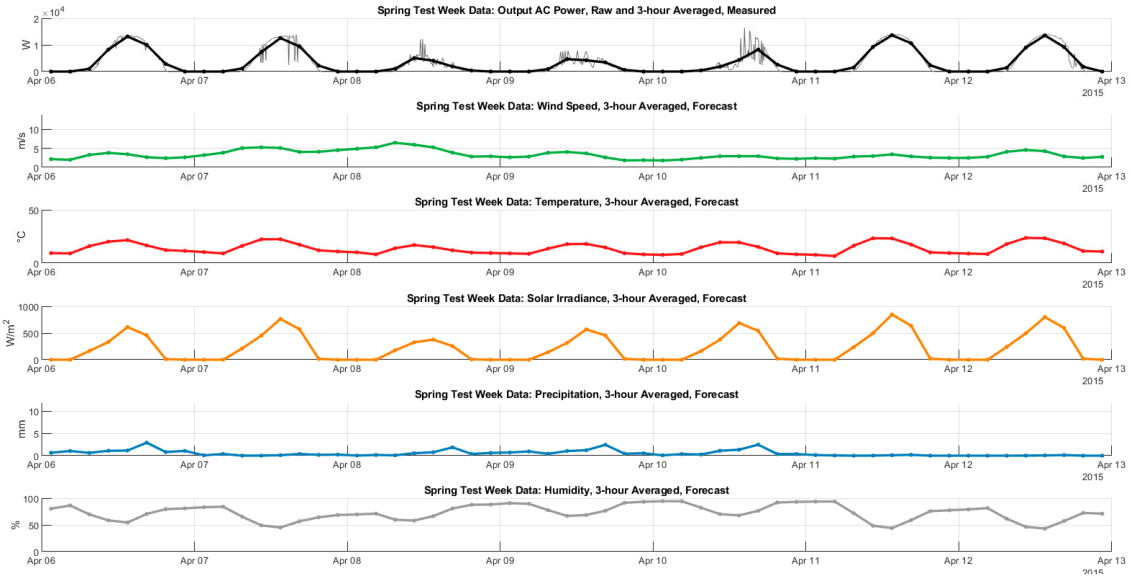

Figure 4.5: Plots of recorded output power and Global Forecast System (GFS) meteorological data for the spring test week.

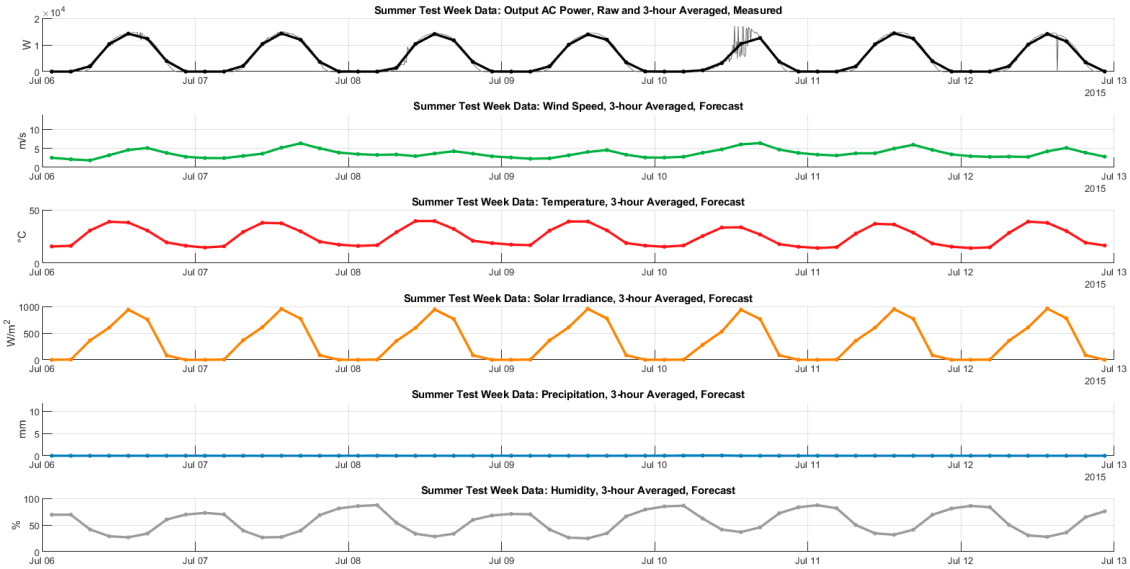

Figure 4.6: Plots of recorded output power and GFS meteorological data for the summer test week.

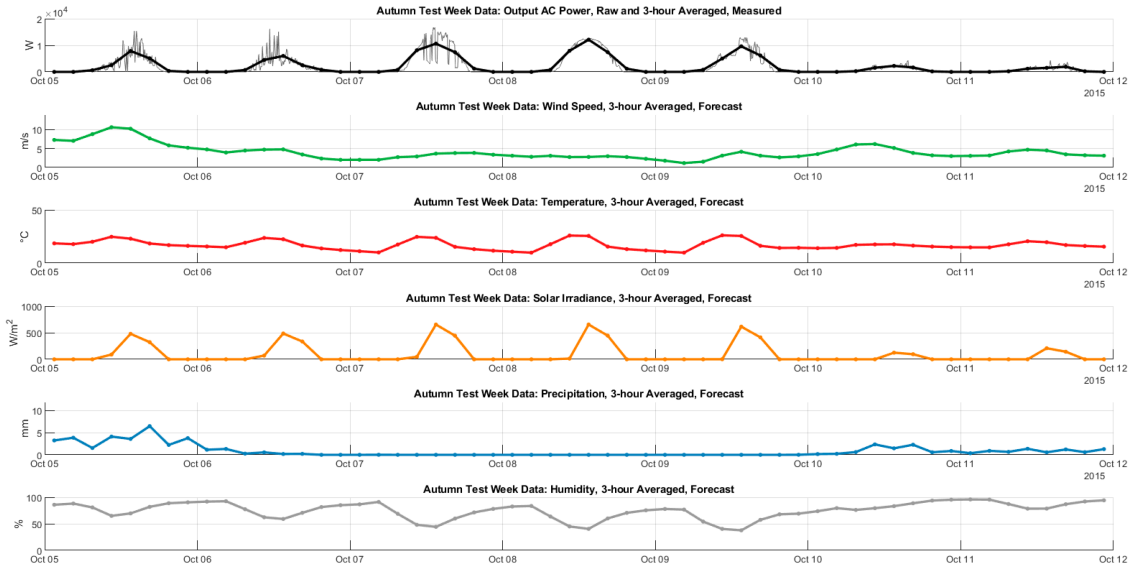

Figure 4.7: Plots of recorded output power and GFS meteorological data for the autumn test week.

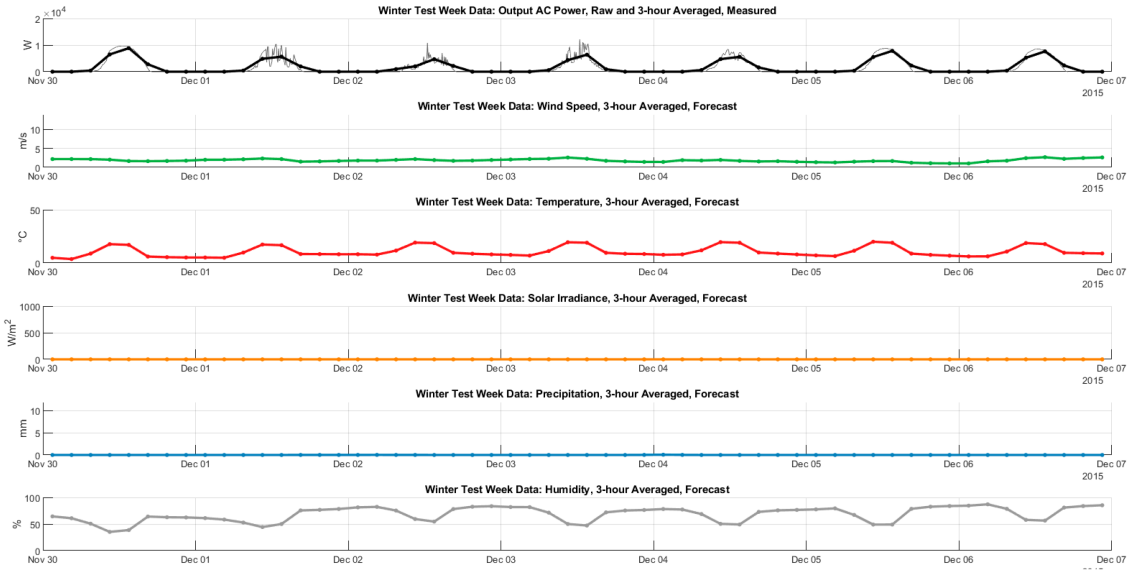

Figure 4.8: Plots of recorded output power and GFS meteorological data for the winter test week.

4.5 Results and Discussion

4.5.1 Results of the Proposed Ensemble Algorithm

The results of the proposed ensemble algorithm are shown in Fig. 4.9. The predicted value was plotted, along with confidence intervals of 68%, 95%, and 99.7%. The following points are noted:

- The proposed ensemble algorithm successfully managed to forecast the PV power output, relying only on the historical GFS meteorological data, for all four tests weeks of all seasons;
- The power production in cases when the deterministic model based on irradiance was inadequate (i.e., winter season) was successfully predicted;
- Despite only being provided averaged data, the confidence intervals successfully managed to cover high-frequency fluctuations during most days;
- The confidence interval grows and shrinks in response to such fluctuations even within the same day (e.g., Summer week, day 5);
- The forecasts mostly underestimated the power output. This is favorable to overestimation particularly from the point of view of operators of DG installations.

4.5.2 Comparison and Validation

A comparison between the forecast obtained and that of an irradiance-based numerical model (in (4.15)) and an ANN was used to validate the proposed method. As elaborated in the previous section, the same data were used to train the ANN. Since a random data division and training method was employed (which aimed to minimize the computational time of the ANN), the average of a sufficiently large number of runs of the ANN (i.e., 10,000 runs) was used for a fair comparison.

The comparison was made considering the MAE, RMSD, and NRMSD error criteria for each of the test weeks and is shown in Table 4.4. The different forecasts are visualized in the plots shown in Fig. 4.10. The computational time to forecast all four weeks by the proposed method and the ANN (average of 10,000 runs in each case) is shown in Table 4.5.

By comparing the results of the different models, the following points can be verified:

- According to all error criteria used, the proposed method outperformed the irradiance-based prediction for all seasons. It outperformed the ANN in all seasons except winter;
- Both the ANN and the proposed method managed to provide a reasonably accurate prediction of the output power in the winter, where a numerical irradiance-based model completely fails;
- Despite the ANN being capable of providing a better average error for the winter, the capability of the proposed method to capture high-frequency fluctuations in its confidence intervals provides an advantage over the ANN;

Table 4.4: Comparison of the MAE, RMSD, and NRMSD error criteria for the results obtained for each of the test weeks from the irradiance forecast, ANN, and the proposed method.

Criterion	Method	Winter	Spring	Summer	Autumn
MAE (kW)	Irradiance Forecast	34.6	15.7	17.4	15.3
	Neural Network	10.7	15.5	8.4	7.9
	Proposed Method	12.6	14.0	3.6	7.7
RMSD (kW)	Irradiance Forecast	3.062	2.138	2.508	1.857
	Neural Network	0.949	2.114	1.203	0.951
	Proposed Method	1.115	1.914	0.523	0.928
NRMSD (%)	Irradiance Forecast	34.6	15.7	17.4	15.3
	Neural Network	10.7	15.5	8.4	7.9
	Proposed Method	12.6	14.0	3.6	7.7

- The proposed method was extraordinarily fast in terms of computational time, being 32 times faster than the ANN while outperforming the ANN in the majority of situations.

4.5.3 Prospects for Future Work

After testing the proposed method, confirming its validity, and taking note of its superior performance particularly in terms of providing an accurate forecast with high computational efficiency, the following recommendations are provided for future work following on this study:

- The effect of using additional meteorological variables (e.g., absolute and relative atmospheric pressure) should be investigated in terms of the forecast accuracy and computational burden;
- Optimal tuning of the bandwidth coefficients should be studied. This can be performed in a pre-processing stage (e.g., with correlation analysis) or using a reinforcement learning-based design in which the values are self-tuned every time the code is run. In the latter, using an optimization method to determine the optimal values may be an option for a hybrid structure;

Table 4.5: Comparison of the computational time between the proposed method and the ANN.

	Computational Time to Forecast all Four Weeks (Average of 10,000 runs)
Neural Network	1.46 s
Proposed Method	0.045 s

- Due to the fact of its high computational efficiency and its reliance only on publicly available historical weather forecasts, the proposed method seems to have great potential to be applied to forecast RES-based DG. As such, follow-up work should test the proposed method on other RES technologies such as wind power. Moreover, while the study focused on RES-based DG forecasting, the method can be employed for any local forecasting (e.g. load demand forecasting), paving the way to the fully decentralized energy system paradigm.

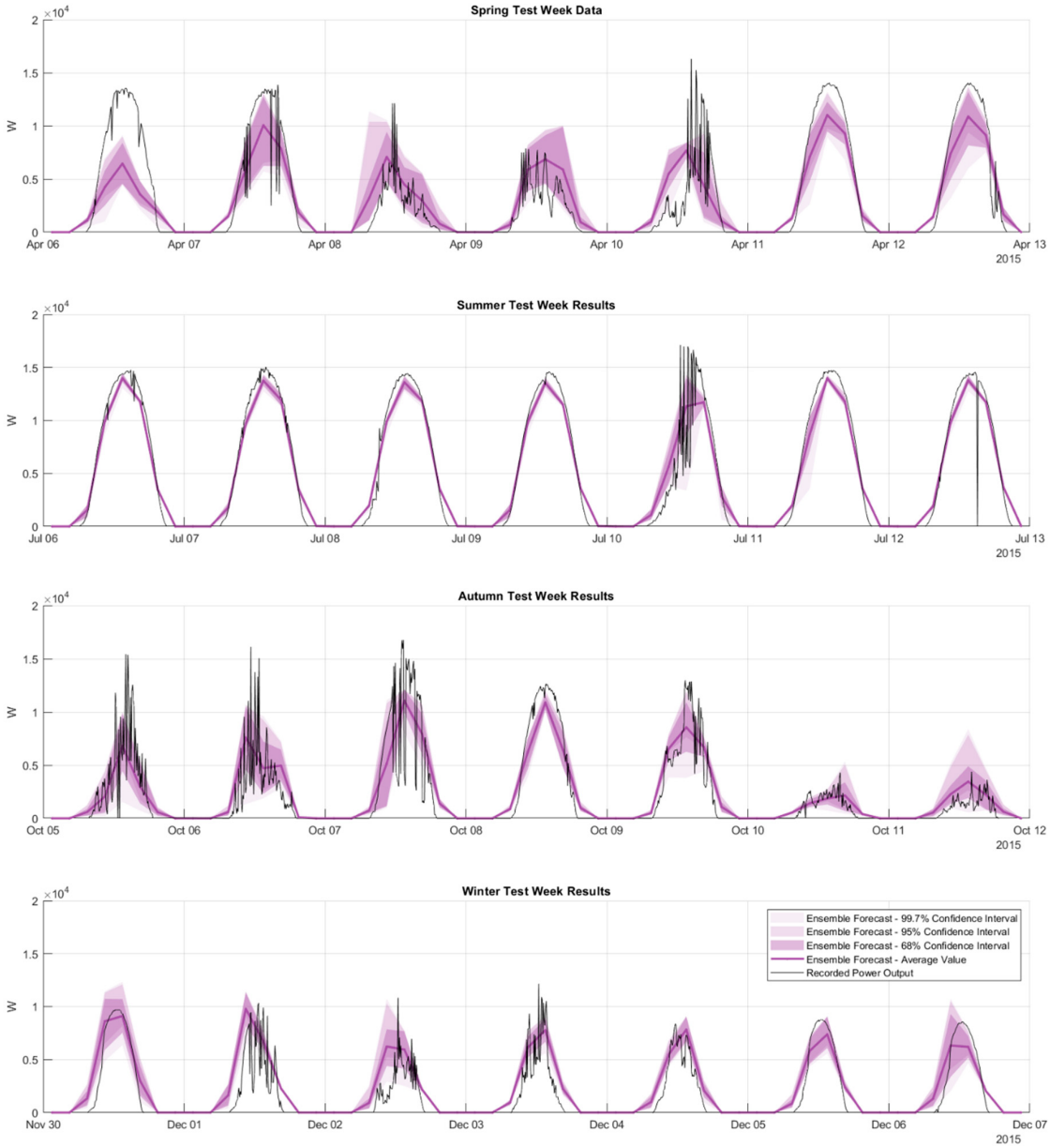

Figure 4.9: Results of the proposed algorithm for all four seasons, showing real output power (un-averaged) and predicted output power. Confidence intervals of 68%, 95%, and 99.7% are highlighted.

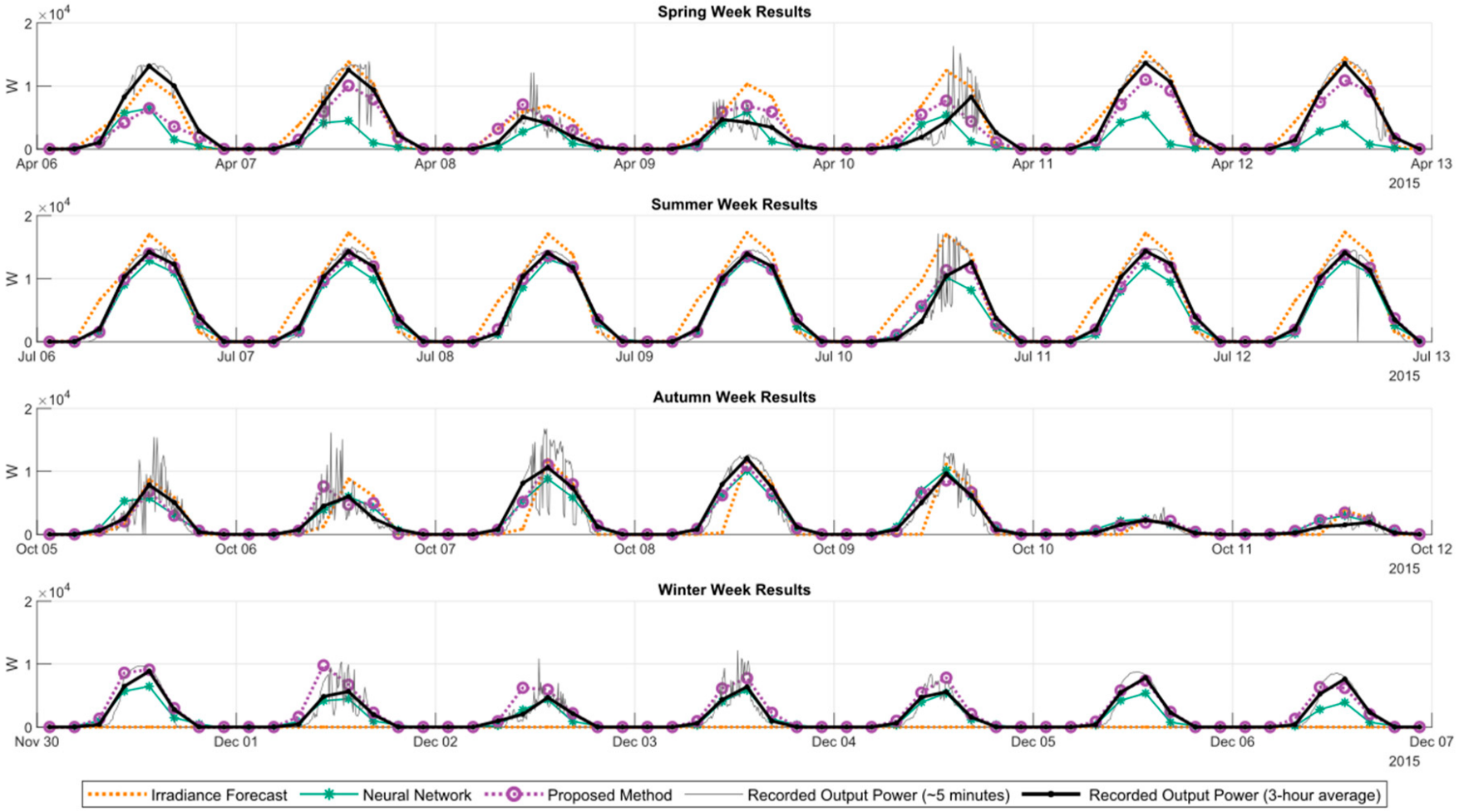

Figure 4.10: Comparison of results obtained by irradiance forecast estimate, ANN, and the proposed method for all four seasons.

4.6 Conclusions

In this chapter, a novel ensemble algorithm based on kernel density estimation (KDE) was proposed to forecast RES-based DG. The proposed method relies solely on publicly available historical series of independent input variables (i.e., historical meteorological data) and the corresponding local output (i.e., recorded power generation). Given a new case (with forecasted meteorological variables), the resulting power generation was forecasted. For the new case to be forecasted, a KDE-based similarity index was used to determine a set of most similar cases from the historical dataset. Then, the corresponding outputs of the most similar cases were used to calculate an ensemble prediction for the forecasted power generation. The proposed method was tested by considering meteorological and recorded power generation from a PV installation around the city of Coimbra, in the center region of Portugal. Despite only being given averaged data as inputs, the developed algorithm was capable of predicting uncertainties associated with high frequency variations in weather conditions, outperforming deterministic prediction based on solar irradiance forecasts. The proposed method outperformed an ANN in most cases while being exceptionally faster (32 times). Given its exceptional computational efficiency and its reliance solely on public data (weather forecasts) and local metered data (power generation), it is a convenient tool for use by owners or operators of DG installations, including small-scale prosumers, to effectively forecast their expected generation without depending on private/proprietary data or divulging their own.

The method developed in this chapter enables fully decentralized local forecasting, compatible with the cloud-based IoE paradigm. While the study focused on RES-based DG forecasting, the method can be employed for any local forecasting (e.g. load demand forecasting).

In the next chapter, the KDE-based similarity index concept is extended to develop a novel machine learning method for fully decentralized power flow management.

Chapter 5

Cloud-based Power Flow Management with Cooperative Information Exchange

Traditional power systems continually employed probabilistic methods to address uncertainties in an accurate and computationally efficient manner. The modern dismantling of the centralized operation paradigm is creating a renewed interest in probabilistic methods and their machine learning (ML) successors as potential enablers for fully decentralized smart grids (SG). In this chapter, a conceptual model is constructed for the transition from a fully centralized operation of a SG to a decentralized one, proposing the transition scheme between the two paradigms. A novel ML algorithm for fully decentralized operation is proposed, formulated, implemented and tested. The proposed algorithm relies solely on local historical data for local agents to accurately predict their optimal control actions without knowledge of the physical system model or access to historical data of other agents. The capability of cloud-based cooperative information exchange was augmented through a new concept of s-index activation codes, being encoded vectors shared between agents to improve their operation without sharing raw information. The proposed algorithm was evaluated using a modified IEEE 24-bus test system and synthetically generated historical operation data based on typical load profiles. A week-ahead high-resolution (15-minute) fully decentralized operation case was tested. The proposed algorithm is shown to guarantee less than 0.1% error compared to a centralized operation case and outperforming a NN model. The proposed algorithm is shown to be exceptionally accurate while being highly computationally efficient, and has great potential as a versatile model for fully decentralized operation of SGs.

Chapter Highlights and Novel Contributions:

- A conceptual model is constructed for the transition from a fully centralized operation of a SG to a decentralized one, proposing the transition scheme between the two paradigms.
- In a fully decentralized SG run by local agents, a novel ML algorithm is proposed and formulated (building on the method developed in chapter 4) to enable this transition and into cloud-based fully decentralized system operation.
- The proposed algorithm relies solely on the local historical data for each agent to accurately predict optimal control action without being given any information on the physical system from outside their local zones (i.e., full grid structure is unknown), and without access to historical data from other agents. As such, the proposed algorithm is designed not only to deal with variable uncertainties, but also missing / lacking information in a decentralized system.
- The proposed algorithm incorporates the capability of cloud-based cooperative information exchange without sharing private/raw data (e.g., local historical datasets or control actions taken locally). This is performed by proposing a new concept of an s-index vector, which is an encoded information that can be shared between agents to improve their control action predictions without sharing raw information.

Relevant Publication(s):

M. Lotfi, C. Monteiro, G.J. Osorio, M. Javadi, M.S. El-Moursi J.P.S. Catalão, "A Fully Decentralized Machine Learning Algorithm for Optimal Power Flow Management in Smart Grids with Cooperative Information Exchange," in *International Journal of Electrical Power & Energy Systems*
Submitted, In Review.

M. Lotfi, S. Fikry, G. J. Osório, M. Javadi, S. F. Santos and J. P. S. Catalão, "A Hybrid Probabilistic Algorithm for Computationally Efficient Estimation of Power Generation in AC Optimal Power Flow," *2020 IEEE 14th International Conference on Compatibility, Power Electronics and Power Engineering (CPE-POWERENG)*, 2020, pp. 169-174.
Published: https://doi.org/10.1109/CPE-POWERENG48600.2020.9161685

Chapter Nomenclature

Abbreviation	Definition
DR	Demand Response
DSM	Demand Side Management
DER	Distributed Energy Resources
FFT	Fast Fourier Transform
IoE	Internet of Energy
IoT	Internet of Things
KDE	Kernel Density Estimation
ML	Machine Learning
MAPE	Mean Average Percentage Error
MC	Monte Carlo
NW-KDE	Nadarya Watson Kernel Density Estimation
OPF	Optimal Power Flow
P2P	Peer to Peer
ERSE	Portuguese Energy Regulation Services Entity
pf	Power Factor
PLF	Probabilistic Load Flow
P-OPF	Probabilistic Optimal Power Flow
PPF	Probabilistic Power Flow
PDF	Probability Distribution Function
RTS	Reliability Test System
RES	Renewable Energy Resources
SG	Smart Grid

5.1 Introduction

5.1.1 Background and Motivation

Despite the profound differences between modern smart grids (SG) and traditional power systems of the past, the primary function remains unchanged: Achieve a balance between power generation and demand, doing so at the minimal possible cost while ensuring system reliability and stability. Optimal power flow (OPF) management is at the heart of this, aiming at identifying optimal generation capacity of controllable/dispatchable generators in a power grid such that the total demand is met. OPF ensures that an electrical power grid is operating at a minimal total cost given the current demand profile and its technical and security constraints. OPF analysis is indispensable for power system operators, being continuously employed to ensure that the system is running at minimal or near-minimal operating costs [144].

In a traditional power system, the system operator is a single central entity with access to all measurable variables in the power grid. Accordingly, constructing a deterministic AC power flow model is possible [105]. The AC-OPF thus incorporates all constraints, including the available generators' costs and limitations, grid structure, and associated safety constraints (e.g. bus voltage angle and transmission line power limits), to obtain the exact solution for ideal generation levels of individual generators. However, a deterministic AC power flow and the resulting AC-OPF models are both highly complex and highly non-linear, making it a formidable task to mathematically construct for each specific case, in addition to being computationally expensive to solve. Therefore, there has always been an interest in scientific literature to develop simplified and computationally efficient models, popularizing linear programming approaches [145, 146].

Linearized OPF models do alleviate the mathematical complexity and computational expense. However, they suffer from critical drawbacks. First, the obtained solution, while deterministic in nature, is approximate and may lack in accuracy. Furthermore, linearization approaches can only be applied if the objective function(s) are differentiable and continuous, and they do not consider uncertain or unknown variables model [147].

The presence of the latter has been an issue even for traditional power systems. While a centralized system operator would have access to all measurable variables in the grid, uncertain parameters in the model persist for two reasons. First, in conventional power systems not all variables are constantly being metered or measured. Second, the increased presence of renewable energy sources (RES) as non-dispatchable sources inherently creates uncertain parameters in the model [148].

Alternatively, quasi-deterministic and probabilistic methods have been developed to solve for power flow and OPF in the presence of missing / unmeasurable data and RESs uncertainties [149]. Quasi-deterministic methods, such as Monte-Carlo (MC) simulations, account for uncertain variables by randomly generating a sufficiently large number of input samples to cover the entire uncertainty range and obtaining a deterministic solution for each sample. Thus, the uncertainty range of input variables is used to generate an uncertainty range of the outputs. While this provides accurate and complete information on grid behavior, it is often computationally expensive [149].

Probabilistic approaches employ statistical models to convert probability distributions of input parameters to those of the outputs. Those have a significantly higher computational efficiency and do not necessitate constructing a physical system model, however they require knowledge of the uncertain variables' probability distributions from a historical dataset, being predecessors to modern machine learning (ML) algorithms [150].

In order to clearly identify the state-of-the-art progress on the development of probabilistic and ML methods for new SG management paradigms, a review of historical literature of the original probabilistic methods was first performed and is presented.

5.1.2 Historical Literature Review: History of Probabilistic Methods for Traditional Power Systems

Decades ago and prior to proliferation of renewable/non-dispatchable generation, stochastic behavior in electrical power grids existed essentially on the load side; hence the original name: "Probabilistic Load Flow" (PLF) which is still used interchangeably with probabilistic power flow (PPF). In 1974, Borkowska [151] published one of the pioneering papers to propose, implement, and test a PLF method for power system operation and planning.

The proposed method was used to obtain probability distribution functions (PDF) of branch (transmission line) power flows given those of input loads. First, three assumptions were made to simplify complex nonlinear equations: 1) linear relationship between branch flows and net nodal loads (linearized around expected values), 2) independence of active and reactive power, and 3) power balance is a function of the sum of input and output powers only (i.e. independent of individual nodal values).

Branch flow PDFs were then obtained by evaluating a recursive set of convolution integrations of the input and output PDFs. This could be used to obtain practically valuable information such as the probability of a line flow exceeding a certain value (e.g. capacity limit) or the realistically possible range for line loads. A major drawback of Borkowska's technique was that a very large number of convolution integrations (number of branches multiplied by the number of input and output PDFs) that had to be evaluated. This restricted the method to smaller networks due to limitations of both computational speed and memory, especially at the time, limiting its applicability to real life scenarios.

In 1981, Allan et al. [152] realized this issue and exploited frequency-domain multiplication, with Fast Fourrier Transforms (FFT), as a computationally efficient alternative to time-domain convolution integration. The results proved FFT to be superior to convolution both in terms of computational efficiency and accuracy. In addition to proposing a more efficient PLF method, the study performed multiple important validation studies. First, the results of PLF were compared against those of MC-5000 [1] for a case of high load value uncertainty (15x usual standard deviation). The results were highly similar with a slight skew in the PDFs which was not significant for practical applications where realistic uncertainties are much lower.

[1] Monte-Carlo simulations are labeled as MC-X, where X is the total number of samples generated.

Second, the use of central limit theorem was considered. Results showed that even when all input variables had a normal distribution, the output did not due to the inherent non-linearity of the system. Therefore, it was concluded that the theorem should not be used regardless of the system size. This method was later extended by Hatziargyriou et al. in 1993 [153] incorporating a probabilistic model for wind turbines. The PLF method of Allan et al. [152] was adapted to radial distribution networks and considered uncertainties in short-term (hourly) wind speed forecasts and corresponding uncertainties in produced active power and absorbed reactive power.

An alternative to convolution/FFT was proposed by Zhang & Lee in 2004 [154]. The proposed algorithm relied on the statistical premise that two distributions with equal moments must also have equal cumulants. Thus, one can be computed from the other. The algorithm started by calculating moments, thereby the cumulants, of injected power. Linearized equations are then used to calculate cumulants, thereby the moments, of line flows. PDFs of line flows are finally constructed from their moments using Gram-Charlier expansion. The study found that at least 7th order Gram-Charlier expansions should be used to provide accurate output PDFs. The proposed approach was significantly faster than MC simulations.

The different variations of PLF mentioned so far are all characterized as analytical PLF methods (refer to Fig. 5.2). Analytical PLF methods still perform deterministic power flow calculations, however they employ statistical theories and probabilistic approaches to model the input uncertainties and determine the corresponding output uncertainty range in a computationally efficient manner (compared to quasi-deterministic methods).

Following the development of PLF techniques in literature, another category of PLF – approximate PLF – was being proposed. As will be shown subsequently, those are the direct predecessors of state-of-the-art work on probabilistic and ML algorithms of most recent literature. The main reason for the delay in developing approximate PLF techniques is that the statistical/mathematical theories they are based on were first discovered around the same time as PLF itself (the first point estimation method was published in 1975 [155], one year after Borkowska's [151] paper). Moreover, more modern computing technologies motivated the application of such methods in the field of electrical power systems (the first point estimation method applied to PLF was in 2005 by Su et al. [156]).

While many point estimation methods were developed since then, they are all based on the same premise. Consider some variable y which is a function of random variables $\{v_1, v_2, \ldots v_{Nv}\}$. Let $y = f(v_1, v_2, \ldots v_{Nv})$ with f being a deterministic function and N_V being the number of random variables. A point estimation method is intended to approximate the first few moments of y and thereby estimate its PDF by evaluating f a number of times around each random input variable.

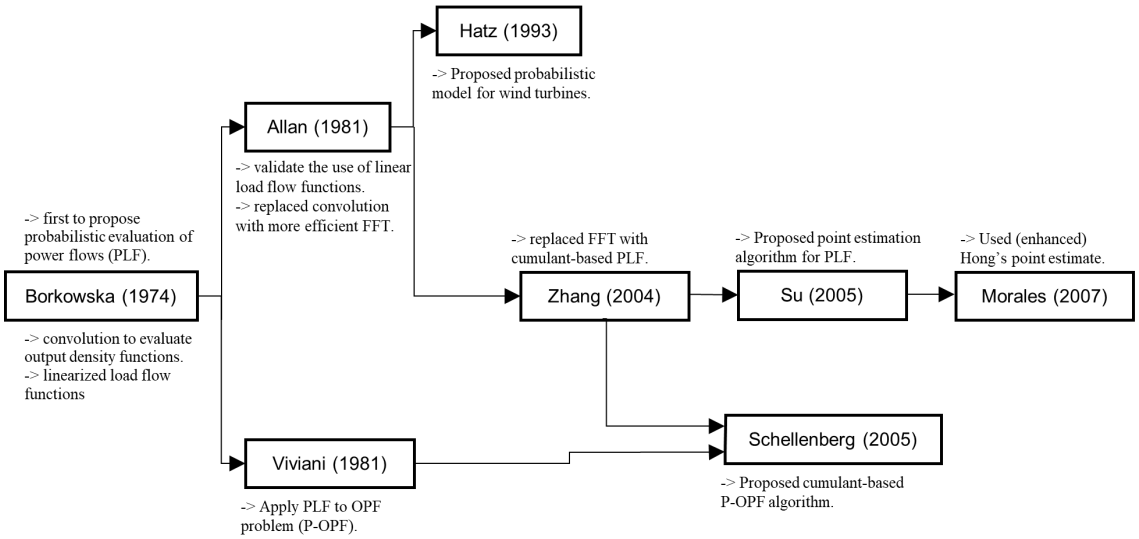

Figure 5.1: Historical timeline of pioneering papers in literature to apply statistical and probabilistic theories to power flow and OPF problems in traditional/centralized power systems.

While this may seem similar to a MC simulation, the main and crucial difference lies in point estimation methods concentrating statistical information calculated on the points for each random input and thereby only requiring a significantly lower number of evaluations for a large number of random inputs. For comparison, MC has a complexity [2] of $O(M^N)$, varying exponentially with the grid size, or number of buses M, and the number of random variables N.

On the other hand, even the earliest point estimation methods are between $O(2N)$ and $O(4N)$ [157], varying linearly with larger problems, which is the same as analytical PLF methods, all while deterministic methods being more computationally efficient than convolutions, FFT, or cumulant-based evaluations. In addition, the linearization of the power flow equations ceases to be necessary, so in the case of high variance random variables in a network the original equations can be used, unlike analytical PLF.

Su [156] was the first to propose a PLF algorithm based on a point-estimation method in 2005. The method used is a "two-point" estimation one. I.e., two samples are evaluated for each random/uncertain variable, and therefore it is $O(2N)$, equivalent to Hong's point estimation [157]. The method was 25 times faster than MC with the results being in very good agreement. It should be noted that a relatively small network (6-bus) was used as the test case, so the implemented algorithm was assumed to run exponentially faster than MC for larger more complex networks

[2] MC simulations can be run with an infinitely large number of samples. The time complexity is based on the number of samples, more that which no numerically significant improvement is obtained (solution is converged).

This was verified a year later when Morales & Pérez-Ruiz [157] performed a more detailed analysis using four different point estimation schemes, including the one proposed by [156]. A significantly larger network (118-bus) was used, and by comparing the resulting PDF's with MC simulations, it was concluded that $2N+1$ estimation schemes perform the best in terms of computational efficiency and provide high accuracy results even with a large number of random input (continuous or discrete) variables. The $2N+1$ point estimation was found to significantly outperform the $2N$ scheme used by [156] especially with a large number of random inputs, by performing only one additional calculation, and therefore it was recommended for use with large networks.

A simultaneous effort was underway to develop probabilistic models for the OPF and optimal dispatch problems. One of the pioneering papers to propose a probabilistic OPF (P-OPF) method was that of Viviani & Heydt in 1981 [158]. Dispatchable generators were modeled using second-order cost functions, and the control vector (for ideal generation levels) was modelled as a vector of PDFs by using Gram-Charlier expansion. The results showed excellent agreement with MC simulations for a small (8-bus) system, which was used as a test case due to limited computational capabilities of the time.

More than two decades later, in 2005, Schellenberg et al. [159] combined the work of Viviani & Heydt [158] and Zhang & Lee [154] to propose a cumulant-based P-OPF method. More modern computing technology allowed the method to be tested on a much larger 118-bus system. The simulations showed the proposed method provided highly accurate results with a computational efficiency an order of magnitude better than MC.

This section provided a review of some of the most influential papers in historic literature which pioneered the application of probabilistic and statistical theories to power flow and OPF methods (represented in Fig. 5.1). From this historical literature review, one can categorize power flow and OPF methods in traditional/centralized power systems into four categories (as shown in Fig. 5.2): deterministic, quasi-deterministic, analytical PPF, and approximate PPF. The different advantages and drawbacks of these methods are qualitatively compared in Table 5.1, according to the evaluated literature.

5.1.3 State-of-the-Art Review: Operation of Modern Smart Grids

In modern SGs, Internet-of-Things (IoT) enabling creates an abundance of measured data from even the smallest devices in the system, which is in fact the main identifier of SGs compared to a traditional grid: implementation of smart metering and communication infrastructures [89, 160].

This largely eliminates uncertainty caused by missing/unmeasurable variables in SGs. However, the combined effect of distributed energy resource (DER) proliferation, increased RESs penetration, and highly dynamic loads due to demand-side management (DSM) and demand response (DR) policies results in new sources of uncertainty, even for a centralized system operator with global data access [105, 161].

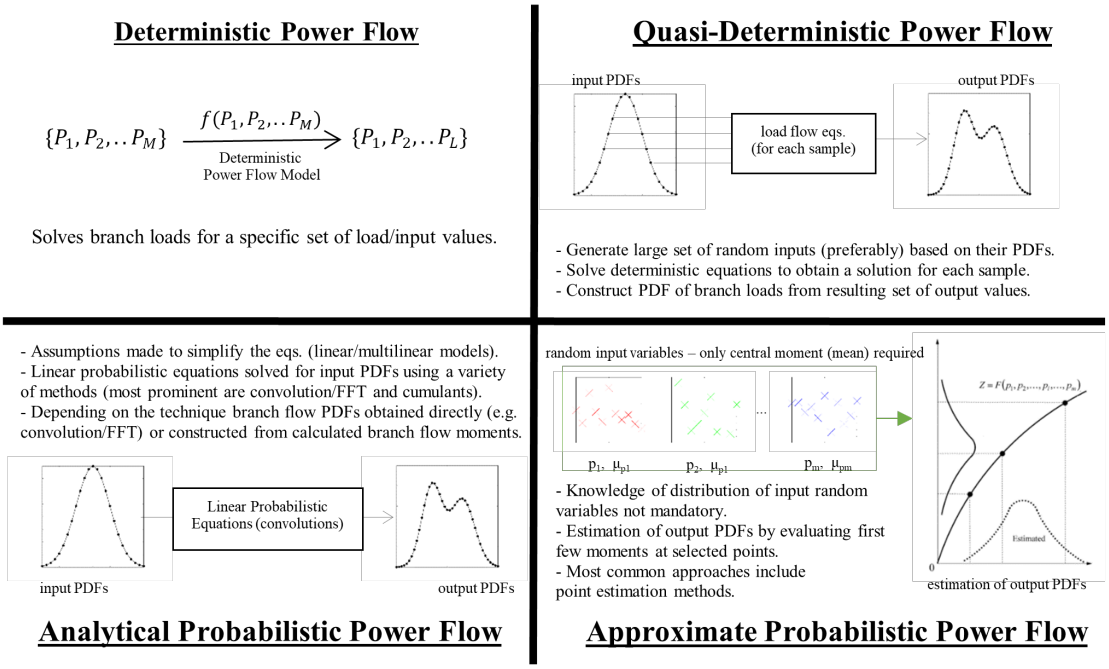

Figure 5.2: Illustration and description of different categories of methods employed for power flow and OPF in traditional/centralized power systems.

On top of that, recent technological, societal, and policy changes are resulting in a call for decentralized operation of SGs, associated with paradigms whose names are increasingly seen in scientific and technical literature such as citizen-run energy communities, peer-to-peer (P2P) energy trading, and the Internet-of-Energy (IoE). In these paradigms, a transition from a centralized operation structure to a decentralized one is advocated [98].

Table 5.1: Qualitative comparison of different categories of methods employed for power flow and OPF.

Category of PF/OPF Method	**Deterministic**	**Quasi-Deterministic**	**Probabilistic (Analytical)**	**Probabilistic (Approximate)**
Complexity of mathematical model / equations.	●●○	●●○	●●●	●○○
Complexity of computational implementation / program.	●○○	●○○	●●○	●●●
Computational expense (running time and memory)	●○○	●●●	●●○	●○○
Capability to incorporate uncertain / random variables.	✗	✓	✓	✓
Grid physical model replaceable with historical data (ML extension possible).	✗	✗	✗	✓

While there are several technical, economical, and environmental benefits of this shift, it adds an additional layer of operational challenges. Contrary to a central operator, decentralized agents would only have access to local data, adding a significant level of uncertainty and inaccessible information from other parts of the grid. In this case, a deterministic power flow or OPF model is not possible to construct by multiple individual agents to whom information (including the physical model) on other regions of the grid may not always be known [162].

To deal with this challenge, two solution efforts exist. The deterministic approach involves the use of decomposition techniques, in which deterministic power flow or OPF global functions are decomposed into a set of local ones to be solved by individual agents, with each local function being dependent on the solutions of the local functions of other agents. Therefore, an iterative procedure is employed where local solutions are interchanged between agents until a convergence is achieved for all local functions i.e., global consensus found.

However, multiple drawbacks are associated with this approach. First, decomposition techniques often suffer from convergence issues and are difficult to generalize for use with a generic power system configuration (i.e., they must be tuned/configured for each system to achieve acceptable convergence). Second, the exchange of local function solutions between local agents must be highly synchronized for real-world applicability, making it heavily reliant on secure communication infrastructures with low latency. Finally, the incorporation of uncertain variables is very complex, if not impossible, in real-world applications [163, 164, 99].

This leads to the second solution effort, revisiting probabilistic methods and their ML successors as viable solutions for the decentralized operation of SGs without the aforementioned problems. IoT-enabling and cloud computing capabilities now make it possible for probabilistic/ML algorithms to replace centralized system operators [150]. In traditional systems, the main drawback of these methods was reliance on historical data, which is no longer an issue in modern SGs (on the contrary, data redundancy is often brought up as an issue in the IoT paradigm).

The challenge in this case is to develop new algorithms in which agents can cooperate to achieve optimal global performance (as in OPF analysis), without sharing private/personal data to fit the new fully decentralized SG management paradigm. Probabilistic and ML techniques make use of historical data to provide fast and accurate predictions of solution variables even in the presence of high levels of uncertainty. Moreover, these methods rely solely on statistical relationships between input and output variables without requiring a deterministic model of the physical system to be constructed.

This makes them ideal to deal with the aforementioned problems of decentralized operation. Moreover, they do not suffer the drawbacks of deterministic decomposition-based techniques (lack of general applicability, convergence issues, reliance on low-latency communication infrastructures, and difficulty to incorporate uncertain parameters) [165].

From the conducted review of pioneering works and subsequent categorization of methods employed to traditional / centralized power systems, it was evident that the fourth category, the "approximate" PPF/P-OPF methods are the predecessors of modern day probabilistic and ML algorithms [150].

A major step in this evolution is the replacement of simple point estimates with non-parametric methods, which does not assume any statistical properties of the inputs to be known *a priori*.

Moreover, a point estimation (i.e., a deterministic calculation at the sampled points) is not needed and can be fully replaced with a historical dataset of input/output pairs, from which non-parametric methods directly estimate density distributions and corresponding output PDFs. Thus, the approach becomes purely a ML one where knowledge of a grid physical model is unnecessary. Kernel density estimation (KDE) has become the most popular non-parametric method in scientific literature, not only in the field of power systems but across the different applications of ML due to its reliability and computational efficiency [166].

Cao & Yan [167] performed a two-stage P-OPF analysis on a grid with multiple wind farms. First, input PDFs of wind generation were estimated, followed by MC simulations in which sampling was done based on the generated PDFs. By constructing a combined PDF for all wind farms with wind speed dependence, its effects were analyzed on the P-OPF results as compared to using individual PDFs of the wind farms. By comparing KDE (non-parametric) and parameter estimation, the PDF produced by KDE and corresponding P-OPF results was found to be more accurate than parameter estimation.

Other studies such as [168, 169] have performed similar analyses, in which KDE was used to estimate the PDFs of uncertain input variables (particularly from renewable generation).

The results of these studies are all in agreement with [167], reaffirming that using non-parametric methods in general and KDE in particular to estimate uncertain input variables in PPF is superior to parametric techniques. The aforementioned studies solely employed KDE as a pre-processing method, performing quasi-deterministic power flow analysis rather than exploiting KDE's full potential to replace MC simulations for PPF, which was performed by other works in literature.

Another study [170] applied KDE for PPF analysis of 14 and 118- bus systems with high levels of uncertainty and relying on historical operation data measurements. The method demonstrated accurate results with respect to the field measurements. In [171], a KDE-based method was proposed for PPF of unbalanced distribution networks. The method was tested on modified IEEE 13- and 37- bus test systems and compared against MC-3000 and 2N+1 point estimation. The results showed that the proposed KDE-based PPF method was superior to both MC and point estimation both in terms of computational time and results accuracy.

A recent study [172] proposed and tested PPF algorithms based on holomorphic embedding, KDE, and saddle point approximation. The study compared various approximate PPF techniques to analytical and quasi-deterministic ones. The proposed methods were tested on modified IEEE 14- and 118-bus test systems with high levels of uncertainty, and compared against MC-150000, 2N+1 point estimation, and other methods.

The results clearly show the effectiveness of the proposed PPF methods and their superiority in terms of computational effort, while providing the same level of accuracy as MC simulations. The paper recognized the potential of approximate PPF methods in terms of their independence of the physical system model and flexibility in application, recommending their use for complex networks and energy management in modern SGs where historical operation data is available.

Aside from operation, the application of KDE-based methods is recently observed in other areas of SGs research, namely in forecasting. Indeed, by employing PPF/P-OPF based on historical data with a ML model, the problem is modeled similar to a forecasting problem in which a desired output is to be predicted based on historical inputs. Examples of this are [124] which proposed a cooperative forecasting model for electricity market prices based on KDE and [173] which proposed a KDE-based ensemble algorithm for solar power forecasting (the work presented in the previous chapter).

5.1.4 Novel Contributions

In this chapter, a novel ML algorithm for fully decentralized power flow management of SGs is proposed, formulated, implemented, and tested. The proposed method was inspired by the forecasting model of [124] and [173] (work presented in the previous chapter), combining the cooperative approach of the former and the ensemble prediction of the latter.

5.2 Proposed Methodology

In this section, the conceptual model for decentralized operation of a SG is described. Then, the mathematical formulation of the proposed ML method for fully decentralized OPF management in this paradigm is presented. Finally, the cooperative information exchange capability of the proposed algorithm is illustrated.

5.2.1 Conceptual Model

In Fig. 5.3, an illustration of the conceptual model for a transition between a centralized (left) and decentralized (right) operation paradigm for an electrical power grid is illustrated. In the centralized paradigm, the system operator would have global access to all measurable variables in the system, and issue control signals to all controllable ones.

For a given grid, multiple overlaying models exist (e.g. corresponding to functions of real-time operation and dispatch, operation planning and unit commitment, voltage and frequency control, etc.). For each of those functions, the system operator would have a historical log of all input (measured) variables from the grid and the corresponding control actions taken (historical system states). In the case of OPF management, the logged historical system states can correspond to load values of the network and the corresponding ideal generation levels of all dispatchable generators.

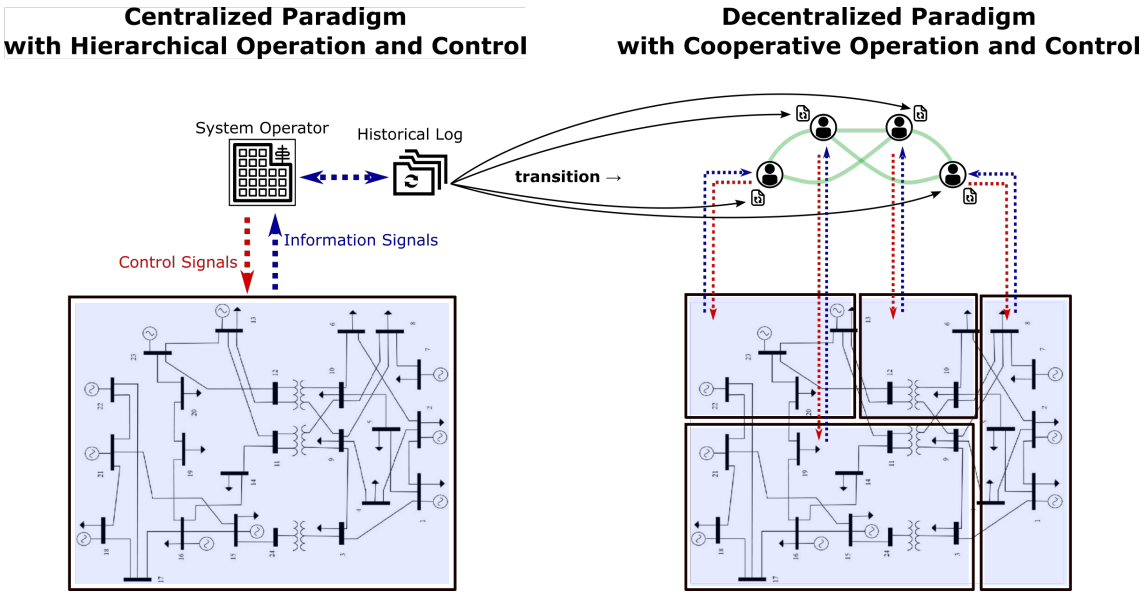

Figure 5.3: Illustration of the conceptual model for a transition between a centralized (left) and decentralized (right) operation paradigm of power grids. Green lines correspond to information exchange.

On the right of Fig. 5.3, the decentralized paradigm is illustrated, in which the centralized system operator is replaced by individual agents. Agents control local regions, where the agent has direct access to measured variables and can issue control actions. The agents in this fully decentralized operation paradigm are speculated to be individual utility operators, small-scale energy communities, or autonomous microgrids as demonstrated by [160, 99, 174].

In the transition from the centralized to the decentralized paradigm, each agent would be handed over a subset of the system operator's historical dataset, only containing input/output variables specific to their respective zone. From this point onwards, agents utilize their individual historical datasets to manage local zones of control using a ML approach which continuously updates their datasets as new control signals are issued for new system states.

At the beginning of the transition the information inherited from the retired system operator, although partial, can guarantee accurate prediction of control actions which lead to both local and global optimization of system performance. However, with time the information provided from the time of the centralized paradigm becomes obsolete, and thus a continuous cooperation scheme between the agents is required to exchange useful information without having to share private and/or raw local data.

5.2.2 Generalized Mathematical Formulation

Consider a system that at any given instant has a set of measurable independent input variables **V**. To ensure global applicability of the developed ML method, all the system input variables are considered as uncertain variables (i.e., $|\mathbf{V}| = N_V$) as shown in (5.1). Moreover, no knowledge of the physical system model is known a priori, and thus no input variable interdependencies are assumed.

$$\mathbf{V} = \{v_1, v_2, \ldots, v_{N_V}\} \tag{5.1}$$

A set **Y** is defined in (5.2), containing N_y output variables, each of which is a function of the input vector, through an unknown system model, as shown in (5.3).

$$\mathbf{Y} = \{y_1, y_2, \ldots, y_{N_Y}\} \tag{5.2}$$

$$\mathbf{Y} = f(\mathbf{V}) = f(\{v_1, v_2, \ldots, v_{N_V}\}) \tag{5.3}$$

Thus for all recorded system states, a historical dataset of operation **H** exists for the system matching the input and output vectors as shown in (5.4)-(5.5).

$$\mathbf{H} = \{H_\mathbf{1}, H_\mathbf{2}, \ldots H_{N_H}\} \tag{5.4}$$

$$H_k = \{\underbrace{y_1^{hist,k}, y_2^{hist,k}, \ldots, y_{N_y}^{hist,k}}_{\text{historical outputs at timestep } k}, \underbrace{v_1^{\text{hist},k}, v_2^{hist,k}, \ldots, v_{N_V}^{\text{hist},k}}_{\text{historical inputs at timestep } k}\} \quad \forall k = 1, 2, \ldots, N_H \tag{5.5}$$

For an updated system state, a new set of input variables $\mathbf{V}^{new}$ is measured as shown in (5.6), for which a corresponding set of output variables $\mathbf{Y}^{new}$ exists as shown in (5.7).

$$\mathbf{V}^{\text{new}} = \left\{v_1^{\text{new}}, v_2^{\text{new}}, \ldots, v_{N_V}^{\text{new}}\right\} \tag{5.6}$$

$$\mathbf{Y}^{\text{new}} = f(\mathbf{V}^{\text{new}}) = f\left(\left\{v_1^{\text{new}}, v_2^{\text{new}}, \ldots, v_{N_V}^{\text{new}}\right\}\right) \tag{5.7}$$

The objective of the proposed ML algorithm is to predict the value of $\mathbf{Y}^{new}$, provided only $\mathbf{V}^{new}$ and **H**, without any knowledge of the physical system model. The proposed ML algorithm (visualized in Fig. 5.4) is comprised of three main steps.

In the first step, a **similarity index (s-index)** between each historical system state and the new one is calculated using Nadarya-Watson KDE (NW-KDE), which evaluates a product of Gaussian kernel functions of all variables [124], as shown in (5.8), to obtain an s-index with a value between 0 and 1 for each historical state, resulting in the vector of s-indices **S** as shown in (5.9)-(5.10).

$$s_k = \left(\prod_i^{N_V} e^{-\frac{1}{2}\left(\frac{v_i^{hist,k} - v_i^{new}}{b_i}\right)^2} \right)^{\frac{1}{N_V}}, \quad \forall \quad k = 1,2,\ldots,N_H \tag{5.8}$$

$$0 \leq s_k \leq 1, \quad \forall \quad k = 1,2,\ldots,N_H \tag{5.9}$$

$$\mathbf{S} = \{s_1, s_2, \ldots s_{N_H}\} \tag{5.10}$$

For each variable i, the Gaussian kernel function bandwidth b_i determines the sampling window relative to the statistical range of the historical samples of this variable. A coefficient α_i can be used to tune the individual bandwidth value for each variable as shown in (5.11).

$$b_i = \alpha_i \left(\max_k \left(v_i^{hist,k} \right) - \min_k \left(v_i^{hist,k} \right) \right); \quad \forall k = 1,2,\ldots,N_H, i = 1,2,\ldots,N_V \tag{5.11}$$

Accordingly, α_i serves as a normalized tuning coefficient, whose value can be set between 0 (exclusive) and 1 (inclusive) as shown in (5.12), corresponding to a bandwidth value between zero (exclusive) and the maximum range of the historical values of the variable (inclusive).

$$0 < \alpha_i \leq 1 \quad \forall \quad i = 1,2,\ldots,N_V \tag{5.12}$$

The second step in the proposed method is to generate an activation vector for the most similar historical cases based on the calculated s-index vector. This can be done in two ways. First, a cut-off value can be set to activate all cases with an s-index above a certain value. The second, and the one used in this study, is to activate a fixed number of the top N_S historical cases from (highest N_S s-indices). In both cases, the result is an activation vector $\mathbf{A}$, whose elements are binary values as shown in (5.13)-(5.14).

$$\mathbf{A} = \{A_1, A_2, \ldots, A_{N_H}\} \tag{5.13}$$

$$A_k \in \{0,1\} \quad \forall \quad k = 1,2,\ldots,N_H \tag{5.14}$$

The activation vector is used to extract the most similar cases from the historical dataset. Thus, a subset $\mathbf{H^S}$ is extracted by discarding all cases whose corresponding activation value is zero. The original indices of the extracted cases $\mathbf{H^S}$ (in the original set $\mathbf{H}$) are preserved in vector $\mathbf{I^S}$. This is represented mathematically using (5.15)-(5.17) and is illustrated in Fig. 5.4.

$$H_k \in \mathbf{H^S} \Leftrightarrow A_k = 1 \quad \forall \quad k = 1,2,\ldots,N_H \tag{5.15}$$

$$\mathbf{I^S} = \{I_1^S, I_2^S, \ldots, I_{N_S}^S\} \tag{5.16}$$

$$\mathbf{H^S} = \left\{ H_{I_1^S}, H_{I_2}^S, \ldots H_{I_{N_S}^S} \right\} \tag{5.17}$$

The third and final step is to predict the output variables $\mathrm{Y}^{\mathrm{new}}$ using an ensemble of the extracted most similar historical cases. The simplest approach is to calculate the mean value of each output variable from the extracted historical values as shown in (5.18).

Confidence intervals can be obtained by applying simple univariate KDE to obtain the out variables' PDFs and the corresponding confidence interval bounds as represented mathematically in (5.19)-(5.21), where $\rho_{1/2x\%}$ corresponds to the x^{th} percentile. The lower and upper bounds of the x^{th} percentile for each predicted output y_j^{new} are expressed as $\hat{y}_{j,lb,x\%}^{new}$ and $\hat{y}_{j,ub,x\%}^{new}$ as shown in (5.20) and (5.21), respectively.

$$y_j^{\mathrm{new}} \approx \hat{y}_j^{\mathrm{new}} = \frac{\sum_{l=1}^{N_S} \left(y_j^{\mathrm{hist},I_l^S} \right)}{N_S} \quad \forall j = 1,2,\ldots,N_Y \tag{5.18}$$

$$\hat{y}_{j,lb,x\%}^{new} \leq \hat{y}_j^{new} \leq \hat{y}_{j,ub,x\%}^{\mathrm{new}} \quad \forall j = 1,2,\ldots,N_Y \tag{5.19}$$

$$\hat{y}_{j,lb,x\%}^{new} = \rho_{\frac{1}{2}(100-x)\%} \left(\left\{ y_j^{hist,I_1^S}, y_j^{hist,I_2^S}, \ldots, y_j^{nist,I_{N_S}^S} \right\} \right) \quad \forall j = 1,2,\ldots,N_Y \tag{5.20}$$

$$\hat{y}_{j,ub,x\%}^{new} = \rho_{\frac{1}{2}(100+x)\%} \left(\left\{ y_j^{hist,I_1^S}, y_j^{hist,I_2^S}, \ldots, y_j^{hist,I_{N_S}^S} \right\} \right) \quad \forall j = 1,2,\ldots,N_Y \tag{5.21}$$

5.2.3 Application to Decentralized OPF with Cooperative Information Exchange

In the case of an OPF problem, the input variables are the bus loads and the output variables are the ideal generation levels. In the decentralized operation paradigm, each agent would only have a historical dataset with variables in their regions of operation. From the presented mathematical formulation it can be seen that the proposed ML model is independent of the physical grid model, and thus even with a limited number of historical variables the prediction of the outputs can still be obtained.

One of the novel contributions of this work is the capability of the proposed method to enable the cooperative information exchange without sharing private/raw data (e.g., local historical datasets or control actions taken locally). With the proposed method, this can effectively be performed by publicly sharing the activation vector $\mathbf{A}$ or the corresponding indices $\mathbf{I^S}$.

In this way, the exchanged indices of activated historical cases would greatly improve the output prediction of other agents by giving them insight on relevant historical cases from the perspective of other agents and thereby the global performance of the system, without exposing any local/private information from the transacting agent's local database or the need for any central coordination. Accordingly, a distributed energy cloud operation scheme is enabled by the proposed method, as illustrated in Fig. 5.5.

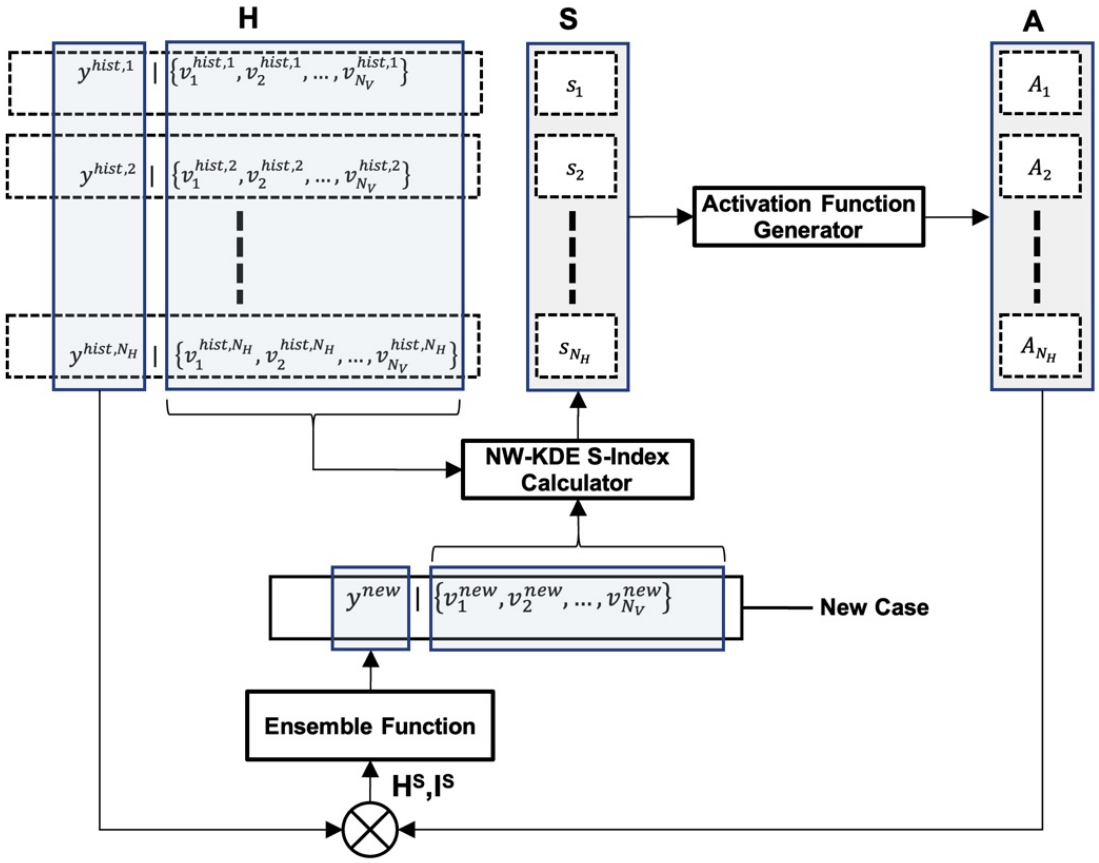

Figure 5.4: Illustrative flowchart of the proposed and implemented ML algorithm.

The activation functions (**A**) therefore serve as encoded, yet useful, information which is broadcast into a public energy cloud and can be shared with other agents in the decentralized system. A few final remarks about the proposed algorithm and cooperation scheme are noted before proceeding to the case study and analysis:

- The size of the historical database does not need to be the same for all agents. In case a distributed energy cloud operation is adopted, standardized implementation is foreseen. However, even in the unlikely case where no standard database size is present activated historical cases can be shared based on their timestamps rather than index in the dataset.

- The tunable parameters of the proposed method are the normalized bandwidth coefficients α_i and N_S. While tuning of these parameters can improve the prediction accuracy, it will be shown in the next sections that the proposed algorithm is highly versatile, such that applying default values for all the parameters still guarantees highly accurate output predictions.

- The proposed method is highly computationally efficient. While the computational implementation is demanding, all operations are based on simple direct array multiplications and manipulations. The high computational efficiency of the implementation will also be demonstrated in the next sections.

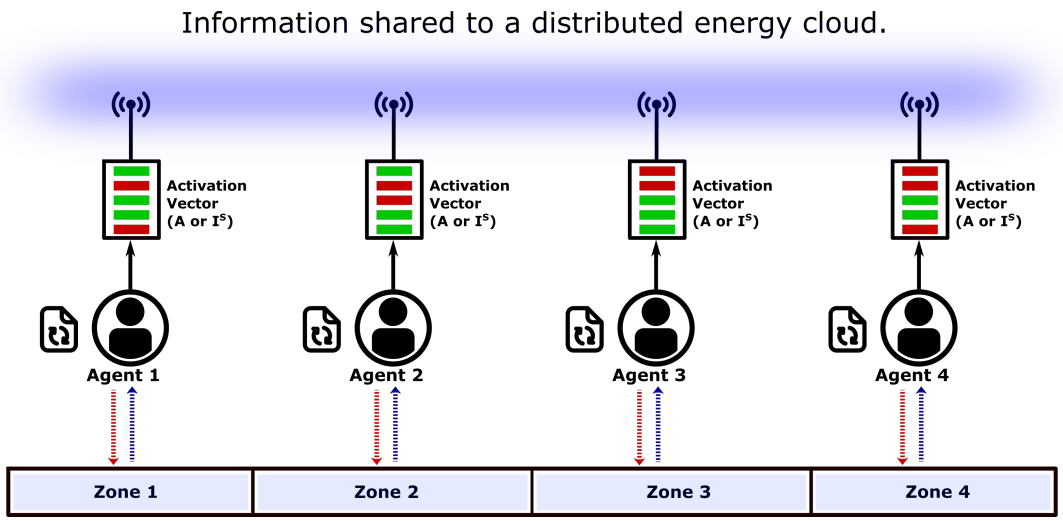

Figure 5.5: Illustration of the cooperative information exchange made possible by the proposed and implemented ML algorithm, enabling a distributed energy cloud operation scheme.

- The proposed algorithm was proposed and implemented as original code by the authors using MATLAB R2020b, on a standard laptop computer with an Intel Core i7-8550U CPU @ 1.80 GHz, 16.0 GB RAM, and a Windows 10 64-bit operating system.

5.3 Case Study and Validation Analyses

5.3.1 Modified IEEE 24-Bus Test System

To demonstrate and validate the proposed algorithm, a case study was constructed based on a modified IEEE 24-bus reliability test system (RTS), whose single line diagram is shown in Fig. 5.6. The 24-bus network has 33 transmission lines, in addition to five transformers separating the two voltage levels in the network (138 kV and 230 kV). A total of 33 generators (G1, G2, ... , G33), including one synchronous generator (G15), are incorporated.

For the purpose of power flow analyses, active power generators that are both 1) connected to the same bus, and 2) have the same cost functions, are aggregated as a single generation station or utilities [175]. Applying this to the considered 24-bus RTS results in 14 utilities (U1, U2, ... , U14) being the active power generation stations of the system. In the decentralized operation paradigm, these generation utilities are considered to be the decentralized operating agents of the system, spread across five zones of operation (Z1, Z2, Z3, Z4, Z5) as is also shown in Fig. 5.6.

The zones are listed in Table 5.2, including the corresponding buses and utilities therein. Accordingly, in the case of an OPF analysis, each utility as a decentralized operating agent has access only to historical load values from its own zone (i.e., loads at buses inside its zone).

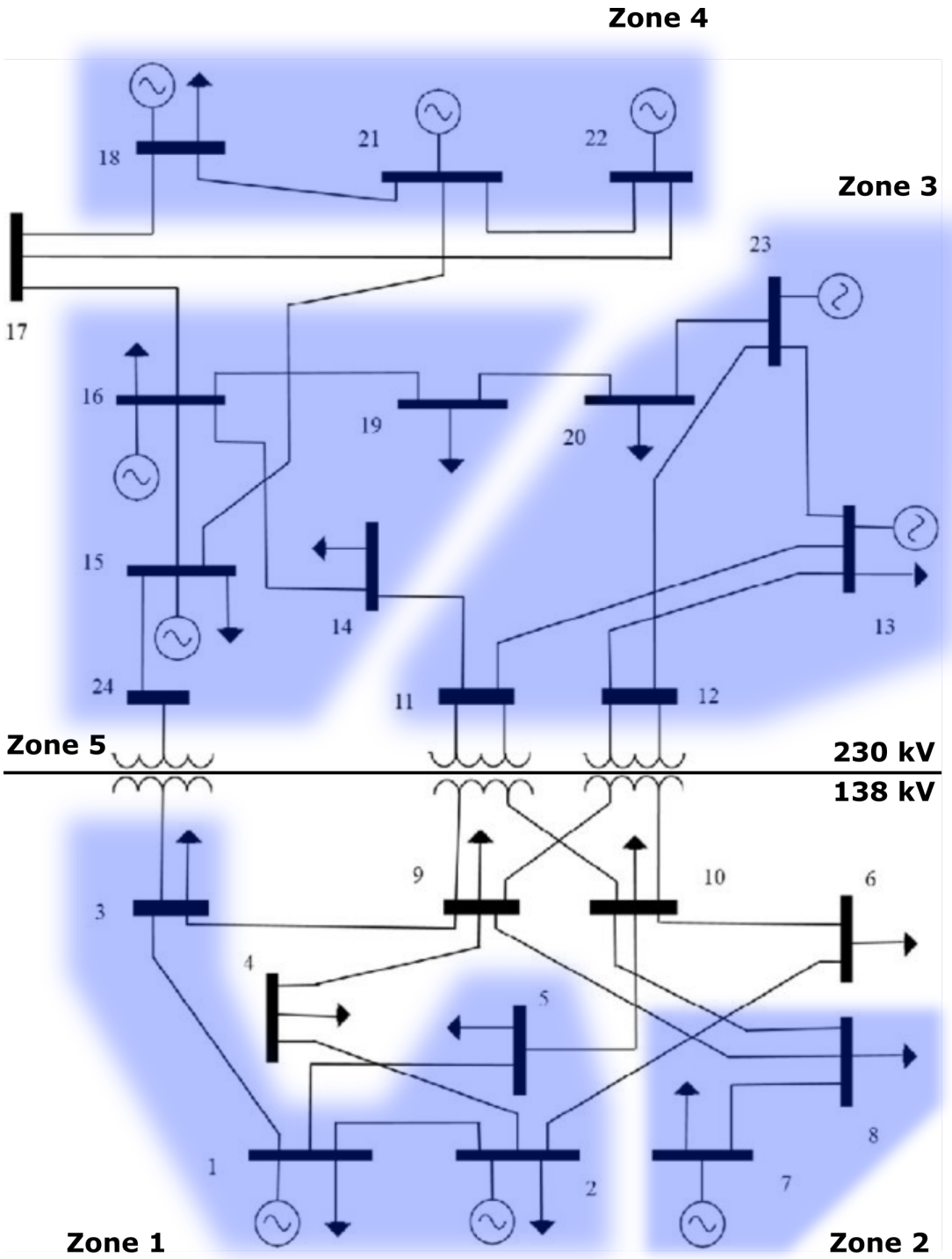

Figure 5.6: Modified IEEE 24-bus test system showing the defined zones.

Table 5.2: Zones of the test system under analysis, and the corresponding buses and utilities within.

Zone	Buses	Utilities
Z1	1, 2, 3, 5	U1, U2, U3, U4
Z2	7, 8	U5
Z3	11, 12, 13, 20, 23	U6, U13, U14
Z4	18, 21, 22	U10, U11, U12
Z5	14, 15, 16, 19, 24	U7, U8, U9

The utilities do not have knowledge of each other's historical generation values (only their own). Table 5.3 lists all 14 utilities, the corresponding zone, incorporated generators, and their respective operating costs represented as coefficients of a quadratic cost function model as described in [176]. In the decentralized operation paradigm, the utilities do not have knowledge of the full grid topology (incidence matrix is unknown), only having knowledge of transmission line connections inside their respective zones.

It can be observed that the designated zones are diverse in terms of both size and structure. This was intended to test the versatility of the proposed algorithm. Furthermore, load buses 4, 6, 9, and 10 are not incorporated in any zone and therefore historical information from them is only provided when the energy cloud / cooperative information exchange is enabled.

This way, they are considered as self-managing microgrids (with self-consumption) which can still share their activation vectors in the proposed scheme for every new system state, however have no control actions over the system. In this sense, the case study can also demonstrate the applicability of the proposed algorithm for the decentralized management of interconnected multi-microgrids with varying sizes, local generation capacity, and self-consumption.

Table 5.3: Utilities of the test system under analysis (considered the decentralized operating agents) including the zone association, incorporated generator number, and the coefficients for the individual generator cost functions.

Utility	Bus	Zone	Incorporated Generators	PGmin	PGmax	a	b	c	MUT	MDT	RD, RU	SU	SD	IH
U1	B1	Z1	G1, G2	16	20	400.7	130	0	1	1	30	5	5	-10
U2	B1	Z1	G3, G4	15.2	76	212.3	16.1	0.01414	8	4	20	596	596	10
U3	B2	Z1	G5, G6	16	20	400.7	130	0	1	1	30	5	5	-10
U4	B2	Z1	G7, G8	15.2	76	212.3	16.1	0.01414	8	4	20	596	596	10
U5	B7	Z2	G9, G10, G11	25	100	781.5	43.7	0.05267	8	8	70	566	250	6
U6	B13	Z3	G12, G13, G14	69	197	832.8	48.6	0.00717	12	10	30	775	443	-8
U7	B15	Z5	G16, G17, G18, G19, G20	2.4	12	86.4	56.6	0.32841	4	2	10	68	38	-3
U8	B15	Z5	G21	54.3	155	382.2	12.4	0.00834	8	8	30	953	260	12
U9	B16	Z5	G22	54.3	155	382.2	12.4	0.00834	8	8	30	953	260	12
U10	B18	Z4	G23	100	400	395.4	4.42	0.00021	1	1	200	0	0	20
U11	B21	Z4	G24	100	400	395.4	4.42	0.00021	1	1	200	0	0	20
U12	B22	Z4	G25, G26, G27, G28, G29, G30	10	50	0.001	0.001	0	0	0	50	0	0	8
U13	B23	Z3	G31, G32	54.3	155	382.2	12.4	0.00834	8	8	30	953	260	8
U14	B23	Z3	G33	140	350	665.1	11.9	0.0049	24	48	40	4468	1915	8

5.3.2 Synthetically Generated Historical Data

To synthetically generate the historical dataset of centralized operation (as described in Section 5.2.1), that reflects realistic conditions, a typical transmission systems' annual load profile provided by the Portuguese Energy Regulation Services Entity (ERSE) was used [118]. The load profile is high resolution (15-minute) for the full year of 2019 (35040 time steps).

To apply the normalized load profile to the current network, the annual peak load was set to correspond to the marginal operation of the network at maximum loadability (considering bus voltage angle and transmission line power limits). To determine this, the network is modeled and simulated using MATPOWER 7.0, and the total load of the system is gradually increased by incrementing individual bus loads while maintaining their original power factor (pf).

The maximum loadability occurs at the point when any infinitesimal increase in individual bus loads would render an AC-OPF solution infeasible (violating network constraints). By performing this, the maximum loadability of this network was found to be 3334.50 MW (total load). The maximum (active power) loadability of individual load buses (PD^{max}) and their pf is detailed in Table 5.4 (note that non-load buses have a pf of zero).

In this way, the normalized typical load (based on Portuguese transmission systems) can be applied to the current network by setting the annual peak load at each bus to its maximum loadability. A synthesized historical dataset could now be generated by performing the following steps:

Step 1: Calculate active power load at each bus b, and the corresponding reactive power load, for each timestep in the load profiles.

$$PD_b^{\text{hist},t} = P_t^{\text{typical}} \cdot PD_b^{\max} \quad \forall b \in \{1,2,\dots 24\}, t \in \{1,2,\dots,35040\} \tag{5.22}$$

$$QD_b^{\text{hist,t}} = PD_b^{\text{hist,t}} \cdot pf_b \quad \forall b \in \{1,2,\dots 24\}, t \in \{1,2,\dots,35040\} \tag{5.23}$$

Step 2: Perform a deterministic AC-OPF calculation to determine the corresponding active power generation levels of each utility, for each timestep in the load profiles.

$$\left\{PG_{U1}^{hist,t}, PG_{U2}^{hist,t}, \dots, PG_{U14}^{\text{hist},t}\right\} \xleftarrow{AC-OPF} \left\{\begin{array}{l} PD_1^{hist,t}, PD_2^{hist,t}, \dots, PD_{24}^{hist,t} \\ QD_1^{hist,t}, QD_2^{hist,t}, \dots, QD_{24}^{hist,t} \end{array}\right\} \quad \forall t \in \{1,2,\dots,35040\} \tag{5.24}$$

With this a historical dataset for a full year (15-minute resolution) is obtained. The day of the year and hour of the day are added as independent input variables in addition to the power loads at all buses. The total load for the generated historical operation is plotted in Fig. 5.7.

Two assumptions made to construct this case study are duly noted and justified. The first assumption is regarding the presence of renewable generation in the system. In a modern SG renewable generation sources are indispensable and therefore must be incorporated.

Table 5.4: Maximum loadability (peak annual load) at each load bus and corresponding pf.

Load Bus	**pf**	**PDmax (MW)**	**Load Bus**	**pf**	**PDmax (MW)**	**Load Bus**	**pf**	**PDmax (MW)**
1	0.9799	126.36	**7**	0.9806	146.25	**15**	0.9802	370.89
2	0.9794	113.49	**8**	0.9797	200.07	**16**	0.9806	117.00
3	0.9795	210.60	**9**	0.9795	204.75	**18**	0.9798	389.61
4	0.9801	86.58	**10**	0.9796	228.15	**19**	0.9797	211.77
5	0.9811	83.07	**13**	0.9799	310.05	**20**	0.9800	149.76
6	0.9795	159.12	**14**	0.9804	226.98	**Peak Annual Load**		3334.50

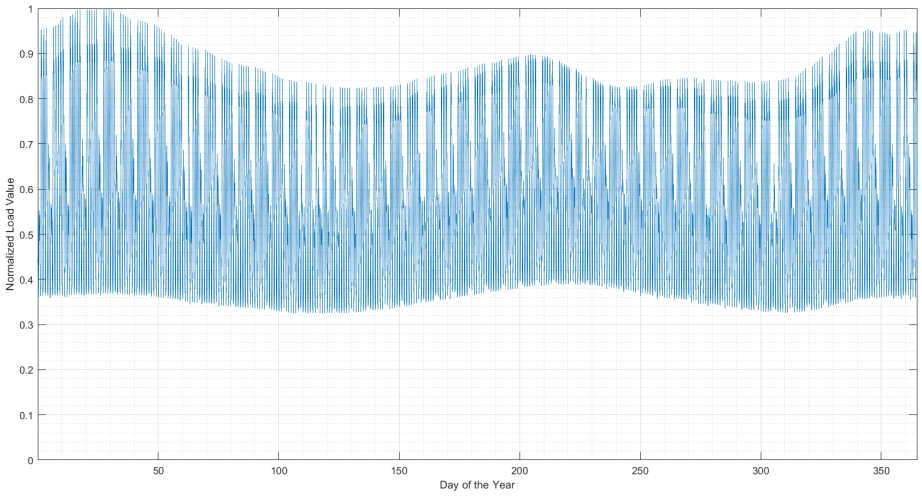

Figure 5.7: Plot of the historical total load (1 year with 15-minute resolution.)

This is done by choosing the ERSE profiles which correspond to aggregated users with self-consumption by local generation, and therefore the considered load profiles for the transmission system already account for renewable generation and self-consumption on the distribution system level, according to Portuguese electrical systems design and operating conditions.

Second, the synthetically generated historical operation data does not consider events such as outages, line failures, unit maintenance, etc. While these events have an impact on power flow, the proposed method is a pure ML one. I.e., their presence in the historical data does not affect the algorithm and/or results since there is no physical model, only a statistical one.

Such events would simply be additional input variables in the NW-KDE activation function generator if the new case corresponds to the same situation. The scope of this chapter is to propose, implement, and validate the proposed algorithm. For the purpose of having a benchmark study and a control experiment, such events are therefore not considered to ensure proper testing and validation of the implemented algorithm, but are recommended to be studied in future work.

Step 3: In accordance with the conceptual model presented in Section 5.2.1, decompose the historical dataset into local datasets available for each agent/utility in the system according to their local variables. With the local datasets extracted, each agent can then employ the proposed methodology in Section 5.2.2. and participate in the cooperative information exchange cloud model described in Section 5.2.3.

To demonstrate the local datasets available to each agent U1 is taken as an example, which is located at bus 1 (B1) in zone 1 (Z1). By referring to Table 5.2, Z1 contains buses 1, 2, 3, and 5. Therefore, for U1, N_V is equal to 6 (load values at four buses, hour of the day, day of the year). By applying this to all utilities, the local historial datasets are represented in (5.25)-(5.38), being the extension of (5.5) considering locally available information. With this, the proposed algorithm can now be implemented locally at each utility.

$$\text{at U1:} \quad H_k = \left\{ \underbrace{PG_{U1}^{\text{hist,t}}}_{\text{historical generation U1}}, \underbrace{PD_1^{\text{hist,t}}, PD_2^{\text{hist,t}}, PD_3^{\text{hist,t}}, PD_5^{\text{hist,t}}}_{\text{historical load values in Zone 1 (U1)}}, \underbrace{\tau(t)}_{\text{hour of the day}}, \underbrace{\delta(t)}_{\text{day of the year}} \right\} \tag{5.25}$$

$$\forall t \in \{1, 2, \ldots, 35040\}$$

$$\text{at U2:} \quad H_k = \left\{ \underbrace{PG_{U2}^{\text{hist,t}}}_{\text{historical generation U2}}, \underbrace{PD_1^{\text{hist,t}}, PD_2^{\text{hist,t}}, PD_3^{\text{hist,t}}, PD_5^{\text{hist,t}}}_{\text{historical load values in Zone 1 (U2)}}, \underbrace{\tau(t)}_{\text{hour of the day}}, \underbrace{\delta(t)}_{\text{day of the year}} \right\} \tag{5.26}$$

$$\forall t \in \{1, 2, \ldots, 35040\}$$

$$\text{at U3:} \quad H_k = \left\{ \underbrace{PG_{U3}^{\text{hist,t}}}_{\text{historical generation U3}}, \underbrace{PD_1^{\text{hist,t}}, PD_2^{\text{hist,t}}, PD_3^{\text{hist,t}}, PD_5^{\text{hist,t}}}_{\text{historical load values in Zone 1 (U3)}}, \underbrace{\tau(t)}_{\text{hour of the day}}, \underbrace{\delta(t)}_{\text{day of the year}} \right\} \tag{5.27}$$

$$\forall t \in \{1, 2, \ldots, 35040\}$$

$$\text{at U4:} \quad H_k = \left\{ \underbrace{PG_{U4}^{\text{hist,t}}}_{\text{historical generation U4}}, \underbrace{PD_1^{\text{hist,t}}, PD_2^{\text{hist,t}}, PD_3^{\text{hist,t}}, PD_5^{\text{hist,t}}}_{\text{historical load values in Zone 1 (U4)}}, \underbrace{\tau(t)}_{\text{hour of the day}}, \underbrace{\delta(t)}_{\text{day of the year}} \right\} \tag{5.28}$$

$$\forall t \in \{1, 2, \ldots, 35040\}$$

$$\text{at U5:} \quad H_k = \left\{ \underbrace{PG_{U5}^{\text{hist},t}}_{\text{historical generation of U5}}, \underbrace{PD_7^{\text{hist},t}, PD_8^{\text{hist},t}}_{\text{historical load values in Zone 2 (U5)}}, \underbrace{\tau(t)}_{\text{hour of the day}}, \underbrace{\delta(t)}_{\text{day of the year}} \right\} \quad (5.29)$$

$$\forall t \in \{1,2,\ldots,35040\}$$

$$\text{at U6:} \quad H_k = \left\{ \underbrace{PG_{U6}^{\text{hist},t}}_{\text{historical generation U6}}, \underbrace{PD_{11}^{\text{hist},t}, PD_{12}^{\text{hist,t}}, PD_{13}^{\text{hist,t}}, PD_{20}^{\text{hist},t}, PD_{23}^{\text{hist},,t}}_{\text{historical load values in Zone 3 (U6)}}, \underbrace{\tau(t)}_{\text{hour of the day}}, \underbrace{\delta(t)}_{\text{day of the year}} \right\}$$

$$\forall t \in \{1,2,\ldots,35040\} \quad (5.30)$$

$$\text{at U7:} \quad H_k = \left\{ \underbrace{PG_{U7}^{\text{hist},t}}_{\text{historical generation U7}}, \underbrace{PD_{14}^{\text{hist},t}, PD_{15}^{\text{hist},,t}, PD_{16}^{\text{hist},t}, PD_{19}^{\text{hist},t}, PD_{24}^{\text{hist},t}}_{\text{historical load values in Zone 5(U7)}}, \underbrace{\tau(t)}_{\text{hour of the day}}, \underbrace{\delta(t)}_{\text{day of the year}} \right\}$$

$$\forall t \in \{1,2,\ldots,35040\} \quad (5.31)$$

$$\text{at U8:} \quad H_k = \left\{ \underbrace{PG_{U8}^{\text{hist},t}}_{\text{historical generation U8}}, \underbrace{PD_{14}^{\text{hist},t}, PD_{15}^{\text{hist},,t}, PD_{16}^{\text{hist},t}, PD_{19}^{\text{hist},t}, PD_{24}^{\text{hist},t}}_{\text{historical load values in Zone 5(U8)}}, \underbrace{\tau(t)}_{\text{hour of the day}}, \underbrace{\delta(t)}_{\text{day of the year}} \right\}$$

$$\forall t \in \{1,2,\ldots,35040\} \quad (5.32)$$

$$\text{at U9:} \quad H_k = \left\{ \underbrace{PG_{U9}^{\text{hist},t}}_{\text{historical generation U9}}, \underbrace{PD_{14}^{\text{hist},t}, PD_{15}^{\text{hist},,t}, PD_{16}^{\text{hist},t}, PD_{19}^{\text{hist},t}, PD_{24}^{\text{hist},t}}_{\text{historical load values in Zone 5(U9)}}, \underbrace{\tau(t)}_{\text{hour of the day}}, \underbrace{\delta(t)}_{\text{day of the year}} \right\}$$

$$\forall t \in \{1,2,\ldots,35040\} \quad (5.33)$$

$$\text{at U10:} \quad H_k = \left\{ \underbrace{PG_{U10}^{\text{hist},t}}_{\text{historical generation U10}}, \underbrace{PD_{18}^{\text{hist},t}, PD_{21}^{\text{hist},t}, PD_{22}^{\text{hist},t}}_{\text{historical load values in Zone 4 (U10)}}, \underbrace{\tau(t)}_{\text{hour of the day}}, \underbrace{\delta(t)}_{\text{day of the year}} \right\} \tag{5.34}$$

$$\forall t \in \{1,2,\ldots,35040\}$$

$$\text{at U11:} \quad H_k = \left\{ \underbrace{PG_{U11}^{\text{hist},t}}_{\text{historical generation U11}}, \underbrace{PD_{18}^{\text{hist},t}, PD_{21}^{\text{hist},t}, PD_{22}^{\text{hist},t}}_{\text{historical load values in Zone 4 (U11)}}, \underbrace{\tau(t)}_{\text{hour of the day}}, \underbrace{\delta(t)}_{\text{day of the year}} \right\} \tag{5.35}$$

$$\forall t \in \{1,2,\ldots,35040\}$$

$$\text{at U12:} \quad H_k = \left\{ \underbrace{PG_{U12}^{\text{hist},t}}_{\text{historical generation U12}}, \underbrace{PD_{18}^{\text{hist},t}, PD_{21}^{\text{hist},t}, PD_{22}^{\text{hist},t}}_{\text{historical load values in Zone 4 (U12)}}, \underbrace{\tau(t)}_{\text{hour of the day}}, \underbrace{\delta(t)}_{\text{day of the year}} \right\} \tag{5.36}$$

$$\forall t \in \{1,2,\ldots,35040\}$$

$$\text{at U13:} \quad H_k = \left\{ \underbrace{PG_{U13}^{\text{hist},t}}_{\text{historical generation U13}}, \underbrace{PD_{11}^{\text{hist},t}, PD_{12}^{\text{hist},t}, PD_{13}^{\text{hist,t}}, PD_{20}^{\text{hist,t}}, PD_{23}^{\text{hist},t}}_{\text{historical load values in Zone 3 (U13)}}, \underbrace{\tau(t)}_{\text{hour of the day}}, \underbrace{\delta(t)}_{\text{day of the year}} \right\}$$

$$\forall t \in \{1,2,\ldots,35040\} \tag{5.37}$$

$$\text{at U14:} \quad H_k = \left\{ \underbrace{PG_{U13}^{\text{hist},t}}_{\text{historical generation U14}}, \underbrace{PD_{11}^{\text{hist},t}, PD_{12}^{\text{hist},t}, PD_{14}^{\text{hist,t}}, PD_{20}^{\text{hist,t}}, PD_{23}^{\text{hist},t}}_{\text{historical load values in Zone 3 (U14)}}, \underbrace{\tau(t)}_{\text{hour of the day}}, \underbrace{\delta(t)}_{\text{day of the year}} \right\}$$

$$\forall t \in \{1,2,\ldots,35040\} \tag{5.38}$$

5.3.3 Performed Analyses

The case study is now fully constructed and validation studies can be performed. Using the generated historical datasets, the proposed algorithm is tested by employing a fully decentralized week-ahead operation planning for OPF in the grid with very high-resolution (15 minute). The total system load profile for the test week, shown in Fig. 5.8, was generated based on the average summer values of the yearly load profile. Individual input variables (bus loads) at each time step are generated by maintaining the ratio of load buses in the test system and dividing the total system load accordingly. Three studies were performed:

Study 1: In the first study the validity of the proposed algorithm is demonstrated, and the influence of tunable parameters is showcased. In this study, the full algorithm is employed, including the cooperative information exchange scheme between the agents. Coefficients α_i were defined as follows:

- α_{in}: coefficient for historical input variables from sources which are physically connected to the utility (i.e. load values of the same bus).
- α_{out}: coefficient for historical input variables which are not physically connected to the utility (i.e. load value of bus other than that of the utility).
- α_{hour},α_{day}: coefficients the day of the year and hour of the day for each historical case, respectively.

Study 2: In the second study, the proposed cloud-based cooperative information exchange is investigated by comparing the results for each agent with and without the exchanged activation functions.

Study 3: In the third and final case study, the performance of the proposed algorithm is assessed in comparison with a NN.

For all studies, the results are compared against the centralized scenario with a deterministic AC-OPF model. The results of all three studies are presented subsequently in the next section.

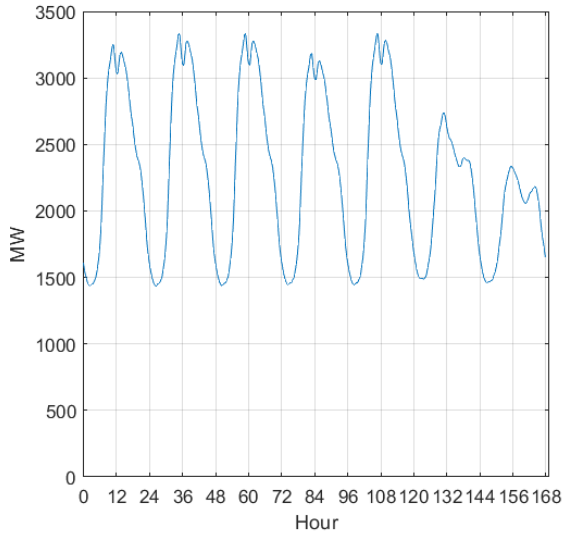

Figure 5.8: Total load profile for the considered test week (15-minute resolution).

5.4 Simulation Results

5.4.1 Study 1: Validation and Parameter Tuning

In this study, the proposed algorithm is validated and the effect of tunable parameters (normalized bandwidth coefficients α_i and N_S) is assessed. Two scenarios are compared. In the first, all normalized bandwidth coefficients α_i are set to 0.5. This can be considered the "default" value of the coefficients. In the second scenario, the coefficients are tuned by generating random value combinations until the error falls below a certain threshold. Here, it is noted that on the machine used for implementation, the algorithm run time was recorded to be less than 4 seconds.

Tuning the parameters ran in less than 1 minute for each utility. This was around the same time that the training time of the NN used in the third study . Therefore, the tuning process was very fast, even for the demanding high resolution week-ahead test case considered. Plots of the results of selected utilities are shown in Fig. 5.9, and the detailed results for all utilities are listed in Table 5.5. It is noted that U1, U3, and U12 are found to have a zero load factor throughout the test week (refer to Fig. 5.10) and are therefore they excluded from the results of this study and subsequent ones. Multiple observations are made:

- The proposed algorithm is shown to have exceptionally high accuracy. With tuned parameters, the moving average percentage error (MAPE), relative to centralized AC-OPF, was well below 0.1% for all utilities. From the plots in Fig. 5.9, it can be seen that the exact and predicted values are tightly overlayed, being hardly distinguishable.

- Even with untuned parameters set to a default value of 0.5 arbitrarily, for the majority of the cases the predicted generation profile was still estimated with reasonable accuracy.

- The utilities predictions most affected by parameter tuning were U5 and U6 which incorporate large high cost generators resulting in the high-frequency fluctuations during peak load hours which were only predicted accurately after parameter tuning. U7 was similarly critical due to the three acute ramps in generation during the test week, which were accurately predicted after parameter tuning. Finally, U10 and U11 being high load factor utilities (Fig. 5.10) and in an energy exporting zone (Fig. 5.11) were sensitive to parameter tuning (although the untuned solution still had a 1% error, which is satisfactory).

By performing this study, the validity of the proposed algorithm is demonstrated, and the influence of tunable parameters is showcased. The tuned algorithm is validated to be exceptionally accurate in predicting the ideal generation levels in the decentralized operation paradigm.

5.4.2 Study 2: Effect of Cooperative Information Exchange

In this study, the effect of the incorporated cloud-based information exchange model was assessed. The results of this study are shown in Fig. 5.12 and Table 5.6. The following observations are made:

- The results show that the cooperative information exchange between the decentralized agents has a profound impact on the accuracy of their predicted generation values.
- By comparing the results against the information provided in Fig. 5.10 and 5.11, it can be seen that this is especially the case with utilities that have: a) a high load factor (expensive generators) and b) exist in zones that are net exporters of energy in the grid. This is expected, since such utilities would heavily rely on any information from other parts of the grid since they mainly respond to peak loads from zones that are net importers of energy in the grid.
- Another important observation is made by comparing the results of this study with the first one. It can be seen that the impact of the implemented cooperative information sharing model is significantly higher than parameter tuning, both in terms of the confidence intervals (shaded parts of the plots), and overall accuracy (MAPE).

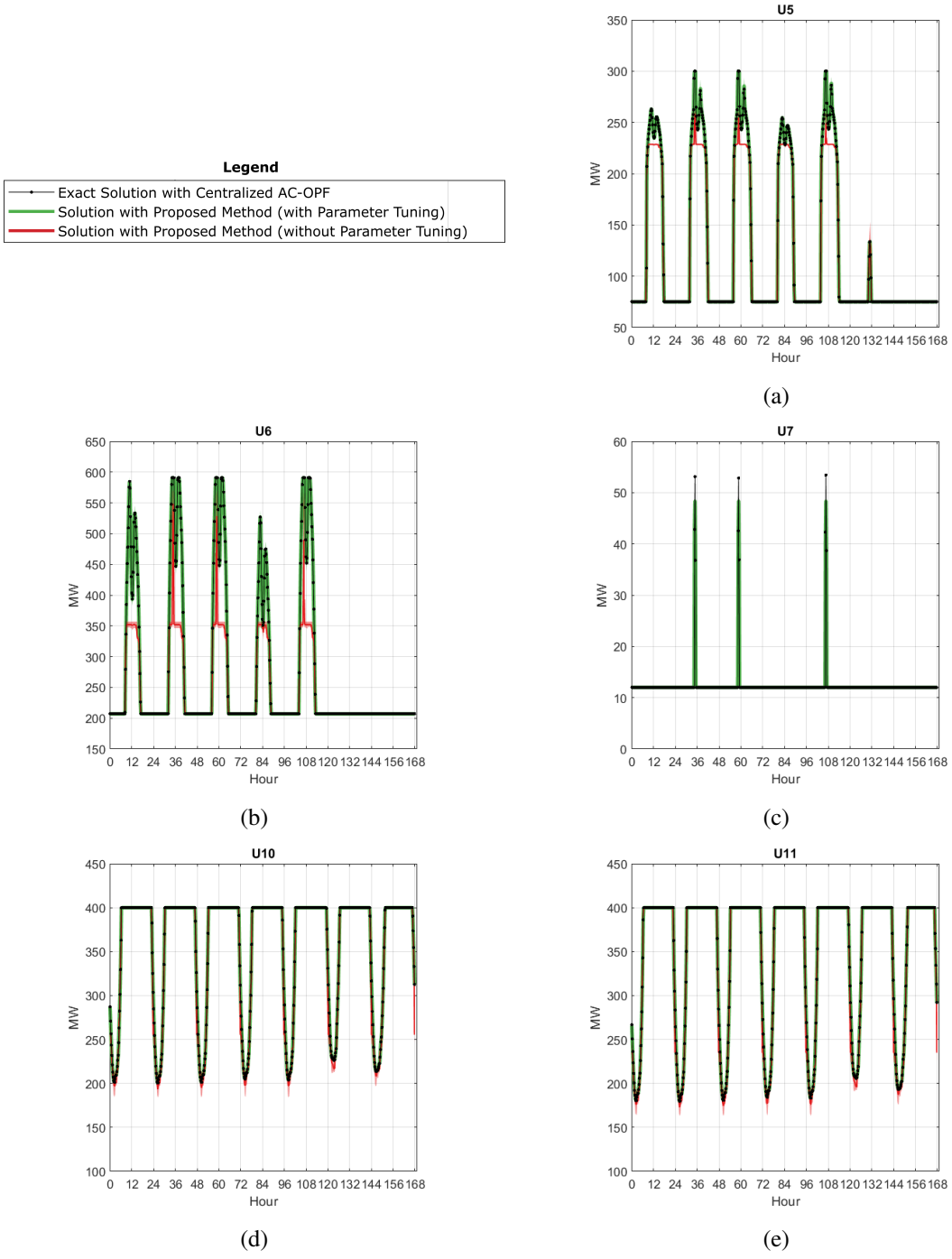

Figure 5.9: Results of the first study: predicted week-ahead generation profile (15-minute resolution) by (a) U5, (b) U6, (c) U7, (d) U10, and (e) U11, with and without parameter tuning, compared against a centralized solution.

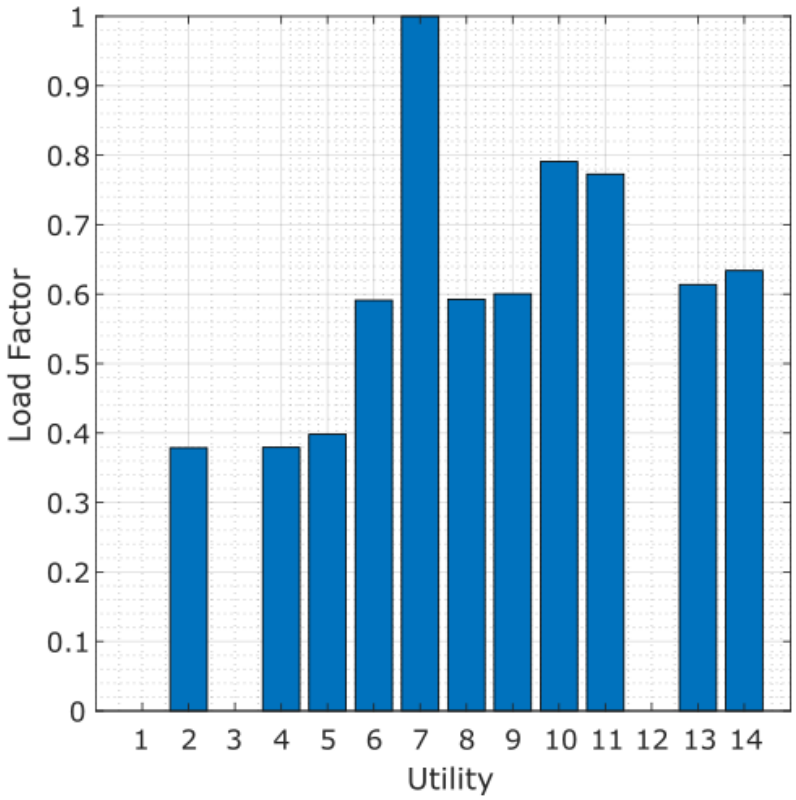

Figure 5.10: Average load factors of the utilities.

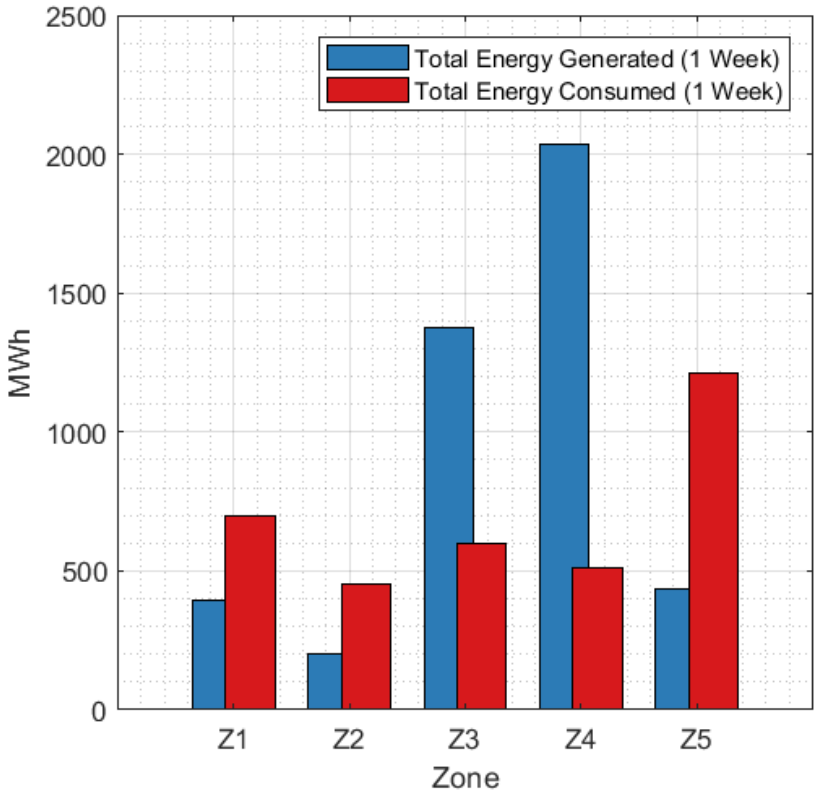

Figure 5.11: Total energy import/export by each zone for the considered week.

Table 5.5: Results of the first study: tuned parameters and MAPE.

Utility	Scenario	Tunable Parameters					MAPE
		N_S	α_{out}	α_{in}	α_{day}	α_{hour}	
U2 (Zone 1)	U2 - Default	10	0.50	0.50	0.50	0.50	0.3790 %
	U2 - Tuned	**9**	**0.05**	**0.60**	**0.90**	**0.70**	**0.0386 %**
U4 (Zone 1)	U4 - Default	10	0.50	0.50	0.50	0.50	0.3788 %
	U4 - Tuned	**9**	**0.05**	**0.95**	**0.70**	**0.95**	**0.0383 %**
U5 (Zone 2)	U5 - Default	10	0.50	0.50	0.50	0.50	2.2590 %
	U5 - Tuned	**16**	**0.05**	**0.55**	**0.90**	**0.40**	**0.0573 %**
U6 (Zone 3)	U6 - Default	10	0.50	0.50	0.50	0.50	6.1020 %
	U6 - Tuned	**25**	**0.05**	**0.45**	**0.75**	**0.80**	**0.0534 %**
U7 (Zone 5)	U7 - Default	10	0.50	0.50	0.50	0.50	0.9695 %
	U7 - Tuned	**4**	**0.05**	**0.30**	**0.85**	**0.35**	**0.0628 %**
U8 (Zone 5)	U8 - Default	10	0.50	0.50	0.50	0.50	0.3234 %
	U8 - Tuned	**36**	**0.05**	**0.40**	**0.95**	**0.55**	**0.0328 %**
U9 (Zone 5)	U9 - Default	10	0.50	0.50	0.50	0.50	0.3041 %
	U9 - Tuned	**9**	**0.05**	**0.35**	**0.75**	**0.65**	**0.0338 %**
U10 (Zone 4)	U10 - Default	10	0.50	0.50	0.50	0.50	0.9498 %
	U10 - Tuned	**36**	**0.05**	**1.00**	**0.70**	**0.40**	**0.0500 %**
U11 (Zone 4)	U11 - Default	10	0.50	0.50	0.50	0.50	1.0449 %
	U11 - Tuned	**25**	**0.05**	**0.10**	**0.95**	**0.55**	**0.0474 %**
U13 (Zone 3)	U13 - Default	10	0.50	0.50	0.50	0.50	0.3104 %
	U13 - Tuned	**25**	**0.05**	**1.00**	**0.55**	**0.95**	**0.0275 %**
U14 (Zone 3)	U14 - Default	10	0.50	0.50	0.50	0.50	0.2732 %
	U14 - Tuned	**25**	**0.05**	**0.15**	**0.80**	**1.00**	**0.0221 %**

5.4.3 Study 3: Comparison with other Methods

In the final study, the proposed algorithm was compared against another ML approach: a NN algorithm. In this scenario, each agent would utilize a feed-forward NN, as the one used in [177], to predict their generation profiles from their local historical datasets. The choice of a NN for comparison is apt for several reasons. First, the proposed algorithm is a ML one, and thus a comparison with a fundamental ML approach is due.

Second, the same local historical datasets can be used for the NN training process. Finally, the utilized feed-forward FF NN is well-established and robust so it would provide a solid benchmark comparison for an implemented ML algorithm. Five critical (worst) cases from the previous two analyses (i,e, U2, U5, U6, U7, and U10) were used for this current study, with one representative utility from each zone. The results are shown in Table 5.7.

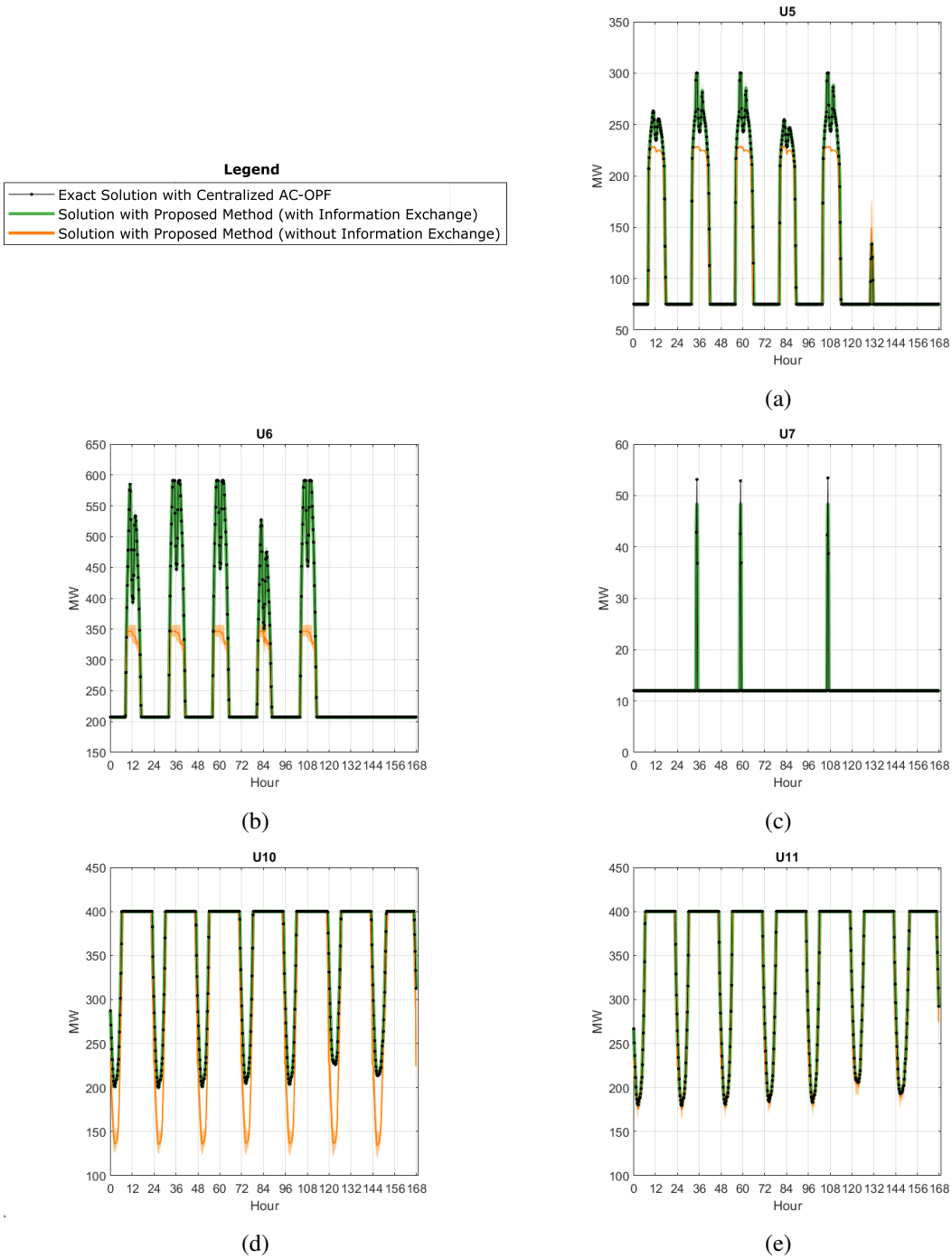

Figure 5.12: Results of the second study: predicted week-ahead generation profile (15-minute resolution) by (a) U5, (b) U6, (c) U7, (d) U10, and (e) U11, with and without information exchange, compared against a centralized solution.

Table 5.6: Results of the second study: MAPE for each utility with and without the implemented cooperative information exchange.

Utility	Scenario	MAPE
U2 (Zone 1)	**Proposed Cooperative Information Exchange**	**0.0386 %**
	Without Information Exchange	0.6760 %
U4 (Zone 1)	**Proposed Cooperative Information Exchange**	**0.0383 %**
	Without Information Exchange	0.9969 %
U5 (Zone 2)	**Proposed Cooperative Information Exchange**	**0.0573 %**
	Without Information Exchange	3.6187 %
U6 (Zone 3)	**Proposed Cooperative Information Exchange**	**0.0534 %**
	Without Information Exchange	0.0694 %
U7 (Zone 5)	**Proposed Cooperative Information Exchange**	**0.0628 %**
	Without Information Exchange	0.9695 %
U8 (Zone 5)	**Proposed Cooperative Information Exchange**	**0.0328 %**
	Without Information Exchange	0.4277 %
U9 (Zone 5)	**Proposed Cooperative Information Exchange**	**0.0338 %**
	Without Information Exchange	0.0321 %
U10 (Zone 4)	**Proposed Cooperative Information Exchange**	**0.0500 %**
	Without Information Exchange	8.0720 %
U11 (Zone 4)	**Proposed Cooperative Information Exchange**	**0.0474 %**
	Without Information Exchange	0.7267 %
U13 (Zone 3)	**Proposed Cooperative Information Exchange**	**0.0275 %**
	Without Information Exchange	1.1598 %
U14 (Zone 3)	**Proposed Cooperative Information Exchange**	**0.0221 %**
	Without Information Exchange	0.2732 %

Table 5.7: Results of the third study: MAPE with the proposed algorithm compared to a NN result.

Utility	Scenario	MAPE
U2 (Zone 1)	**Proposed Algorithm**	**0.0386 %**
	Neural Network (averaged)	0.2252 %
U5 (Zone 2)	**Proposed Algorithm**	**0.0573 %**
	Neural Network (averaged)	0.4193 %
U6 (Zone 3)	**Proposed Algorithm**	**0.0534 %**
	Neural Network (averaged)	0.1678 %
U7 (Zone 5)	**Proposed Algorithm**	**0.0628 %**
	Neural Network (averaged)	0.1126 %
U10 (Zone 4)	**Proposed Algorithm**	**0.0500 %**
	Neural Network (averaged)	0.1822 %

By inspecting the results of this study the following points are noted:

- The proposed algorithm outperforms the NN for all cases. The NN is shown to guarantee a MAPE < 0.5% , while for the proposed method MAPE < 0.1%.
- It was mentioned that the training time of the NN was around the same time as the tuning process of the proposed algorithm. However, a key difference is the fact that the NN training process must be rerun for any new output variable introduced, while the proposed algorithm is tuned once for each utility / agent.
- With this being said, the proposed algorithm not only outperforms the NN in terms of accuracy but also in terms of computational time, since the proposed method's average running time is 4 seconds (for the high resolution week-ahead test case considered).
- The NN network results are dependent on the training process which contains random elements. I.e., the results of the NN are different each time the training process is re-run (hence the averaged results presented in Table 5.7). This is not the case for the proposed algorithm, which provides the same results given the same historical dataset being used, being more reliable than a NN.
- A final important point to note is that one of the main novel contributions of the proposed algorithm is its capability to accommodate cooperative information exchange to enhance the results of individual agents.
- A NN implementation (and other ML algorithms) do not accommodate this, since local datasets are used to train the NN. Therefore to improve the NN results it would be required to further augment or pre-process the historical data itself, and afterwards reperform the training process.
- In the case of the proposed algorithm, the designed cooperative information exchange framework allows agents to dynamically improve their results dynamically while the algorithm is running, adding a significant level of versatility to the proposed approach as opposed to a NN and other ML algorithms (not to mention the higher computational efficiency).

5.5 Conclusions

In this chapter, a novel ML algorithm for fully decentralized power flow management of SGs was proposed, formulated, implemented, and tested. The proposed algorithm relies solely on the local historical data for each local agent to accurately predict their optimal control actions without being given any information on the physical system from outside their local zones (i.e., full grid structure is unknown), and without access to historical data from other agents. The capability of cloud-based cooperative information exchange without sharing private/raw data (e.g., local historical datasets or control actions taken locally) was incorporated through a new concept of an s-index vector, calculated using NW-KDE and represents the similarity between each historical case and the one being predicted.

The s-index and corresponding activation codes of historical cases are encoded vectors which can be shared between agents to improve their control action predictions without sharing raw information. The algorithm was tested using a modified IEEE 24-bus test system and synthetically generating historical operation data based on typical load profiles from Portuguese transmission networks. Based on a demanding, high-resolution (15-minute) week-ahead fully decentralized operation case, the results showed that the proposed algorithm guarantees an accurate prediction with less than 0.1% error compared to a centralized operation case.

The proposed cooperative information exchange also provides opportunities for transactive information exchange using peer-to-peer or cloud-based platforms for cooperative operation by decentralized agents.

Part III

Adapting End-User Energy Management Models

Chapter 6

Residential Prosumer Scheduling in Transactive Energy Networks

In this chapter, a novel fully distributed strategy for joint scheduling of consumption and trading within transactive energy networks is proposed. The aim is maximizing social welfare, which itself is redefined and adapted for peer-to-peer prosumer-based markets. In the proposed scheme, hourly energy values are calculated to coordinate the joint scheduling of consumption and trading, taking into consideration both preferences and needs of all network participants. Electricity market prices are scaled locally based on hourly energy values of each prosumer. This creates a system where energy consumption and trading are coordinated based on the value of energy use throughout the day, rather than only the market price. For each prosumer, scheduling is done by allocating load (consumption) and supply (trading) blocks, maximizing the energy value globally and locally within the network. The proposed strategy was tested using a case study of typical residential prosumers. It is shown that the proposed model could provide potential benefits for both prosumers and the grid, albeit with a user-centered, fully distributed management model which relies solely on local scheduling in transactive energy networks.

Chapter Highlights and Novel Contributions:

- A novel algorithm for fully distributed joint scheduling of energy consumption and trading in residential transactive energy networks is proposed.
- "Energy Value Signals" are proposed as an alternative means of quantifying social welfare, which is redefined and adapted for peer-to-peer prosumer-centered networks.
- The scheduling tool runs locally at each prosumer in order to achieve a maximum global "energy value" throughout the network, simultaneously leveraging consumption scheduling preferences and minimizing costs.
- It is shown that the proposed model provides potential benefits for both the prosumers and the grid, albeit with a user-centered, fully distributed approach.
- Since all calculations run locally at each prosumer, no exchange of private information is needed to achieve fully distributed management of the network, enabling a cloud-based approach for residential prosumer energy management in the IoE paradigm.

Relevant Publication(s):

M. Lotfi, C. Monteiro, M.S. Javadi, M. Shafie-khah and J.P.S. Catalão, "Optimal Prosumer Scheduling in Transactive Energy Networks Based on Energy Value Signals," *2019 International Conference on Smart Energy Systems and Technologies (SEST)*, 2019, pp. 1-6.
Published: https://doi.org/10.1109/SEST.2019.8849017

Chapter Nomenclature

Abbreviation	Definition
DER	Distributed Energy Resources
DR	Demand Response
DSM	Demand Side Management
EP	Energy Premiums
FiT	Feed in Tariff
IEP	Indexed Electricity Price
IoT	Internet of Things
NM	Net Metering
RTP	Real Time Pricing

6.1 Introduction

It is no secret that energy systems are undergoing a substantial paradigm shift, unleashing societal and economic chain reactions rivaled in magnitude by no less than those of the 18th Century industrial revolution. Three centuries and three industrial revolutions later, engineers and policy makers find themselves facing a wave of unprecedented technical breakthroughs and societal changes to which existing structures and mechanisms need to be adapted. The ability to harness and use energy has been the backbone of human development ever since discovering the controlled use of fire. With human civilization now taking a similar leap into advancing the way energy is harnessed and used, it is necessary to revisit energy quantification as a resource, and the way it is managed and traded [178, 179].

6.1.1 State-of-the-Art

The rise of "prosumers" (producers and consumers of energy, simultaneously), was driven by the many recent technological advancements for energy generation (primarily electrical) from local resources, and those to store it, both of which were seldom possible at an economically adequate level of conversion efficiency for small-scales before the current decade [180]. Simultaneously, the increased attention towards the "demand"-side by means of the development of new enabling technologies, and more importantly by the enactment of legislation to direct demand side management (DSM) and demand response (DR) policies, has inspired the mindset of moving towards more user-centric and decentralized energy systems [89]. This was further enabled by the rise of the Internet of Things (IoT), and strengthened information infrastructures which allow for real-time communication, data analysis, and decision-making to take place in modern smart grids [76].

The most pressing issue is adapting existing structures and frameworks to this proliferation of small-scale resources. This gives more power to prosumers, dismantling established structures of energy markets, especially with regards to the relationship between the grid and the prosumer sides [98]. With prosumer-centered energy trading emerging as a disruptive scenario, there is little literature available with concrete solutions to this paradigm shift. Most offered solutions are based on traditional approaches such as the Feed-in-Tariff (FiT) or Energy Premiums (EP). These models are vastly outdated and were initially meant as incentives in the early days of distributed energy resources (DER) penetration, and never meant as a permanent approach upon which new management tools are to be developed [180, 181]. The proposed solutions so far can be said to exist between two extremes.

The first, more outdated, extreme is where prosumers with installed local generation either store any surplus generation or feed it into the grid, either for no payment at all (especially in the case of EPs or DER-subsidy programs) or in exchange for a flat-rate (the case of FiT). In all cases, this class of solutions is economically unfair for the prosumers as they are seldom compensated for services they provide to the grid [98].

The other, recently more popular, extreme is referred to as net-metering (NM) in which the grid pays prosumers the full grid price for feeding-in their surplus generation, acting as their "battery" [182]. This approach is inherently interlinked with the implementation of price-based DR programs, particularly real-time pricing (RTP), which is the only current framework of establishing a link between market conditions and the prosumers [183].

Many DR programs are already implemented in different markets around the world. Although DR was not originally established for this purpose, it can temporarily suffice as a way of managing this sudden proliferation of prosumers in order to ensure an economic benefit for both sides. Moreover, almost all currently implemented DR programs are based on centralized or hierarchical structures in which the grid-side operator is in control [89, 181, 45]. However, a shift towards more user-centric systems with fully distributed management is inevitable in case of prosumer-dominated energy networks. As such, the use of DR as a temporary solution will have to be replaced soon by a more permanent energy management framework. One solution rapidly gaining interest is peer-to-peer trading, which is now enabled by distributed ledger and optimization technologies [98, 99, 184, 185].

6.2 Methodology and Formulation

Being inherently a "social" concept, it is important to reestablish the underlying definition of social welfare before proceeding to quantify it mathematically or incorporate it in any model. The Oxford dictionary defines social welfare as:

"The well-being of a community or society,
especially with regard to
health and economic matters." [186]

From there, the concept is extended to the definition used in the domain of economics:

"The well-being of the entire society.
Social welfare is not the same as standard of living
but is more concerned with the quality of life." [187]

Here we can establish that social welfare emphasizes the way in which resources are allocated and used within a society, i.e. quality, rather than the collective availability or cost of this resource i.e., quantity or total standard of living. This is important to establish before proceeding to mathematically modeling and quantifying social welfare for application in the context of electrical power systems.

6.2.1 Status-Quo of Social Welfare Models

In power systems scientific research, a vast majority of the literature uses the Bergson-Samuelson function [188] (or an adaptation thereof) to quantify social welfare [189, 58, 190]. In this model, a number of individuals in a society ($i = 1,2,\ldots,n$) require some commodity (x) which is allocated in different amounts to each of them (x_i). The desire or need of each individual to this utility (i.e., how much they would be willing to pay for every additional unit of this utility) can be expressed using a utility function for each individual and their allocation: $u_i(x_i)$. The opposite applies for the supplier of a utility: the utility function in this case represents how much it would cost for them to generate an additional unit of the commodity (in this case the value is negative). The Bergson–Samuelson model thereby defines social welfare as a function of all individual utility functions in the society [188]:

$$W_{BS} = f\left(u_1\left(x_1\right), u_2\left(x_2\right), \ldots u_n\left(x_n\right)\right) \tag{6.1}$$

This general definition was adapted for double-sided bidding competitive electricity markets by the majority of literature, to obtain the form shown in (6.2).

$$W_{BS} = \sum_i U_i\left(Q_2(i)\right) - \sum_j C_j\left(Q_0(j)\right) - C_T \tag{6.2}$$

In this case, the social welfare function represents the sum of utility functions of consumers and generators of energy, in addition to the transmission and/or grid costs (C_T). The benefit of a consumer to use purchased energy is incorporated by means of their utility function [188].

6.2.2 Social Welfare of Prosumers

It is clear that the existing approach of quantifying this benefit of energy use does not apply to the newly emerging paradigm of prosumer-based transactive energy networks. First, in this paradigm, there is no clear distinction between the supply and demand sides in the same manner quantified by the utility functions.

Secondly, a prosumer's benefit of using energy may not always depend only on their desire to use their loads/appliances, but may depend also on current market conditions which may make it more profitable for them to transact their generated energy rather than use it, or vice versa.

6.2.3 Energy Value Signals

Consider a residential prosumer that has a varying number of schedulable appliances α_i. These loads are scheduled for different timeslots t of each day. The scheduling of the appliances can be mathematically represented by means of an allocation matrix A, described as follows:

$$A_t^{\alpha} := A(t,\alpha) = \begin{cases} 1, & \text{if } \alpha \text{ is on in } t \\ 0, & \text{if } \alpha \text{ is off in } t \end{cases} \tag{6.3}$$

Based on their preferences, the prosumer can control an energy value signal for each load, which reflects the value of allocating energy consumption to this load during various timeslots of the day. In our proposed model, we define this energy value signal ζ_t as follows:

$$\zeta_t^{\alpha} = \mu_t^{\alpha} \cdot \gamma + P_t^G \tag{6.4}$$

In this case, the prosumer's value of allocating energy to an appliance α during timeslot t is obtained by scaling the current price of electricity from the grid (P_t^G) by means of a user-defined preference of (μ_t^{α}) and a rigidity factor R. The energy value matrix can then be compiled as follows, with the same dimensions as the allocation matrix.

$$\mathrm{Z}_{t,\alpha} := \mathrm{Z}(t,\alpha) = \zeta_t^{\alpha} \tag{6.5}$$

The preference μ_t^{α} defined as a real number between one and the maximum value of R_{max}:

$$\mu_t^{\alpha} \in \mathbb{R} \cap [0,1] \tag{6.6}$$

The rigidity R is defined as an integer between one and a upper limit value of R_{max}:

$$R \in \mathbb{Z} \cap [1, R_{\max}] : 2 < R_{\max} \tag{6.7}$$

This rigidity factor determines a prosumer's flexibility to allocate a load to different hours. A scaling factor is then used:

$$\gamma = f\left(\gamma_b, R, P_t^G\right) := \frac{(R-1)}{(R_{\max}-1)} \cdot \gamma_b \cdot P_t^G \tag{6.8}$$

On the other hand, the total energy supply available throughout the day consists of contracted power the grid and all prosumers making offers for the decision-making window:

$$\sigma \in \mathrm{S} = \{G, \Psi\} \tag{6.9}$$

And the set of prosumers is defined accordingly:

$$\psi \in \Psi = \left\{\psi_1, \psi_2, \ldots, \psi_{N_\psi}\right\} \tag{6.10}$$

Each prosumer offers a price to supply electricity for every hour. In our proposed framework, this price needs to be less than the grid price, but also higher than the price to feed-in to the grid. Operating between both extremes of FiT and NM, we choose a more moderate indexed electricity price (IEP).

$$P_t^{\psi} = \kappa_t^{\psi} \cdot P_t^G \tag{6.11}$$

The competitiveness coefficient κ reflects the "greediness" of each prosumer when making their offers: i.e., the higher the offer, the greater the profit made by this prosumer albeit with a greater risk of not selling their energy due to better offers. This value drives the competitiveness between prosumers in the proposed transactive energy market model.

This limitation is based on the IEP as a fraction of the grid price. In this sense, if the competitiveness of a prosumer is too high and fails to transact their energy offer, the alternative is feeding their surplus energy to the upper level of the grid.

$$\phi_t^{IEP} = \frac{P_t^{IEP}}{P_t^G} \tag{6.12}$$

Looking back to the reference prosumer, the amount of energy transacted from a supplier (prosumer or the grid) is expressed as:

$$\tau_t^{\sigma} \in \mathbb{R} \cap [0, \omega_t^{\sigma}] \tag{6.13}$$

As such, partial transactions from each supplier can be made with a maximum amount equal to the offered quantity ω_t^{σ} from that prosumer for that timeslot. An important aspect of this model is that the reference prosumer enters the market themselves by making energy offers from locally generated energy. The self-consumption of the prosumer is thereby a result of them self-transacting the energy. I.e., there is no discrimination between the prosumers offering energy supply in the scheduling model; it is only based on the offered prices for each timeslot.

6.2.4 Prosumption Scheduling

With all relevant definitions now established, it is possible to implement a tool for coordinated scheduling between energy consumption and trading scheduling which can be summarized in threes steps as follows:

Step 1: Sort incoming offers from suppliers in ascending order of cost for each timeslot.

Step 2: Schedule consumption blocks based on defined energy value of each block for each timeslot, such that the maximum energy value is achieved for the day, constrained by the maximum available power supply.

Step 3: Execute consecutive energy transactions from suppliers in descending order of cost based on calculated consumption schedule.

Table 6.1: Schedulable loads in the reference prosumer's residential household.

α - Load Description	Power (kW)	Duration (h)
α_1 - Space Heaters	3.0	6
α_2 - Oven and Stove	2.0	2
α_3 – Clothes Iron	1.0	1
α_4 - Clothes Dryer	3.0	3
α_5 - Clothes Washer	1.0	3
α_6 - Dishwasher	2.0	1
α_7 - Refrigerator	0.5	20
α_8 - Entertainment (TV / PC)	0.4	4
α_9 - Base Load	2.0	24
α_{10} - Lighting	0.6	16

6.3 Case Study and Analysis

To demonstrate the proposed framework, we consider a typical household with the schedulable loads listed in Table 6.1. The scheduling is performed for a 24-hour-ahead period with hourly timeslots for energy consumption and transaction scheduling. In Fig. 6.1, the total available energy offered from the grid or prosumers for each hour is shown. The prosumer is assumed to have a contracted power of 10.35 kW with the grid, which sets their maximum hourly load. The green bars show the energy offers made from different prosumers connected to the transactive energy network for this decision- making horizon.

Table 6.2: Hourly prices for energy offers from the grid (G) and prosumers ($\Psi_1, \Psi_2, ..., \Psi_{10}$) in the transactive energy network.

t	G	Ψ_1	Ψ_2	Ψ_3	Ψ_4	Ψ_5	Ψ_6	Ψ_7	Ψ_8	Ψ_9
1	0.057	1.000	1.000	1.000	1.000	1.000	1.000	1.000	1.000	1.000
2	0.051	1.000	1.000	1.000	1.000	1.000	1.000	1.000	1.000	1.000
3	0.050	1.000	1.000	1.000	1.000	1.000	1.000	1.000	1.000	1.000
4	0.048	1.000	1.000	1.000	1.000	1.000	1.000	1.000	1.000	1.000
5	0.047	1.000	1.000	1.000	1.000	1.000	1.000	1.000	1.000	1.000
6	0.049	1.000	1.000	1.000	1.000	1.000	1.000	1.000	1.000	1.000
7	0.048	1.000	1.000	1.000	1.000	1.000	1.000	1.000	1.000	1.000
8	0.050	1.000	1.000	1.000	1.000	1.000	1.000	1.000	1.000	1.000
9	0.053	1.000	1.000	1.000	1.000	1.000	1.000	1.000	1.000	1.000
10	0.054	0.049	0.050	0.051	0.053	0.051	0.052	0.054	0.051	0.050
11	0.058	0.053	0.058	0.058	0.053	0.058	0.053	0.055	0.057	0.055
12	0.059	0.057	0.056	0.057	0.058	0.058	0.055	0.054	0.058	0.059
13	0.060	0.054	0.057	0.057	0.057	0.059	0.054	0.056	0.057	0.059
14	0.059	0.057	0.059	0.054	0.059	0.056	0.057	0.059	0.055	0.058
15	0.059	0.057	0.058	0.054	0.055	0.054	0.054	0.059	0.056	0.056
16	0.053	0.052	0.052	0.053	0.053	0.052	0.053	0.051	0.051	0.049
17	0.053	0.050	0.051	0.053	0.052	0.051	0.051	0.052	0.053	0.052
18	0.060	0.057	0.059	0.055	0.054	0.056	0.058	0.054	0.059	0.055
19	0.068	0.062	0.067	0.067	0.067	0.063	0.062	0.067	0.066	0.062
20	0.070	1.000	1.000	1.000	1.000	1.000	1.000	1.000	1.000	1.000
21	0.070	1.000	1.000	1.000	1.000	1.000	1.000	1.000	1.000	1.000
22	0.067	1.000	1.000	1.000	1.000	1.000	1.000	1.000	1.000	1.000
23	0.067	1.000	1.000	1.000	1.000	1.000	1.000	1.000	1.000	1.000
24	0.066	1.000	1.000	1.000	1.000	1.000	1.000	1.000	1.000	1.000

In this case, nine prosumers are making offers with different maximum energy quantities and prices for each hour. Different prices (including transmission costs) offered by each supplier are shown in Table 6.2, with the reference prosumer (the one doing the scheduling) personally participating in this market, being represented as prosumer one, or Ψ_1. The hourly prices from the grid are shown in red, with darker values being higher. For each hour, the prices offered by prosumers are shaded from lightest to darkest, relative to how much less they are compared to the grid price of that hour.

It is obvious that all prosumers have solar-based generation. Different generation scenarios, in addition to different randomized uncertainties have been modeled for each prosumer to reflect a realistic case. As previously elaborated in Section 6.2.3, the values in Table 6.2 show that the prosumers offer energy at hourly prices, which are between the grid price and the IEP: refer to (9) and (10). In this case, we assume the IEP to be 10% of the grid price. Different prosumers make more or less competitive offers each hour based on their strategy.

In this case study, we assume the hourly competitive coefficient, κ, for each prosumer to vary randomly. The hourly energy offers are visualized in Fig. 6.2, which clearly shows multiple aspects of the considered transactive energy market.

First, the grid hourly prices reflect the implementation of some real-time pricing (RTP) DR program, reflecting higher prices in times of higher demand for residential consumption. This will be re-emphasized shortly with the introduction of the prosumer preferences for appliance scheduling.

As such, the existence of both a fully decentralized transactive energy market for prosumers and a market for large utilities will be shown to not be mutually exclusive. Rather, the interaction between the two may very well lead to more efficient systems. While this is out of the scope of this study, this interaction will be the focus of future studies on this proposed framework, in which this model can be scaled to what is sometimes referred to as “fractal” energy systems.

This brings up the second aspect to infer from Figure 2. A prosumer’s bidding strategy can have a significant effect on market dynamics, including strategies of other prosumers. This dynamic interaction is not only confined within the prosumers transactive network, but extends to the grid. The main motive of DR programs and RTP was to incentivize active participation from consumers. This idea can be extended to this prosumer-based model, with the prosumers’ bidding strategies within their network having a significant effect on grid prices, enabling a two-way interaction between grid prices, prosumer prices, and a dynamically changing IEP index, resulting in a varying bidding margin for prosumers. This will be addressed in future studies on this framework.

The final step to setup up the case study is for the reference prosumer to indicate their preference for the allocation of the appliances. This is shown in Table III, in which these values are normalized and transformed to calculate the value signals.

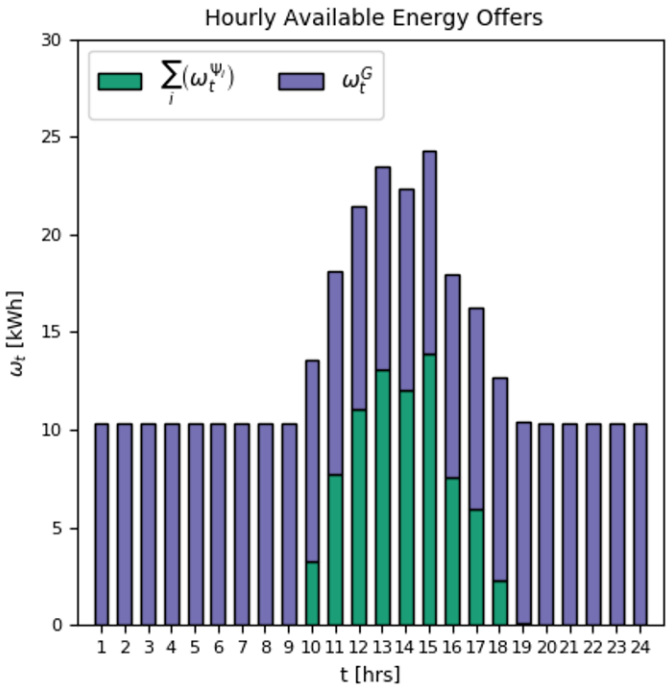

Figure 6.1: Hourly available energy from suppliers in the transactive network: Grid (purple) and Prosumers (green).

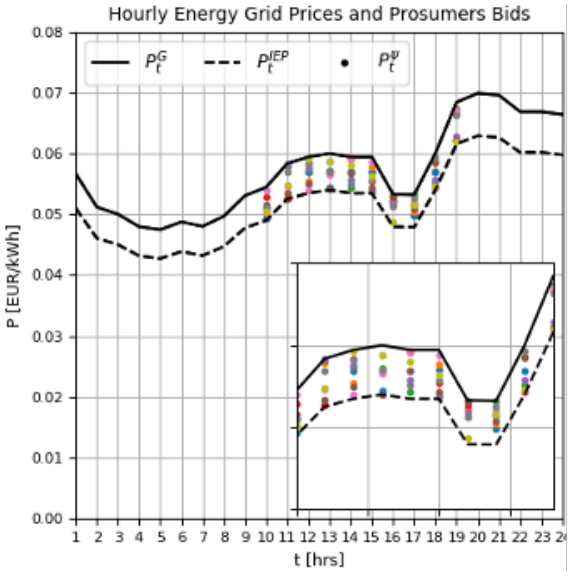

Figure 6.2: Hourly values of energy price corresponding to: grid supply (solid black line), grid-indexed electricity price (dashed black line), and prosumers in the transactive network (different colored dots corresponding to different prosumers). Hours with prosumer offers (during the day hours due to reliance on solar generation) are zoomed in on the bottom-right corner.

6.4 Results and Discussion

The optimal schedule is obtained using the approach highlighted in Section 6.3.4. In this study, an exhaustive search code implemented using Python was used. The model takes a fraction of a second to run, showing that by employing a more superior optimization algorithm it can run in real-time. Table IV shows the resulting allocation matrix $\mathrm{A}(t, \alpha)$.

It can be seen that the scheduling tool attempted as much as possible to adhere to user preferences, subject to also minimizing the energy cost and thereby maximizing the total value of energy for each hour (the objective function of the optimization model).

For instance, the space heater (α_1) was scheduled two hours before the preferred hours for the prosumer, due to the significantly higher availability of (cheaper) energy supplied through other prosumers in the transactive network. The same applies to the refrigerator (α_7), scheduled at 1:00. This can be seen in Fig. 6.3.

Table 6.3: Reference prosumer preferences for applicance allocation (1->lowest, 3->highest).

t	a_1	a_2	a_3	a_4	a_5	a_6	a_7	a_8	a_9
1	1	1	1	1	1	1	1	1	1
2	1	1	1	1	1	1	1	1	1
3	1	1	1	1	1	1	1	1	1
4	1	1	1	1	1	1	1	1	1
5	1	1	1	1	1	1	1	1	1
6	1	1	1	1	1	1	1	1	1
7	1	1	1	2	1	1	1	1	1
8	1	1	1	2	1	1	1	1	1
9	1	1	1	2	1	2	1	1	1
10	1	1	1	2	1	3	1	1	1
11	1	1	1	2	1	3	1	1	1
12	1	1	1	2	1	3	1	1	1
13	1	1	1	2	1	3	2	1	1
14	1	1	1	2	1	3	3	1	1
15	1	1	1	2	1	2	3	1	1
16	2	1	1	2	1	1	3	1	1
17	2	1	1	1	1	1	1	1	1
18	2	1	2	1	1	1	1	1	1
19	2	2	3	1	2	1	1	3	1
20	2	3	2	1	3	1	1	3	1
21	2	2	1	1	3	1	1	3	1
22	1	1	1	1	2	1	1	3	1
23	1	1	1	1	1	1	1	3	1
24	1	1	1	1	1	1	1	3	1

Table 6.4: Obtained allocation matrix for appliances.

t	a_1	a_2	a_3	a_4	a_5	a_6	a_7	a_8	a_9
1	0	0	0	0	0	0	1	0	1
2	0	0	0	0	0	0	1	0	1
3	0	0	0	0	0	0	1	0	1
4	0	0	0	0	0	0	1	0	1
5	0	0	0	0	0	0	1	0	1
6	0	0	0	0	0	0	1	0	1
7	0	0	0	1	0	0	1	0	1
8	0	0	0	1	0	0	1	0	1
9	0	0	0	1	0	0	1	0	1
10	0	0	0	0	0	1	1	0	1
11	0	0	0	0	0	0	1	0	1
12	0	0	0	0	0	0	1	0	1
13	0	0	0	0	0	0	1	0	1
14	1	0	0	0	0	0	1	0	1
15	1	0	0	0	0	0	1	0	1
16	1	0	0	0	0	0	1	0	1
17	1	0	0	0	0	0	1	0	1
18	1	0	0	0	0	0	1	0	1
19	1	1	1	0	0	0	1	0	1
20	0	1	0	0	1	0	1	0	1
21	0	0	0	0	1	0	0	1	1
22	0	0	0	0	1	0	0	1	1
23	0	0	0	0	0	0	0	1	1
24	0	0	0	0	0	0	0	1	1

It can be seen that from 11:00 to 15:00, the energy is 100% supplied from the prosumers in the transactive network. This corresponds to a significant reduction of energy cost during those hours, as shown in Fig. 6.4.

Concerning energy trading, it can be seen that while energy cost was minimized as much as possible, this did not come at the cost of sacrificing the reference prosumer's welfare, with the peak load occurring at 19:00, when there was in fact no supply from the transactive network of prosumers. However, the maximum possible utilization of cheaper energy from the transaction energy was achieved as can be seen in Fig. 6.3. This can also be seen in Fig. 6.4, where the maximized energy value signal can be compared to the hourly energy cost.

By being more flexible in their consumption preferences (refer to Table 6.3), the reference prosumer can guide the scheduling tools to give more weight to cost reduction, and vice versa.

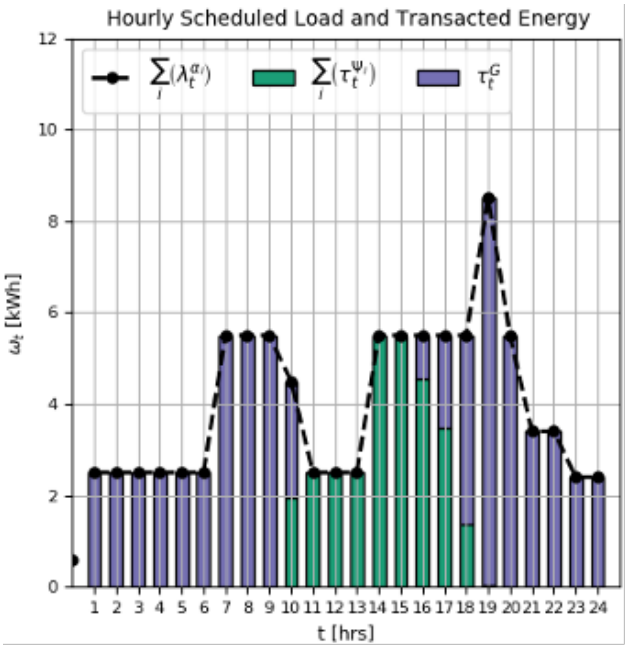

Figure 6.3: Hourly scheduled load and transacted energy. The total hourly load is shown using the black dotted line, the energy purchased from the grid is shown using the purple bars, and the total transacted energy from the prosumers in the transactive network is shown using the green bars.

Finally, we can now compare our proposed framework with the traditional approaches existing on both extremes as discussed in Section 6.1. By comparison with the case of net metering, our model exhibits a potential benefit for the upstream grid as it does not have to pay for energy generated locally by the consumers as they pay each other locally within the transactive network. In addition, our framework provides the coordinated scheduling of prosumers in a fully distributed manner, without the need of a central operator, while always providing a guarantee that the generated electricity will be paid for regardless of the "presumption" schedules of the users in the network. The only thing that varies (maximized) is the global value of energy, but in all cases, any locally generated energy will be paid for, with the worst-case scenario corresponding to the lower bidding margin of the IEP. On the other hand, comparison with systems where the prosumers are not paid for fed-in energy, it is obvious that this framework provide a benefit for the prosumers. In fact, the proposed framework can be directly applied to such systems, as an extreme case of having a zero-valued IEP bidding margin. All in all, the proposed model can provide potential economic benefits to both the grid and prosumer, while being user- centric and fully distributed.

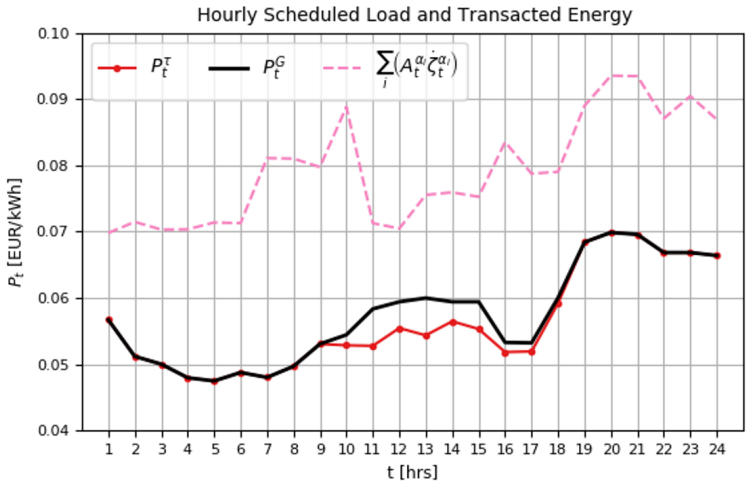

Figure 6.4: Hourly energy price paid by reference prosumer (red line), electricity price from the grid (black) and the maximized energy value signal (pink dashed line).

An important aspect to note is that the reference prosumer is participating in the transactive energy market, and with no discrimination between buying energy from themselves or other prosumers. The only deciding factor is offered price from each prosumer. This is important for the market dynamics, as there are hours when the prosumer can profit more by selling it to another rather than self-consuming (or in this case, self-transacting) it. In this study, we consider all the offered prices already including the transmission and grid connection costs. However, the transactive network can be a virtual one rather than physical, and follow-up work can investigate the effect of the presence of prosumers from different low-voltage networks.

6.5 Conclusions

In this study, we propose and test a novel framework for distributed management of transactive energy networks. Energy value signals are proposed as an alternative means of quantifying social welfare for prosumer-centered networks. Afterwards, a coordinated scheduling algorithm for joint scheduling of energy consumption and trading is formulated. The scheduling tool runs locally at each prosumer in order to achieve a maximum global energy throughout the network. Rather than minimizing energy costs as traditional models do, in this case we maximize energy value, which we propose as a new way of quantifying social welfare for prosumer networks, simultaneously leveraging consumption scheduling preferences and minimizing costs. Energy value reflects the value set by the user of allocating energy for a certain usage at a certain time. These user preferences are input locally resulting in the optimal schedule of each prosumer, which in turn affects the price of energy globally in a similar manner to demand response programs. The local energy transactions are guided within a margin relative to the upstream grid prices. It was shown that the proposed model could provide potential benefits for both prosumers and the grid, albeit with a user- centered, fully distributed approach to schedule energy consumption and trading in transactive energy networks of prosumers. Since all calculations run locally at each prosumer, no exchange of private information is needed to achieve fully distributed management of the network. For future work, the effect of employing such a model on power flow and grid connection costs should be investigated in detail in order to confirm the applicability of this approach on existing power systems. Moreover, investigation of the effect of employing different bidding strategies by the prosumers should be performed, in order to ensure transparency and verification can be guaranteed between the prosumers.

Chapter 7

Design of Fully Electric Public Transport Systems and Charging Infrastructures

In this chapter, a generalized mathematical formulation is proposed to model a generic fully electric public transport system, and a mixed-integer linear programming (MILP) optimization is used to determine the optimal design of the system in terms of charging infrastructure deployment (with on-route and off-route charging), battery sizing, and charging schedules for each route in the network. Three case studies are used to validate the proposed model while demonstrating its universal applicability. First, the design of three individual routes with different characteristics is demonstrated. Then, a large-scale generic transport system with 180 routes, consisting of urban and suburban routes with varying characteristics is considered and the optimal design is obtained. Afterwards, the use of the proposed model for a long-term transport system planning problem is demonstrated by adapting the system to a 2030 scenario based on forecasted technological advancements. The proposed formulation is shown to be highly versatile in modeling a wide variety of components in an electric bus (EB) transport system and in achieving an optimal design with minimal TOC.

Chapter Highlights and Novel Contributions:

- A universal mathematical model for fully electric public transport networks is developed using mixed-integer linear programming (MILP) to minimize the total ownership cost (TOC).
- The proposed model determines the optimal design of transport networks in terms of charging, battery sizing, and charging schedules for each route in the network. Dynamic electricity tariffs are incorporated in the model.
- Three case studies are considered: optimization of individual routes (case study 1), design of large-scale system (case study 2), and long-term planning of large-scale transport systems adapting to a 2030 scenario based on forecasted technological advancements (case study 3).

Relevant Publication(s):

M. Lotfi, P. Pereira, N. G. Paterakis, H. A. Gabbar and J. P. S. Catalão, "Optimal Design of Electric Bus Transport Systems With Minimal Total Ownership Cost," in *IEEE Access*, vol. 8, pp. 119184-119199, 2020.
Published: https://doi.org/10.1109/ACCESS.2020.3004910

M. Lotfi, P. Pereira, N. Paterakis, H.A. Gabbar, J.P.S. Catalão, "Optimizing Charging Infrastructures of Electric Bus Routes to Minimize Total Ownership Cost," *2020 IEEE International Conference on Environment and Electrical Engineering and 2020 IEEE Industrial and Commercial Power Systems Europe (EEEIC / I&CPS Europe)*, 2020, pp. 1-6.
Published: https://doi.org/10.1109/EEEIC/ICPSEurope49358.2020.9160687

Chapter Nomenclature

Abbreviation	Definition
AML	Algebraic Modeling System
CC	City Center
DC	Depot Charger
DER	Distributed Energy Resource
EB	Electric Bus
ESS	Energy Storage System
EV	Electric Vehicle
FC	Flash Charger
FLC	Fuzzy Logic Controller
GA	Genetic Algorithm
HF	High Frequency
LD	Long Distance
LF	Low Frequency
LV	Low Voltage
MD	Medium Distance
MILP	Mixed Integer Linear Programming
MIP	Mixed Integer Programming
MPC	Model Predictive Control
MV	Medium Voltage
NLP	Non Linear Programming
SD	Short Distance
SoC	State of Charge
SU	Suburban
TC	Terminal Charger
TOC	Total Ownership Cost

7.1 Introduction

7.1.1 Background and Motivation

In the context of public transport systems, the transition to a fully electric fleet is quite easy to carry out for three main reasons: First, due to heavy usage, public transport buses are frequently replaced and thus EBs can gradually replace conventional buses in the fleet without causing any interruption. Second, public transportation schedules are largely fixed (on the short-to-medium term), and thus individual upgrades to EBs can be seamlessly performed. Third, investment stability is mostly guaranteed in the public transportation sector, which facilitates the acquisition of new EB technologies [1]. In addition to the aforementioned facts, EB fleets have been shown to have a lower total ownership cost (TOC) compared to their conventional counterparts [191].

With all this being said, the main challenge hindering the transition thereto is the complexity involving designing an optimal charging infrastructure which meets the needs of the transport system and adheres to techno-economic constraints while maintaining the minimal TOC of the system [1]. With this being the primary motivation behind this work, a survey or recent scientific literature has been performed to identify the state-of-the-art progress on this topic.

7.1.2 State-of-the-Art Survey

In a recent study [192], the design of an EB transport system was optimized in terms of the fleet size and mix (with specifications of different bus types), and the charging infrastructure. The study identified that range limitation is indeed a main hurdle in electrification of public transport systems and that optimal design thereof is of paramount importance. By modeling the transport network of two European cities, a genetic algorithm (GA) was used obtain the optimal mix of EB models and the required number of each. The objective function of the GA was formulated as the TOC.

The authors in [193] used an enhanced GA algorithm combined with a departure time adjustment procedure to optimize EB deployment scheduling for a given bus route. The proposed model was applied to a bus route from a real-world public transit system in Nanjing, China. The results of the study showed that by applying the proposed model to optimize EB deployment and scheduling on that route, the operating costs are decreased due to the reduced number of deployed buses and drivers, as compared to experience-based scheduling used in the real-world scenario.

Another study [194] utilized a GA as an optimization approach for EB-based public transport systems. A realworld transit network in China was modeled, and the objective was to determine the optimal EB scheduling and charging infrastructure in order to meet the (constraint) scheduled routes with minimal charging costs. A sensitivity analysis was used to assess the economic viability of the charging power and discharging depth (direct functions of charging infrastructure and EB schedules, respectively).

Table 7.1: A synopsis of recently published studies addressing the optimization of electric bus public transportation networks.

Reference	Computational Model	Charging Infrastructure	Charging Schedule	Routes	Battery Capacity	Bus Deployment
[193]	**GA**	Constraint	Constraint	Constraint	Constraint	**Decision Variable**
[194]	**GA**	Constraint	**Decision Variable**	Constraint	Constraint	**Decision Variable**
[195]	**NLP**	Constraint	**Decision Variable**	Constraint	Constraint	Constraint
[196]	**FLC**	Constraint	**Decision Variable**	Constraint	Constraint	Constraint
[197]	**MILP**	**Decision Variable**	Constraint	Constraint	**Decision Variable**	Constraint
[198]	**MIP**	**Decision Variable**	Constraint	Constraint	Constraint	Constraint

In [195], the target of the study was to evaluate the interaction between EB public transportation networks and the electrical grid, in the presence of dynamic pricing. A nonlinear programming (NLP) model was used to determine the optimal charging schedule for EBs of eight EB routes in Shenzhen, China. The proposed optimization framework was employed to determine the charging schedules which would provide a tradeoff between meeting the transportation network constraints and minimizing the power grid congestions.

Similarly, [196] aimed at optimizing the power exchange between the public transport network and the power grid through the use of fuzzy logic control (FLC) to control the energy flow between the charging infrastructure and the EBs in the predefined transport network. The proposed model was used to perform simulations based on EB routes in Assam, India, and was shown to improve the voltage profile of the power grid while adhering to the transport network requirements and route schedules.

While the main focus of some studies was optimizing the EB schedules, others were concerned with optimizing the charging infrastructure, given a specified EB fleet. The previous studies [192, 194], like many others, considered only the presence of a charger at the EB depot, meaning they to return to the original depot in order to recharge. Other studies tackled this problem by considering other locations for energy storage systems (ESSs) and/or fast chargers throughout the network which can be used to charge the EBs without having to make a full trip back.

In [197], mixed-integer programming (MIP) was used to minimize the TOC of a real world transportation network of a town in the United States. The optimal deployment of fast charging stations and ESS throughout the network was achieved. Similarly, another study [198] utilized MIP to for optimal charging station planning for a transport network of a city in China. The objective in this case was to determine the optimal sizing and siting of the charging stations, which minimizes the total cost at each stage of the planning problem.

The most recent scientific literature addressing the problem of optimizing EB public transport networks have been surveyed, and compiled in Table 7.1. The conducted literature survey led to two main findings:

- All surveyed scientific publications have been concerned with the optimization of one or two elements of the transport system, with the other aspects being considered as model constraints.

- All studies were performed on specific case studies based on existing transport networks in real-world cities. No studies were found to model generic networks or testing the universal applicability of the proposed model.

Accordingly, in this work a universal mathematical model for fully electric public transportation networks is developed and formulated as a mixed-integer linear programming (MILP) optimization problem with the objective of minimizing the TOC. The nature of the proposed model is universal, i.e., any set of routes, buses, and type of charging infrastructure can be considered as a parameter or a decision variable. In this sense, the model is highly versatile and can be used to optimize existing systems or to design new ones.

7.2 Public Transport Network Model

In Fig. 7.1, a public transport system is illustrated along with its components. A generic system is comprised of the following components:

- **Depot**: The depot is where the buses are dispatched from, and is where they park and charge while they are not in service.
- **Electric Bus**: The electric buses (EBs) are the backbone of the network, traversing the routes with passengers on board. EBs have onboard batteries which are recharged at designated charging locations in the network.
- **Routes**: The routes are the paths which EBs must traverse to transport passengers. Routes are made up of bus stops and are scheduled. The scheduling can be based on a specific time at which the EB must arrive/depart from/to each spot, or a frequency for the EBs to traverse the route (e,g. 1 bus to pass by a stop every X minutes).
- **Terminals**: Terminals are usually bus stops at which several routes intersect and therefore have an allocated area and infrastructure for use by the EBs
- **Charging Infrastructure**: The charging infrastructure provides the energy needs of the system. The chargers where buses can recharge their batteries can be off-route (e.g. at depots) or on-route (e.g. at terminals).

As illustrated in Fig 7.1, three main types of chargers are currently available commercially [199, 200, 201]. The first is the depot charger (DC), typically used to charge the buses during the time when they are out of service and parked at the depot (off-route). DCs typically have rated powers ranging from 50 kW to 100 kW, intended for slow charging of the batteries overnight or while they are out of service.

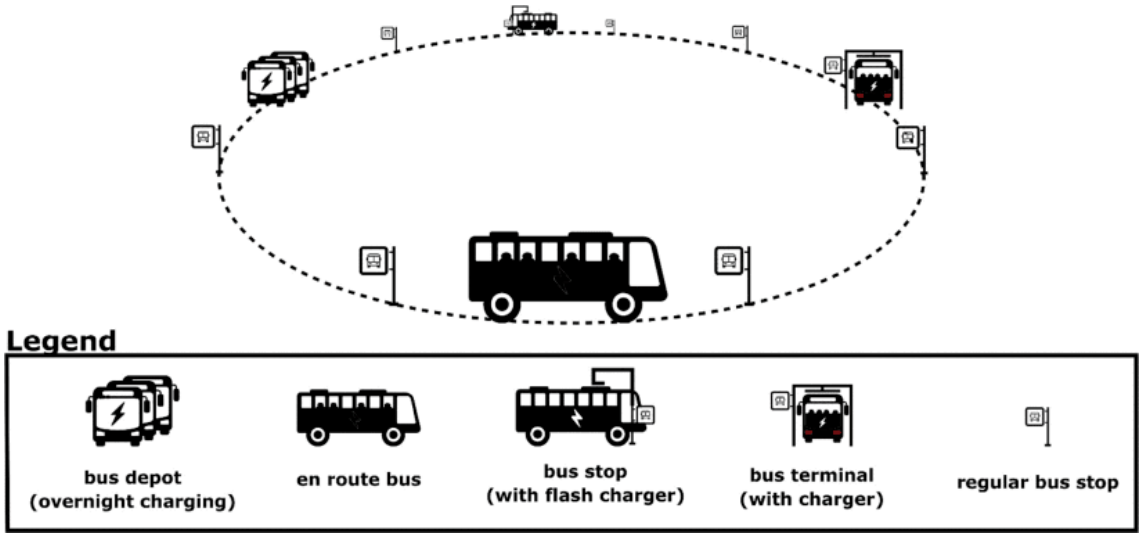

Figure 7.1: Illustration of a generic public transport network and its components: depots, buses, routes, stops, terminals, and charging infrastructure.

The second type of chargers is the terminal charger (TC). As the name suggests, a TC is typically installed for on-route charging at main terminals, with its rated power ranging from 500 kW to 600 kW. The TC charges the onboard battery through a converter, typically connected to the medium voltage (MV) power grid through a substation transformer at the terminal, as illustrated in Fig 7.2.

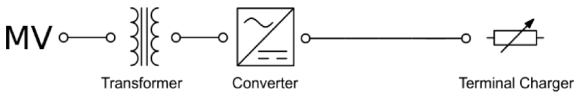

Figure 7.2: Schematic of a TC grid connection.

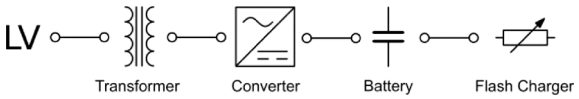

Figure 7.3: Schematic of a FC grid connection.

The third type is the flash charger (FC) illustrated in Fig. 7.3, used for on-route fast charging at regular stops, typically has a rated power ranging from 400 kW to 500 kW. Unlike the TC, the FC is installed at regular stops, and thus is connected to the low voltage (LV) power grid, typically coupled with a battery to avoid causing a load spike on the LV grid, which would be more sensitive to such load fluctuations as opposed to the MV ones. Another reason is that buses spend more time stopped at terminals (a few minutes) compared to regular stops (a few seconds).

In fact, this is the main technical difference between TCs and FCs. Although their costs and rated powers are similar, the main different influencing the choice between the maximum time at which EBs can spend charging at either.

From a cost perspective, on-route chargers are typically associated with much higher (an order of magnitude) capital costs than depot chargers. The investment is justified by their fast charging rates, which allow EBs to charge onroute, decreasing the parking time at the depot, and thereby minimizing the number of idle buses in the network and total investment in batteries. This is one of the trade-offs which upholds the need for an optimization model for designing the charging infrastructure.

Accordingly, all three types of commercially available charging infrastructures (DC, TC, and FC chargers) and their aforementioned technical and economic characteristics are to be considered in the current model.

Most commercially available EBs are fitted with batteries with capacities ranging from 80 kWh to 320kWh [202, 203]. As such, in the current model the battery capacity of EBs assigned to each route are modeled as a design variable for the optimization problem.

Defining generic routes is crucial to establish an adequate framework for the optimization model. Routes can be categorized based on two key parameters [192, 202]:

Average Distance Between Stops: This parameter is an indicator of the route location. Routes within large cities or densely populated areas are associated with shorter average distances between stops compared to those in suburban areas. This is expressed as:

$$d_r^s = \frac{L_r}{N_r^s - 1} \tag{7.1}$$

where d_r^s is the average distance between stops for route r. L_r is the length of route r, and N_r^s is the number of stops in route r.

Average Daily Distance: Considering normal operation in which an EB is assigned a specific route each day, this is expressed as:

$$d_r^d = \frac{H_r}{T_r} \cdot L_r = N_r^t \cdot L_r \tag{7.2}$$

where d_r^d is the average daily distance on route r. H_r is circulating hours of route r (difference between first and last bus of the day), T_r is the average duration of the route, and N_r^t is the daily number of trips in route r.

Having defined these two key parameters, generic routes can be categorized into different types to provide physical meaning. In this study, the categorization defined in Table 7.2 is used to describe different routes in the case studies. Accordingly, generic routes can be categorized into city (CC) or suburban (SU) routes based on d_r^s , or as short (SD), medium (MD), or long distance (LD) based on d_r^d.

Table 7.2: Categorization of generic routes into: city center (CC), suburban (SU), short distance (SD), medium distance (MD), and long distance (LD).

		d_r^d (km)		
		<200	200-250	>250
d_r^s (km)	<0.3	**CC-SD**	**CC-MD**	**CC-LD**
	>0.3	**SU-SD**	**SU-MD**	**SU-LD**

7.3 Optimization Model

As any optimization problem, the proposed MILP model consists of two main elements: the objective function and problem constraints, which are detailed subsequently.

7.3.1 Objective Function

Note that in the current formulation the TOC is calculated as an annual value. Electricity charging costs are operating costs and therefore the annual value can be calculated directly. However, the charging infrastructure and battery costs have capital investments, and therefore the capital cost is divided by the equipment lifetime and summed to the yearly operating costs to obtain their equivalent annual cost:

$$annual\ cost = \frac{capital\ cost}{life\ time} + annual\ operating\ cost \tag{7.3}$$

The objective function to be minimized represents the TOC of the transport system and is shown in (7.4). For each route in the system, the annual TOC is calculated as the summation of five cost terms. The five cost terms, from left to right, correspond to: the annual running cost of the depot station(s), annual ownership costs of batteries for all buses in circulation, annual ownership cost of all the entire charging infrastructure, annual electricity cost for on-route charging (by TCs and FCs), and finally the annual electricity cost for off-route charging (by DCs). Each of the five terms is elaborated in (7.5)-(7.9).

$$\min \mathbf{TOC} = \sum_{r \in R} \left(C_r^{depot} + C_r^{batteries} + C_r^{chargers} + C_r^{onroute} + C_r^{offroute} \right) \tag{7.4}$$

$$C_r^{depot} = d_r \cdot C^d \tag{7.5}$$

$$C_r^{batteries} = \sum_{k \in B^r} \left(b_{k,r} \cdot C^B \right) \tag{7.6}$$

$$C_r^{chargers} = \sum_{i \in I^r} \sum_{h \in H} x_{i,h,r} \cdot C_h^C \tag{7.7}$$

$$C_r^{onroute} = \sum_{i \in I^r} \sum_{j \in J^r} \left(e_{i,j,r} \cdot C^E_{i,j,r} \right) \cdot d_{year} \cdot n_r^{bus} \tag{7.8}$$

$$C_r^{offroute} = e_{end,r} \cdot C^E_{end,end,r} \cdot d_{year} \cdot n_r^{bus} \tag{7.9}$$

The first term (C_r^{depot}) corresponds to the depot charger annual TOC for each route r and is expressed in (7.5). The term is a multiplication of a binary variable (d_r) representing the existence of the depot charger (for route r) multiplied by the annual ownership cost of running a depot charger (C^d).

The second term, ($C_r^{batteries}$) , is the annual TOC of all batteries in route r and is shown in (7.6). For each route, this is the summation of the battery costs of each bus k deployed to this route (B^r is the set of all buses deployed to route r) which is calculated as the capacity of each battery $b_{k,r}$ multiplied by its annual ownership cost (C^B) per-kWh.

The third term ($C_r^{chargers}$) is shown in (7.7) and corresponds to the annual cost of the charging infrastructure on each route r. Here, i and h are the positive integer indices for the stops and charger type, respectively, and I^r and H are the set of all stops in route r and set of available on-route charger types, respectively. For each route r, $x_{i,h,r}$ is a binary variable indicating the presence of a charger of type h at stop i, and C_h^C is the annual ownership cost of a charger of type h. Accordingly, $C_r^{chargers}$ is calculated for each route r as the sum of the annual cost of all present charger types (decided by the binary variable) at each stop, and is summed for all stops.

The fourth and fifth terms in (7.8) and (7.9) correspond to the total cost of energy supplied to recharge the batteries through on-route and off-route chargers, respectively.

In (7.8), j corresponds to the index of the trip in J^r, which is the set of all daily trips made on route r (the number of daily trips made on each route is determined by the frequency of the route). For each route r, $e_{i,j,r}$ and $C^E_{i,j,r}$ are the energy charged at stop i during trip j, and the corresponding cost per unit of electricity, respectively. d_{year} is the number of days in a year, set as 365, and n_r^{bus} is the total number of buses traversing the route. This last value can be calculated based on the two parameters of each route which were introduced in (7.1) and (7.2), as is shown in (7.10):

$$n_r^{bus} = \frac{H_r}{N_r^t} \cdot F_r^b \tag{7.10}$$

In (7.10), F_r^b is the frequency of buses is route r and the other variables have been defined previously. Accordingly, $C_r^{onroute}$ is calculated for each route r as the sum of the annual cost of electricity charged at all stops, for all trips.

In (7.9), the final term of the TOC objective function is shown ($C_r^{offroute}$) which is the cost of electricity charged offroute (while the EBs parked or are not in service) for route r. In this equation, $e_{end,r}$ and $C^E_{end,end,r}$ and correspond to the energy charged at the end of the route (i.e., off-route), and the corresponding cost per unit of electricity, respectively. It is important to note that in this formulation, the last stop in a bus schedule corresponds to the depot. However, this does not dictate the presence of a charger at the depot (DC), which is a decision variable dependent on the binary variable d_r . With all the terms being defined, the objective function for the transport system TOC is evaluated as the summation of the total costs of all routes in the network, denoted by set R.

7.3.2 Constraints

The constraints of the optimization problem can be divided into four groups:

7.3.2.1 Infrastructure Constraints

The first constraint is associated with the charging infrastructure, and guarantees that at each stop there is only one type of charger installed (based on the binary decision variable $x_{i,h,r}$ which was previously introduced), as is represented in (7.11).

$$\sum_{h\in H} x_{i,h,r} \leq 1, \quad \forall r \in R,\ \forall i \in I^r \tag{7.11}$$

7.3.2.2 Battery Constraints

The second set of constraints are associated with the batteries onboard the EBs, and are represented by (7.12)-(7.14). To protect the health of the batteries, for each bus , the battery State-of-Charge (SoC), denoted by $E_{i,j,k,r}$, must be within the upper and lower bounds $\bar{B}$ and $\underline{B}$, as set by (7.12) and (7.13), respectively. As defined in the previous section, $b_{k,r}$ is the capacity of the battery installed on bus k deployed to route r. Constraint (7.14) sets the SoC boundary conditions to be at the maximum value ($\bar{B} \cdot b_{k,r}$), i.e., the EB starts each trip from the depot with full charge. It is important to note that with the circular bus route nature, the first and last stops are the same (i.e., stop $i = 1$ is the same as $i = end$) . Hence, the SoC at both, $E_{1,j,k,r}$ and $E_{end,j,k,r}$ are equal as set by (7.14). Constraints (7.12)-(7.14) are applied globally: at each stop in each route for all buses deployed to all routes.

$$E_{i,j,k,r} \leq \bar{B} \cdot b_{k,r}, \quad \forall r \in R, \forall i \in I^r, \forall j \in J^r, \forall k \in K^r \tag{7.12}$$

$$E_{i,j,k,r} \geq \underline{B} \cdot b_{k,r}, \quad \forall r \in R, \forall i \in I^r, \forall j \in J^r, \forall k \in K^r \tag{7.13}$$

$$\begin{aligned} E_{1,j,k,r} = & E_{end,j,k,r} = \bar{B} \cdot b_{k,r}, \\ & \forall r \in R, \quad \forall i \in I^r, \forall j \in J^r, \forall k \in K^r \end{aligned} \tag{7.14}$$

7.3.2.3 Charged Energy Constraints

The third set of constraints in (7.15)-(7.21) are related to the energy exchange between the EBs and the charging infrastructure. First, (7.15) ensures that energy can only be injected from the electrical grid to the EBs through the chargers and not vice-versa. This constraint can easily be modified or removed in case bi-directional energy flow with the power grid is possible and to be considered. Constraint (7.16) dictates that if there is no charger installed at a stop ($x_{i,h,r} = 0$), then the energy exchanged at that stop must be equal to zero ($e_{i,j,r} = 0$). Constraint (7.17) sets the charging power according to the charger type installed at a stop ($x_{i,1}, x_{i,2}, etc.$), matching it to the corresponding maximum charging capacity of this charger type ($\bar{E}_1$, $\bar{E}_2$, etc.).

Constraints (7.18) and (7.19) impose $x_{i,h,r}$ that there can only be one type of charger at each stop in each route. In case there is a depot charger ($d_r = 1$), the constraint (7.20) limits charging at the end of each trip to correspond to the maximum charging capacity of the depot charger ($\bar{E}_{DC}$). Constraint (7.21) imposes that there must be a charger installed at the first/last stop of each route, such that if there is no depot charger ($d_r = 0$), charger type 1 (e.g. terminal charger) is imposed on that stop to comply with constraint (7.14). In this sense, the model optimizes the design of the system by choosing between the depot charger and the cheapest opportunity charger depending on which is more cost effective. In real-life terms, this is seen in the case that some routes start/end at terminal (with a TC) and other start and end at the main depot (with a DC).

$$e_{i,j,r} \geq 0, \quad \forall r \in R, \forall i \in I^r, \forall j \in J^r \tag{7.15}$$

$$\sum_{h \in H} x_{i,h,r} = 0 \Longrightarrow e_{i,j,r} = 0, \quad \forall r \in R, \forall i \in I^r, \forall j \in J^r \tag{7.16}$$

$$x_{i,h,r} = 1 \Longrightarrow e_{i,j,r} \leq \bar{E}_h, \quad \forall r \in R, \forall i \in I^r, \forall j \in J^r \tag{7.17}$$

$$\sum_{h \in H} x_{i,h,r} \geq 0, \quad \forall r \in R, \forall i \in I^r \tag{7.18}$$

$$\sum_{h \in H} x_{i,h,r} \leq 1, \quad \forall r \in R, \forall i \in I^r \tag{7.19}$$

$$d_r = 1 \Longrightarrow e_{end,j,r} \leq \bar{E}_{DC}, \quad \forall r \in R, \forall j \in J^r \tag{7.20}$$

$$d_r = 0 \Longrightarrow, x_{\text{end},1,r} = 1, \quad \forall r \in R \tag{7.21}$$

7.3.2.4 Energy Balance Constraints

The final constraint in (22) is associated with the total energy balance of the system, such that the total SoC consumed by all buses is equal to the total SoC charged.

The equation is applied for all buses deployed to all routes in the network, such that for each bus, the sum of the SoC difference between all subsequent stops ($E_{i,j,k,r} - E_{i-1,j,k,r}$) must be equal to the total energy charged at all stops (including the terminal or depot).

$$\begin{aligned} \sum_{i=2...end} \left(E_{i,j,k,r} - E_{i-1,j,k,r} + e_{i,j,k,r}\right) = 0 \\ \forall r \in R, \quad \forall j \in J^r, \forall k \in K^r \end{aligned} \tag{7.22}$$

7.3.3 Computational Implementation

The YALMIP package (version R20181012) was used as the algebraic modeling language (AML) for the proposed model, on MATLAB (version R2019b). The Gurobi solver (version 8.0) was used to optimize the system using MILP.

Here it is important to note that the model of the system and the optimization algorithm employed are distinct. The main objective of this work is to formulate a generalized mathematical formulation which allows the modeling of all components of any generic fully electric public transport network. Given that the design problem is offline in nature, the choice of deterministic optimization is generally favored over a meta-heuristic one, which would yield sub-optimal solutions. The choice of a MILP optimization solver was due to its deterministic nature which guarantees the global optimal value for any given case using the proposed formulation

7.4 Case Studies

7.4.1 Description of the Different Case Studies

In order to validate and demonstrate the universal applicability of the proposed optimization model on a wide range of problems, **three case studies were performed**:

1. In the **first case study**, **three generic routes** are constructed with **different lengths**. The proposed model is used to determine the optimal design, sizing, and siting of the charging infrastructure in addition to the sizing of the batteries for each of the given routes.

2. In the **second case study**, a generic **transportation network** is constructed based on a combination of **180 different routes**, belonging to all six categories (CC-SD, CC-MD, CC-LD, SU-SD, SU-MD, and SU-LD). The optimal design, sizing, and siting of charging infrastructure in addition to the sizing of the batteries for all deployed EBs and routes **in the entire system** is determined.

3. In the **third case study**, a long-term transport network planning problem is investigated, by studying the **effect of long-term (10-year ahead) forecasted change** on battery, energy, and other technology costs on the results obtained in the second case study. A comparative analysis is then performed between the **present-day (2020) and future (2030) scenarios** in terms of the TOC of the network and its respective breakdown.

Table 7.3: Specifications of routes used for the first case study.

	Route A	Route B	Route C
Number of Trips (per day)	5	15	15
Number of Stops (per trip)	75	60	80
Total Number of Stops (per day)	375	900	1200
Trip Length (km)	20	15	20
Bus Size (m)	18	18	24
Average Consumption (kWh/km)	1.8	1.8	2.2

Table 7.4: Classification of commercially available EBs according to average energy consumption [1, 2, 3].

Bus Type	Average Consumption (kWh/km)
12-meter	1.2
18-meter or articulated	1.8
24-meter or double articulated	2.2

Table 7.5: Techno-economic specifications of chargers.

	DC	TC		FC	
Charger Classification	Depot	On-Route		On-Route	
Model	Standard	Slow	Fast	Slow	Fast
Rated Power (kW)	50	400	600	400	600
Maximum Charging Time	5 hours	3 minutes		10 seconds	
Capital Cost (EUR)	98k	278k	280k	278k	280k
Operating Cost (EUR/year)	100	2k		2k	
Lifetime (years)	20	20		20	

Table 7.6: Techno-economic specifications of the batteries.

Capital Cost (EUR/kWh)	250
Operating Cost (EUR/year)	-
Battery Lifetime (years)	5
State-of-Charge Upper Boundary (%)	90
State-of-Charge Lower Boundary (%)	10

The three defined case studies allow the validation of the proposed model in terms of its applicability on different classes of transport system design problems, namely the **optimization of specific routes (case study 1)**, **design of large-scale system (case study 2)**, and **long-term investment planning of large-scale transport systems (case study 3)**.

7.4.2 Case Study Definition and Results

7.4.2.1 Case Study 1: Optimal Design of Individual Bus Routes

In this first case study, the objective is to test and validate the proposed mathematical formulation, by attempting to determine the optimal charging infrastructure deployment and battery sizing for individual EB routes. For this purpose, three generic routes are constructed with different lengths, as detailed in Table 7.3. Based on length of the route, different bus sizes are needed for each route, whose specifications are in accordance with Table 7.4. Techno-economic specifications of commercially available chargers to choose from and the batteries are provided in Tables 7.5 and 7.6, respectively (based on information by Siemens and ABB Canada [200, 201]). The latter are constrained between 80 kWh and 320 kWh with 20 kWh increments. In the first case study, n_r^{bus} is set to unity for all routes, i.e. one EB dispatched to each route.

The result for the optimal charger deployment in Route A is shown in Fig. 7.4a. As can be seen, only the depot charger with a 50 kW power rating is sufficient to sustain the energy demand of the EB throughout its 5 cycles of the route per day. The result of the optimal battery capacity was 260 kWh. In Fig. 7.4b, one can see that a full charge at the depot can sustain the full daily cycle of the route by the EB before reaching the minimum bound of 10

With Route B being significantly longer (threefold the distance of Route A), investment in a higher charging power is necessary. In Fig. 7.5a, the optimal deployment is shown to be that of one 600 kW TC to sustain the route. With this, only a 80 kWh battery is needed. As such, the optimal solution as here as opposed to Route A consisted of investing in a more powerful charger while saving the costs by using smaller batteries on the deployed EB The optimal charging schedule is shown in Fig. 7.5b, where it can be seen that the EB occasionally stops at charges at the TC to recharge its battery throughout the day, guaranteeing a full SoC at the end of the route for its next deployment.

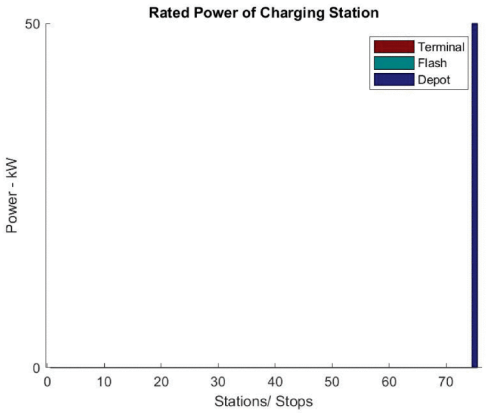

(a) Charger deployment.

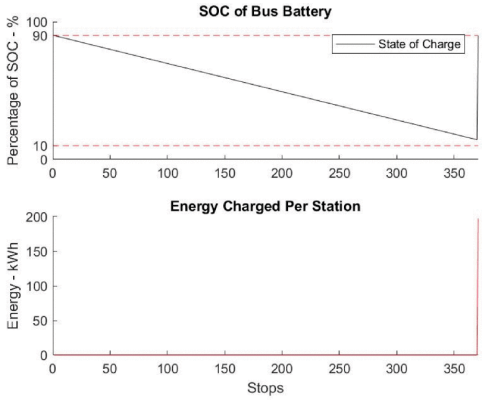

(b) Battery SoC variation (top) and energy charged at each station (bottom).

Figure 7.4: Results for Route A.

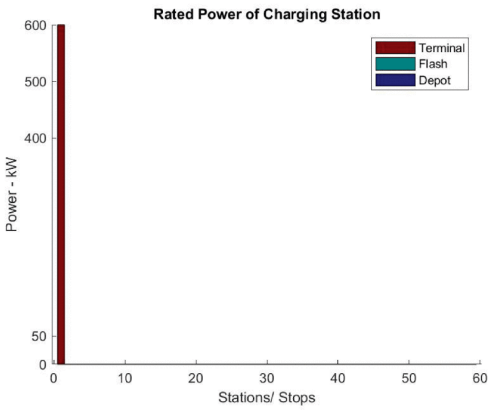

(a) Charger deployment.

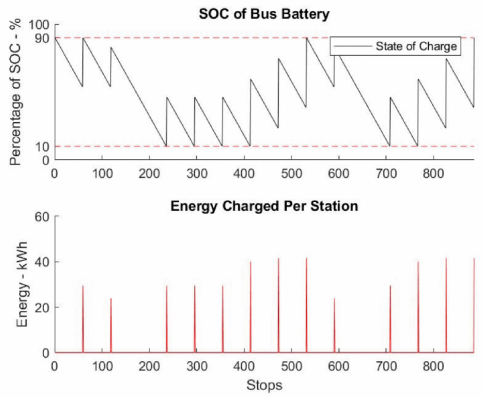

(b) Battery SoC variation (top) and energy charged at each station (bottom).

Figure 7.5: Results for Route B.

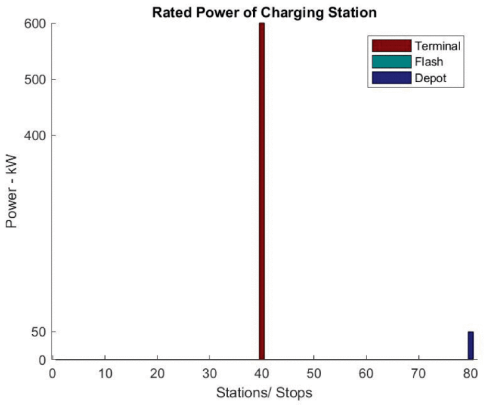

(a) Charger deployment.

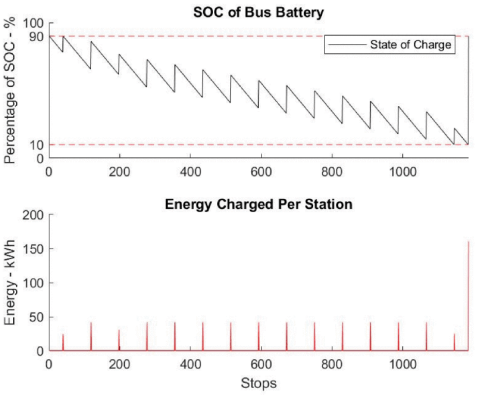

(b) Battery SoC variation (top) and energy charged at each station (bottom).

Figure 7.6: Results for Route C.

Table 7.7: Resulting optimal design and total ownership cost breakdown for each of the first case study routes.

	Route A	**Route B**	**Route C**
Optimal Battery Size (kWh)	260	80	200
Number of DC (50 kW)	1	0	1
Number of TC (500 kW)	0	0	0
Number of TC (600 kW)	0	1	1
Number of FC (400 kW)	0	0	0
Number of FC (500 kW)	0	0	0
Cost of Chargers (EUR/year)	5000	16000	21000
Cost of Batteries (EUR/year)	13000	4000	10000
Cost of Electricity (EUR/year)	3918	11181	18614
Annual TOC (EUR/year)	21918	31181	49614

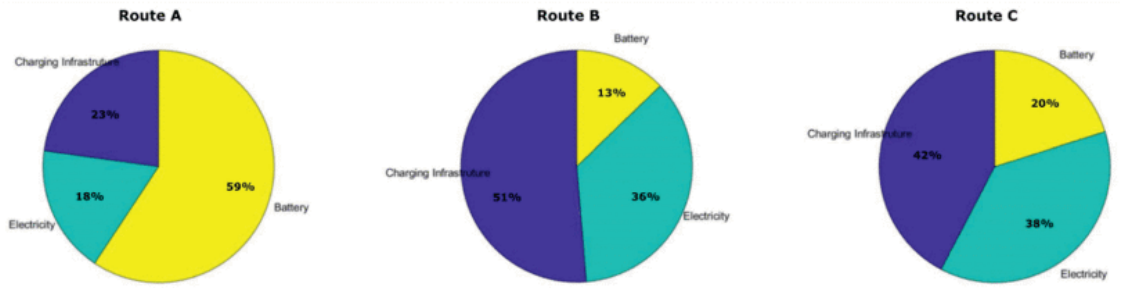

Figure 7.7: Breakdown of the optimal design TOC for the first case study routes: Route A TOC (left, total of 21918 EUR/year), Route B TOC (center, total of 31181 EUR/year), Route C TOC (right, total of 49614 EUR/year).

For Route C (the longest of the three), the optimal charger configuration consisted of both a 600 kW TC and a 50 kW DC (as shown in Fig. 7.6a), with a medium-sized 200 kWh battery capacity for deployed EBs. The SoC variation throughout the day (Fig. 7.6b) shows that the EB stops to recharge its battery every cycle of the route, gradually decreasing the SoC at the end of every cycle. Finally, at the end of the day, the EB is recharged at the depot to a full SoC for its next deployment.

The optimal annual TOC (objective function of the model) and its breakdown for each route are illustrated in Fig. 7.7 and detailed in Table 7.6.

One can observe that for the shortest Route (A), the lowest TOC is encountered and investment in high capacity batteries on board the deployed EB is sufficient to support the route requirements. In this case, investment in high power and/or fast chargers is not cost-effective, with only the DC sufficing.

As the length of the route increases as in Route B, one can see that the optimal design involves investing more in the charging infrastructure, and the trade-off between battery capacity and charging power becomes cost-effective. However, as the route length is further increased in Route C, a more complex design is needed in terms of charger types and battery sizing. It is noteworthy that for these three routes, (all being CC-type routes), the installation of a FC is not found to be cost-effective.

7.4.2.2 Case Study 2: Optimal Design of Electric Bus Transport Systems

In the second case study, the proposed optimization model is tested and validated for the design of a full electric bus transport system. While the objective is to test the applicability of the proposed model for any generic transport network, it is important to also maintain the true-to-life nature of the case study.

Therefore, two major cities with high EB presence who also publicly provide their full bus route information have been analyzed: Paris, France [204] and London, UK [205]. The routes were categorized based on the categories proposed in Table II, and the corresponding statistics are presented in Fig. 11. Due to the large metropolitan nature of both transport networks, it was predictable that the routes would be almost equally divided between CC and SU types (44% and 56%, respectively). Also, as expected, the majority of city routes were short-distance (CC-SD), while the majority of suburban routes were long-distance (SU-LD), with the two types combined making up more than half of the total routes (53%).

Following this analysis, it is possible to generate a set of routes which represents a generic public transport system, while maintaining its realism by emulating the route category distribution of real-life public transport systems. Accordingly, a generic public transport network consisting of 180 routes was constructed. The routes were generated based on random pairs of d_r^s and d_r^d values (defined in Section 7.2 and Table 7.2), while maintaining the share of the route categories as per the real world systems (as in Fig. 7.8). The key parameters (d_r^s and d_r^d) for each of the 180 routes forming the generic public transport network are shown in Fig. 7.9.

With the routes defined, the proposed MILP model can be used to optimize the design of the charging infrastructure and battery sizing to achieve a minimum TOC of this generic transport network. The techno-economic specifications of the EBs, chargers, and batteries are used according to Table 7.4, Table 7.5, and Table 7.6, respectively.

Average hourly electricity prices for the European energy market [206] are used (distributed based on respective scheduling of stops). In addition, due to the nature of urban environments with frequent breaking and stopping, an added penalty of 10% increased electricity consumption per kilometer driven is used for CC routes to estimate these effects in the generic network. The frequency for all the routes is set to a high frequency (HF) of 15 minutes, and the EB deployment is calculated according to (7.10).

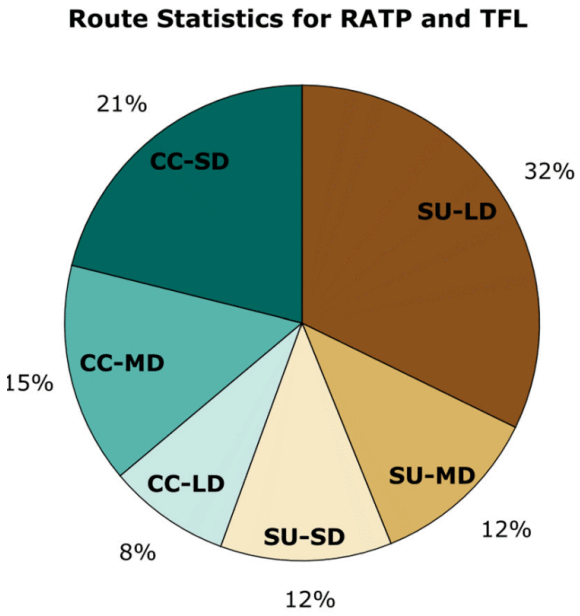

Figure 7.8: Breakdown of the different route categories based on the networks of RATP and TFL.

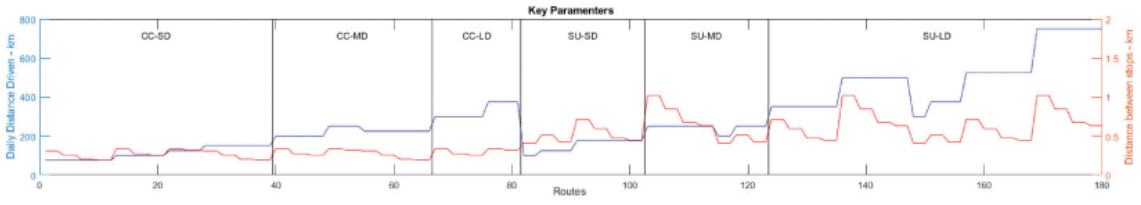

Figure 7.9: Key parameters (d_r^s, and d_r^d) for each of the 180 routes making up the generic public transport network for the second case study.

The results for the optimal charger deployment and battery sizing for the entire network are shown in Fig.7.10. For CC-SD and CC-MD routes, the charging infrastructure is seen to be mainly comprised of TCs along with low-capacity batteries, with a few exceptions where an additional DC and augmented battery capacity is needed, when the distance between stops is larger and the bus type has a higher consumption. Only one CC-LD route requires the use of a FC, and this can be attributed to the high energy consumption of this route. For suburban routes, it is clear that there is an increased reliance on on-route charging with increased battery capacities. This is especially the case for longer-distance routes, when the use of FC becomes common, as the distance between stops and the total length of the routes become very large.

The results in Fig. 7.11 for the TOC breakdown shows that for all SD routes (CC or SU), the majority of the TOC corresponds to battery costs, followed by charging infrastructure and electricity costs. For MD and LD routes, the majority of the TOC becomes that of the charging infrastructure, followed by electricity (more prominent due to larger distances), and then batteries (less prominent due to more frequent on-route charging).

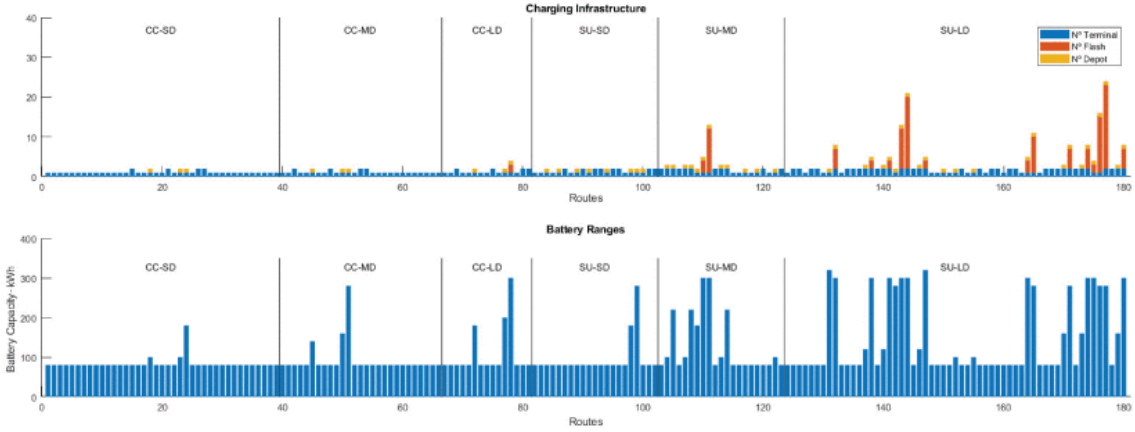

Figure 7.10: Results for the optimal charging infrastructure (top) and battery sizing (bottom) for all 180 routes of the generic public transport network under study, with a HF.

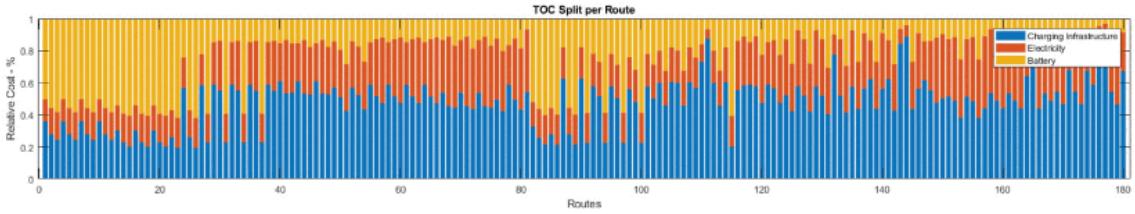

Figure 7.11: Breakdown of the resulting TOC for all 180 routes of the generic public transport network under study, with a HF.

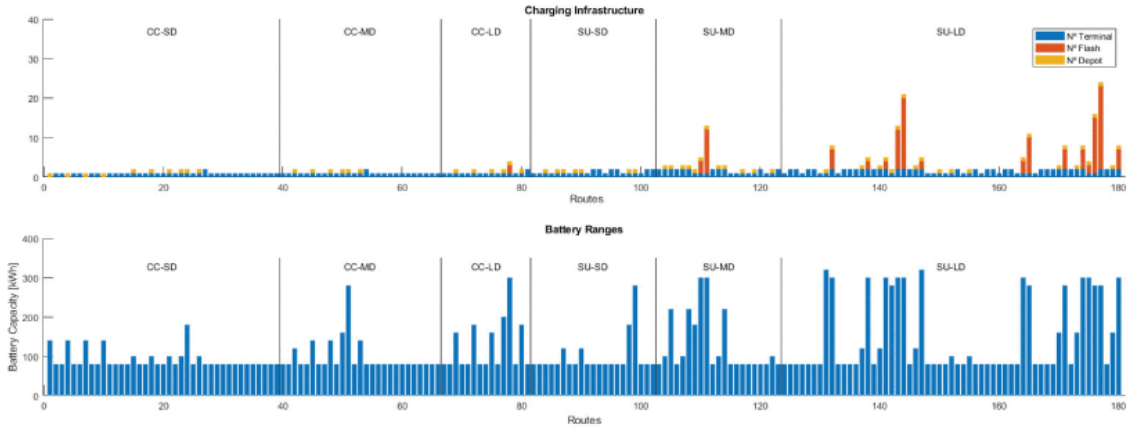

Figure 7.12: Results for the optimal charging infrastructure (top) and battery sizing (bottom) for all 180 routes of the generic public transport network under study, with a LF (reduced by a factor of 4 compared to the HF case).

These patterns appear to be the same for both CC and SU routes. That is, despite the fact that suburban routes have a higher TOC than their city counterparts, the TOC breakdown (percentage share of batteries, charging infrastructure, and electricity consumption) is significantly more dependent on the length of the route (SD/MD/LD) rather than the distance between stops (CC/SU).

In order to analyze the effect of the route frequencies, the simulation is repeated for the same network, albeit with a low frequency (LF) 1 hour instead of 15 minutes (i.e., all routes reduced by a factor of 4 compared to the former HF case). The results are shown in Fig. 7.12. For the most part, the solution is very similar to the HF case, with a few differences noted. First, for SD routes, it can be observed that with a lower overall number of buses traversing the routes, it becomes more cost-effective to invest in DCs and larger battery capacities. Overall, HF routes have a higher number of TC due to their larger bus fleet, prioritizing cost reduction in batteries while LF ones with smaller bus fleets rely on bigger batteries with the additional DCs.

7.4.2.3 Case Study 3: Long-Term Investment Planning for a Fully Electric Public Bus Transport System - 2030 Scenario

The final case study used to validate the proposed model is based on a long-term planning problem, in which investment options are analyzed considering the forecasted change in the cost of acquiring and operating technologies.

By considering the predictions made in the report by Bloomberg [207], the constructed network in the previous case study is modified for a 2030 scenario (10 years ahead) by making the following modifications:

- Battery cost reduced to 62 EUR/kWh.
- Upper range of battery capacities increased to 400 kWh.
- Decrease in flash charger cost by 40% for stops close in proximity (due to increased ease of sharing one transformer and converter for FCs closer to each other).
- Decrease in terminal charger cost by 10% due to technological advancements.
- Remove the electricity consumption penalty for CC routes (due to the foreseen advance in regenerative breaking technologies).

For this updated 2030 scenario, the model is re-run for both the HF and LF cases, and the results are shown in Fig. 7.13 and Fig. 7.14, respectively. Three main changes are observed:

First, there is a clear increase in DC deployment, with larger battery capacities in CC-SD and SU-SD routes, regardless of the bus frequency. This effect is to be expected as the estimated decrease in battery cost overcomes the advantages of TCs.

Secondly, despite their (future) costs being sharply reduced in this scenario, FCs appear even less often than they did (being deployed rarely and only for SU-MD and SU-LD due to high energy consumption requirements).

Third, for LF routes there is a significant increased reliance on larger battery capacities and less on fast charging infrastructure, with batteries taking up a larger percentage share of the route TOCs as opposed to the 2020/present-day scenario. This may suggest that according to the assumptions used for the 2030 scenario, benefits from cost reductions in battery technologies will outweigh those in fast charging technologies.

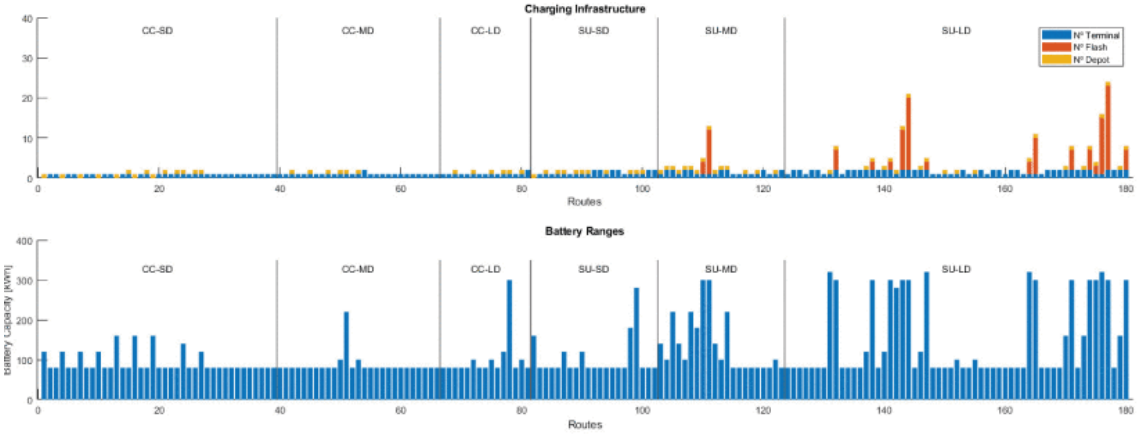

Figure 7.13: Results for optimal charging infrastructure (top) and battery sizing (bottom) for all 180 routes of the generic public transport network under study, with HF, for 2030 scenario.

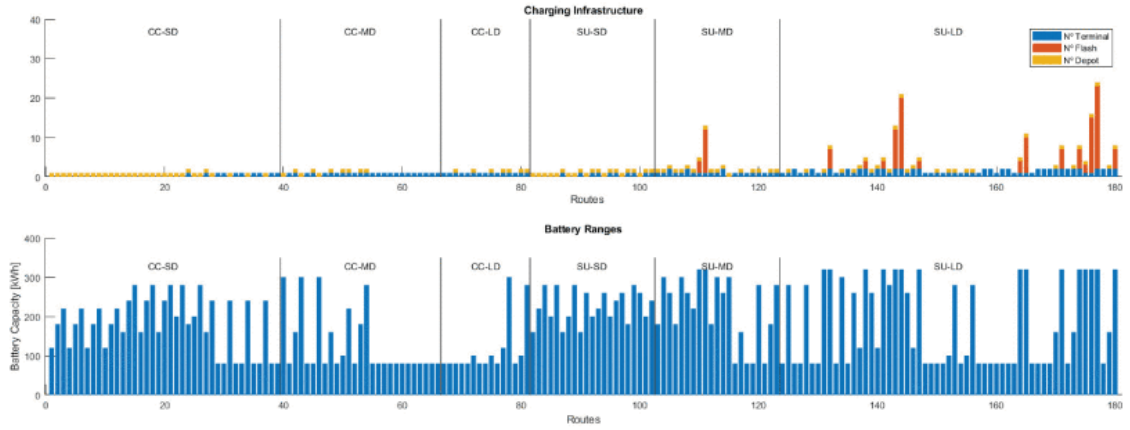

Figure 7.14: Results for optimal charging infrastructure (top) and battery sizing (bottom) for all 180 routes of the generic public transport network under study, with LF, for 2030 scenario.

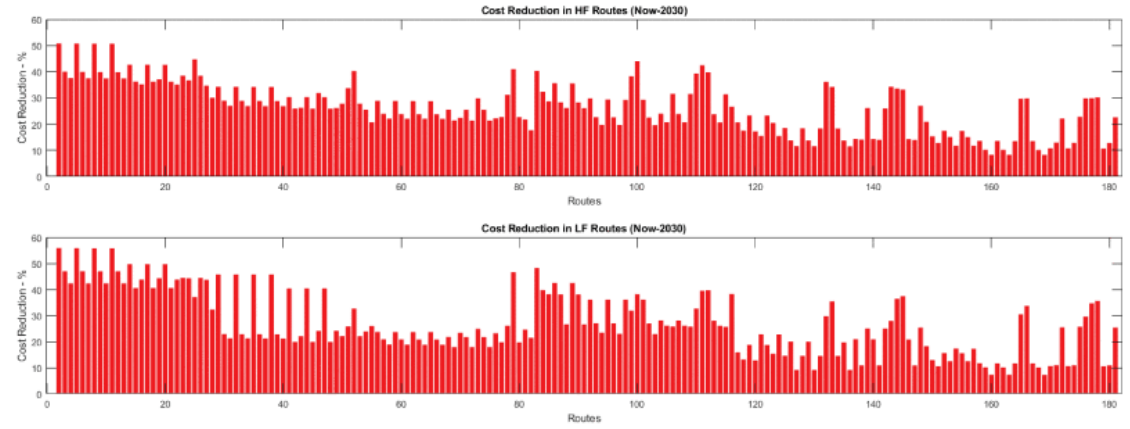

Figure 7.15: Route TOC decrease in 2030 scenario (relative to the 2020/present-day scenario), shown for the HF (top) and LF (bottom) cases.

In Fig. 7.15, the percentage decrease in the TOC (relative to the 2020/present-day scenario) is shown for all the routes and for the HF and LF cases. It is clear that there is a considerable decrease (>30%) in the TOC of SD routes, and a smaller decrease (>10%) for LD ones. This is due to the same reasons expressed above, with SD being shown to be more dependent on larger battery capacities and thereby achieving more saving with advanced and cheaper technologies thereof. HF routes can be seen to expect higher cost reductions, although this can be attributed to the fact that a larger fleet translates to higher contribution from batteries, leading to a greater impact of the aforementioned points, increasing the overall cost reduction. Overall, from this analysis one can see that the current trend and policies in electrification of public transport systems are well justified for long-term prospects.

It is important to note that this case study is merely used here to showcase the applicability of the proposed model in analyzing future scenarios. The assumptions made for the 2030 scenario were for demonstration purposes, and an exact analysis of forecasted techno-economic values is a very complex problem and indeed out of the scope of the current work. With this being said, the applicability of the proposed model to analyze different forecasts for future scenarios has been validated, and is indeed recommended for future research building up on this work, which is discussed in more detail in the next section.

7.5 Discussion and Recommendations for Future Work

The proposed MILP optimization model's applicability on any generic EB route or public transport system was demonstrated. In the first case study the model was shown to determine the optimal charging infrastructure deployment, battery sizing, and charging schedule for individual routes. In the second case study, the proposed model was shown to determine the optimal design on the level of a full system, determining the optimal charging infrastructure deployment, battery sizing, and charging schedule for all routes which guarantee the minimal TOC. Finally, in the third case study, it was shown that the proposed model can be used to analyze different future scenarios for long-term planning of planning of public transport systems.

As such, the proposed model was shown to be versatile in the sense that it can be used for a wide spectrum of problems and applied on any generic transport network. This also presents a lot of opportunities for future research building up on this work. Several recommendations can be made for future and follow-up studies by discussing the findings of this work:

- The case studies were purposefully chosen as generic cases in order to emphasize that the proposed model is not case-specific and not specifically fitted to any existing network structure or problem. While this is useful to showcase the versatility and universal nature of the proposed mathematical model, one limitation of the use of generic case studies is the lack of a benchmark to compare the optimal solution against. In other words, if no optimization model is employed, then in this case the system would be an "arbitrarily" or "heuristically" designed one (in literature this is sometimes referred to as an "experience-based" approach [193]), and in the case of a generic system there would be an infinitely large number of sub-optimal possible designs to consider. With MILP optimization employed, being a deterministic method in nature, the global optimal solution is guaranteed, so this does not retract any of the conclusions made from the performed case studies. However, since most real-life systems are designed using said "experience-based" approaches [193], it would be insightful to model full-scale real-life public transport networks and highlight the potential benefit of applying the proposed to improve their design. Moreover, using the proposed model to optimize real-life transport networks from different countries/regions may provide valuable insight on regional differences to consider and evaluate design considerations in different regions.

- Although hourly varying electricity prices corresponding to modern SGs and their demand-side management strategies were considered in this model and the case studies, more complex grid interaction can be modeled between EB networks and the power grid. Previous studies such as [195] have evaluated such "grid-interactive" bus operation problem for existing networks. The benefits of grid-interaction can be leveraged if considered early-on in the design phase, and can increase profitability since ancillary services provided to the grid can bring about considerable profit for the network owner [114]. No studies were found to consider this aspect. As such, its incorporation into the optimization model is recommended for future studies building up on this current study.

- Accounting for resource sharing can be an interesting and valuable point to consider. For instance, sharing the charging infrastructure with other transport networks (belonging to different owners/companies), or other facilities such as EV parking lots [208] can be mutually beneficial to both parties and help decrease overall TOC, and thereby recommended to be analyzed in future work. Moreover, battery swapping strategies for EVs were shown to improve the techno-economic operation of consumer-owned EVs, as shown in [209], and therefore a potentially viable strategy to be used to further improve EB systems.

- In the third case study, a 2030 scenario was analyzed based on several assumptions for future technology advancements. A similar sensitivity analysis is recommended to be performed for present-day scenarios, albeit in different countries or regions. Globally, costs of acquiring and operating different technologies, in addition to implemented socioeconomic policies significantly vary between different regions. This is recommended as a future analysis as it can provide insight on different transport electrification strategies required.

- The impact of regenerative braking as a future technological advancement which can decrease city route electricity consumption was briefly highlighted in the third case study. Recently published works [210, 211, 212, 213] have investigated the use of intelligent control algorithms to enhance the driving strategies, also with the objective of decreasing losses due to frequent braking in urban settings. The incorporation of such algorithms in this model is recommended for future follow-up work, in order to analyze the cost-efficiency of acquiring these technologies on the design of the EB transport systems.

- The proposed model was developed to consider any type of on-route or off-route charging infrastructures with any techno-economic properties. However, in the performed case studies, only the two most common on-route charges commercially available were considered. It is recommended that follow-up work consider other newly emerging fast charging technologies [214]. On-site storage devices (which can be modeled as a generic off-route charging infrastructure in the proposed formulation), especially newly emerging technologies such as fuel cells [215] or flywheels [216], should also be considered in the design of public transport systems.

7.6 Conclusions

In this chapter, a mathematical model for fully electric public transport networks was formulated, and MILP optimization was implemented to minimize the TOC of a public transport system. The generic nature of the model was guaranteed by allowing the consideration of any set of routes, different EB models, battery capacities, and different charging technologies as input for the model. In this sense, the model is versatile and can be used to optimize already existing systems or design new ones due to its generic formulation. Three case studies were used to validate the proposed model while demonstrating its universal applicability. First, the design of three individual routes with different characteristics was demonstrated. Then, a large-scale generic transport system with 180 routes, consisting of urban and suburban routes with varying characteristics was considered and the optimal design was obtained and analyzed in detail. Afterwards, the use of the proposed model for a long-term transport system planning problem was demonstrated by adapting the system to a 2030 scenario based on forecasted technological advancements. The proposed model and formulation was shown to be highly versatile in modeling a wide variety of components in an EB transport system and in achieving an optimal design with minimal TOC. A number of recommendations for future work were made, including the incorporation of power grid-interactive designs for future transport systems, considering the interaction with other transport networks or EV parking lots, or the consideration of on-route charging through newly emerging technologies.

Chapter 8

Energy Management in Smart Industries with Optimal Task Scheduling

An original graph-based model and algorithm for optimal industrial task scheduling is proposed in this chapter. The innovative algorithm designed, dubbed "Dijkstra Optimal Tasking" (DOT), is suitable for fully distributed task scheduling of autonomous industrial agents for optimal resource allocation, including energy use. The algorithm was designed starting with the fundamentals of graph theory, from the ground up, to guarantee a generic nature, making it applicable on a plethora of tasking problems and not case-specific. For any industrial setting in which mobile agents are responsible for accomplishing tasks across a site, the objective is to determine the optimal task schedule for each agent, which maximizes the speed of task achievement while minimizing the movement, thereby minimizing energy consumption cost. The DOT algorithm is presented in detail in this chapter, starting from the conceptualization to the mathematical formulation based on graph theory, having a thorough computational implementation and a detailed algorithm benchmarking analysis. The choice of Dijkstra as opposed to other shortest path methods (namely, A* Search and Bellman-Ford) in the proposed graph-based model and algorithm was investigated and justified. An example of a real-world application based on a refinery site is modeled and simulated and the proposed algorithm's effectiveness and computational efficiency is duly evaluated. A dynamic obstacle course was incorporated to effectively demonstrate the proposed algorithm's applicability to real-world applications.

Chapter Highlights and Novel Contributions:

- Model a generic tasking problem using graph theory to guarantee applicability to a wide range of modern problems (particularly in the industrial and transportation sectors).
- Design and implement an original graph-based model and algorithm for task scheduling by a limited number of autonomous mobile agents.
- Perform several benchmarking analyses to determine the computational complexity of the proposed algorithm, optimal setting of tunable parameters, and assessing the performance of the proposed algorithm incorporating different shortest path methods (Dijkstra, A* Search and Bellman-Ford).
- Ensure the computational efficiency of the algorithm to enable application in real-time.
- Demonstrate the proposed algorithm considering a case study based on a real-world industrial site, including the effect of dynamic (moving) obstacles.

Relevant Publication(s):

M. Lotfi, G.J. Osório, M. Javadi, A. Ashraf, M. Zahran, G. Samih, J.P.S. Catalão, "A Dijkstra-Inspired Graph Algorithm for Fully Autonomous Tasking in Industrial Applications," in *IEEE Transactions on Industry Applications*
Revised Version Submitted

M. Lotfi, A. Ashraf, M. Zahran, G. Samih, M. Javadi, G.J. Osório, J.P.S. Catalão, "A Dijkstra-Inspired Algorithm for Optimized Real-Time Tasking with Minimal Energy Consumption," *2020 IEEE International Conference on Environment and Electrical Engineering and 2020 IEEE Industrial and Commercial Power Systems Europe (EEEIC / I&CPS Europe)*, 2020, pp. 1-6.
Best PhD Paper Award (1st Place)
Published: https://doi.org/10.1109/EEEIC/ICPSEurope49358.2020.9160688

Chapter Nomenclature

Abbreviation	Definition
CD	Cooldown
CDF	Cooldown Function
DER	Distributed Energy Resources
DOT	Dijkstra Optimal Tasking
DR	Demand Response
DRW	Directed Random Walk
EB	Electric Bus
EV	Electric Vehicle
FCD	Fixed Cooldown
SCD	Scaled Cooldown
SoC	State of Charge
SPF	Shortest Path First
ZCD	Zero Cooldown

8.1 Introduction

In an exceedingly dynamic and digital world, the old saying of "time is money" presents itself in all modern problems. Energy systems witnessed momentous change during the past few decades [89], which in turn affected all sectors that are heavily energy-dependent, including industrial and transport sectors [217].

Despite the advancement of technologies leading to overall abundance or resources, increased social and technical complexities associated with the availability of resources make the optimal management thereof of paramount importance [218].

In addition to the added complexity of the energy supply infrastructure, process automation levels are at an all-time high, making it necessary to develop and deploy new algorithms for optimized task management in order to guarantee cost-efficiency and reliability of these automated processes [219, 220].

8.1.1 Literature Review

A rundown of recent scientific studies is performed and subsequently presented to establish the state-of-the-art of scientific literature addressing optimal task scheduling and management in modern automated systems. As previously mentioned, two of the most affected sectors are the industrial and transport sectors [217], with maximizing cost-efficiency already of pivotal importance for the two.

For the transport sector, there has been a lot of recent focus on developing optimal management algorithms for consumer-owned electric vehicle (EV) fleets [221], with an emphasis on cost-optimal energy management in the presence of hybrid technologies [3] and considering smart homes [222] and other modern solutions for optimal utilization of distributed energy resources (DERs) [114]. This is especially important with dynamic electricity pricing schemes adopted through demand response (DR) implementation [89, 217].

Recent research on this matter was not only confined to consumer-owned EVs, with a lot of research also investigating smart public transport systems with increased proliferation of electric buses (EBs) and smart charging infrastructures [196]. The priority is ensuring cost-efficiency of the systems [192] through optimal scheduling [194]. This has been thoroughly addressed in the previous chapter and associated publication [56].

In industrial applications, optimal management of time and resources is even more critical due to the profit-centered character of industry, throughout the wide-ranging spectrum of industrial specializations. In the context of smart factories, multi-agents systems are proposed as a model for coordination between autonomous systems working on performing preset tasks in factories with high levels of automation and a smart communication infrastructure [223].

The adoption of intelligent algorithms for optimal task scheduling in industry has been shown to result in significant cost savings, whether performed by automated mobile agents or human labor. Such saving are crucial for industries and economic growth [224].

Algorithms for optimal task-handling are being investigated for a wide array of applications, ranging from coordinating autonomous self-driving EVs [225], to cooperative robotics [226], industrial site inspection [227], and the management of modern warehouses [228]. As such, the development of these algorithms for optimal cost-efficiency of task handling, regardless of the type of task, becomes imperative for modern industries.

With increased intertwining of modern systems and cross-industry designs it becomes even more important to design algorithms for generic systems [61], which are not application-specific, and could be employed regardless of the target sector, be it smart factories, modern warehouses, EV fleet management, etc.

In this study, we propose, implement, and validate a novel algorithm for optimal task scheduling, dubbed "Dijkstra Optimal Tasking" (DOT), initially conceptualized (by the author of this thesis) in [55]. The proposed algorithm is generic in nature, meaning that it can be adapted to different problems in which a limited number of mobile agents are required to perform a number of tasks, with minimal energy consumption.

In this chapter the proposed algorithm is documented in detail, including: the conceptual model, mathematical formulation, algorithm design, and computational implementation. A thorough benchmarking analysis is performed to determine optimal settings of tunable parameters and determine the time complexity. A case study is used to demonstrate a real-world application.

8.2 Algorithm Design

8.2.1 Conceptual Model

A generic task scheduling problem in a modern industrial setting is illustrated in Fig. 8.1. The main elements thereof can be defined and listed as follows:

Map: is a confined space where all the tasks and mobile agents are located. All events and scheduling are performed within this local environment.

Mobile Agent: is an agent which can move around the map and perform tasks. The agent is electric, meaning it consumes electric energy on a local battery as a cost of movement. This agent could be autonomous or human-operated (e.g. Segway, electric pallet jack, or golf cart).

Charging Station: is where the mobile agent is stationed to recharge onboard batteries. Although commonly found on the edges of the maps, they can be located anywhere across the traversable map.

Tasks: must be reached by a mobile agent in order to be accomplished. This is generic, i.e., in inspection problems the task is merely for the agent to be there every period of time. In handling problems, the agent must stay until task completion.

Obstacles: are non-traversable areas. The mobile agent must plan a path around them to reach tasks or charging stations.

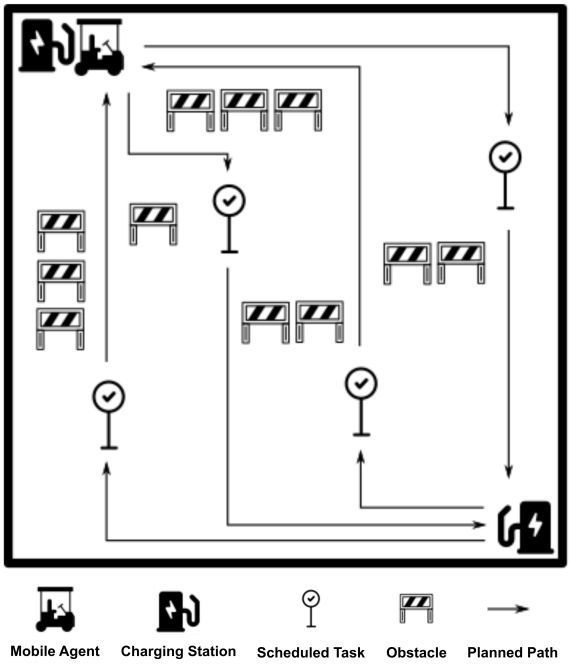

Figure 8.1: An illustration of a generic tasking problem: A mobile agent needs to perform specified tasks located at different locations in a confined map, in the presence of non-traversable obstacles. The movement is associated with energy consumption and recharging is performed at set locations.

8.2.2 Mathematical Formulation: Graph Theory Model

These are the defining elements of any generic industrial task scheduling problem, and an algorithm aiming to provide a non-case-specific solution must be capable of incorporating them in a versatile and flexible manner.

Graph theory provides the tools to mathematically model such a problem and is therefore chosen to construct the basis of the proposed algorithm. The first step is to divide the map into a mesh of equidistant and isomorphic "cells". The size of each cell should be based on the smallest element in the map. By doing so, the problem can be defined as a graph G whose elements are mathematically defined subsequently.

$$G = (\mathbf{V}, \mathbf{E}) \tag{8.1}$$

8.2.2.1 Graph Vertices

The graph defined in (8.1) consists of a set of vertices $\mathbf{V}$ (which correspond to the "cells"), and a set of edges $\mathbf{E}$.

$$i \in \mathbf{V}, \quad \forall i \in \mathbb{Z} \cap [0, |\mathbf{V}| - 1] \tag{8.2}$$

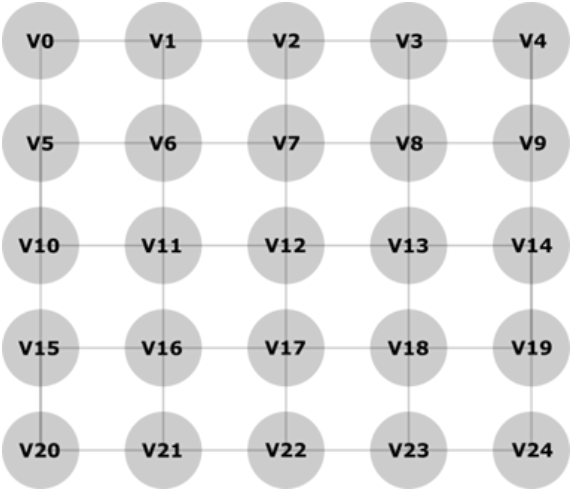

Figure 8.2: An illustration of five-by-five map modeled as a lattice graph. Cells are assigned as vertices in the graph, and connections between adjacent vertices correspond to edges of the graph.

As defined in (8.2), $\mathbf{V}$ is a set of vertices $i : \{0, 1, \ldots, |V| - 1\}$. At this stage it is established that a zero-based numbering convention (initial element assigned index 0) is used throughout this chapter, due to its compatibility with graph theory modeling and algorithm design. The vertices are numbered sequentially, row-by-row, as shown in Fig. 8.2.

The equidistant and isomorphic division of the map results in a "lattice graph" (illustrated in Fig. 8.2), a unique type of graph whose properties can be exploited. First, the size of the graph is decided by the number of rows m and number of columns n. The total number of vertices is easily expressed as in (8.3).

$$|\mathbf{V}| = m \cdot n \tag{8.3}$$

Afterwards, each vertex in the lattice graph can be uniquely mapped to a row and column value $R(i)$ and $C(i)$ in a set of rows $\mathbf{R}$ and columns $\mathbf{C}$, respectively. Being a single-values unique mapping between the sets, no two different vertices (i, j) can have both the same row and column values as shown in (8.4), and the sets have the same size as shown in (8.5).

The mapping functions of the row and column values for each vertex i is done using (8.6) and (8.7), respectively. In (8.6) the row number of node i is obtained by applying the *modulo* operator of i to n (remainder of division), while the column is calculated using integer (truncated) division in (8.7). This is a simple demonstration of the advantage of using zero-based numbering to obtain simple and computationally efficient operations within the graph.

$$(C(i) = C(j)) \wedge (R(i) = R(j)) \leftrightarrow i = j \tag{8.4}$$

$$|\mathbf{C}| = |\mathbf{R}| = |\mathbf{V}| \tag{8.5}$$

$$R(i) = (i \bmod n) \tag{8.6}$$

$$C(i) = [(m \cdot i)/|\mathbf{V}|] \tag{8.7}$$

The x and y coordinates of each vertex on the original (physical) map can be retrieved using (8.8) and (8.9), where d_x and d_y correspond to the horizontal and vertical spacing between cells, respectively.

$$x(i) = C(i) \cdot d_x \tag{8.8}$$

$$y(i) = R(i) \cdot d_y \tag{8.9}$$

For equidistant and isomorphic spacing, this is simplified by setting $d_x = d_y = \Delta v$. Furthermore, the relationship between row and column values of adjacent vertices the graph is defined using (8.10)-(8.13).

$$R(i) = R(i-1) \leftrightarrow \text{row}(i) > 0 \tag{8.10}$$

$$C(i) = 1 + C(i-1) \leftrightarrow R(i) > 0 \tag{8.11}$$

$$C(i) = C(i-n) \leftrightarrow C(i) > 0 \tag{8.12}$$

$$R(i) = 1 + R(i-n) \leftrightarrow C(i) > 0 \tag{8.13}$$

Finally, vertices are identified as boundary vertices (set **B**) or interior domain (set **D**) nodes according to (8.14) and (8.15).

$$i \in \mathbf{B} \leftrightarrow i \in \mathbf{V} \wedge ((R(i) \cdot C(i) = 0) \vee ((R(i) - m + 1) \cdot (C(i) - n + 1) = 0)) \tag{8.14}$$

$$i \in \mathbf{D} \leftrightarrow i \in \mathbf{V} \wedge i \notin \mathbf{B} \Rightarrow \mathbf{D} = \mathbf{V} - \mathbf{B} \tag{8.15}$$

8.2.2.2 Graph Edges

The other main element of the graph is the set of edges, **E**. An edge is a set of two vertices i, j that are connected in the graph. The set of all possible edges **E** can be defined using the condition in (8.16).

While loops (an edge connecting a node to itself, or subsequently a path which starts and ends at the same node) are mathematically possible in a generic graph, they do not exist in this mode, as it would correspond to indefinite circling in a closed "loop" within the map. Thus, the condition $i \neq j$ is imposed in (8.16). Moreover, the modeled graph is an undirected one, hence the condition in (8.17).

$$\mathbf{E} \subseteq \{\{i,j\} \mid (i,j) \in \mathbf{V} \wedge i \neq j\} \tag{8.16}$$

$$\{i,j\} = \{j,i\} \forall (i,j) \in \mathbf{V} \tag{8.17}$$

Based on this property, all edges of the lattice graph can be constructed by defining an edge between all interior domain vertices and their adjacent neighbors. This is mathematically expressed using the interjection in (8.18).

$$\exists \{\mathrm{i,j}\} \in \mathbf{E} \leftrightarrow (i \in \mathbf{D}) \wedge ((|i-j|=1) \vee (|i-j|=n)) \tag{8.18}$$

The total number of edges in the graph can be obtained using the expression in (8.19).

$$|\mathbf{E}| = (m-1) \cdot n + (n-1) \cdot m = 2 \cdot m \cdot n - m - n \tag{8.19}$$

8.2.2.3 Shortest Paths

The constructed lattice graph is a connected graph, meaning that any two set of vertices i, j can connected using a number of edges. The simplest connection is a walk, in which a sequence of edges joins two vertices. A walk can either be finite or infinite, in which the edges contained in the sequence need not to be unique.

A path is defined as a walk in which all the elements are unique, i.e., every vertex in the path is only visited once. Some path $P(i,j)$ connecting i and j is therefore defined in (8.20), with K being the number of elements in the path.

$$\mathrm{P(i,j)} = (P_0, P_1, \ldots P_{K-1}) \mid \{P_0, P_1, \ldots P_{K-1}\} \in \mathbf{V} \wedge (P_0, P_{K-1}) = (i,j) \tag{8.20}$$

For every set of vertices i and j, there exists a finite number of paths between them, where $\Pi_{i,j}$ is a set containing all possible paths $P(i,j)$. In a weighted graph every edge E is associated with a weight value $\omega(E)$ such that $\mathbf{E} \mapsto \omega$, with the latter being the set of edge weights. Accordingly, the weighted length $l(P)$ of a path can be calculated as shown in (8.21).

$$l(P) = \sum_{k=0}^{K-1} \omega\left(\{P_k, P_{k+1}\}\right) \tag{8.21}$$

This function can be used to map $\Pi_{i,j} \mapsto \mathbf{L}_{i,j}$ (set of corresponding path weighted lengths). The graph distance between two vertices is defined in (8.22) as the weighted length of the shortest path between them:

$$d(i,j) = \min\left\{\mathbf{L}_{i,j}\right\} \tag{8.22}$$

Dijkstra's algorithm [229] is one of the most popular and well-established fundamental SPF algorithms in graph theory. The algorithm is a highly computationally efficient algorithm finding the shortest path between two nodes in a graph as expressed in (8.23).

$$\text{SPF} : (i,j) \rightarrow P(i,j) \ni l(P(i,j)) = d(i,j) \tag{8.23}$$

It is duly noted that the proposed model accommodates the use of any shortest path method, and not necessarily Dijkstra. The choice of Dijkstra as opposed to other alternatives is discussed and analyzed in detail in Section 8.3.3. With the mathematical formulation being specified, the designed algorithm can now be expressed in terms of the graph elements and defined relations.

8.2.3 Designed Algorithm and Computational Implementation

Recalling the original motive, the objective of the proposed algorithm is to be generic in nature, easily adaptable to different problems with elements defined in 8.2.1. To do this, the designed algorithm was implemented in an object-oriented programming environment. The pseudocode is shown in Algorithm 1, followed by a detailed description of the implementation.

```
1  Input Map, TaskList, MobileAgents
2  while isRunning do
3    tau += 1
4      for each A in MobileAgents
5        if A.isCharging then
6            A.chargeStep()
7            if A.fullyCharged then
8                A.isCharging := false
9                tau += 1
10           end if
11       else if A.atStation then
12         A.path ← DijkstraSPF(A.orSta,A.deSta)
13         A.atStation := false
14       else
15         A.loc[t] ← A.move(path,loc[t-1])
16         if map[A.loc[t]].isStation then
17           A.atStation := true
18           tau += tau
19         else
20           Map.vertexHeat[loc[t]] += INC
21         end if
22         for each N in Map.vertexHeats
23           N-=Map.CDF()
24         end for
25       end if
26     end for
27     Map.refresh()
28     TaskList.refresh()
29     MobileAgents.refresh()
30 end while
```

Algorithm 1: Pseudocode of the developed DOT algorithm.

1. ***Map*** *(Class)*: The industrial site map model is implemented as a class. A map object contains all information about the graph (edges and vertices) and the class methods to update them.

2. ***Agent*** *(Class)*: Each agent is modeled as a class. The class contains information about the agent, e.g. its current location, battery state-of-charge (SoC), current path and the class methods to update all the aforementioned values.

3. ***Checkpoints*** *(Class Property of Map, Agent)*: Checkpoints are locations in the map where the agents stop between map traversals. Checkpoints don't necessarily have to also contain a charging stations, whilst all charging stations are checkpoints, since the agent can stop at a station and not charge depending on its current path or schedule.

4. ***Timer*** *(Global Variable)*: The time t is constantly incremented as a global counter in the implemented program with any update in the map. Given a lattice graph, the movement time from one node to the other can be used as the unit of time if all agents are the same model (i.e., same speed), which is common in most industrial facilities. MAXTIME can be used as a termination criterion for the program.

$$t \in \mathbf{t} = (0, 1, \dots \text{ MAXTIME }) \tag{8.24}$$

5. ***Traversal Timer*** *(Class Property of Map, Agent)*: A second time variable is incorporated to increase the versatility of the algorithm. Since the algorithm relies on the agents traversing between checkpoints, the flow of time can be alternatively tracked as a counter of the number of traversals the agent makes. This traversal time τ is the one used to keep track of the vertex properties and update the heat values in the map. A good feature of this implementation, which provides the versatility, is that τ can always be set simply as $\tau = t$ in the code, switching back to real time in the dependent functions according to the type of tasking problem at hand. Like MAXTIME, TMAX can also be used as a termination criterion. A mapping $\tau(t)$ can give the current increment time at any t.

$$\tau \in \tau = (0, 1, \dots \text{ TMAX }) \tag{8.25}$$

6. ***Heat Values*** *(Class Property of Map)*: Each vertex has a time-varying "heat" value $H(i,t)$ assigned to it in the Map class. The movement cost through an edge is defined as the mean of the heat values of the two connected vertices as in (8.26).

$$\omega(\{i,j\},t) = \frac{1}{2}(H(i,t) + H(j,t)) \forall \{i,j\} \in \mathbf{E}, t \in \mathbf{t} \tag{8.26}$$

This heat property is the main premise of the designed algorithm and is used to establish all other relations to model a given problem and calculate the task scheduling. Heat values of the vertices are continuously updated to "guide" each agent through the shortest path in the graph such that all tasks are achieved while traversing between its checkpoints (Fig. 3).

7. ***Obstacles*** are directly incorporated by setting a very large number as heat value in that vertex. In this manner, obstacles can be modeled in a very computationally efficient way (as opposed to the use of exceptions or conditional statements), since the movement to/from that vertex is never chosen over any other alternative. This number is imposed as the largest float value of the machine where the algorithm is running, which for most modern processors is 1.7976^{308}.

8. ***Tasks***, on the contrary, are by setting a low value, depending on the type and/or urgency of each task. This acts as an "attractor" for the mobile agent since the Dijkstra SPF algorithm will be attracted to pass through that vertex when constructing the path instead of other alternatives. Once an agent has reached a vertex with a task, the heat value of this vertex is incremented. In this way, the movement cost to/from this location is increased, removing the "attractor" as the task is accomplished. A "cooldown" effect is applied by decrementing heat values of all vertices with each increment of t, such that for an idle map with no activity, heats are eventually reset to their initial values.

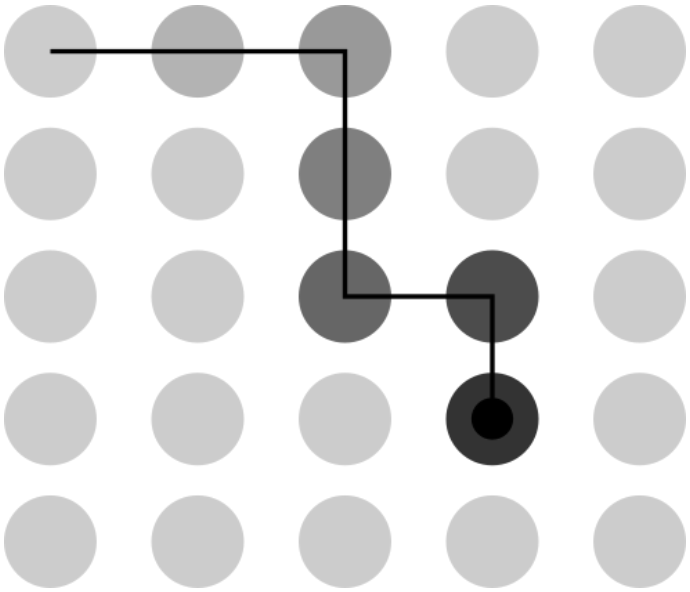

Figure 8.3: Vertex properties being updated as the mobile agent moves and follows a path through the map.

To sum up the flow of the algorithm:

- The industrial site or facility is modeled as a lattice graph.
- Each vertex has a heat property that is updated with every increment of time t based on the mobile agents' movement through the map, the flow of time, and nature of the tasks to be performed (as visualized in Fig. 8.3). The heat value update is done by incrementation and cooldown.
- Tasks and obstacles are modeled by setting the heat value accordingly to guide the agents.
- The heat values set the edge weights for the graph.
- The pathing of each mobile agent between its checkpoints is determined using Dijkstra's SPF (or an alternative shortest path method) every increment of traversal time τ.

The algorithm was implemented using Python 3.6.7. All subsequent tests were run on a standard laptop computer with an Intel Core i7-8550U CPU @ 1.80 GHz, 16.0 GB RAM, and Windows 10 64-bit operating system.

8.3 Parameter Tuning and Benchmark Testing

In this section, tuning parameters of the algorithm are identified, and a benchmark analysis is performed to test the proposed algorithm on a benchmark case, assess the appropriate values for the parameters, and analyze the computational performance and time complexity of the algorithm.

Finally, the choice of the most adequate shortest path method (Dijkstra is justified by discussing other commonly employed shortest path methods is graph theory (A* Search and Bellman-Ford) and performing a comparative analysis between feasible candidates.

8.3.1 Identifying Tunable Parameters

From the algorithm description it can be seen that there are two main parameters which can be used to tune the algorithm:

1. *Increment Value*: The first tuning parameter is the incremental heat value of a vertex once an agent completes a task there. This is defined as INC in (2.27). Note that this function is only invoked once an agent reaches a vertex marked with a task.

$$H(i,t) = H(i,t) + \text{INC}, \quad \text{if task completed} \tag{8.27}$$

2. *Cooldown Function*: This second tuning parameter is how the vertex heat values of the whole graph are updated every time increment t. This is defined as a function CDF in (2.28).

$$H(i,t) = CDF(i, H(i,t), t) \tag{8.28}$$

In this study, four different types of functions are considered. A Fixed Cooldown (FCD) decrements the $H(i,t)$ by a constant value CD every time increment, while a Zero Cooldown sets $CD = 0$ as in (8.29) and (8.30). In (8.31) and (8.32), exponential functions are used instead for a scaled cooldown (SCD), making the cooldown value increase exponentially with every traversal time. In SCD1 and SCD2, the initial decrement values are 1 and 0, respectively. T_{obj} scales the function, increasing the exponential growth as $T_{obj} \to 0$, as shown in (8.33).

$$CDF_{FCD}(i,H(i,t),t) = H(i,t) - \text{CD} \tag{8.29}$$

$$\text{CDF}_{ZCD}(i,H(i,t),t) = H(i,t) - \text{CD}, \quad \text{CD} = 0 \tag{8.30}$$

$$CDF_{scd1}(i,H(i,t),t) = H(i,\tau(t)-1) - e^{\text{CDS}\cdot\tau(t)} + 1 \tag{8.31}$$

$$CDF_{Scd2}(i,H(i,t),t) = H(i,\tau(t)-1) - e^{\text{CDS}\cdot\tau(t)} \tag{8.32}$$

$$\text{SCD} = |V| \cdot \log\left(\frac{\text{T}_{obj}}{\text{TMAX}}\right) \tag{8.33}$$

8.3.2 Benchmark Analysis and Limit Testing

The objective of benchmark analysis is limit-testing the proposed algorithm by conducting a parametric study to assess the performance and stability of the solution A generic case study is used based on the facility inspection problem [227].

In this problem, a mobile agent travels between the charging stations, at the top-left and bottom-right corners of the map. The mobile agent must inspect the site, making sure all areas are frequently visited and no areas are ignored. The inspection problem makes for an ideal benchmark case study for limit testing, since it is an extreme case of the task scheduling problem: every vertex of the map is itself a task since the goal is to patrol the full map continuously.

The ideal solution in this case is for the agent to be pathed across the map to avoid any areas of the map being neglected on the long term (i.e., avoid some areas being visiting more than others as much as possible). Three benchmark studies and limit tests were performed.

8.3.2.1 Benchmark Test 1: Time Complexity Analysis

When proposing a new computational algorithm, one of the most important features to establish is its time complexity. The time complexity of the Dijkstra SPF (computing only one traversal of the map) is $\Theta(|\text{V}| \cdot \log|\text{V}|)$. Using analytical analysis of the implemented code, the time complexity of the proposed algorithm was determined to be $\Theta\left(|\text{V}| \cdot (\log|\text{V}|)^3\right)$.

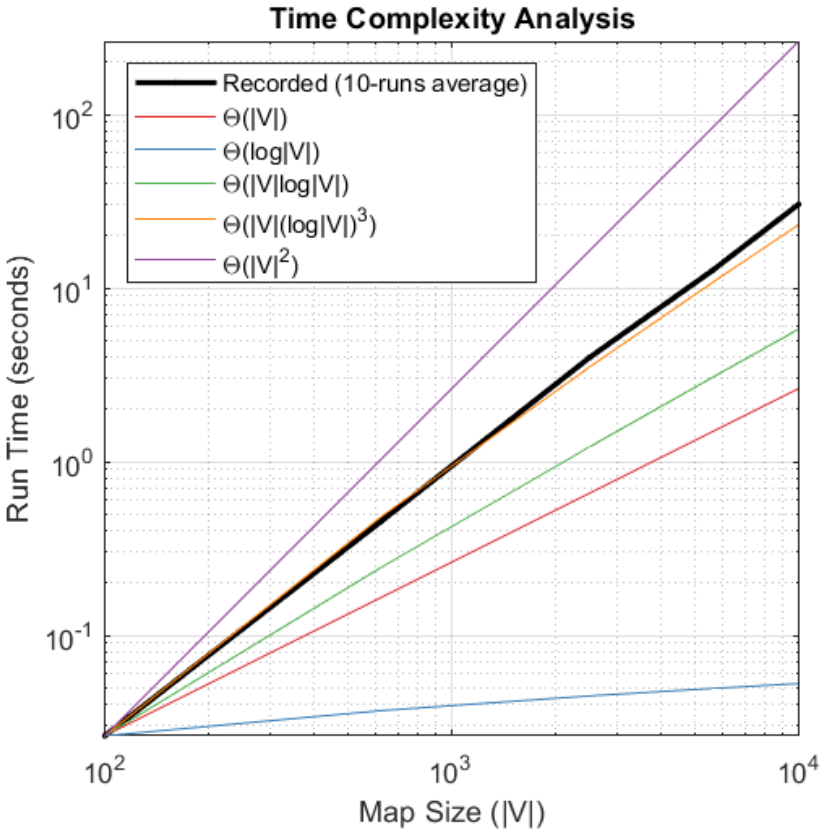

Figure 8.4: Results for the first benchmark test: time complexity analysis showing the recorded run time vs. other time complexities in big-Θ notation. The designed algorithm is confirmed to be $\Theta\left(|V| \cdot (\log |V|)^3\right)$.

The benchmark problem is run for a grid size of 10x10, 25x25, 50x50, 75x75, and 100x100. The ZCD function was used (chosen for simplicity, since the choice is irrelevant and doesn't affect the time complexity results since all the CDF functions are $\Theta(1)$). The termination criterion was set as TMAX=100 (100 traversals). For each map size the code is run 10 times, and the average run time is recorded.

The results are plotted in Fig. 8.4 in comparison to other common time complexities of graph algorithms, expressed in big-Θ notation. From the results, it is indeed confirmed to be $\Theta\left(|V| \cdot (\log |V|)^3\right)$.

The small offset for larger values is attributed to approaching physical limits of memory allocation on a laptop PC. Thus, the proposed algorithm is deemed computationally efficient, being marginally slower than Dijkstra's SPF for a single shortest path solution, yet faster than any $\Theta\left(N^2\right)$ algorithm, i.e., $\Theta(|V| \cdot \log |V|) < \Theta\left(|V| \cdot (\log |V|)^3\right) < \Theta\left(N^2\right)$.

8.3.2.2 Benchmark Test 2: INC and CDF Selection

The second benchmark test aims to test the effect of varying the value of INC and the choice of the CDF. To perform a full parametric analysis which considers the grid size as well, the testing is performed and comparatively evaluated on small (10x10), medium (25x25), and large (50x50) maps.

For each map size, ten different INC values are tested, varying from 0.5·|V| to 5·|V| with increments of 0.5·|V|. For each value of INC, the problem is run using each of the four proposed CDF functions (i.e., a total of 3 maps x 10 INC values x 4 CDF runs). For each run, the termination criterion was set as TMAX=100 (100 traversals). As a performance metric the number of times each vertex was visited/inspected by the agent is counted, recalling that the anticipated solution is to have no uninspected parts of the grid.

In Fig. 8.5, the number of uninspected nodes at the end of each run (at $\tau = TMAX = 100$) is plotted for all cases. Another performance metric is associated with the frequencies of vertex inspections. The ideal solution is for the number of visits for the maps vertices to be as close to the median value as possible (i.e., no parts are neglected compared to others).

To analyze this, a box plot with summary statistics for each run of the medium map is shown in Fig. 8.6. In this sense what is desired is to have: 1) no zero values; and 2) minimum inter-quartile range. From the results in Fig. 8.5 and Fig. 8.6, the following points can be made by observing both performance metrics:

- ZCD is the only CDF that provides a stable operation, being independent of the grid size.
- If a FCD is to be chosen, its value should be set as a function of INC (proportional thereto) to guarantee improved performance.
- In comparison, SCD1 and SCD2 do not perform as well and are less stable. SCD1 shows more stability than SCD2, but better tuning of the function is necessary.

The results of this third benchmark test strengthen the points made previously. ZCD and FCD both provide stable performance, with the number of traversals required converging to a finite value as the grid size is increased. However, FCD is dependent on the INC value, thus being proportional to the grid size for a stable operation. SCD1 and SCD2 are shown to have stability problems in their current form for large maps.

It can be argued that the SCD function may provide better performance depending on the type of tasking problem involved. While this may be true, the objective of this test is to determine the choice of parameters that guarantee a reliable and stable operation for any type of tasking problem, thus establishing a “benchmark” for the designed algorithm. Nevertheless, the implementation makes it flexible for users to freely tune these parameters to best fit the specific problem.

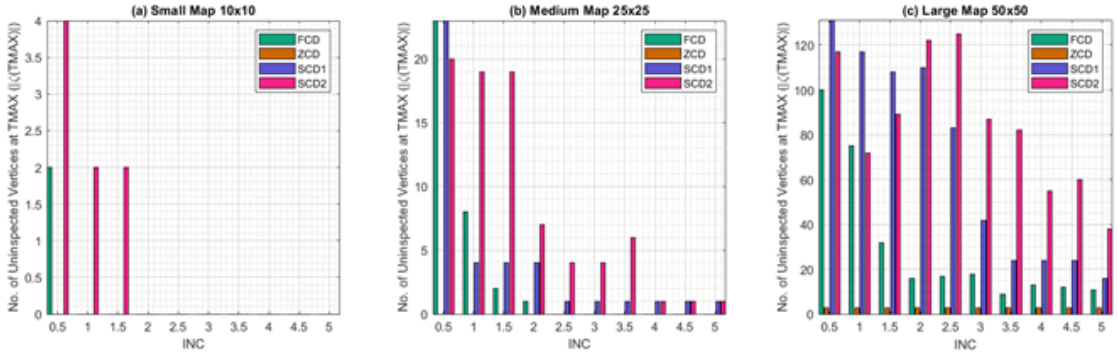

Figure 8.5: Results for the second benchmark test: number of uninspected vertices at τ=TMAX=100. Results are shown for the total of number of runs corresponding to: 3 maps x 10 INC values x 4 CDF choices.

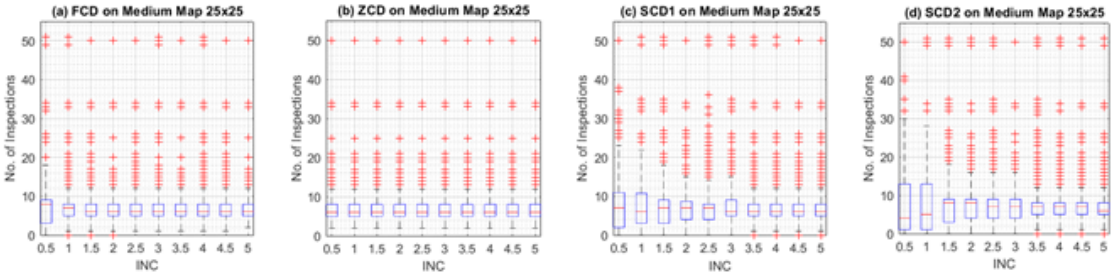

Figure 8.6: Results for the second benchmark test: box plot to show summary statistics of the number of vertex inspections at τ=TMAX=100. A box plot for each of the 10 INC values x 4 CDF choices is plotted for the medium 25x25 map. The blue boxes correspond to the 25th to 75th percentile range. The red line is the median value, and the whiskers show the maximum and minimum values. Outliers (>1.5 times inter-quartile range) are shows as red crosses.

Therefore, from the benchmark analysis it is possible to show that: 1) the proposed algorithm is $\Theta\left(|V| \cdot (\log |V|)^3\right)$ and 2) ZCD is recommended as the "default" option for the CDF, being the most reliable and least dependent on other parameters.

8.3.2.3 Benchmark Test 3: Stability and Termination Criteria

By using TMAX as the termination criterion in the previous study, it was observed that the number of required traversals to fully span the map is dependent both on the tunable parameters and the grid size. It is very critical to verify that the number of traversals required to fully span the map does not diverge with the grid size, i.e., it is critical to establish the stability of the algorithm and the CDF functions and INC values.

Therefore, another limit test is performed by letting the simulation run for a very large number of traversals (TMAX = 500) and recording the number of traversals required to inspect the full grid once all nodes have been inspected at least once. The results are listed in Table 8.1 and plotted in Fig. 8.7.

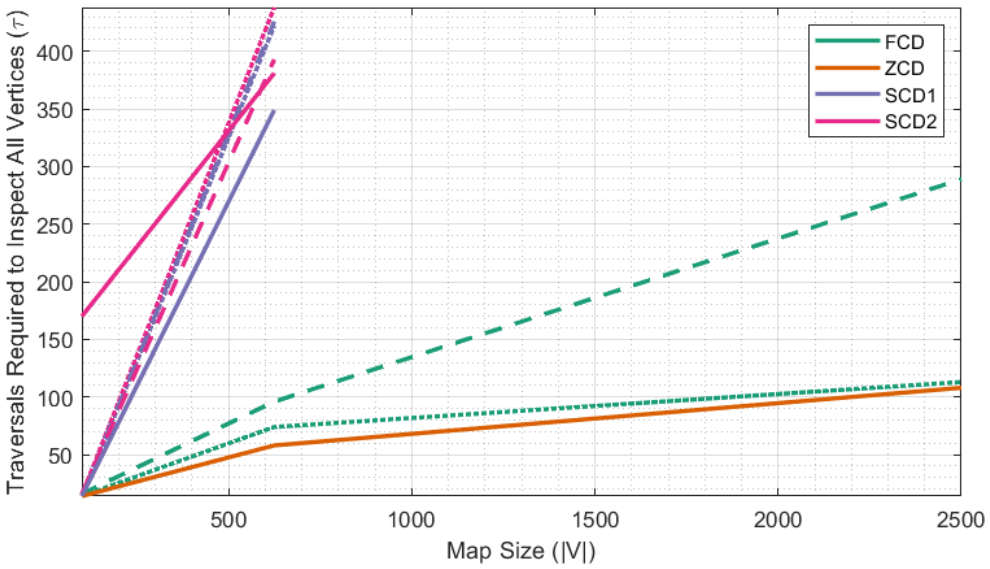

Figure 8.7: Results for the third benchmark test: number of traversals required to inspect the full map relative to the map size, for each CDF selection. Dotted, dashed, and solid lines correspond to INC=1|V|, 3|V|, and 5|V|, respectively.

Table 8.1: Results for the third benchmark test: the number of traversals required to inspect the full map with different sizes, INC values, and CDFs.

CDF	**Map Size (|V|)**	**INC**		
		1|V|	**3|V|**	**5|V|**
FCD	**100**	36	16	14
	625	>500	96	74
	2500	>500	289	113
ZCD	**100**	14	14	14
	625	58	58	58
	2500	108	108	108
SCD1	**100**	170	16	15
	625	381	393	438
	2500	>500	>500	>500
SCD2	**100**	14	14	14
	625	349	426	422
	2500	>500	>500	>500

8.3.3 Choice of the Shortest Path Method

In the designed and implemented algorithm, for each traversal of a mobile agent through the modeled map, Dijkstra's SPF method is used to determine the path taken of the mobile agent. Since the shortest path is guided by the node values set iteratively according to the designed algorithm (as the map dynamically changes), the obtained path would maximize the tasks being achieved while minimizing the movement cost (and hence, electricity consumption).

Indeed, numerous other shortest path methods exist in graph theory applications, with common well-known alternatives to Dijkstra's SPF being A* Search and Bellman-Ford [230].

All the aforementioned methods achieve the same objective: find the shortest path between two nodes in a weighted graph.

The designed graph-based model and algorithm are versatile such that any shortest path method can be used, and the same results would be achieved, since the shortest path for a given state of the map (node values and corresponding edge weights) would be the same regardless of the method used to find it.

In this case, the choice of the most suitable shortest path method to incorporate in the proposed algorithm depends on the computational burden. To justify the choice of Dijkstra as opposed to other alternatives, a discussion thereof and a comparative analysis is performed in this section.

By reperforming the benchmark analysis considering all three candidates (Dijkstra, A* Search, and Bellman-Ford), Dijkstra was shown to guarantee the best performance in terms of computational complexity (and thereby scalability) for the proposed algorithm. In Fig. 8.8, A* Search and Bellman-Ford are seen to have a similar performance, being significantly slower than Dijkstra, especially for larger maps.

Another critical point to note is that with the proposed model and algorithm, Bellman-Ford is unable to converge to a solution when all the edge weights are equal (e.g., in the first iteration), and an alternative method must be employed whenever this occurs.

This issue does not occur neither with Dijkstra nor with A* Search, which both robustly find the shortest path in all iterations for all map conditions. Therefore, the use of Bellman-Ford is not recommended, and the two feasible candidates are Dijkstra and A* Search.

Both methods provide the same results for the designed model and algorithm, with Dijkstra being superior in terms of computational time, especially for larger maps (i.e., better scalability). Therefore, Dijkstra's method is shown to guarantee a reliable performance while providing the fastest computational time (which is critical as the proposed algorithm is intended for real-time application).

Nevertheless, the implementation of the proposed model and algorithm makes it flexible for users to use any shortest path method at their convenience. A comparison between the choice of Dijkstra and A* Search in the proposed model and algorithm is revisited in the next section considering a real-world application.

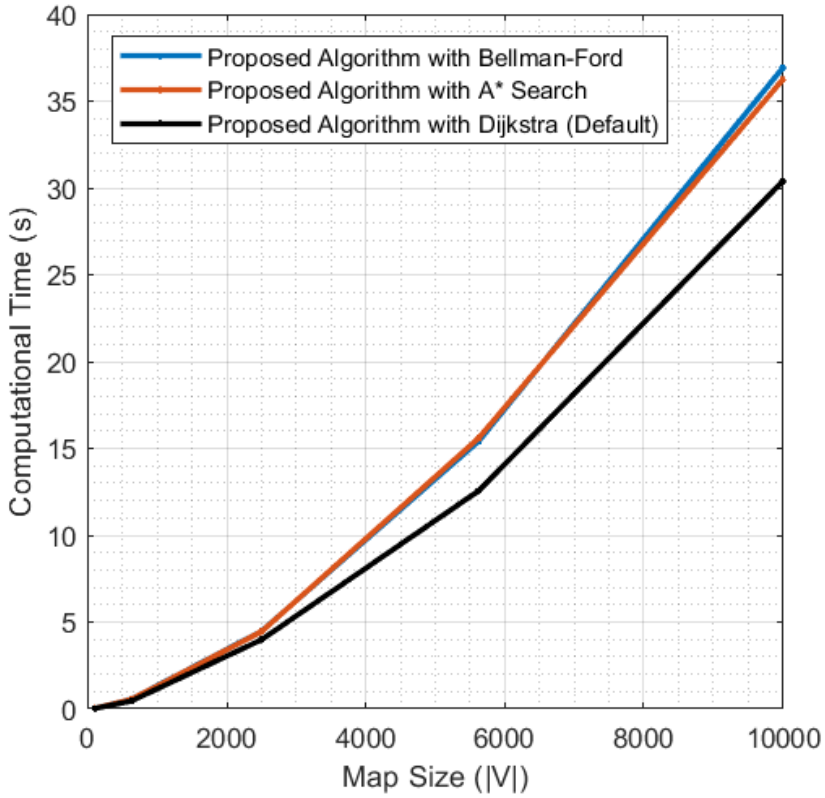

Figure 8.8: Comparing the performance of the proposed algorithm while using Dijkstra, A* Search, and Bellman-Ford for different map sizes.

8.4 Real-World Application

In this section, a real-world case study is used to demonstrate the applicability of the proposed algorithm to real-life problems. An oil refinery located at coordinates (53.090, 14.254) is considered. Due to their nature, oil refineries require constant safety inspection, particularly with the hazardous nature involving the oil tanks and pipelines on the site. These refineries span very large areas, and so automating the safety inspection process is highly desired.

8.4.1 Validation Case Study with Stationary Obstacles

In this case study, one autonomous mobile agent is allocated to perform the security inspection and patrolling the refinery, as shown in Fig. 8.9 (left). The SMP S5.2 series security robot 2020 model [4] is considered as a commercially available option for an autonomous mobile agent, with its specifications listed in Table 8.2. Thus, the objective is to test the performance of the proposed DOT algorithm in effectively scheduling its fully autonomous operation in the sites' safety inspection. In this first case study, only stationary obstacles are considered.

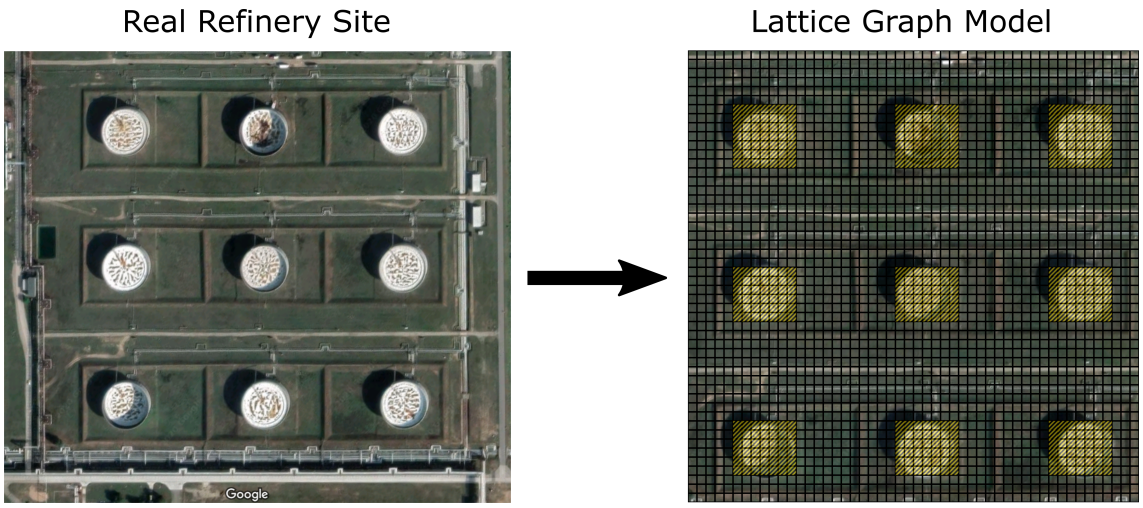

Figure 8.9: Satellite image of the oil refinery located at coordinates (53.090, 14.254) used as for the case study (left), and modeling as a lattice graph (right) with the obstacles/non-traversable vertices highlighted in yellow. The real-life area of the site is 350x350 m^2.

The physical limitations of the agent's motion must be considered to determine the correct discretization of the lattice graph. The dimension of each grid element Δv must be larger than both the minimum width of the patrol path (S3) and the minimum turning radius (S4). Meanwhile, the grid elements must also be smaller than the minimum object recognition range of the onboard cameras and detection systems (S5). This is expressed in (8.34).

$$\max(S3, S4) \leq \Delta v \leq S5 \tag{8.34}$$

With the real site area being 350x350 (m^2), a spacing Δv=7m would satisfy (8.38), thus resulting in a 50x50 grid as shown in Fig. 8.8 (right). The graph can then be constructed as formulated in Section 8.2. As mentioned, obstacles (in this case being the tanks) are modeled by setting the vertex heat values to 1.7976^{308}. Each time step would correspond to the average traveling time between two vertices at the agent's average autonomous traveling speed (S2), as shown in (8.35).

$$\Delta t = \Delta v \cdot S2 = 0.035h \tag{8.35}$$

The agent's onboard battery SoC is updated according with each timestep to (8.36). The charging and discharging values (per timestep) are calculated according to (8.37) and (8.38). The minimum allowed SoC is 0.1. Accordingly, the maximum range of a fully charged agent is be obtained in (8.40).

$$\mathrm{SoC}(t) = \begin{cases} \mathrm{SoC}(t-1) - \mathrm{SoC}_{\mathrm{disharge}}\,, & \text{if moving} \\ \mathrm{SoC}(t-1) + \mathrm{SoC}_{\mathrm{charge}}\,, & \text{if charging} \end{cases} \tag{8.36}$$

$$\mathrm{SoC}_{\ \mathrm{discharge}} = 100 \cdot \frac{\Delta v}{S1}\% = 0.029\% \tag{8.37}$$

Table 8.2: Specifications of the mobile agent used for the case studies (SMP S5.2 series 2020 model) [4].

S1 - Cruising Range	24 km
S2 - Autonomous Traveling Speed (average)	5 km/h
S3 - Width of Patrol route path (minimum)	0.9 m
S4 - Turning Radius (minimum)	5 m
S5 - Object Recognition Range (minimum)	50 m
S6 - Operating Time (average)	12 h
S7 - Charging Time (average)	5 h
S8 - On-Board Battery Capacity	3 kWh
S9 - Charger Power	600 W

$$\text{SoC}_{\text{ charge}} = 100 \cdot \frac{\Delta t \cdot S9}{S8}\% = 0.7\% \tag{8.38}$$

$$\text{max range} = (1 - \text{SoC}_{\text{min}}) \cdot S1 = 19.2 \text{ km} \tag{8.39}$$

The algorithm is run for this problem with ZCD and INC=1. In order to simulate the real-life case, the termination criteria is set according to the maximum range at full charge, by setting *MAXTIME*=3085. In this sense, the case study aims to assess the effectiveness of the algorithm in scheduling the agent's inspection paths through the map, making the best use of one full battery charge.

It has been mentioned that the proposed algorithm is the first of its kind in generically model the industrial task scheduling problem for autonomous agents. While this is a novel contribution, it does add a difficulty since there were no similar existing algorithms to use for comparison at the time of this work, especially in terms of the problem modeling.

Obtaining a deterministic solution is not possible, as it would require a full graph search to be performed being $\Theta(|V|!)$, corresponding to more than 1.6^{7411} path determinations, which is infeasible even on high-performance computers.

However, there are multiple graph theory algorithms for path spanning and sampling that can be modified for this purpose. Accordingly, the directed random walk (DRW) algorithm [231], [232] was used with two variations: normal (DRW1), and brute-force (DRW2). Those algorithms are detailed in Appendix B.

In addition, the case study is used to reaffirm the choice of Dijkstra's SPF as opposed to the other feasible alternative (A* Search) in the proposed model and algorithm. While it is anticipated that both Dijkstra and A* Search would yield the same results and the main advantage of choosing Dijkstra would be in the computational efficiency, this is revalidated by comparing the results of the proposed algorithms using both shortest path methods.

The objective now is to evaluate a) how effectively is the site being inspected by the assigned agent and b) how efficiently is this being done by limiting the operation to one full battery charge. Four evaluation criteria are used:

- Percentage of Site Area Inspected [%].
- Mean number of vertex visits.
- Mean Area per Charge Consumed [m^2/kWh]
- Ratio of Algorithm Running Time to Real Operating Time.

Snapshots of the resulting paths through the site by the DOT algorithm are visualized in Fig. 8.10, and the performance metrics are compared with those of DRW1 and DRW2 in Fig. 8.11. The latter are also listed in Table III. The proposed algorithm outperforms the others in all performance metrics.

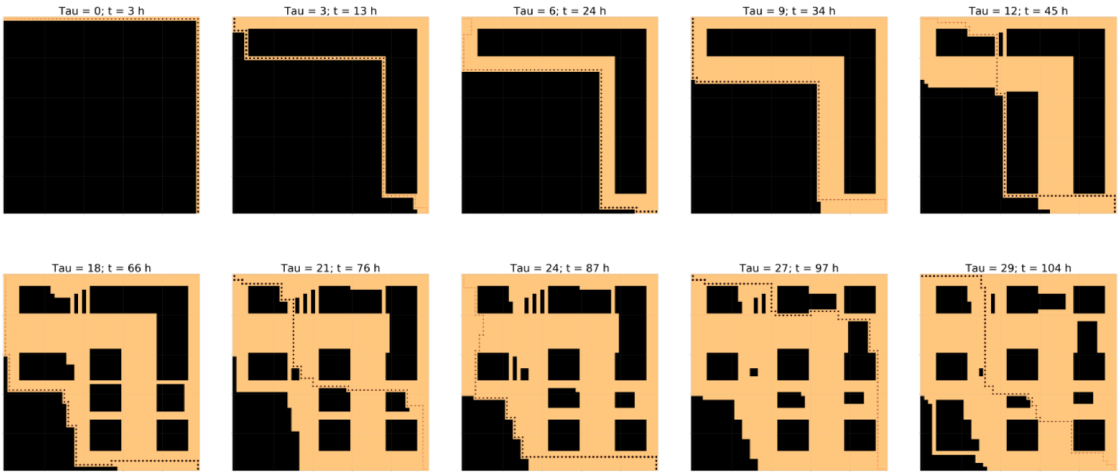

Figure 8.10: Snapshots visualizing the resulting paths through the site by the DOT algorithm at τ=(0,3,6,9,12,18,21,24,27,28) on a single onboard battery charge. Dark and light colored nodes correspond to inspected vs. uninspected vertices, respectively.

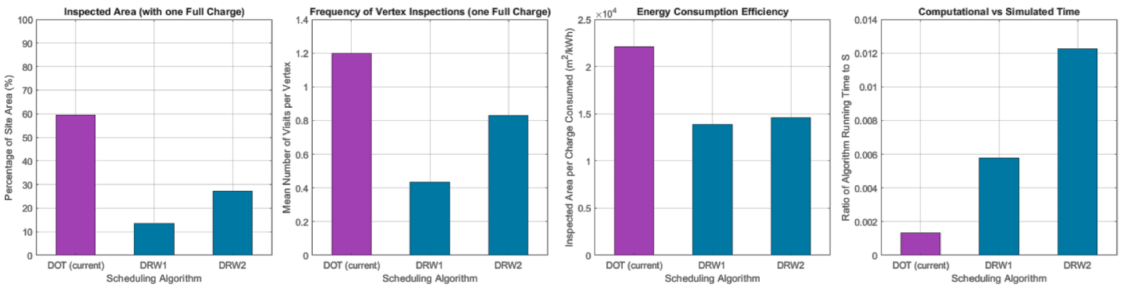

Figure 8.11: Comparison between the proposed DOT algorithm vs. DRW1 and DRW2 in terms of the performance metrics: a) Percentage of Site Area Inspected [%], b) Mean number of vertex visits, c) Mean Area per Charge Consumed [m^2/kWh], and d) Ratio of Algorithm Running Time to Real Operating Time.

Table 8.3: Performance metrics for DOT (proposed algorithm with Dijkstra), proposed algorithm with A* search, DRW1, and DRW2 with stationary obstacles only (using only one full battery charge).

Performance Metric	Method Used for Task Scheduling			
	Proposed Graph Model and Algorithm		DRW1	DRW2
	With Dijkstra SPF	With A* Search		
Algorithm Running Time (s)	**3.99**	**4.5**	**36.6**	**17.2**
Mean number of vertex visits	1.20	1.20	0.43	0.83
Total area inspected (m^2)	57526	57526	13083	26313
Percentage site area inspected (%)	60%	60%	14%	27%
Area per Charge Consumed (m^2/kWh)	22103	22103	13874	14569

It is noted that the algorithm run time is calculated per map traversal as a normalized figure. As anticipated, the choice of Dijkstra or A* has no effect on the performance metrics except the computational time, where the choice of Dijkstra outperforms A* Search (by 12.5%).

Note that the DRW algorithms have a random element and the results shown are for optimized runs (best cases). Therefore, the actual real-life performance of DRW is worse than shown here, as opposed to the deterministic solution of the proposed DOT.

The results shown are for an operation limited to one full battery charge to simulate a real-life restriction. Removing this constraint (with recharging or a substitute agent) results in even better performance by DOT compared to DRW. Finally, it is worth noting that the ratio of scheduled real time to the algorithm running time is 1000, confirming that DOT is deployable for real time scheduling of autonomous agents.

It can be seen in Fig. 8.10 how the obstacles were provided directly in the map data input file without the need for any conditional statement modifications to the code. Applying a heat value of 1.7976^{308} guaranteed that the obstacle vertices are never selected in computed paths. This provides great versatility, since new obstacles can be introduced or moved in real-time, a feature which is not possible by other graph methods that construct random paths such as DRW. To demonstrate this, a second case study with dynamic (mobile) obstacles is performed.

8.4.2 Case Study with Stationary and Mobile Obstacles

In this case study, two dynamic (mobile) obstacles are introduced into the map. In the real-world setting, this would correspond to construction work along the pipelines in the oil refinery, which would in untraversable by the mobile agent during its inspection patrols. This is illustrated in Fig. 8.12, with dynamic obstacles 1 and 2 set on a path that is eastbound and westbound, respectively. The speed of the obstacles is set to 3m/h, corresponding to a realistic relocation of maintenance workers along the pipelines.

Snapshots of the resulting paths through the site by the DOT algorithm is visualized in Fig. 8.13, and the performance metrics are shown in Table IV.

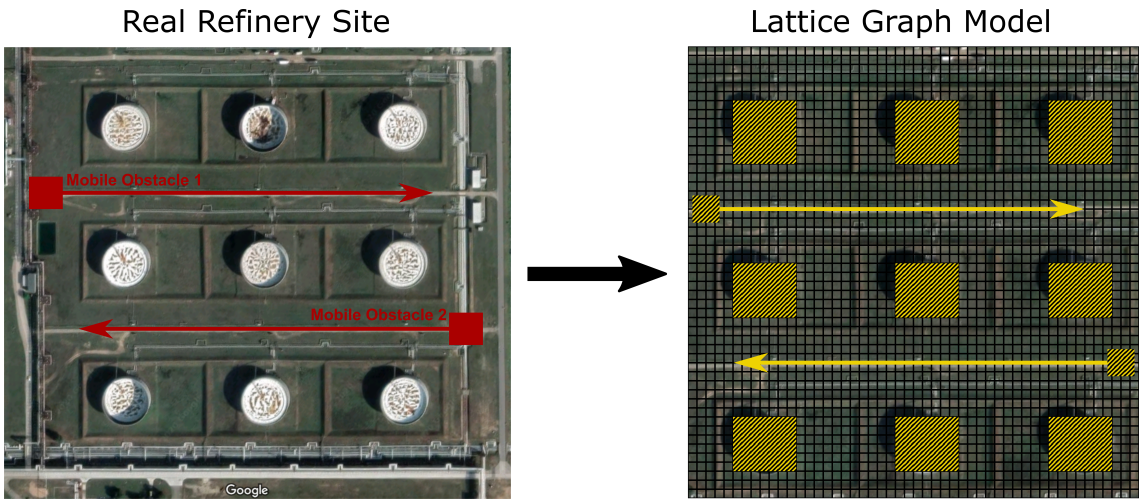

Figure 8.12: Satellite image of the oil refinery located at coordinates (53.090, 14.254), including mobile obstacles used as for the second case study (left), and modeling as a lattice graph (right) with the obstacles/non-traversable vertices highlighted in yellow (stationary and mobile). The real-life area of the site is 350x350 m^2.

The presence of dynamic obstacles slightly increases the computational burden (due to the necessity of updating the node heat values every time the obstacle moves). Moreover, the presence of the moving obstacles seems to (very slightly) facilitate the inspection problem, since it forces the mobile agent to cover a wider area to avoid the additional obstacles present.

It is verified that the resulting paths for the agent never intersect with neither the stationary nor the dynamic (moving) obstacles, while successfully maximizing the inspected area for an operation limited to one full battery charge to simulate a real-life restriction.

To reaffirm the statements made in Section III.C regarding the choice of Dijkstra as opposed to other shortest path, the case study with dynamic obstacles is re-simulated using the proposed method, incorporating A* Search instead of Dijkstra. As anticipated and previously stated (also as the results of the first case study showed), the choice of the shortest path method does not affect the results. Dijkstra is demonstrated again to guarantee the best computational efficiency and algorithm stability.

The objective of this chapter was to clearly describe the proposed model and algorithm present the mathematical formulation. A thorough limit testing was performed to recommend the set of parameter settings (i.e., INC and CDF) and the choice of the shortest path method (i.e., Dijkstra), that guarantees reliable and stable execution of the algorithm, in addition to minimal computational burden.

However, the algorithm was designed such that the building blocks can be easily changed by the users (e.g., choice of the shortest path method), without influencing the results). This is in fact a compelling advantage of the proposed graph model and algorithm, being that the obtained solution is independent on the choice of the shortest path function.

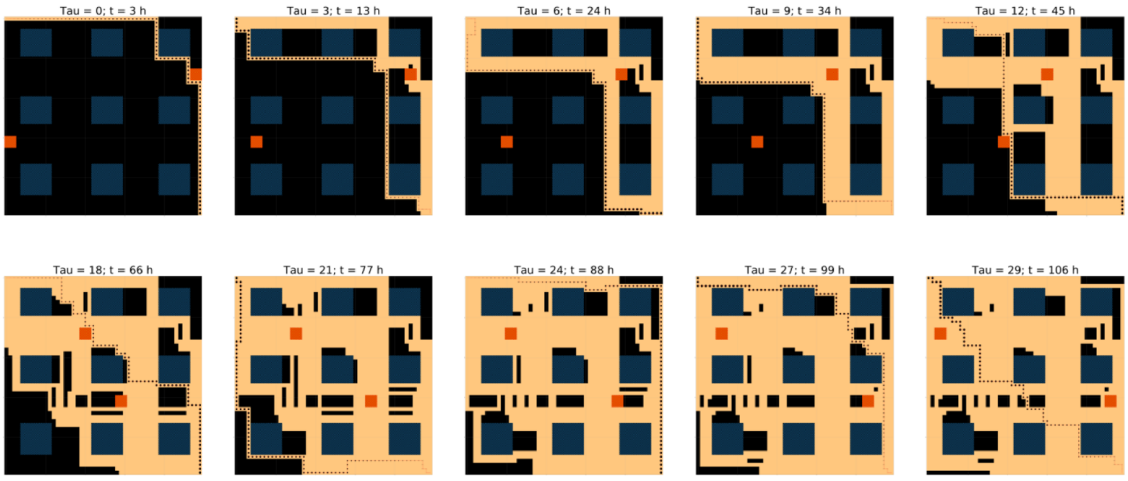

Figure 8.13: Snapshots visualizing the resulting paths through the site by the DOT algorithm at τ=(0,3,6,9,12,18,21,24,27,28) on a single onboard battery charge. Dark- and light-colored nodes correspond to inspected vs. uninspected vertices, respectively. Blue and red squares correspond to stationary and mobile obstacles, respectively. The dotted path corresponds to the agent's current path at the given time.

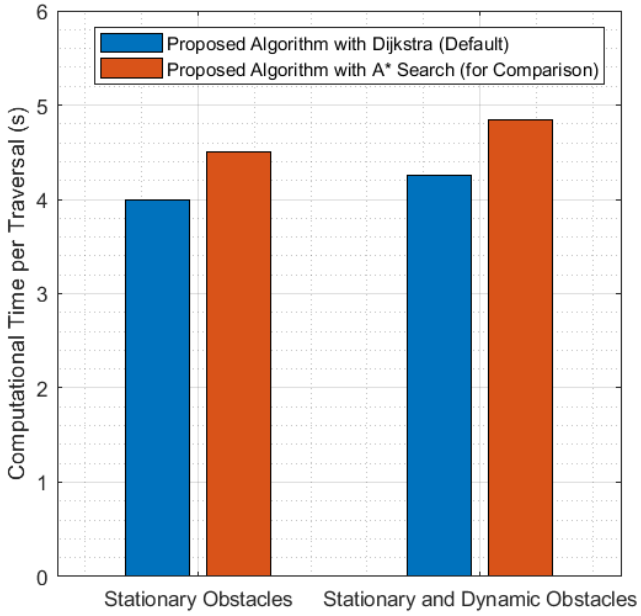

Figure 8.14: Comparing the computational performance of the proposed algorithm while using Dijkstra vs. A* Search in the presence of stationary obstacles only (left) and stationary and dynamic obstacles (right).

Table 8.4: Performance metrics for DOT (proposed algorithm with Dijkstra) vs. Proposed algorithm with A* considering dynamic obstacles (using only one full battery charge).

Performance Metric	**Proposed Graph Model and Algorithm**	
	With Dijkstra (DOT)	**With A*Search**
Algorithm Running Time (s)	**4.25**	**4.85**
Mean number of vertex visits	1.21	1.21
Percentage site area inspected (%)	61%	61%
Area per Charge Consumed (m^2/kWh)	22235	22235

In this way, the designed algorithm is versatile and can be easily adapted or modified by users for different industrial tasking problems cases while guaranteeing a reliable and robust performance for real world applications.

8.5 Conclusions

An innovative graph-based model and algorithm for optimal task scheduling was proposed, implemented and tested. The designed DOT algorithm was designed based on graph theory to guarantee a generic nature, making it applicable on a plethora of tasking problems and not being case-specific. For any industrial setting where mobile agents are responsible for accomplishing tasks across a site, an optimal task schedule for each agent is obtained to maximize the speed of the task achievement with high energy consumption efficiency. The algorithm's versatility in modeling different problems and high computational efficiency make it perfectly suitable for a fully distributed task scheduling of autonomous agents. A real-world case study has demonstrated the effectiveness of the proposed algorithm for an industrial site inspection problem, including the presence of dynamic (moving obstacles). In future work, the algorithm can be applied to other problems in smart industries with dynamic environments where energy consumption efficiency is required as a top priority.

This concludes the third part of this thesis, where new energy management models for the residential, transport, and industry sectors are developed. The next and final part revisits the research questions, summarizes the work performed in the thesis listing the main innovations, summarizes the conclusions, and presents prospects for future work.

Part IV

Final Remarks and Recommendations for Future Work

Chapter 9

Final Discussion and Response to Research Questions

In this chapter, the research questions of the this thesis are revisited and answered in detail based on, and referencing to, the research work presented in all previous chapters. The secondary research questions are each individually addressed first, aggregating a comprehensive answer to the primary research question.

9.1 Secondary Research Questions

1) Can individual and proprietary data models from the IoE paradigm be used to leverage DSM and DR services from individual prosumers and microgrids (cluster of prosumers) thereby improving global operation of dispersed energy systems?

In Chapter 1, the origins of Demand-Side Management (DSM) and Demand Response (DR) and initial motives for their inception were identified and regional differences investigated. The historical evolution of DR and DSM were analyzed using a novel scientometric approach of both legislative and scientific research literature from the past four decades.

It was shown that DR has historically emerged globally as a subset of DSM only through smart meter (SM) roll-out, the establishment of Smart Grids (SG) advanced communication infrastructures, and the market rules that promoted the willingness of the consumers to increase their active participation. Thus, it is established that even historically, the use of data models involving individual prosumers is a key enabler to DR implementation.

Increased Internet-of-Things (IoT)-enabling of SG and high penetration of scalable and distributed energy resources in recent years is resulting in the emergence of the Internet of Energy (IoE), seen as the SG 2.0. In this IoE paradigm being a fully decentralized network of energy prosumers, DR will continue to be a vital aspect of the grid in future Transactive Energy (TE) schemes, which aim for more user-centered, energy-efficient, cost-saving, energy management approaches. More physically decentralized and interconnected energy systems motivate the investigation of decentralized data models to manage them as opposed to centralized operators.

In Chapter 2 it was concluded that technical models and processes developed in an IoE paradigm should be:

1. **distributed** (fully decentralized),
2. **efficient at data analysis** (with efficient forecasting and optimization capabilities),
3. **scalable**, and
4. **user-friendly** (plug and play).

Therefore data models developed to leverage DR and DSM services should follow these design requirements in the IoE paradigm.

The use of Blockchain and cloud computing has been shown to enable successful implementation of peer to peer (P2P) based models to leverage DR and DSM services from individual prosumers and microgrids (cluster of prosumers) and thereby indeed improve global operation of dispersed energy systems.

In Chapter 3 a complex analysis is conducted where a cloud-based Energy Management System (EMS) coordination framework is proposed. The EMS of both individual prosumers and aggregators, Electric Vehicle (EV) parking lot operators, both actively participated in a fully implemented DR and DSM services of a considered SG. Synergistic coordination of the EMSs is evaluated through a cloud-based data model. Technical and economic benefits for all participants (grid operator, EV owners, and parking lot EMS aggregator) have been demonstrated.

Therefore, the answer to this research question is: *Individual and proprietary data models from the IoE paradigm can indeed be used to leverage DSM and DR services from individual prosumers and microgrids (cluster of prosumers) and improve global operation of dispersed energy systems.*

2) Can local (fully decentralized) optimization and data analytics functions enable global integration of demand-side flexibility in the energy market, system operation, and planning?

In Chapter 3, the developed and considered EMSs all aimed at leveraging demand-side flexibility. The home energy management system (HEMS) for homeowners considered real-time pricing for active DR implementation. The parking lot energy management system (PLEMS) provided ancillary services (namely in the reserve and regulation markets).

Through the presence of implemented DSM and DR measures, local optimization and data analytics can indeed enable global integration of demand-side flexibility in the energy market. Furthermore, coordination between these local optimization systems through a cloud-based approach can further leverage flexibility and enhance system operation.

In Chapter 7 this is also demonstrated for the case of a fully electrified public transport networks, showing that the development of the generalized optimization algorithm leverages the demand flexibility (through optimal charging schedules with dynamic pricing considered), system operation (through optimal design of the systems and dispatching to reduce costs), and planning (through optimal battery sizing and charging infrastructure deployment). In addition, the optimization model is shown to enable long term planning (10-year ahead).

Therefore, the answer to this research question is: *Local (fully decentralized) optimization and data analytics functions can indeed enable global integration of demand-side flexibility in the energy market, system operation, and planning.*

3) Can optimal prosumption scheduling of individual agents in a decentralized energy system (using information signals from other individual agents contrary to top-down centralized control) result in global optimal operation?

In Chapter 5, a conceptual model was constructed for the transition from a fully centralized operation of a SG to a decentralized one, proposing the transition scheme between the two paradigms. In a fully decentralized SG run by local agents, a novel machine learning (ML) algorithm was proposed and formulated (building on the method developed in Chapter 3) to enable this transition and into cloud-based fully decentralized system operation. The proposed algorithm incorporates the capability of cloud-based cooperative information exchange without sharing private/raw data (e.g., local historical datasets or control actions taken locally).

This is performed by proposing a new concept of an s-index vector, which is an encoded information that can be shared between agents to improve their control action predictions without sharing raw information. Based on a demanding, high-resolution (15-minute) week-ahead fully decentralized operation case, the developed algorithm guarantees an accurate prediction of optimal operation with less than 0.1% error compared to a centralized operation case.

In addition, in Chapter 6 a novel framework for distributed management of TE networks was proposed and tested. A coordinated scheduling algorithm for joint scheduling of energy consumption and trading was developed. The scheduling tool runs locally at each prosumer in order to achieve a maximum global energy throughout the network. It was shown that the proposed model could provide potential benefits for both prosumers and the grid, albeit with a user-centered, fully distributed approach to schedule energy consumption and trading in transactive energy networks of prosumers. Since all calculations run locally at each prosumer, no exchange of private information is needed to achieve fully distributed management of the network.

Therefore, the answer to this research question is: *Optimal prosumption scheduling of individual agents in a decentralized energy system (using information signals from other individual agents contrary to top-down centralized control) can indeed result in global optimal operation.*

4) Do decentralized data models provide an effective and sustainable solution for the operation of physically decentralized energy systems?

In Chapter 2, it was elaborated that decentralization occurs at three different and distinguishable layers:

- **Decentralization of power systems**: Physical disaggregation of power generation.
- **Decentralization of information systems**: Distributed data as in the IoT paradigm.
- **Decentralization of energy markets**: Is the case with P2P energy trading between prosumers.

Moreover, it was demonstrated that decentralization of information systems creates two main problems: data redundancy and data security/privacy. Therefore, developed decentralized data models must handle address both problems to offer an effective solution for the operation of decentralized power systems.

The latter is made possible with the development of Blockchain-based systems, enabling fully decentralized, cryptographically secured, and consensus-based networks. It is important to elaborate here that Blockchain is not necessarily associated with energy markets, and the technology can be used to provide a secure communication infrastructure (for information "transaction") regardless of the energy market structure. The application of Blockchain to energy systems has been discussed in detail in Chapter 2.

Meanwhile, cloud computing capabilities now make it possible for probabilistic and ML algorithms to overcome the data redundancy problem. This was extensively studied and proved through the novel methods developed and analyses conducted in Chapters 3, 4, and 5.

Therefore, the answer to this research question is: *Decentralized data models provide an effective and sustainable solution for the operation of physically decentralized energy systems; enabled by cloud computing capabilities, ML algorithms, and secure communication infrastructures.*

5) Could new models be created and developed to enable a fully decentralized P2P energy and information trading platform?

In Chapter 5, the developed ML algorithm for fully decentralized power system operation incorporates the capability of cloud-based cooperative information exchange without sharing private/raw data (e.g., local historical datasets or control actions taken locally) of the individual agents. This is performed by proposing a new concept of an s-index vector, which is an encoded information that can be shared between agents to improve their control action predictions without sharing raw information. The results of the conducted case study have shown that the cooperative information exchange between the decentralized agents has a profound impact on the accuracy of their predicted generation values. Therefore, this model provides opportunities for transactive information exchange using peer-to-peer or cloud-based platforms for cooperative operation by decentralized agents, assessing the "value" of traded / transacted information.

In the case of small-scale residential prosumers: In Chapter 6 a novel algorithm for fully distributed joint scheduling of energy consumption and trading in residential transactive energy networks was proposed. An alternative means of quantifying social welfare was conceptualized, which is redefined and adapted for peer-to-peer prosumer-centered networks. With all calculations performed locally at each prosumer, the energy transactions are performed using peer-to-peer trading within a decentralized energy market (e.g. on Blockchain), with no exchange of private information needed to achieve fully distributed management of the community of prosumers.

Therefore, the answer to this research question is: *New models can indeed be created and developed to enable a fully decentralized P2P energy and information trading platform; both for grid operation and small-scale prosumer management.*

6) In the future cloud-based IoE paradigm, how can energy management models be adapted for end-users in different sectors (namely: residential, transport, and industry).

This research question has been addressed explicitly and extensively in Part III of the thesis.

For the residential sector: In Chapter 6, "Energy Value Signals" were proposed and formulated as an alternative means of quantifying social welfare for residential prosumers, which is redefined and adapted for peer-to-peer prosumer-centered networks. Based on this, a fully distributed joint scheduling of energy consumption and trading in residential transactive energy networks was proposed. It was shown that the proposed model provides potential benefits for both the prosumers and the grid, albeit with a user-centered, fully distributed approach. Energy value reflects the value set by the user of allocating energy for a certain usage at a certain time. These user preferences are input locally resulting in the optimal schedule of each prosumer, which in turn affects the price of energy globally in a similar manner to DR programs in modern-day SGs. The developed model enables a cloud-based approach for residential prosumer energy management in the IoE paradigm.

For the transport sector: In Chapter 7 a universal mathematical model for fully electric public transport networks was developed to minimize the total ownership cost (TOC). This addressed critical gaps in scientific literature, where: 1) all surveyed literature were found to construct case-specific models (non-generalizeable), and 2) the optimization models targeted only one or two elements of the transport system, with the other aspects being considered as model constraints. Accordingly a universal model was developed model in this thesis, i.e., any set of routes, electric buses, and type of charging infrastructure can be considered either as a parameter or a decision variable. The optimization model accounts for real-time dynamic electricity pricing.

In this sense, the model is highly versatile and can be used for 1) optimal operation of existing systems (through optimal charging schedules with dynamic pricing considered), 2) system operation (through optimal design of the systems and dispatching to reduce costs), and 3) investment planning (through optimal battery sizing and charging infrastructure deployment). Three case studies were used to validate the proposed model while demonstrating its universal applicability. First, the design of three individual routes with different characteristics was demonstrated. Then, a large-scale generic transport system with 180 routes, consisting of urban and suburban routes with varying characteristics was considered and the optimal design was obtained and analyzed in detail. Afterwards, the use of the proposed model for a long-term transport system planning problem was demonstrated by adapting the system to a 2030 scenario based on forecasted technological advancements. Due to the universal nature of the developed optimization model, it can be applied to any public transport network, including electric vehicle (EV) fleets and other emerging electric transport technologies.

For the industry sector: In Chapter 8 an innovative graph-based model and algorithm for optimal task scheduling was proposed, implemented and tested. As with the transport sector, a critical gap in literature was found where all developed solutions are case-specific and not generalizeable. The designed algorithm based on graph theory guarantees a generic nature, making it applicable on a plethora of tasking problems. For any industrial setting where mobile agents are responsible for accomplishing tasks across a site, an optimal task schedule for each agent is obtained to maximize the speed of the task achievement with high energy consumption efficiency. The algorithm's versatility in modeling different problems and high computational efficiency make it perfectly suitable for a fully distributed task scheduling of autonomous agents.

The developed algorithm is applicable in the context of smart industries, where autonomous multi-agent systems are deployed to perform preset tasks with high levels of automation and a advanced communication infrastructures (i.e., IoT-enabled agents with cloud-based coordination). A real world case study has demonstrated the effectiveness of the proposed algorithm in maximizing the task accomplishment of the autonomous industrial agent on one full battery charge, maximizing the energy consumption efficiency.

Therefore, the answer to this research question is: *In the future cloud-based IoE paradigm, cross-sector end-user energy management must be adapted with a focus on the new models being universal and not case specific to ensure interoperability. The models must make also make use of advanced communication infrastructures. These focal aspects are in accordance with the requirements defined earlier for methods developed for the IoE paradigm. Moreover, in the case of the transport and industry sectors the upcoming full electrification thereof. With this mindset, new and innovative optimization scheduling models have been developed in this thesis for the energy management in the residential, transport, and industry sectors.*

9.2 Primary Research Question

Can fully decentralized distributed data models (based on IoT and P2P networks) ensure techno-economic sustainability for electric power systems and cross-sector end-users?

Part I of the thesis (Chapter 1 and Chapter 2) provided a comprehensive and clear definition of the first part of the question "Can fully decentralized distributed data models (based on IoT and P2P networks) ensure techno-economic sustainability". Part II (Chapter 3, 4, and 5) addressed this question for "electric power systems", and Part III (Chapter 6, 7, and 8) for "cross-sector end-users".

With all the secondary research questions addressed, the answer to the primary research question emerges with confidence as an aggregated conclusion of all the outcomes of the work performed in this thesis.

Therefore, the answer to the primary research question is: *Fully decentralized distributed data models (based on IoT and P2P networks) can indeed ensure techno-economic sustainability for electric power systems and cross-sector end-users. The designed models must adhere to the design requirements defined for the IoE paradigm.*

Chapter 10

Final Conclusions and Prospects for Future Work

The work presented in this thesis built on architectures, approaches, and emerging technologies in the IoE paradigm to develop disruptive energy management tools that cover the full spectrum and dimensions of this transition: 1) grid operation (cloud-based coordination, forecasting, and power flow management tools), and 2) cross-sector end-user energy management adaptation to future scenarios (namely: the residential, transport, and industry sectors).

First, the emergence of the IoE paradigm and energy prosumers was exhaustively investigated by conducting a thorough analysis of scientific literature, legislations, and expert reviews. The necessary criteria for tools and methods developed to be compatible with the IoE paradigm have been defined.

Then, cloud-based coordination, forecasting, and power flow management tools are developed for energy management in power systems of the IoE paradigm. First, the coordination of modern-day energy management systems through a cloud based approach to achieve synergistic benefits both for the global system and the end-users (local prosumers) was demonstrated. Then, new disruptive algorithms for fully decentralized forecasting and power flow management of next-generation power systems were developed. A novel KDE method was developed and enables fully decentralized local forecasting for prosumers without depending on private/proprietary data or divulging their own, being compatible with the cloud based IoE paradigm. Afterwards, a novel machine learning algorithm was proposed and formulated to enable the transition into a cloud-based fully decentralized power system operation.

In the next part of the thesis, the adaption of energy management models for cross-sector end-users to future scenarios was investigated. For the residential sector, a combined prosumption scheduling and trading tool based on a new energy value signal concept was developed. For the transport sector, a comprehensive and universal optimization model for charging infrastructure deployment, charge scheduling, battery sizing, and route design for fully electric public transport networks was developed and used to analyze future scenarios. For the industrial sector, an original graph-based model for fully autonomous task scheduling in smart industries was presented to minimize energy consumption.

With complex and disruptive tools developed in this thesis, it opens the door for several paths for future work thereon:

- For economic research: The method developed in Chapters 5 and 6 raised intriguing possibilities regarding the prospects of building business models for information transactions. The "value" of information can be quantified in cooperative operation and forecasting frameworks.
- For systems research: The literature reviews leading to the work in Chapters 7 and 8 have shown a clear delay in the transfer of knowledge between the power systems research on one hand, and the transport and industrial sectors on the other. Very little research was found to investigate the effect of demand response on smart industries and multi-agent autonomous task allocation. Similarly, very little research considers dynamic SG interaction with transport networks. Most SG research focuses on the residential side and consumer-owned EVs. Therefore it is recommended that future work further investigates synergies that can be attained from multi-disciplinary research between these fields as a global system model in the IoE.
- For legal research: The analysis presented in Chapter 1 and 2 clearly show that the legislation was the main instigator to the scientific research and development on DR, DSM, and SGs. Accordingly, if the scientific community is to pursue the development of innovative multi-disciplinary tools to accelerate the development of the IoE, proper legislation should be enacted prompt it.

References

[1] S. Pelletier, O. Jabali, J. E. Mendoza, and G. Laporte, "The electric bus fleet transition problem," *Transportation Research Part C: Emerging Technologies*, vol. 109, pp. 174–193, 2019, doi: https://doi.org/10.1016/j.trc.2019.10.012.

[2] International Energy Agency, "World energy balances overview," International Energy Agency, Tech. Rep., 2019. [Online]. Available: https://www.iea.org/t_c/

[3] X. Hu, C. Zou, X. Tang, T. Liu, and L. Hu, "Cost-optimal energy management of hybrid electric vehicles using fuel cell/battery health-aware predictive control," *IEEE Transactions on Power Electronics*, vol. 35, no. 1, pp. 382–392, 2020, doi: 10.1109/TPEL.2019.2915675.

[4] SMP Robotics, "S5.2 series 2020 models datasheet," 2020. [Online]. Available: https://smprobotics.com/wp-content/uploads/2019/09/security_robot_s5.2_is_prompt_2020.pdf

[5] N. Bassamzadeh, R. Ghanem, S. Lu, and S. J. Kazemitabar, "Robust scheduling of smart appliances with uncertain electricity prices in a heterogeneous population," *Energy and Buildings*, vol. 84, pp. 537–547, 2014, doi: https://doi.org/10.1016/j.enbuild.2014.08.035.

[6] R. Green and I. Staffell, "Electricity in Europe: exiting fossil fuels?" *Oxford Review of Economic Policy*, vol. 32, no. 2, pp. 282–303, 04 2016, doi: 10.1093/oxrep/grw003.

[7] G. M. Masters, *Renewable and Efficient Electric Power Systems*. John Wiley Sons, Inc., 2004. ISBN 3175723993

[8] G. Strbac, "Demand side management: Benefits and challenges," *Energy Policy*, vol. 36, no. 12, pp. 4419–4426, 2008, doi: https://doi.org/10.1016/j.enpol.2008.09.030. Foresight Sustainable Energy Management and the Built Environment Project.

[9] J. Mullins, L. Wagner, and J. Foster, "Price Spikes in Electricity Markets: A Strategic Perspective," School of Economics, University of Queensland, Australia, Energy Economics and Management Group Working Papers 05, Dec. 2010.

[10] T. M. Christensen, A. S. Hurn, and K. A. Lindsay, "Forecasting Spikes in Electricity Prices," *NCER Working Paper Series*, 2011.

[11] CIAB, "Power Generation from Coal: Measuring and Reporting Efficiency Performance and CO2 Emissions," International Energy Agency, Tech. Rep., 2010. [Online]. Available: http://large.stanford.edu/courses/2014/ph240/wolkoff1/docs/power_generation_from_coal.pdf

[12] M. Steen, "Greenhouse Gas Emissions from Fossil Fuel Fired Power Generation Systems," EUROPEAN COMMISSION JOINT RESEARCH CENTRE (DG JRC) INSTITUTE FOR ADVANCED MATERIALS, Tech. Rep., 2001. [Online]. Available: https://publications.jrc.ec.europa.eu/repository/bitstream/JRC21207/EUR19754EN.pdf

[13] H. T. Haider, O. H. See, and W. Elmenreich, "A review of residential demand response of smart grid," *Renewable and Sustainable Energy Reviews*, vol. 59, pp. 166–178, 2016, doi: https://doi.org/10.1016/j.rser.2016.01.016.

[14] E. Muljadi, V. Gevorgian, M. Singh, and S. Santoso, "Understanding inertial and frequency response of wind power plants," in *2012 IEEE Power Electronics and Machines in Wind Applications*, 2012, doi: 10.1109/PEMWA.2012.6316361. pp. 1–8.

[15] P. Fairley, "Can Synthetic Inertia from Wind Power Stabilize Grids?" *IEEE Spectrum*, nov 2016. [Online]. Available: https://spectrum.ieee.org/energywise/energy/renewables/can-synthetic-inertia-stabilize-power-grids

[16] S. A. Pourmousavi and M. H. Nehrir, "Real-time central demand response for primary frequency regulation in microgrids," *IEEE Transactions on Smart Grid*, vol. 3, no. 4, pp. 1988–1996, 2012, doi: 10.1109/TSG.2012.2201964.

[17] P. Warren, "A review of demand-side management policy in the uk," *Renewable and Sustainable Energy Reviews*, vol. 29, pp. 941–951, 2014, doi: https://doi.org/10.1016/j.rser.2013.09.009.

[18] ——, "Electricity demand-side management : best practice programmes for the UK," *WIT Transactions on Ecology and The Environment*, vol. 176, pp. 69–80, 2013, doi: 10.2495/ESUS130061.

[19] M. Albadi and E. El-Saadany, "A summary of demand response in electricity markets," *Electric Power Systems Research*, vol. 78, no. 11, pp. 1989–1996, 2008, doi: https://doi.org/10.1016/j.epsr.2008.04.002.

[20] M. Kopsakangas-Savolainen and R. Svento, *Modern Energy Markets: Real-Time Pricing, Renewable Resources and Efficient Distribution*. Springer Science Business Media, 2012. ISBN 1447129725

[21] L. Meeus, K. Purchala, and R. Belmans, "Development of the internal electricity market in europe," *The Electricity Journal*, vol. 18, no. 6, pp. 25–35, 2005, doi: https://doi.org/10.1016/j.tej.2005.06.008.

[22] P. L. Joskow, "Productivity growth and technical change in the generation of electricity," *The Energy Journal*, vol. 8, no. 1, pp. 17–38, 2021/05/26/ 1987, full publication date: January 1987. [Online]. Available: http://www.jstor.org/stable/41322243

[23] F. A. Wolak, "Market Design and Price Behavior in Restructured Electricity Markets: An International Comparison," in *Deregulation and Interdependence in the Asia-Pacific Region*, ser. NBER Chapters. National Bureau of Economic Research, Inc, December 2000, pp. 79–137. [Online]. Available: https://ideas.repec.org/h/nbr/nberch/8478.html

[24] 91st Congress, "Clean Air Amendments of 1970," pp. 1676–1713, 1970. [Online]. Available: https://www.govinfo.gov/content/pkg/USCODE-2010-title42/html/USCODE-2010-title42-chap85.htm

[25] A. Jordan, "The implementation of eu environmental policy; a policy problem without a political solution?" *Environment and Planning C: Government and Policy*, vol. 17, no. 1, pp. 69–90, 1999, doi: 10.1068/c170069.

[26] R. N. L. Andrews, *Managing the Environment, Managing Ourselves*. Yale University Press, 2021/05/26/ 2006. ISBN 9780300111248. [Online]. Available: http://www.jstor.org/stable/j.ctt5vkwzb

[27] "Celebrating Europe and its environment — European Environment Agency," 2016. [Online]. Available: https://www.eea.europa.eu/highlights/celebrating-europe-and-its-environment

[28] MINISTERIO DE MINERÍA CHILE, "APRUEBA MODIFICACIONES AL D.F.L. N° 4, DE 1959, LEY GENERAL DE SERVICIOS ELECTRICOS, EN MATERIA DE ENERGIA ELECTRICA," 1982. [Online]. Available: https://www.leychile.cl/Navegar?idNorma=3410

[29] 95th Congress, "H.R. 4018 - Public Utility Regulatory Policies Act," 1978. [Online]. Available: https://www.congress.gov/bill/95th-congress/house-bill/4018

[30] 102nd Congress, "H.R. 776 - Energy Policy Act of 1992," 1992. [Online]. Available: https://www.congress.gov/bill/102nd-congress/house-bill/776

[31] 109th Congress, "H.R. 6 - Energy Policy Act of 2005," 2005. [Online]. Available: https://www.congress.gov/bill/109th-congress/house-bill/6

[32] 110th Congress, "H.R. 6 - Energy Independence and Security Act of 2007," 2007. [Online]. Available: https://www.congress.gov/bill/110th-congress/house-bill/6

[33] 111th Congress, "H.R. 1 - American Recovery and Reinvestment Act of 2009," 2009. [Online]. Available: https://www.congress.gov/bill/111th-congress/house-bill/1

[34] "United Kingdom Electricity Act 1989," 1989. [Online]. Available: https://www.legislation.gov.uk/ukpga/1989/29/contents

[35] "United Kingdom Climate Change and Sustainable Energy Act 2006," 2006. [Online]. Available: https://www.legislation.gov.uk/ukpga/2006/19/contents

[36] "United Kingdom Energy Act 2008, c.32," 2008. [Online]. Available: http://www.legislation.gov.uk/ukpga/2008/32/contents

[37] "United Kingdom Energy Act 2011, c.16," 2011. [Online]. Available: https://www.legislation.gov.uk/ukpga/2011/16/contents/enacted

[38] European Parliament and European Council, "EU DIRECTIVE 96/92/EC," 1996. [Online]. Available: https://eur-lex.europa.eu/legal-content/EN/TXT/PDF/?uri=CELEX:31996L0092&from=EN

[39] ——, "EU DIRECTIVE 2003/54/EC," 2003. [Online]. Available: https://eur-lex.europa.eu/resource.html?uri=cellar:caeb5f68-61fd-4ea8-b3b5-00e692b1013c.0004.02/DOC_1&format=PDF

[40] ——, "EU DIRECTIVE 2001/77/EC," 2001. [Online]. Available: https://eur-lex.europa.eu/legal-content/EN/TXT/PDF/?uri=CELEX:32001L0077&from=EN

[41] ——, "EU DIRECTIVE 2009/28/EC," 2009. [Online]. Available: https://eur-lex.europa.eu/legal-content/EN/TXT/PDF/?uri=CELEX:32009L0028&from=EN

[42] ——, "DIRECTIVE 2012/27/EU," 2012. [Online]. Available: https://eur-lex.europa.eu/LexUriServ/LexUriServ.do?uri=OJ:L:2012:315:0001:0056:en:PDF

[43] F. Shariatzadeh, P. Mandal, and A. K. Srivastava, "Demand response for sustainable energy systems: A review, application and implementation strategy," *Renewable and Sustainable Energy Reviews*, vol. 45, pp. 343–350, 2015, doi: https://doi.org/10.1016/j.rser.2015.01.062.

[44] R. Venkatraman and S. K. Khaitan, "A survey of techniques for designing and managing microgrids," in *2015 IEEE Power Energy Society General Meeting*, 2015, doi: 10.1109/PESGM.2015.7286590. pp. 1–5.

[45] N. G. Paterakis, O. Erdinç, and J. P. Catalão, "An overview of demand response: Key-elements and international experience," *Renewable and Sustainable Energy Reviews*, vol. 69, pp. 871–891, 2017, doi: https://doi.org/10.1016/j.rser.2016.11.167.

[46] K. Vu, M. Begouic, and D. Novosel, "Grids get smart protection and control," *IEEE Computer Applications in Power*, vol. 10, no. 4, pp. 40–44, 1997, doi: 10.1109/67.625373.

[47] R. Pratt, "Transforming the u.s. electricity system," in *IEEE PES Power Systems Conference and Exposition, 2004.*, 2004, doi: 10.1109/PSCE.2004.1397713. pp. 1651–1654 vol.3.

[48] H. Kirkham, D. Nightingale, and T. Koerner, "Energy management system design with dispersed storage and generation," *IEEE Transactions on Power Apparatus and Systems*, vol. PAS-100, no. 7, pp. 3432–3441, 1981, doi: 10.1109/TPAS.1981.316686.

[49] R. Dugan, S. Thomas, and D. Rizy, "Integrating dispersed storage and generation(dsg) with an automated distribution system," *IEEE Transactions on Power Apparatus and Systems*, vol. PAS-103, no. 6, pp. 1142–1146, 1984, doi: 10.1109/TPAS.1984.318441.

[50] R. C. Dugan and D. T. Rizy, "Electric distribution protection problems associated with the interconnection of small, disperesed generation devices," *IEEE Transactions on Power Apparatus and Systems*, vol. PAS-103, no. 6, pp. 1121–1127, 1984, doi: 10.1109/TPAS.1984.318438.

[51] M. Lotfi, P. S. João Catalão, M. S. Javadi, A. E. Nezhad, and M. Shafie-khah, "Demand response program implementation for day-ahead power system operation," in *2019 IEEE Milan PowerTech*, 2019, doi: 10.1109/PTC.2019.8810850. pp. 1–6.

[52] P. Siano, "Demand response and smart grids—a survey," *Renewable and Sustainable Energy Reviews*, vol. 30, pp. 461–478, 2014, doi: https://doi.org/10.1016/j.rser.2013.10.022.

[53] J. Torriti, "A review of time use models of residential electricity demand," *Renewable and Sustainable Energy Reviews*, vol. 37, pp. 265–272, 2014, doi: https://doi.org/10.1016/j.rser.2014.05.034.

[54] PwC, "Blockchain – an opportunity for energy producers and consumers?" PwC, Tech. Rep., 2016. [Online]. Available: http://www.pwc.com/gx/en/industries/energy-utilities-mining/power-utilities/publications/opportunity-for-energy-producers.html

[55] M. Lotfi, A. Ashraf, M. Zahran, G. Samih, M. Javadi, G. J. Osório, and J. P. S. Catalão, "A dijkstra-inspired algorithm for optimized real-time tasking with minimal energy consumption," in *2020 IEEE International Conference on Environment and Electrical Engineering and 2020 IEEE Industrial and Commercial Power Systems Europe (EEEIC / I CPS Europe)*, 2020, doi: 10.1109/EEEIC/ICPSEurope49358.2020.9160688. pp. 1–6.

[56] M. Lotfi, P. Pereira, N. G. Paterakis, H. A. Gabbar, and J. P. S. Catalão, "Optimal design of electric bus transport systems with minimal total ownership cost," *IEEE Access*, vol. 8, pp. 119 184–119 199, 2020, doi: 10.1109/ACCESS.2020.3004910.

[57] S. Bahrami, M. H. Amini, M. Shafie-khah, and J. P. S. Catalão, "A decentralized electricity market scheme enabling demand response deployment," *IEEE Transactions on Power Systems*, vol. 33, no. 4, pp. 4218–4227, 2018, doi: 10.1109/TPWRS.2017.2771279.

[58] S. Bahrami, M. H. Amini, M. Shafie-Khah, and J. P. S. Catalão, "A decentralized renewable generation management and demand response in power distribution networks," *IEEE Transactions on Sustainable Energy*, vol. 9, no. 4, pp. 1783–1797, 2018, doi: 10.1109/TSTE.2018.2815502.

[59] E. Rokrok, M. Shafie-khah, P. Siano, and J. P. S. Catalão, "A decentralized multi-agent-based approach for low voltage microgrid restoration," *Energies*, vol. 10, no. 10, 2017, doi: 10.3390/en10101491.

[60] P. S. Anton, R. Silberglitt, and J. Schneider, *The Global Technology Revolution: Bio/Nano/Materials Trends and Their Synergies with Information Technology by 2015*. Santa Monica, CA: RAND Corporation, 2001. [Online]. Available: https://www.rand.org/pubs/monograph_reports/MR1307.html

[61] M. Hermann, T. Pentek, and B. Otto, "Design principles for industrie 4.0 scenarios," in *2016 49th Hawaii International Conference on System Sciences (HICSS)*, 2016, doi: 10.1109/HICSS.2016.488. pp. 3928–3937.

[62] A. D. Maynard, "Navigating the fourth industrial revolution," *Nature Nanotechnology*, vol. 10, no. 12, pp. 1005–1006, Dec 2015, doi: 10.1038/nnano.2015.286.

[63] L. Elliott, "Fourth Industrial Revolution brings promise and peril for humanity," jan 2016. [Online]. Available: http://www.theguardian.com/business/economics-blog/2016/jan/24/4th-industrial-revolution-brings-promise-and-peril-for-humanity-technology-davos

[64] "Ieee standard for information technology - telecommunications and information exchange between systems - local and metropolitan area networks - specific requirements - part 11: Wireless lan medium access control (mac) and physical layer (phy) specifications," *IEEE Std 802.11-2007 (Revision of IEEE Std 802.11-1999)*, pp. 1–1076, 2007, doi: 10.1109/IEEESTD.2007.373646.

[65] A. Nordrum, "Popular Internet of Things Forecast of 50 Billion Devices by 2020 Is Outdated," *IEEE Spectrum*, aug 2016.

[66] Gartner, "Gartner Says 6.4 Billion Connected "Things" Will Be in Use in 2016, Up 30 Percent From 2015 [Press Release]," Gartner, Inc, Barcelona, Tech. Rep., 2015. [Online]. Available: http://www.gartner.com/newsroom/id/3165317

[67] Ericsson, "Ericsson Mobility Report: On the Pulse of the Networked Society," Ericsson, Tech. Rep., 2016.

[68] S. Lucero, "IoT platforms : enabling the Internet of Things," *IHS Technology*, 2016. [Online]. Available: https://cdn.ihs.com/www/pdf/enabling-IOT.pdf

[69] C. MacGillivray, M. Torchia, M. Cinco, M. Kalal, M. Kumar, R. Membrila, A. Siviero, Y. Torisu, and N. Wallis, "Worldwide Internet of Things Forecast Update , 2016 – 2020," *IDC Market Forecast*, p. 40755516, 2017. [Online]. Available: http://www.idc.com/getdoc.jsp?containerId=US40755516

[70] Dimensional Research and ParStream, "Internet of Things (IoT) Meets Big Data and Analytics: A Survey of IoT Stakeholders," Tech. Rep. March, 2015.

[71] A. Meola, "The roles of cloud computing and fog computing in the Internet of Things revolution," *Business Insider*, 2016.

[72] IBM, "What is cloud computing?" 2017. [Online]. Available: https://www.ibm.com/cloud-computing/learn-more/what-is-cloud-computing/

[73] Gartner, "Gartner Says Worldwide IoT Security Spending to Reach $348 Million in 2016 [Press Release]," Gartner, Inc, Tech. Rep., 2016. [Online]. Available: http://www.gartner.com/newsroom/id/3291817

[74] European Parliament and of the Council of 27 April 2016, "Regulation (EU) 2016/679," 2016. [Online]. Available: https://eur-lex.europa.eu/eli/reg/2016/679/oj

[75] A. Jung, "Smart Grid 2.0 Building the Internet of Energy Supply," pp. 1–3, 2010. [Online]. Available: https://www.spiegel.de/international/business/smart-grid-2-0-building-the-internet-of-energy-supply-a-694287.html

[76] N. Bui, A. P. Castellani, P. Casari, and M. Zorzi, "The internet of energy: a web-enabled smart grid system," *IEEE Network*, vol. 26, no. 4, pp. 39–45, 2012, doi: 10.1109/MNET.2012.6246751.

[77] M. Jaradat, M. Jarrah, A. Bousselham, Y. Jararweh, and M. Al-Ayyoub, "The internet of energy: Smart sensor networks and big data management for smart grid," *Procedia Computer Science*, vol. 56, pp. 592–597, 2015, doi: https://doi.org/10.1016/j.procs.2015.07.250. The 10th International Conference on Future Networks and Communications (FNC 2015) / The 12th International Conference on Mobile Systems and Pervasive Computing (MobiSPC 2015) Affiliated Workshops.

[78] K. Wang, J. Yu, Y. Yu, Y. Qian, D. Zeng, S. Guo, Y. Xiang, and J. Wu, "A survey on energy internet: Architecture, approach, and emerging technologies," *IEEE Systems Journal*, vol. 12, no. 3, pp. 2403–2416, 2018, doi: 10.1109/JSYST.2016.2639820.

[79] A. S. Sani, D. Yuan, J. Jin, L. Gao, S. Yu, and Z. Y. Dong, "Cyber security framework for Internet of Things-based Energy Internet," *Future Generation Computer Systems*, 2018, doi: 10.1016/j.future.2018.01.029.

[80] C.-C. Lin, D.-J. Deng, W.-Y. Liu, and L. Chen, "Peak load shifting in the internet of energy with energy trading among end-users," *IEEE Access*, vol. 5, pp. 1967–1976, 2017, doi: 10.1109/ACCESS.2017.2668143.

[81] Q. Sun, R. Han, H. Zhang, J. Zhou, and J. M. Guerrero, "A multiagent-based consensus algorithm for distributed coordinated control of distributed generators in the energy internet," *IEEE Transactions on Smart Grid*, vol. 6, no. 6, pp. 3006–3019, 2015, doi: 10.1109/TSG.2015.2412779.

[82] A. Jindal, N. Kumar, and M. Singh, "A unified framework for big data acquisition, storage, and analytics for demand response management in smart cities," *Future Generation Computer Systems*, vol. 108, pp. 921–934, 2020, doi: https://doi.org/10.1016/j.future.2018.02.039.

[83] P. Tenti and T. Caldognetto, "Optimal control of local area energy networks (e-lan)," *Sustainable Energy, Grids and Networks*, vol. 14, pp. 12–24, 2018, doi: https://doi.org/10.1016/j.segan.2018.03.002.

[84] J. Cao and M. Yang, "Energy internet – towards smart grid 2.0," in *2013 Fourth International Conference on Networking and Distributed Computing*, 2013, doi: 10.1109/ICNDC.2013.10. pp. 105–110.

[85] S. Nakamoto, "Bitcoin: A Peer-to-Peer Electronic Cash System," *www.bitcoin.org*, 2008, doi: 10.1007/s10838-008-9062-0.

[86] M. Swan, *Blockchain: Blueprint for a New Economy*. O'Reilly Media, Inc., 2015. ISBN 978-1-4919-2044-2

[87] European Central Bank, *Virtual currency schemes*. European Central Bank, 2012. ISBN 9789289908627. [Online]. Available: http://www.ecb.europa.eu

[88] ——, "Virtual currency schemes - a further analysis," European Central Bank, Tech. Rep., 2015. [Online]. Available: www.ecb.europa.eu

[89] M. Lotfi, C. Monteiro, M. Shafie-khah, and J. P. S. Catalão, "Evolution of demand response: A historical analysis of legislation and research trends," in *2018 Twentieth International Middle East Power Systems Conference (MEPCON)*, 2018, doi: 10.1109/MEPCON.2018.8635264. pp. 968–973.

[90] Electric Power Research Institute, "The Integrated Grid: Realizing The Full Value of Central and Distributed Energy Resources," *EPRI*, 2014.

[91] W. Cox and T. Considine, "Structured energy: Microgrids and autonomous transactive operation," in *2013 IEEE PES Innovative Smart Grid Technologies Conference (ISGT)*, 2013, doi: 10.1109/ISGT.2013.6497919. pp. 1–6.

[92] W. Inam, D. Strawser, K. K. Afridi, R. J. Ram, and D. J. Perreault, "Architecture and system analysis of microgrids with peer-to-peer electricity sharing to create a marketplace which enables energy access," in *2015 9th International Conference on Power Electronics and ECCE Asia (ICPE-ECCE Asia)*, 2015, doi: 10.1109/ICPE.2015.7167826. pp. 464–469.

[93] M. Pustišek, A. Kos, and U. Sedlar, "Blockchain based autonomous selection of electric vehicle charging station," in *2016 International Conference on Identification, Information and Knowledge in the Internet of Things (IIKI)*, 2016, doi: 10.1109/IIKI.2016.60. pp. 217–222.

[94] N. Z. Aitzhan and D. Svetinovic, "Security and privacy in decentralized energy trading through multi-signatures, blockchain and anonymous messaging streams," *IEEE Transactions on Dependable and Secure Computing*, vol. 15, no. 5, pp. 840–852, 2018, doi: 10.1109/TDSC.2016.2616861.

[95] German Energy Agency, "Blockchain in the energy transition. A survey among decision-makers in the German energy industry," German Energy Agency, Berlin, Tech. Rep., 2016.

[96] J. Mattila, T. Seppälä, C. Naucler, R. Stahl, M. Tikkanen, Alexandra Bådenlid, and J. Seppälä, "Industrial Blockchain Platforms : An Exercise in Use Case Development in the Energy Industry," The Research Institute of the Finnish Economy (ETLA), Tech. Rep., 2016.

[97] J. Horta, D. Kofman, and D. Menga, "Novel paradigms for advanced distribution grid energy management," dec 2017. [Online]. Available: http://arxiv.org/abs/1712.05841

[98] J. Green and P. Newman, "Citizen utilities: The emerging power paradigm," *Energy Policy*, vol. 105, pp. 283–293, 2017, doi: https://doi.org/10.1016/j.enpol.2017.02.004.

[99] E. Münsing, J. Mather, and S. Moura, "Blockchains for decentralized optimization of energy resources in microgrid networks," in *2017 IEEE Conference on Control Technology and Applications (CCTA)*, 2017, doi: 10.1109/CCTA.2017.8062773. pp. 2164–2171.

[100] Q. Duan, N. V. Quynh, H. M. Abdullah, A. Almalaq, T. Duc Do, S. M. Abdelkader, and M. A. Mohamed, "Optimal Scheduling and Management of a Smart City within the Safe Framework," *IEEE Access*, vol. 8, pp. 161 847–161 861, 2020, doi: 10.1109/ACCESS.2020.3021196.

[101] T. Qian, T. Qian, C. Shao, C. Shao, X. Li, X. Li, X. Wang, X. Wang, M. Shahidehpour, and M. Shahidehpour, "Enhanced Coordinated Operations of Electric Power and Transportation Networks via EV Charging Services," *IEEE Transactions on Smart Grid*, vol. 11, no. 4, pp. 3019–3030, 2020, doi: 10.1109/TSG.2020.2969650.

[102] V. H. Nguyen, Q. T. Tran, and Y. Besanger, "SCADA as a service approach for interoperability of micro-grid platforms," *Sustainable Energy, Grids and Networks*, vol. 8, pp. 26–36, 2016, doi: 10.1016/j.segan.2016.08.001. . [Online]. Available: http://dx.doi.org/10.1016/j.segan.2016.08.001

[103] H. Kikusato, K. Mori, S. Yoshizawa, Y. Fujimoto, H. Asano, Y. Hayashi, A. Kawashima, S. Inagaki, and T. Suzuki, "Electric Vehicle Charge-Discharge Management for Utilization of Photovoltaic by Coordination between Home and Grid Energy Management Systems," *IEEE Transactions on Smart Grid*, vol. 10, no. 3, pp. 3186–3197, may 2019, doi: 10.1109/TSG.2018.2820026.

[104] H. Zhang, Z. Hu, Y. Song, and Y. Song, "Power and Transport Nexus: Routing Electric Vehicles to Promote Renewable Power Integration," *IEEE Transactions on Smart Grid*, vol. 11, no. 4, pp. 3291–3301, 2020, doi: 10.1109/TSG.2020.2967082.

[105] K. Kotsalos, I. Miranda, N. Silva, and H. Leite, "A horizon optimization control framework for the coordinated operation of multiple distributed energy resources in low voltage distribution networks," *Energies*, vol. 12, no. 6, 2019, doi: 10.3390/en12061182.

[106] M. Yousefi, A. Hajizadeh, and M. N. Soltani, "A Comparison Study on Stochastic Modeling Methods for Home Energy Management Systems," *IEEE Transactions on Industrial Informatics*, vol. 15, no. 8, pp. 4799–4808, apr 2019, doi: 10.1109/tii.2019.2908431.

[107] M. S. Javadi, A. E. Nezhad, P. H. Nardelli, M. Gough, M. Lotfi, S. Santos, and J. P. Catalão, "Self-scheduling model for home energy management systems considering the end-users discomfort index within price-based demand response programs," *Sustainable Cities and Society*, vol. 68, p. 102792, may 2021, doi: 10.1016/j.scs.2021.102792.

[108] A. Sangswang and M. Konghirun, "Optimal Strategies in Home Energy Management System Integrating Solar Power, Energy Storage, and Vehicle-to-Grid for Grid Support and Energy Efficiency," *IEEE Transactions on Industry Applications*, vol. 56, no. 5, pp. 5716–5728, 2020, doi: 10.1109/TIA.2020.2991652.

[109] M. Yousefi, A. Hajizadeh, M. N. Soltani, and B. Hredzak, "Predictive Home Energy Management System with Photovoltaic Array, Heat Pump, and Plug-In Electric Vehicle," *IEEE Transactions on Industrial Informatics*, vol. 17, no. 1, pp. 430–440, 2021, doi: 10.1109/TII.2020.2971530.

[110] L. Zhang and Y. Li, "Optimal Management for Parking-Lot Electric Vehicle Charging by Two-Stage Approximate Dynamic Programming," *IEEE Transactions on Smart Grid*, vol. 8, no. 4, pp. 1722–1730, jul 2017, doi: 10.1109/TSG.2015.2505298.

[111] S. Hussain, M. A. Ahmed, and Y. C. Kim, "Efficient Power Management Algorithm Based on Fuzzy Logic Inference for Electric Vehicles Parking Lot," *IEEE Access*, vol. 7, pp. 65 467–65 485, 2019, doi: 10.1109/ACCESS.2019.2917297.

[112] M. Shafie-Khah, P. Siano, D. Z. Fitiwi, N. Mahmoudi, and J. P. Catalão, "An innovative two-level model for electric vehicle parking lots in distribution systems with renewable energy," *IEEE Transactions on Smart Grid*, vol. 9, no. 2, pp. 1506–1520, 2018, doi: 10.1109/TSG.2017.2715259.

[113] Y. Zhang and L. Cai, "Dynamic Charging Scheduling for EV Parking Lots with Photovoltaic Power System," *IEEE Access*, vol. 6, pp. 56 995–57 005, 2018, doi: 10.1109/ACCESS.2018.2873286.

[114] H. M. Espassandim, M. Lotfi, G. J. Osorio, M. Shafie-Khah, O. M. Shehata, and J. P. Catalao, "Optimal operation of electric vehicle parking lots with rooftop photovoltaics," in *2019 IEEE International Conference on Vehicular Electronics and Safety, ICVES 2019*. Institute of Electrical and Electronics Engineers Inc., sep 2019, doi: 10.1109/ICVES.2019.8906320. . ISBN 9781728134734

[115] G. J. Osório, M. Gough, M. Lotfi, S. F. Santos, H. M. Espassandim, M. Shafie-khah, and J. P. Catalão, "Rooftop photovoltaic parking lots to support electric vehicles charging: A comprehensive survey," *International Journal of Electrical Power Energy Systems*, vol. 133, p. 107274, 2021, doi: https://doi.org/10.1016/j.ijepes.2021.107274. . [Online]. Available: https://www.sciencedirect.com/science/article/pii/S0142061521005135

[116] M. Lotfi, T. Almeida, M. Javadi, G. J. Osorio, and J. P. Catalao, "Coordinated Operation of Electric Vehicle Parking Lots and Smart Homes as a Virtual Power Plant," in *Proceedings - 2020 IEEE International Conference on Environment and Electrical Engineering and 2020 IEEE Industrial and Commercial Power Systems Europe, EEEIC / I and CPS Europe 2020*. Institute of Electrical and Electronics Engineers Inc., jun 2020, doi: 10.1109/EEEIC/ICPSEurope49358.2020.9160684. . ISBN 9781728174532

[117] T. Almeida, M. Lotfi, M. Javadi, G. J. Osorio, and J. P. Catalao, "Economic Analysis of Coordinating Electric Vehicle Parking Lots and Home Energy Management Systems," in *Proceedings - 2020 IEEE International Conference on Environment and Electrical Engineering and 2020 IEEE Industrial and Commercial Power Systems Europe, EEEIC / I and CPS Europe 2020*. Institute of Electrical and Electronics Engineers Inc., jun 2020, doi: 10.1109/EEEIC/ICPSEurope49358.2020.9160594. . ISBN 9781728174532

[118] Entidade Reguladora dos Serviços Energéticos (ERSE), "Diretiva (extrato) 1/2020, 2020-01-17 - DRE." [Online]. Available: https://dre.pt/web/guest/pesquisa/-/search/128227680/details/normal?l=1

[119] EDP Comercial, "EDP Comercial - Opções horárias." [Online]. Available: https://www.edp.pt/particulares/apoio-cliente/perguntas-frequentes/pt/contratos/novo-contrato/o-que-e-a-opcao-horaria-e-qual-a-melhor-para-mim/faq-4823/

[120] REN, "SIMEE - Daily and Intraday - Prices." [Online]. Available: https://www.mercado.ren.pt/EN/Electr/MarketInfo/MarketResults/OMIE/Pages/Prices.aspx

[121] S. Dev, T. AlSkaif, M. Hossari, R. Godina, A. Louwen, and W. van Sark, "Solar irradiance forecasting using triple exponential smoothing," in *2018 International Conference on Smart Energy Systems and Technologies (SEST)*, 2018, doi: 10.1109/SEST.2018.8495816. pp. 1–6.

[122] M. Gough, M. Lotfi, R. Castro, A. Madhlopa, A. Khan, and J. P. S. Catalão, "Urban wind resource assessment: A case study on cape town," *Energies*, vol. 12, no. 8, 2019, doi: 10.3390/en12081479.

[123] T. J. Formica, H. A. Khan, and M. G. Pecht, "The effect of inverter failures on the return on investment of solar photovoltaic systems," *IEEE Access*, vol. 5, pp. 21 336–21 343, 2017, doi: 10.1109/ACCESS.2017.2753246.

[124] C. Monteiro, I. J. Ramirez-Rosado, L. A. Fernandez-Jimenez, and M. Ribeiro, "New probabilistic price forecasting models: Application to the iberian electricity market," *International Journal of Electrical Power Energy Systems*, vol. 103, pp. 483–496, 2018, doi: https://doi.org/10.1016/j.ijepes.2018.06.005.

[125] "Recent advances in electricity price forecasting: A review of probabilistic forecasting," *Renewable and Sustainable Energy Reviews*, vol. 81, pp. 1548–1568, 2018, doi: https://doi.org/10.1016/j.rser.2017.05.234.

[126] T. Palmer, "The ecmwf ensemble prediction system: Looking back (more than) 25years and projecting forward 25years," *Quarterly Journal of the Royal Meteorological Society*, vol. 145, no. S1, pp. 12–24, 2019, doi: https://doi.org/10.1002/qj.3383.

[127] D. Su, E. Batzelis, and B. Pal, "Machine learning algorithms in forecasting of photovoltaic power generation," in *2019 International Conference on Smart Energy Systems and Technologies (SEST)*, 2019, doi: 10.1109/SEST.2019.8849106. pp. 1–6.

[128] A. Bracale, G. Carpinelli, and P. De Falco, "Developing and comparing different strategies for combining probabilistic photovoltaic power forecasts in an ensemble method," *Energies*, vol. 12, no. 6, 2019, doi: 10.3390/en12061011.

[129] Z. Qian, Y. Pei, H. Zareipour, and N. Chen, "A review and discussion of decomposition-based hybrid models for wind energy forecasting applications," *Applied Energy*, vol. 235, pp. 939–953, 2019, doi: https://doi.org/10.1016/j.apenergy.2018.10.080.

[130] A. Bracale, G. Carpinelli, and P. De Falco, "A probabilistic competitive ensemble method for short-term photovoltaic power forecasting," *IEEE Transactions on Sustainable Energy*, vol. 8, no. 2, pp. 551–560, 2017, doi: 10.1109/TSTE.2016.2610523.

[131] M. W. Ahmad, M. Mourshed, and Y. Rezgui, "Tree-based ensemble methods for predicting pv power generation and their comparison with support vector regression," *Energy*, vol. 164, pp. 465–474, 2018, doi: https://doi.org/10.1016/j.energy.2018.08.207.

[132] J. Thorey, C. Chaussin, and V. Mallet, "Ensemble forecast of photovoltaic power with online crps learning," *International Journal of Forecasting*, vol. 34, no. 4, pp. 762–773, 2018, doi: https://doi.org/10.1016/j.ijforecast.2018.05.007.

[133] X. Zhang, Y. Li, S. Lu, H. F. Hamann, B.-M. Hodge, and B. Lehman, "A solar time based analog ensemble method for regional solar power forecasting," *IEEE Transactions on Sustainable Energy*, vol. 10, no. 1, pp. 268–279, 2019, doi: 10.1109/TSTE.2018.2832634.

[134] L. Liu, M. Zhan, and Y. Bai, "A recursive ensemble model for forecasting the power output of photovoltaic systems," *Solar Energy*, vol. 189, pp. 291–298, 2019, doi: https://doi.org/10.1016/j.solener.2019.07.061.

[135] M. Q. Raza, N. Mithulananthan, J. Li, K. Y. Lee, and H. B. Gooi, "An ensemble framework for day-ahead forecast of pv output power in smart grids," *IEEE Transactions on Industrial Informatics*, vol. 15, no. 8, pp. 4624–4634, 2019, doi: 10.1109/TII.2018.2882598.

[136] C. Pan and J. Tan, "Day-ahead hourly forecasting of solar generation based on cluster analysis and ensemble model," *IEEE Access*, vol. 7, pp. 112 921–112 930, 2019, doi: 10.1109/ACCESS.2019.2935273.

[137] M. AlKandari and I. Ahmad, "Solar power generation forecasting using ensemble approach based on deep learning and statistical methods," *Applied Computing and Informatics*, Jan 2020, doi: 10.1016/j.aci.2019.11.002.

[138] G. Osório, J. Matias, and J. Catalão, "Electricity prices forecasting by a hybrid evolutionary-adaptive methodology," *Energy Conversion and Management*, vol. 80, pp. 363–373, 2014, doi: https://doi.org/10.1016/j.enconman.2014.01.063.

[139] J. P. S. Catalão, H. M. I. Pousinho, and V. M. F. Mendes, "Hybrid wavelet-pso-anfis approach for short-term electricity prices forecasting," in *2011 IEEE Power and Energy Society General Meeting*, 2011, doi: 10.1109/PES.2011.6038968. pp. 1–1.

[140] G. J. Osório, M. Lotfi, M. Shafie-khah, V. M. A. Campos, and J. P. S. Catalão, "Hybrid forecasting model for short-term electricity market prices with renewable integration," *Sustainability*, vol. 11, no. 1, 2019, doi: 10.3390/su11010057.

[141] J. Nowotarski and R. Weron, "To combine or not to combine? Recent trends in electricity price forecasting," Hugo Steinhaus Center, Wroclaw University of Technology, HSC Research Reports HSC/16/01, Jan. 2016. [Online]. Available: https://ideas.repec.org/p/wuu/wpaper/hsc1601.html

[142] "Global Forecast System (GFS) | National Centers for Environmental Information (NCEI) formerly known as National Climatic Data Center (NCDC)." [Online]. Available: https://www.ncdc.noaa.gov/data-access/model-data/model-datasets/global-forcast-system-gfs

[143] The Mathworks Inc., "Statistics and Machine Learning Toolbox User's Guide R2019b," 2019.

[144] H. Abdi, S. D. Beigvand, and M. L. Scala, "A review of optimal power flow studies applied to smart grids and microgrids," *Renewable and Sustainable Energy Reviews*, vol. 71, pp. 742–766, 2017, doi: https://doi.org/10.1016/j.rser.2016.12.102.

[145] F. Capitanescu, "Critical review of recent advances and further developments needed in ac optimal power flow," *Electric Power Systems Research*, vol. 136, pp. 57–68, 2016, doi: https://doi.org/10.1016/j.epsr.2016.02.008.

[146] H. Ergun, J. Dave, D. Van Hertem, and F. Geth, "Optimal power flow for ac–dc grids: Formulation, convex relaxation, linear approximation, and implementation," *IEEE Transactions on Power Systems*, vol. 34, no. 4, pp. 2980–2990, 2019, doi: 10.1109/TPWRS.2019.2897835.

[147] Z. Yang, H. Zhong, A. Bose, T. Zheng, Q. Xia, and C. Kang, "A linearized opf model with reactive power and voltage magnitude: A pathway to improve the mw-only dc opf," *IEEE Transactions on Power Systems*, vol. 33, no. 2, pp. 1734–1745, 2018, doi: 10.1109/TPWRS.2017.2718551.

[148] M. R. M. Cruz, D. Z. Fitiwi, S. F. Santos, S. J. P. S. Mariano, and J. P. S. Cataláo, "Multi-flexibility option integration to cope with large-scale integration of renewables," *IEEE Transactions on Sustainable Energy*, vol. 11, no. 1, pp. 48–60, 2020, doi: 10.1109/TSTE.2018.2883515.

[149] J. C. Beltrán, A. J. Aristizábal, A. López, M. Castaneda, S. Zapata, and Y. Ivanova, "Comparative analysis of deterministic and probabilistic methods for the integration of distributed generation in power systems," *Energy Reports*, vol. 6, pp. 88–104, 2020, doi: https://doi.org/10.1016/j.egyr.2019.10.025.

[150] O. A. Alimi, K. Ouahada, and A. M. Abu-Mahfouz, "A review of machine learning approaches to power system security and stability," *IEEE Access*, vol. 8, pp. 113 512–113 531, 2020, doi: 10.1109/ACCESS.2020.3003568.

[151] B. Borkowska, "Probabilistic load flow," *IEEE Transactions on Power Apparatus and Systems*, vol. PAS-93, no. 3, pp. 752–759, 1974, doi: 10.1109/TPAS.1974.293973.

[152] R. Allan, A. L. Da Silva, and R. Burchett, "Evaluation methods and accuracy in probabilistic load flow solutions," *IEEE Transactions on Power Apparatus and Systems*, vol. PAS-100, no. 5, pp. 2539–2546, 1981, doi: 10.1109/TPAS.1981.316721.

[153] N. Hatziargyriou, T. Karakatsanis, and M. Papadopoulos, "Probabilistic load flow in distribution systems containing dispersed wind power generation," *IEEE Transactions on Power Systems*, vol. 8, no. 1, pp. 159–165, 1993, doi: 10.1109/59.221262.

[154] P. Zhang and S. Lee, "Probabilistic load flow computation using the method of combined cumulants and gram-charlier expansion," *IEEE Transactions on Power Systems*, vol. 19, no. 1, pp. 676–682, 2004, doi: 10.1109/TPWRS.2003.818743.

[155] E. Rosenblueth, "Point estimates for probability moments," *Proceedings of the National Academy of Sciences*, vol. 72, no. 10, pp. 3812–3814, 1975, doi: 10.1073/pnas.72.10.3812.

[156] C.-L. Su, "Probabilistic load-flow computation using point estimate method," *IEEE Transactions on Power Systems*, vol. 20, no. 4, pp. 1843–1851, 2005, doi: 10.1109/TPWRS.2005.857921.

[157] J. M. Morales and J. Perez-Ruiz, "Point estimate schemes to solve the probabilistic power flow," *IEEE Transactions on Power Systems*, vol. 22, no. 4, pp. 1594–1601, 2007, doi: 10.1109/TPWRS.2007.907515.

[158] G. L. Viviani and G. T. Heydt, "Stochastic optimal energy dispatch," *IEEE Transactions on Power Apparatus and Systems*, vol. PAS-100, no. 7, pp. 3221–3228, 1981, doi: 10.1109/TPAS.1981.316651.

[159] A. Schellenberg, W. Rosehart, and J. Aguado, "Cumulant-based probabilistic optimal power flow (p-opf) with gaussian and gamma distributions," *IEEE Transactions on Power Systems*, vol. 20, no. 2, pp. 773–781, 2005, doi: 10.1109/TPWRS.2005.846184.

[160] K. Thirugnanam, M. S. E. Moursi, V. Khadkikar, H. H. Zeineldin, and M. Al Hosani, "Energy management of grid interconnected multi-microgrids based on p2p energy exchange: A data driven approach," *IEEE Transactions on Power Systems*, vol. 36, no. 2, pp. 1546–1562, 2021, doi: 10.1109/TPWRS.2020.3025113.

[161] B. E. Sedhom, M. M. El-Saadawi, M. El Moursi, M. Hassan, and A. A. Eladl, "Iot-based optimal demand side management and control scheme for smart microgrid," *International Journal of Electrical Power Energy Systems*, vol. 127, p. 106674, 2021, doi: https://doi.org/10.1016/j.ijepes.2020.106674.

[162] M. Pasetti, S. Rinaldi, and D. Manerba, "A virtual power plant architecture for the demand-side management of smart prosumers," *Applied Sciences*, vol. 8, no. 3, 2018, doi: 10.3390/app8030432.

[163] K. Christakou, D.-C. Tomozei, J.-Y. Le Boudec, and M. Paolone, "Ac opf in radial distribution networks – part i: On the limits of the branch flow convexification and the alternating direction method of multipliers," *Electric Power Systems Research*, vol. 143, pp. 438–450, 2017, doi: https://doi.org/10.1016/j.epsr.2016.07.030.

[164] ——, "Ac opf in radial distribution networks – part ii: An augmented lagrangian-based opf algorithm, distributable via primal decomposition," *Electric Power Systems Research*, vol. 150, pp. 24–35, 2017, doi: https://doi.org/10.1016/j.epsr.2017.04.028.

[165] W. Lin, Z. Yang, J. Yu, S. Bao, and W. Dai, "Toward fast calculation of probabilistic optimal power flow," *IEEE Transactions on Power Systems*, vol. 34, no. 4, pp. 3286–3288, 2019, doi: 10.1109/TPWRS.2019.2911050.

[166] F. Kamalov, "Kernel density estimation based sampling for imbalanced class distribution," *Information Sciences*, vol. 512, pp. 1192–1201, 2020, doi: https://doi.org/10.1016/j.ins.2019.10.017.

[167] J. Cao and Z. Yan, "Probabilistic optimal power flow considering dependences of wind speed among wind farms by pair-copula method," *International Journal of Electrical Power Energy Systems*, vol. 84, pp. 296–307, 2017, doi: https://doi.org/10.1016/j.ijepes.2016.06.008.

[168] Z. Ren, K. Wang, W. Li, L. Jin, and Y. Dai, "Probabilistic power flow analysis of power systems incorporating tidal current generation," *IEEE Transactions on Sustainable Energy*, vol. 8, no. 3, pp. 1195–1203, 2017, doi: 10.1109/TSTE.2017.2669139.

[169] G. E. Constante-Flores and M. S. Illindala, "Data-driven probabilistic power flow analysis for a distribution system with renewable energy sources using monte carlo simulation," *IEEE Transactions on Industry Applications*, vol. 55, no. 1, pp. 174–181, 2019, doi: 10.1109/TIA.2018.2867332.

[170] Y. Liu, S. Gao, H. Cui, and L. Yu, "Probabilistic load flow considering correlations of input variables following arbitrary distributions," *Electric Power Systems Research*, vol. 140, pp. 354–362, 2016, doi: https://doi.org/10.1016/j.epsr.2016.06.005.

[171] H. Nosratabadi, M. Mohammadi, and A. Kargarian, "Nonparametric probabilistic unbalanced power flow with adaptive kernel density estimator," *IEEE Transactions on Smart Grid*, vol. 10, no. 3, pp. 3292–3300, 2019, doi: 10.1109/TSG.2018.2823058.

[172] A. R. Abbasi, "Probabilistic load flow based on holomorphic embedding, kernel density estimator and saddle point approximation including correlated uncertainty variables," *Electric Power Systems Research*, vol. 183, p. 106178, 2020, doi: https://doi.org/10.1016/j.epsr.2019.106178.

[173] M. Lotfi, M. Javadi, G. J. Osório, C. Monteiro, and J. P. S. Catalão, "A novel ensemble algorithm for solar power forecasting based on kernel density estimation," *Energies*, vol. 13, no. 1, 2020, doi: 10.3390/en13010216.

[174] L. Martirano, S. Rotondo, M. Kermani, F. Massarella, and R. Gravina, "Power sharing model for energy communities of buildings," *IEEE Transactions on Industry Applications*, vol. 57, no. 1, pp. 170–178, 2021, doi: 10.1109/TIA.2020.3036015.

[175] E. Espinosa-Juarez and A. HernÁndez, "A method for voltage sag state estimation in power systems," *IEEE Transactions on Power Delivery*, vol. 22, no. 4, pp. 2517–2526, 2007, doi: 10.1109/TPWRD.2007.905587.

[176] M. S. Javadi, K. Firuzi, M. Rezanejad, M. Lotfi, M. Gough, and J. P. Catalão, "Optimal sizing and siting of electrical energy storage devices for smart grids considering time-of-use programs," in *IECON 2019 - 45th Annual Conference of the IEEE Industrial Electronics Society*, vol. 1, 2019, doi: 10.1109/IECON.2019.8927263. pp. 4157–4162.

[177] M. Lotfi, S. Fikry, G. J. Osório, M. Javadi, S. F. Santos, and J. P. S. Catalão, "A hybrid probabilistic algorithm for computationally efficient estimation of power generation in ac optimal power flow," in *2020 IEEE 14th International Conference on Compatibility, Power Electronics and Power Engineering (CPE-POWERENG)*, vol. 1, 2020, doi: 10.1109/CPE-POWERENG48600.2020.9161685. pp. 169–174.

[178] P. Mallet, P.-O. Granstrom, P. Hallberg, G. Lorenz, and P. Mandatova, "Power to the people!: European perspectives on the future of electric distribution," *IEEE Power and Energy Magazine*, vol. 12, no. 2, pp. 51–64, 2014, doi: 10.1109/MPE.2013.2294512.

[179] F. Griffiths and M. Ooi, "The fourth industrial revolution - industry 4.0 and iot [trends in future i m]," *IEEE Instrumentation Measurement Magazine*, vol. 21, no. 6, pp. 29–43, 2018, doi: 10.1109/MIM.2018.8573590.

[180] T. Medved, E. Lakić, J. Zupančič, and A. F. Gubina, "A review of business models for small prosumers in a post-res subsidy and post-priority dispatch world," in *2017 14th International Conference on the European Energy Market (EEM)*, 2017, doi: 10.1109/EEM.2017.7981998. pp. 1–6.

[181] G. C. Christoforidis, I. P. Panapakidis, G. K. Papagiannis, T. A. Papadopoulos, I. Koumparou, M. Hatzipanayi, and G. E. Georghiou, "Investigating net-metering variant policies: The case of greece," in *2015 IEEE 15th International Conference on Environment and Electrical Engineering (EEEIC)*, 2015, doi: 10.1109/EEEIC.2015.7165486. pp. 2023–2028.

[182] J. Goop, M. Odenberger, and F. Johnsson, "The effect of high levels of solar generation on congestion in the european electricity transmission grid," *Applied Energy*, vol. 205, pp. 1128–1140, 2017, doi: https://doi.org/10.1016/j.apenergy.2017.08.143.

[183] B. Hussain, Q. U. Hasan, N. Javaid, M. Guizani, A. Almogren, and A. Alamri, "An innovative heuristic algorithm for iot-enabled smart homes for developing countries," *IEEE Access*, vol. 6, pp. 15 550–15 575, 2018, doi: 10.1109/ACCESS.2018.2809778.

[184] M. J. Burke and J. C. Stephens, "Political power and renewable energy futures: A critical review," *Energy Research Social Science*, vol. 35, pp. 78–93, 2018, doi: https://doi.org/10.1016/j.erss.2017.10.018. Energy and the Future.

[185] C. Pop, T. Cioara, M. Antal, I. Anghel, I. Salomie, and M. Bertoncini, "Blockchain based decentralized management of demand response programs in smart energy grids," *Sensors*, vol. 18, no. 1, 2018, doi: 10.3390/s18010162.

[186] Oxford Dictionary, "Definition of social welfare in US English:," 2019. [Online]. Available: https://en.oxforddictionaries.com/definition/us/social_welfare

[187] Business Dictionary, "What is social welfare? definition and meaning." [Online]. Available: http://www.businessdictionary.com/definition/social-welfare.html

[188] H. Liu, Y. Shen, Z. B. Zabinsky, C.-C. Liu, A. Courts, and S.-K. Joo, "Social welfare maximization in transmission enhancement considering network congestion," *IEEE Transactions on Power Systems*, vol. 23, no. 3, pp. 1105–1114, 2008, doi: 10.1109/TPWRS.2008.926717.

[189] B. Zhao, A. Zlotnik, A. J. Conejo, R. Sioshansi, and A. M. Rudkevich, "Shadow price-based co-ordination of natural gas and electric power systems," *IEEE Transactions on Power Systems*, vol. 34, no. 3, pp. 1942–1954, 2019, doi: 10.1109/TPWRS.2018.2879801.

[190] H. Hao, C. D. Corbin, K. Kalsi, and R. G. Pratt, "Transactive control of commercial buildings for demand response," *IEEE Transactions on Power Systems*, vol. 32, no. 1, pp. 774–783, 2017, doi: 10.1109/TPWRS.2016.2559485.

[191] L. Mathieu, "Electric Buses arive on time - Marketplace, economic, technology, environmental and policy perspectives for fully electric buses in the EU," Transport Environment, Tech. Rep. November, 2018. [Online]. Available: https://www.transportenvironment.org/sites/te/files/Electricbusesarriveontime.pdf

[192] M. Rogge, E. van der Hurk, A. Larsen, and D. U. Sauer, "Electric bus fleet size and mix problem with optimization of charging infrastructure," *Applied Energy*, vol. 211, pp. 282–295, 2018, doi: https://doi.org/10.1016/j.apenergy.2017.11.051.

[193] X. Zuo, C. Chen, W. Tan, and M. Zhou, "Vehicle scheduling of an urban bus line via an improved multiobjective genetic algorithm," *IEEE Transactions on Intelligent Transportation Systems*, vol. 16, no. 2, pp. 1030–1041, 2015, doi: 10.1109/TITS.2014.2352599.

[194] E. Yao, T. Liu, T. Lu, and Y. Yang, "Optimization of electric vehicle scheduling with multiple vehicle types in public transport," *Sustainable Cities and Society*, vol. 52, p. 101862, 2020, doi: https://doi.org/10.1016/j.scs.2019.101862.

[195] Z. Wu, F. Guo, J. Polak, and G. Strbac, "Evaluating grid-interactive electric bus operation and demand response with load management tariff," *Applied Energy*, vol. 255, p. 113798, 2019, doi: https://doi.org/10.1016/j.apenergy.2019.113798.

[196] M. Bhaskar Naik, P. Kumar, and S. Majhi, "Smart public transportation network expansion and its interaction with the grid," *International Journal of Electrical Power Energy Systems*, vol. 105, pp. 365–380, 2019, doi: https://doi.org/10.1016/j.ijepes.2018.08.009.

[197] Y. He, Z. Song, and Z. Liu, "Fast-charging station deployment for battery electric bus systems considering electricity demand charges," *Sustainable Cities and Society*, vol. 48, p. 101530, 2019, doi: https://doi.org/10.1016/j.scs.2019.101530.

[198] Y. Lin, K. Zhang, Z.-J. M. Shen, B. Ye, and L. Miao, "Multistage large-scale charging station planning for electric buses considering transportation network and power grid," *Transportation Research Part C: Emerging Technologies*, vol. 107, pp. 423–443, 2019, doi: https://doi.org/10.1016/j.trc.2019.08.009.

[199] "The European electric bus market is charging ahead, but how will it develop? | McKinsey." [Online]. Available: https://www.mckinsey.com/industries/oil-and-gas/our-insights/the-european-electric-bus-market-is-charging-ahead-but-how-will-it-develop

[200] IRENA, "Innovation outlook: Smart charging for electric vehicles," IRENA, Tech. Rep., 2019. [Online]. Available: https://www.irena.org/-/media/Files/IRENA/Agency/Publication/2019/May/IRENA_Innovation_Outlook_EV_smart_charging_2019.pdf

[201] ABB Canada, "Electrification of public transport," ABB Canada, Toronto, Tech. Rep., 2018. [Online]. Available: https://search.abb.com/library/Download.aspx?DocumentID=9AKK107046A1570&LanguageCode=en&DocumentPartId=&Action=Launch&DocumentRevisionId=A

[202] M. Rogge, S. Wollny, and D. U. Sauer, "Fast charging battery buses for the electrification of urban public transport—a feasibility study focusing on charging infrastructure and energy storage requirements," *Energies*, vol. 8, no. 5, pp. 4587–4606, 2015, doi: 10.3390/en8054587.

[203] M. Andersson, "Energy storage solutions for electric bus fast charging stations Cost optimization of grid connection and grid reinforcements," Ph.D. dissertation, Uppsala Universitet, 2017. [Online]. Available: http://www.teknat.uu.se/student

[204] "Des bus map of Paris and the île-de-France region | RATP." [Online]. Available: https://www.ratp.fr/en/plans-lignes/plan-des-bus

[205] Transport for London, "Key bus routes in central London," 2020. [Online]. Available: http://content.tfl.gov.uk/bus-route-maps/key-bus-routes-in-central-london.pdf

[206] "Energy prices and costs in Europe | Energy." [Online]. Available: https://ec.europa.eu/energy/en/data-analysis/energy-prices-and-costs

[207] "A Behind the Scenes Take on Lithium-ion Battery Prices | BloombergNEF." [Online]. Available: https://about.bnef.com/blog/behind-scenes-take-lithium-ion-battery-prices/

[208] P. Nunes, R. Figueiredo, and M. C. Brito, "The use of parking lots to solar-charge electric vehicles," *Renewable and Sustainable Energy Reviews*, vol. 66, pp. 679–693, 2016, doi: https://doi.org/10.1016/j.rser.2016.08.015.

[209] Q. Kang, J. Wang, M. Zhou, and A. C. Ammari, "Centralized charging strategy and scheduling algorithm for electric vehicles under a battery swapping scenario," *IEEE Transactions on Intelligent Transportation Systems*, vol. 17, no. 3, pp. 659–669, 2016, doi: 10.1109/TITS.2015.2487323.

[210] H. Tan, H. Zhang, J. Peng, Z. Jiang, and Y. Wu, "Energy management of hybrid electric bus based on deep reinforcement learning in continuous state and action space," *Energy Conversion and Management*, vol. 195, pp. 548–560, 2019, doi: https://doi.org/10.1016/j.enconman.2019.05.038.

[211] Z. Chen, L. Li, X. Hu, B. Yan, and C. Yang, "Temporal-difference learning-based stochastic energy management for plug-in hybrid electric buses," *IEEE Transactions on Intelligent Transportation Systems*, vol. 20, no. 6, pp. 2378–2388, 2019, doi: 10.1109/TITS.2018.2869731.

[212] A. Li, W. Yuan, S. Li, X. Wang, X. Qiu, and L. Xu, "Design and implementation of controller for ehps of intelligent electric bus," *IEEE Access*, vol. 7, pp. 89 400–89 411, 2019, doi: 10.1109/ACCESS.2019.2925899.

[213] X. Tian, Y. Cai, X. Sun, Z. Zhu, and Y. Xu, "An adaptive ecms with driving style recognition for energy optimization of parallel hybrid electric buses," *Energy*, vol. 189, p. 116151, 2019, doi: https://doi.org/10.1016/j.energy.2019.116151.

[214] A. M. Othman, H. A. Gabbar, F. Pino, and M. Repetto, "Optimal electrical fast charging stations by enhanced descent gradient and voronoi diagram," *Computers Electrical Engineering*, vol. 83, p. 106574, 2020, doi: https://doi.org/10.1016/j.compeleceng.2020.106574.

[215] S. Mudaliyar and S. Mishra, "Coordinated voltage control of a grid connected ring dc microgrid with energy hub," *IEEE Transactions on Smart Grid*, vol. 10, no. 2, pp. 1939–1948, 2019, doi: 10.1109/TSG.2017.2783972.

[216] H. A. Gabbar and A. M. Othman, "Flywheel-based fast charging station – FFCS for electric vehicles and public transportation," *IOP Conference Series: Earth and Environmental Science*, vol. 83, p. 012009, aug 2017, doi: 10.1088/1755-1315/83/1/012009.

[217] J. A. P. Lopes, A. G. Madureira, M. Matos, R. J. Bessa, V. Monteiro, J. L. Afonso, S. F. Santos, J. P. S. Catalão, C. H. Antunes, and P. Magalhães, "The future of power systems: Challenges, trends, and upcoming paradigms," *WIREs Energy and Environment*, vol. 9, no. 3, p. e368, 2020, doi: https://doi.org/10.1002/wene.368.

[218] R. K. Jain, J. Qin, and R. Rajagopal, "Data-driven planning of distributed energy resources amidst socio-technical complexities," *Nature Energy*, vol. 2, no. 8, p. 17112, Aug. 2017, doi: 10.1038/nenergy.2017.112.

[219] M. Chowdhury and M. Maier, "Local and nonlocal human-to-robot task allocation in fiber-wireless multi-robot networks," *IEEE Systems Journal*, vol. 12, no. 3, pp. 2250–2260, 2018, doi: 10.1109/JSYST.2017.2661282.

[220] V. Ortenzi, M. Controzzi, F. Cini, J. Leitner, M. Bianchi, M. A. Roa, and P. Corke, "Robotic manipulation and the role of the task in the metric of success," *Nature Machine Intelligence*, vol. 1, no. 8, pp. 340–346, Aug 2019, doi: 10.1038/s42256-019-0078-4.

[221] A. Ovalle, A. Hably, S. Bacha, G. Ramos, and J. M. Hossain, "Escort evolutionary game dynamics approach for integral load management of electric vehicle fleets," *IEEE Transactions on Industrial Electronics*, vol. 64, no. 2, pp. 1358–1369, 2017, doi: 10.1109/TIE.2016.2615042.

[222] X. Hou, J. Wang, T. Huang, T. Wang, and P. Wang, "Smart home energy management optimization method considering energy storage and electric vehicle," *IEEE Access*, vol. 7, pp. 144 010–144 020, 2019, doi: 10.1109/ACCESS.2019.2944878.

[223] S. Wang, J. Wan, D. Zhang, D. Li, and C. Zhang, "Towards smart factory for industry 4.0: a self-organized multi-agent system with big data based feedback and coordination," *Computer Networks*, vol. 101, pp. 158–168, 2016, doi: https://doi.org/10.1016/j.comnet.2015.12.017. Industrial Technologies and Applications for the Internet of Things.

[224] X. Gong, Y. Liu, N. Lohse, T. De Pessemier, L. Martens, and W. Joseph, "Energy- and labor-aware production scheduling for industrial demand response using adaptive multiobjective memetic algorithm," *IEEE Transactions on Industrial Informatics*, vol. 15, no. 2, pp. 942–953, 2019, doi: 10.1109/TII.2018.2839645.

[225] B. Beirigo, F. Schulte, and R. Negenborn, "Dual-mode vehicle routing in mixed autonomous and non-autonomous zone networks," in *2018 21st International Conference on Intelligent Transportation Systems (ITSC)*, 2018, doi: 10.1109/ITSC.2018.8569344. pp. 1325–1330.

[226] A. Khamis, A. Hussein, and A. Elmogy, *Multi-robot Task Allocation: A Review of the State-of-the-Art*. Cham: Springer International Publishing, 2015, pp. 31–51. ISBN 978-3-319-18299-5

[227] C. Liu, *Multi-Robot Task Allocation for Inspection Problems with Cooperative Tasks Using Hybrid Genetic Algorithms*. ISBN 978-3-86219-551-0

[228] C. Sarkar, H. S. Paul, and A. Pal, "A scalable multi-robot task allocation algorithm," in *2018 IEEE International Conference on Robotics and Automation (ICRA)*, 2018, doi: 10.1109/ICRA.2018.8460886. pp. 5022–5027.

[229] E. W. Dijkstra, "A note on two problems in connexion with graphs," *Numerische Mathematik*, vol. 1, no. 1, pp. 269–271, Dec 1959, doi: 10.1007/BF01386390.

[230] D. K. Smith, "Shortest Paths," *Networks and Graphs*, pp. 27–45, 2003, doi: 10.1533/9780857099570.27.

[231] S.-Y. Huang, X.-W. Zou, and Z.-Z. Jin, "Directed random walks in continuous space," *Physical Review E*, vol. 65, no. 5, May 2002, doi: 10.1103/physreve.65.052105.

[232] B. Ribeiro, P. Wang, F. Murai, and D. Towsley, "Sampling directed graphs with random walks," in *2012 Proceedings IEEE INFOCOM*, 2012, doi: 10.1109/INFCOM.2012.6195540. pp. 1692–1700.

Appendix A

Annual GFS and PV Generation Data

This Appendix is associated with Chapter 4

.

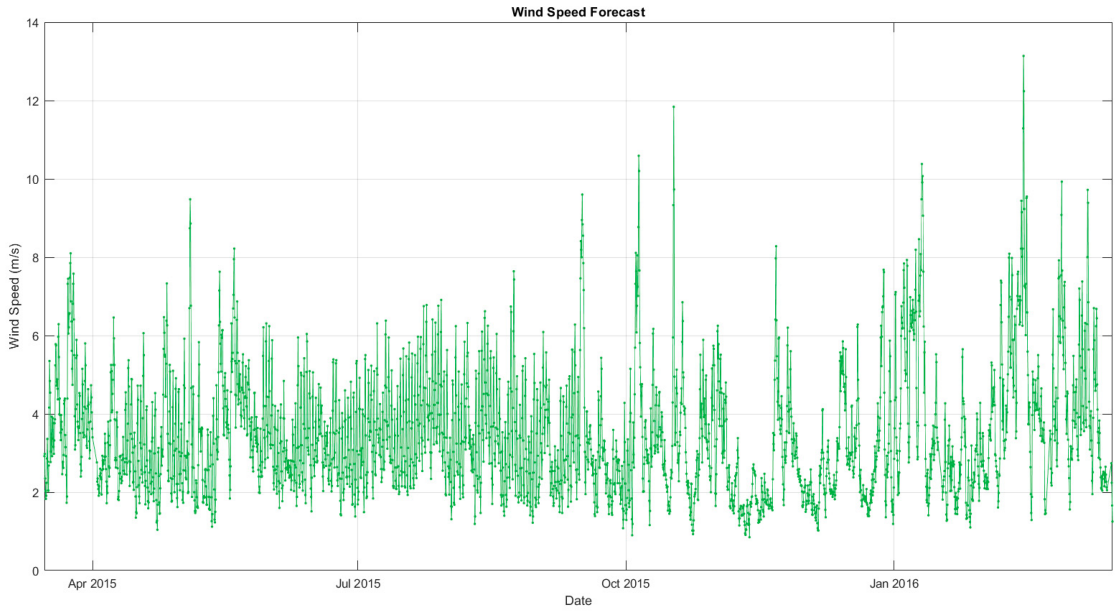

Figure A.1: Annual wind speed data for the case study provided by GFS.

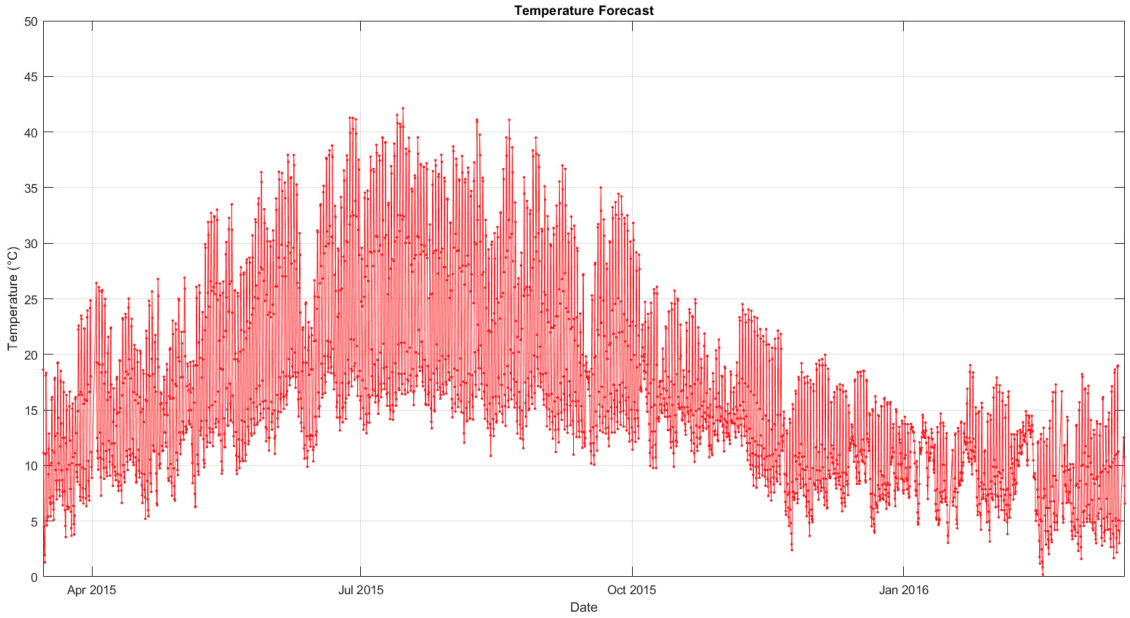

Figure A.2: Annual temperature data for the case study provided by GFS.

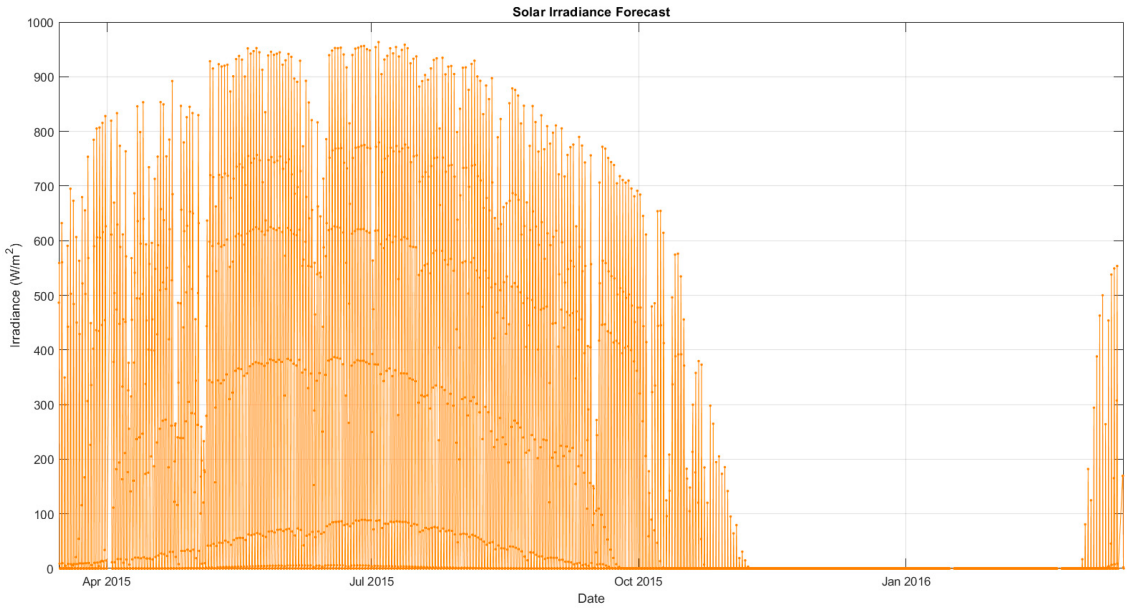

Figure A.3: Annual solar irradiance data for the case study provided by GFS.

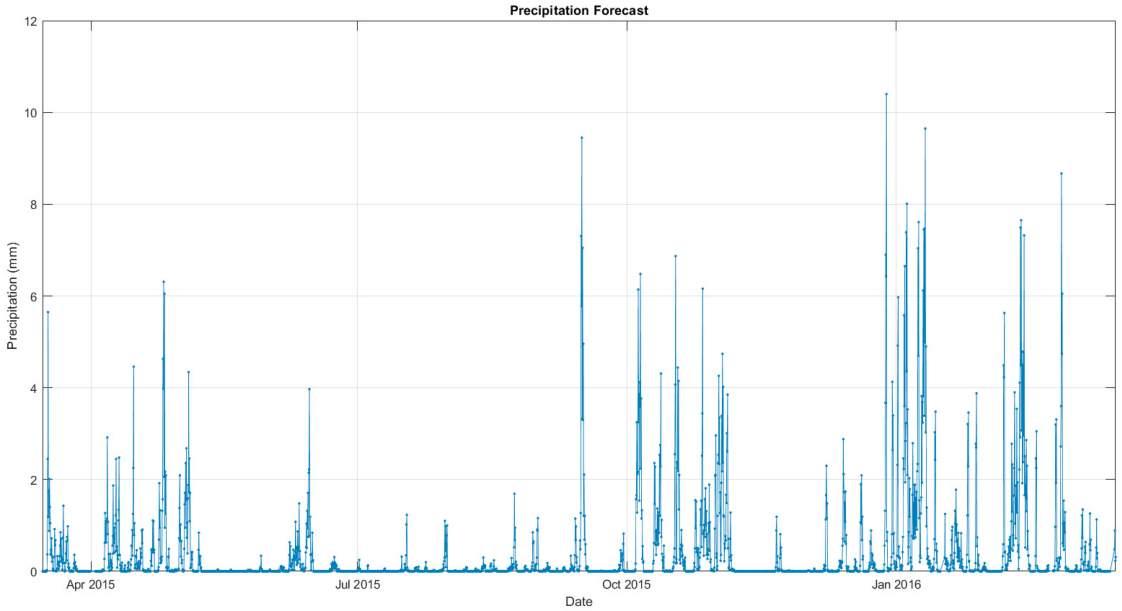

Figure A.4: Annual precipitation data for the case study provided by GFS.

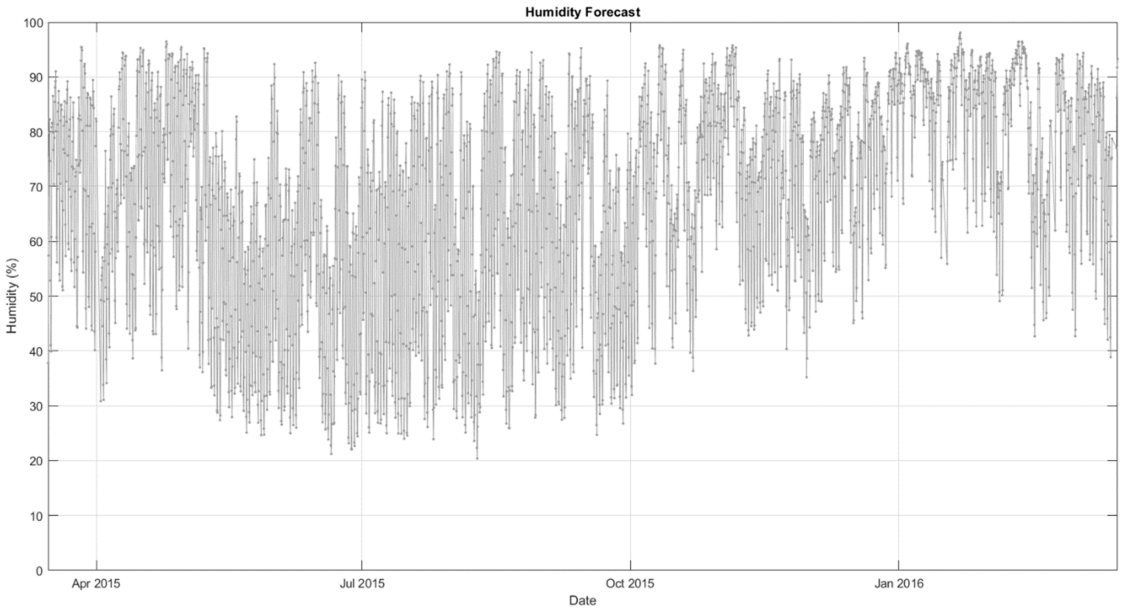

Figure A.5: Annual humidity data for the case study provided by GFS.

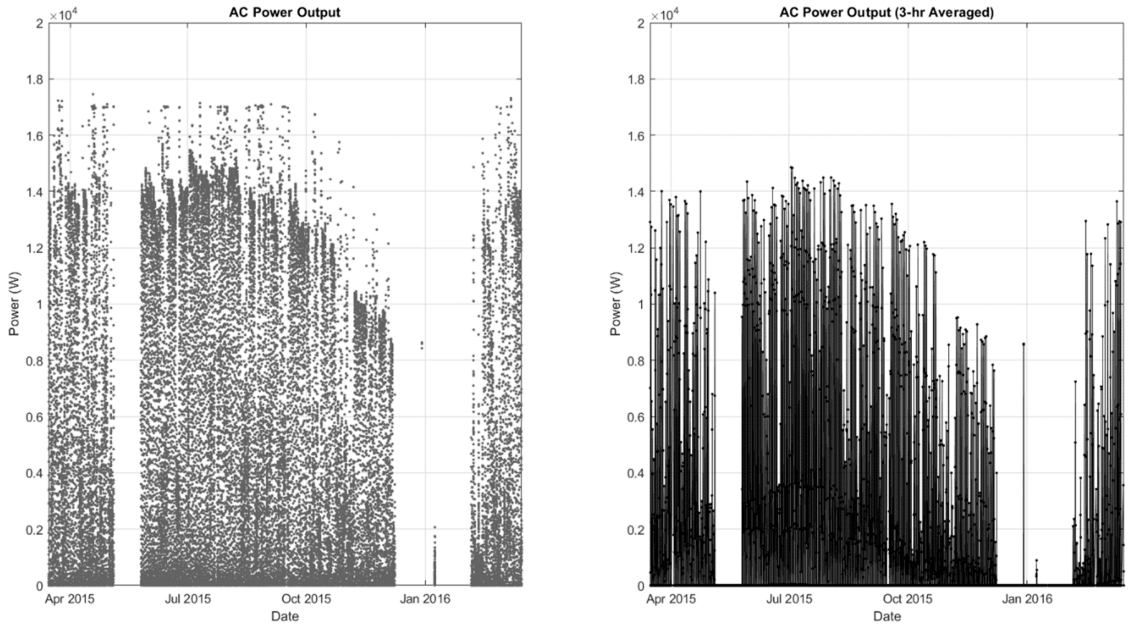

Figure A.6: Annual recorded AC output power data for the case study: recorded (left) and averaged for GFS synchronization (right).

Appendix B

Directed Random Walk Algorithm

This Appendix is associated with Chapter 8

.

In a random walk, the next vertex j in a path is chosen at random from the neighbors of a vertex i. In this study a variation of this is used for comparison with DOT, a directed random walk (DRW) [231, 232]. In a DRW the next vertex is chosen randomly, but the probability of a vertex being chosen is inversely proportional to its distance from the destination. This is illustrated in Fig. B.1, where the current vertex *i* has four neighbors 1, 2, 3, and 4, with the distances (Cartesian) to the destination being d1, d2, d3, and d4, respectively.

The next vertex in the path is selected using a roulette wheel approach. The aim is to have a random selection while assigning a higher priority to vertices closer to the destination. Therefore, the selection probability is proportional to d', which is the inverse (1/d) of the Cartesian distance. A random variable X is generated such that X=U(0,sum(d1',d2'd3',d4'), based on an uniform distribution. As illustrated in Fig B.2, the probability of each of the neighbors being selected is proportional to its inverse distance from the destination. With the random element performed, the results reported in this study are based on the 25th percentile (best case) of 1000 runs. The DRW guarantees to provide a finite path; however, the random element can result in excessively long ones. Therefore, two variations of the DRW were used in this work: normal (DRW1) and an improved brute force one (DRW2). At the beginning of every traversal while stationed at a checkpoint, a path is calculated. Once a path requires the agent to drop below SoC minimum, the pathing is halted. With DRW2, ten trials are attempted at finding a shorter path until the solution is halted, in which case the agent must recharge before proceeding, since no shorter path can be found that can be traversed with the remaining SoC.

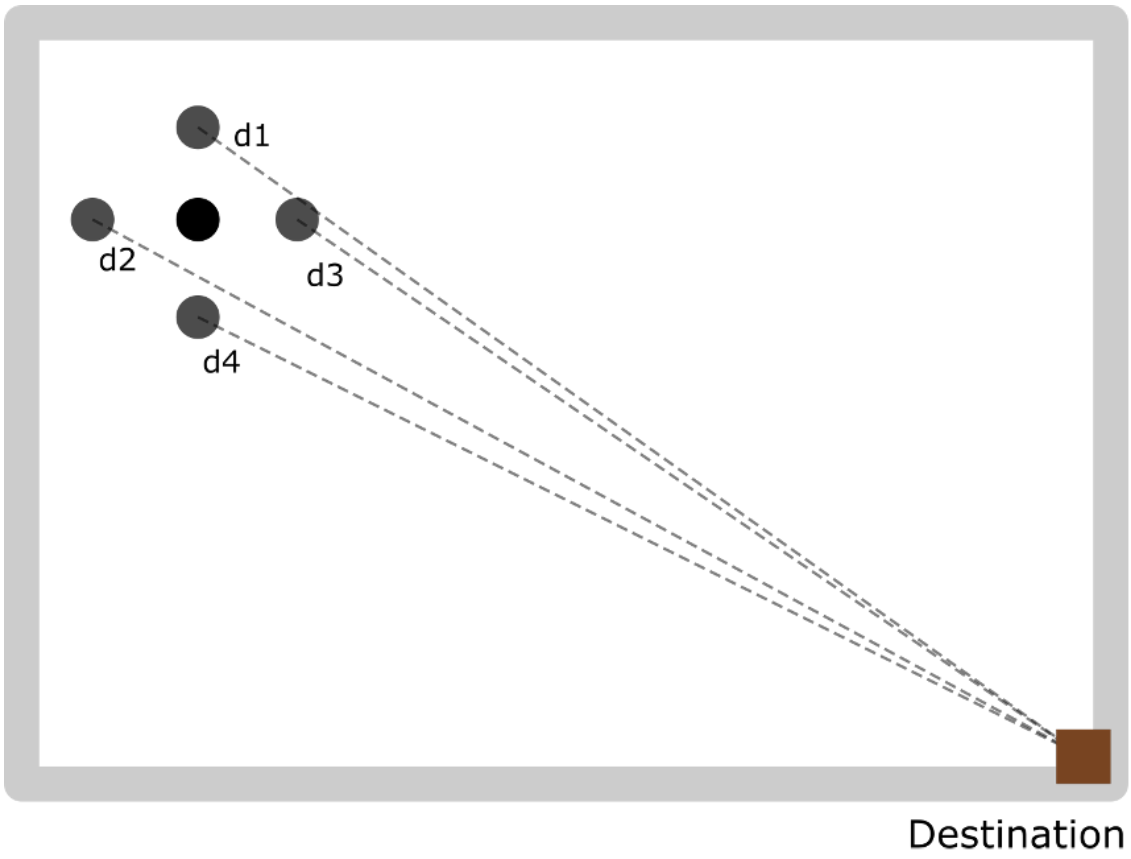

Figure B.1: Illustration of current node i , neighboring nodes, and their Cartesian distance to the destination.

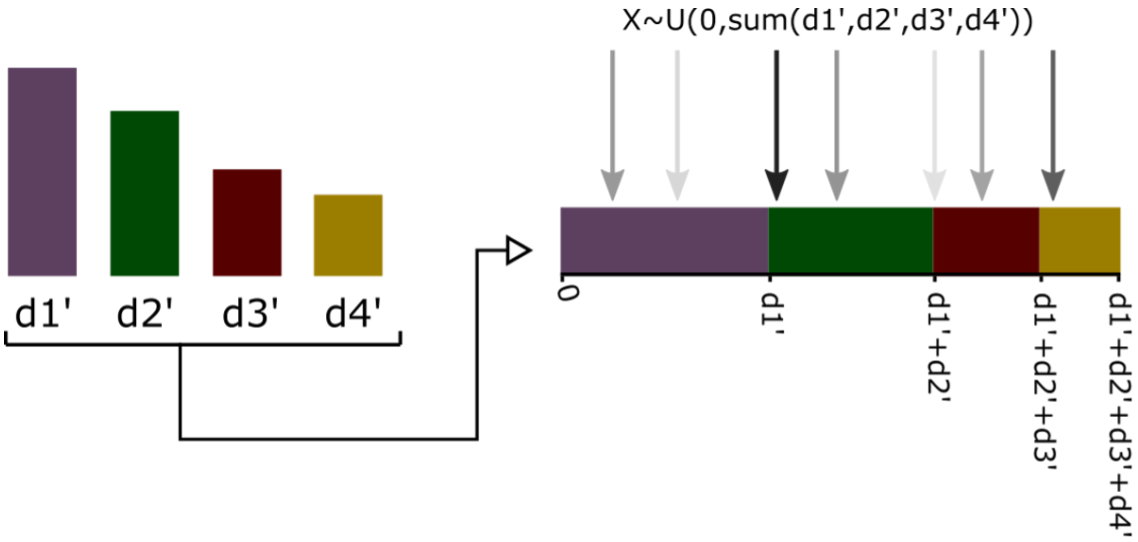

Figure B.2: Constructing the roulette wheel selection.